Development of novel composite materials with defects induced gigantic positive and negative permittivity

by

Hossein Talebinezhad

A dissertation submitted to the Graduate Faculty of
Auburn University
in partial fulfillment of the
requirements for the Degree of
Doctor of Philosophy

Auburn, Alabama
August 03, 2019

Keywords: Permittivity, Nonlinearity, SPS, Defects, Negative-permittivity, Annealing

Approved by

ZhongYang Cheng, Chair, Professor of Materials Engineering
Majid Beidaghi, Assistant Professor of Materials Engineering
Dong-Joo Kim, Alumni Professor of Materials Engineering
Minseo Park, Professor of Physics

Abstract

Dielectrics respond to an electrical field with a polarization. They are high demands for electronic circuits and electrical system. There is a particular need to develop dielectrics with a high breakdown field for several applications such as energy storage, capacitors, transistors. Moreover, in the past decades developing new materials with negative permittivity are in broad interest. The reason for such attention lies on the usage of those materials on applications like cloaking, tunable electronic, microstrip antenna and transistors.

For developing the dielectric materials for different applications, composites are used to manipulate materials properties. In the composites, polymers and glasses are extensively used due to their high breakdown field. These composites usually exhibit low permittivity due to their matrix properties. In this study, the defects are used to improved ceramic-glass composites permittivities and the conductivity nonlinearity change just as the conclusion.

The first part of this research, is the dielectric characterization of $CaCu_3Ti_4O_{12}$ $(CCTO)/SiO_2$ ceramics with high permittivity. Many efforts aimed at reducing high dielectric loss and increasing low breakdown field which is essential for energy storages. One of the most common approaches for improving the performance of $CCTO$ is using insulative additive aiming grain-boundaries microstructure and properties. In this regards, SiO_2 as an approved insulator is the right candidate which we used to control dielectric loss of $CCTO$ and improve its breakdown field. The ceramic composite was made with core-shell structure by SiO_2 layers around $CCTO$ particles obtained by the sol-gel method. The composites with different percentage of SiO_2 and the various sintered temperature was made to evaluate the glass-ceramic behavior carefully. There is a significant change on microstructure when composites with an adequate amount of SiO_2 was sintered above 1060 ^0C. Dielectric properties of ceramics were influenced by the formation of the second phase and defects in grain structure. Moreover, the

composites pose improvement in nonlinearity which can be considered to be used in varistor applications.

The second part of research is focus on BTO ($BaTiO_3$)/SiO_2 Composites. The BTO ceramics which has ferroelectric properties exhibit high permittivity with strong temperature dependence. The BTO composites with SiO_2 are one of the most used materials in energy storage application which has lower the permittivity and the dielectric loss. In this work, the Spark Plasma Sintering (SPS) was used to induced defects and oxygen vacancies in BTO-SiO_2 ceramics. Ceramics was fabricated with two different size powders and pretreatment to help the understanding of each parameter contributions. Ceramics posses gigantic permittivity up to $10^5 - 10^6$ due to induced defects. It is interesting to find the permittivity can be negative by applying DC bias. Furthermore, the negative permittivity can be found in the low-frequency test. The negative permittivity result can be fitted with the Drude model very well that indicates the electrons are almost free. It is believed that the gigantic positive and negative permittivity is due to polaron electrons with pretty low energy barriers which can easily overcome by an electrical field. Based on our knowledge, these ceramics posses smallest plasma frequency among all epsilon negative materials.

To confirm the influence of oxygen vacancies on SPS ceramics properties, they were annealed in the air. The ceramic color and features show that the annealing changes the oxygen vacancies concentration which can provide ceramics with permittivity that surpasses the conventional sintering and acceptable dielectric loss. The fully annealed sample can result in high energy density with thin PE loop. In the other hand, the partially annealed samples still can possess similar properties to the SPS sample. The ability to tune the properties can lead to many possibilities in using such materials.

Acknowledgments

I would like to acknowledge everyone supported me during my doctoral studies. Foremost, I would like to express my most profound appreciation to my parents and dedicate all my success to them. My academic accomplished would not have been possible without their warm love, and endless support. And also special thanks to my family, Mr. Amin Talebinejad, Dr. Ali Talebinejad and Ms. Neda Moosavifard, whom their continuous support made this dissertation possible.

I would like to express my sincere gratitude to Prof. Cheng, for his guidance, motivation, enthusiasm, and immense knowledge. Under his supervision, I accomplished many achievements and publications during my studies. Moreover, I am thankful to Dr. Yong Tong, Dr. Xu Lu, and Mr. Weiye Wang for their collaboration and contribution to various projects during my doctoral studies. I would also like to thank my other lab mates that include Ms. Liangxi Li, Mr. Wei Yi, Mr. Jiachen Liu, Mr. Yancen Cai, Mr. Jindong Wei, and Dr. Lin Zhang for making my experience in the smart materials lab and graduate school exciting and fun. I would like to thank my friends Dr. Hamid Ghaedinia, Dr. Ali Khoshkhoo, Mr. Mohammadnaser Ansari, Dr. Nila Ghanei, Ms. Bahareh Karimi, Ms. Shekoofeh Gheitani, Mr. Jafar Orangi and Mr. Navid Etebari for their help and support through the experiments and studies.

Thanks are also due to the (MSFC, NASA) for the financial support that I otherwise would not have been able to develop my scientific discoveries. More specifically, I would like to thank Mr. Curtis Hill, Dr. Dennis Tucker, Dr. Terry Rolin for their significant contribution and for providing me with powders and sample for dielectric studies. Last but not least, I would like to thank the rest of my dissertation committee members (Prof. Beidaghi, Prof. Kim, and Prof. Park) for their great support and invaluable advice.

Table of Contents

List of Figures

List of Tables

Chapter 1

Introduction and literature review

There is a growing need for materials with high electrical energy storage and high permittivity. These materials are needed for the applications including mobile electronic devices, stationary power systems, hybrid electric vehicles and also high-performance capacitors. These materials should have high permittivity while perform in the high electrical field. Other variables such as flexibility and being environmental friendly are important as well. Therefore, composites that combine all those properties are needed. In this regard, glass-ceramic composites are favored because of their high permittivity and ability to perform in the high electrical field make them good candidate in this area. In the case of energy storage, lossy materials with high permittivity might not be favorable. However, there are many application which need materials with such properties like varistors, microwave absorbing, electromagnetic attenuation, shielding fields, cloaking, superlens, wave filters, and superconductors. Moreover, recently, random composites with the negative permittivity open new area of interest and research for these types of materials.

1.1 Dielectric study

There is a wide range of application in electrical industries that use dielectric materials which are insulators with high permittivities. In this section, the dielectric properties of materials are listed and described and materials with high positive and negative permittivity introduced.

Capacitance is an electrical term that can be defined as the ability to store electrical charge. So the amount of electrical charge that can be accumulated by applying a voltage V into the two parallel metal plate which are separated by a distance of L is called the capacitance

[5, 63].

$$C = \frac{q}{V} \tag{1.1}$$

Where q is an accumulative charge on the surface of metal plates. The two geometry parameters of plates area and distance between them are determining the capacitance.

However, the capacitance also depends on the materials inserted in between the two metallic

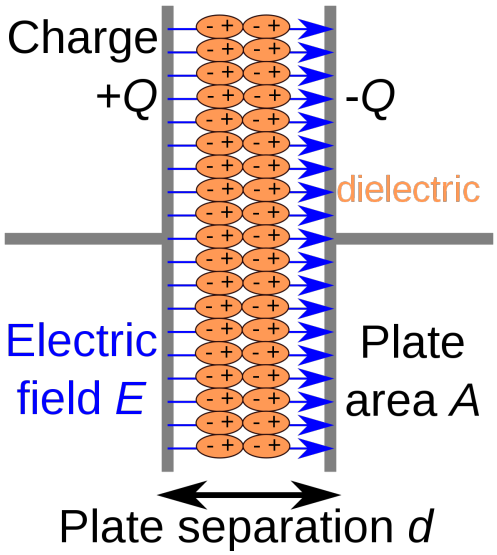

Figure 1.1: The effect of dielectric on charge separation in parallel-plate capacitor by applying the electric field [29].

plates. The relation between those parameters can be shown as below:

$$C = \varepsilon\varepsilon_0 \frac{A}{L} \tag{1.2}$$

In this equation, A and L are plates area and the distance between them. ε is the dielectric constant which is also called relative permittivity, and ε_0 is empty-space permittivity constant $(8.85 * 10^{-12} F/m)$. Equation. 1.2 shows that by inserting materials between two conductors, the ability to store the charges increases which is due to the separation between positive and negative charge can be occurred when an electric field applied.

1.1.1 Polarization

The formation of dipoles by applying an electrical field is called polarization. In the result of this process, inside the dielectric medium the electrical field strength is weakened. The term of dielectric displacement (D) is usually replacing polarization which is representative of surface charge density.

$$D = \varepsilon\varepsilon_0 E = \varepsilon_0 E + P \tag{1.3}$$

$$P = (\varepsilon_r - 1)\varepsilon_0 E \tag{1.4}$$

In this formula, P is the dielectric polarization which is responsible for the increase in the charge density by inserting dielectric material between two conductive plates. The polarization density P of a dielectric materials can be calculated by dividing the dipole moment dp to the Volume dV:

$$P = \frac{dp}{dV} \tag{1.5}$$

While the electrical field applied to dielectric materials, the electrical charge in a sample is moved from their normal equilibrium position. Dielectric polarization depends on the frequency which is known as the ability of displacement. Non-instantaneously response of electrical charges like atoms and molecules to the AC electrical field result in the dependence of permittivity to the frequency. By the electrical field, the dipole moment formed with positive and negative charge separation corresponds to nuclei and electrons respectfully, from atom and molecules. There are three main polarization found in materials among which electronic polarization present in all materials [28].

Various types of polarization can be found in dielectric materials. Their contribution depends on the time of the process. The relaxation time corresponding to characteristic frequency can be explained by Debye theory. Based on this theory materials dipole can mechanically

moved freely before characteristic frequency which cause polarization but cannot follow AC electrical field in shorter time. Polarizations categorized can be ranked based on their speed of polarization. Electron polarization exhibiting with frequency larger than 10^{15} is the fastest followed by the ionic polarization with the frequency range of 10^{10} to 10^{13}. The ionic polarization is common in the ionic material which by applying an external field, anions and cations are displaced and net dipole moment increases. Moreover, the dipole (orientation) polarization can be detected in a spectrum of 10^{3}-10^{6}.The third polarization mechanism is called molecular or orientation which response to the permanent dipoles which can align in an external electric field [7, 12].

For frequencies smaller than 10^{3} Hz, the interfacial or space charge polarization is causes the

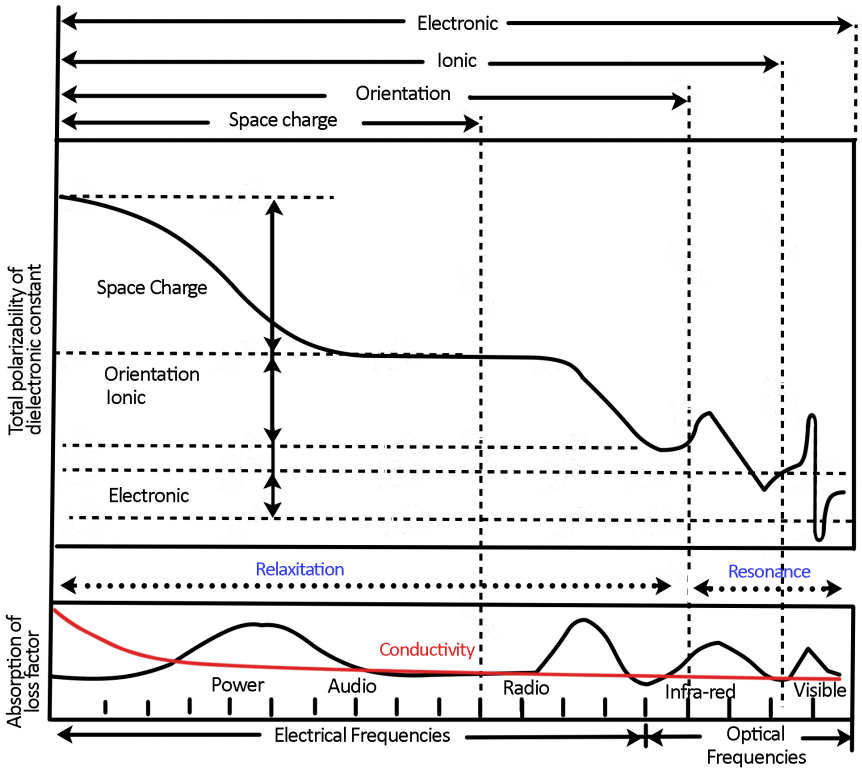

Figure 1.2: Dielectric responds over different frequency depends on polarization [4].

dielectric behavior and it is believed that electron hopping which is responsible for this type of polarization cannot follow the AC field at the higher frequencies. This polarization results

in large dielectric imaginary part values due to moving free carriers inside the material and usually shows an inverse linear relationship with the DC conductivity [17].

1.1.2 Dielectric constant and loss

Polarizations in dielectric materials strongly depends on the frequency, and at high frequencies, some polarizations may breakdown. This is due to transformation of energy to the heat which is known as a dielectric loss. In other word, under AC electrical field, the complex permittivity is fuction of the frequency [5]:

$$\varepsilon_r = \varepsilon_r' - j\varepsilon_r'' \tag{1.6}$$

In which ε_r' and ε_r'' correspond to the real and imaginary part of permittivity. In dielectric materials, ε_r' is responsible for energy stored in medium and ε_r'' is a loss of energy. In the suggested systems, the imaginary part can be rewritten where:

$$\epsilon^{"} = \epsilon_C^{"} + \epsilon_r^{"} \tag{1.7}$$

The term, $\epsilon_r^{"}$ is responsible for the delay on material by a relaxation or the resonance. Whenever the DC conductivity is involved in the dielectric response of medium, the imaginary part will includes $\epsilon_C^{"}$ which can be described as the following formula.

$$\epsilon_C^{"} = \frac{\sigma_{dc}}{\omega\epsilon_0} \tag{1.8}$$

On the other hand, the $\epsilon_r^{"}$ is dependent on the type of relaxation and system configuration of the medium and in the ideal case of Debye relaxation it can be written as the following equations:

$$\epsilon_r^{"} = \frac{(\epsilon_s - \epsilon_\infty)\omega\tau}{1 + \omega^2\tau^2} \tag{1.9}$$

$$\epsilon_r^{'} = \epsilon_\infty + \frac{\epsilon_s - \epsilon_\infty}{1 + \omega^2\tau^2} \tag{1.10}$$

The dielectric loss of a material can be defined as the ration of the dielectric constant imaginary part to the real part which represents the energy loss of a dielectric material [63].

$$tan\delta = \frac{\varepsilon_r'}{\varepsilon_r''} \tag{1.11}$$

The loss of dielectric materials can also be displayed by the imaginary part which is produced from the delay due to the frequency dependence of polarization. The phase difference between the current and the voltage corresponds to the loss which is 90 degrees for an ideal dielectric [98].

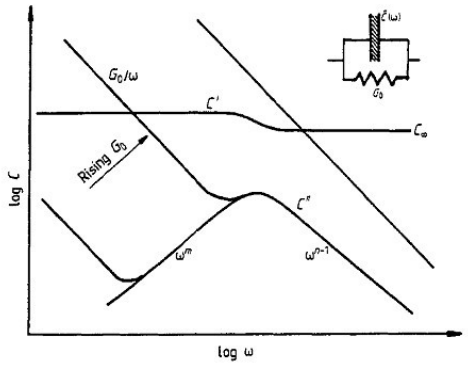

Figure 1.3: The effect of conductivity on imaginary part [98].

Kramers-Kronig

The dielectric response of materials can be written as the following equation:

$$R(q,\omega) = R(q,\infty) + \frac{1}{\pi} * \int_0^\infty \frac{d\omega'^2 * ImR(q,\omega')}{\omega'^2 - \omega' - i\delta} \tag{1.12}$$

$$\epsilon(q,0) = 1 + \frac{1}{\pi} * \int_0^\infty \frac{d\omega'^2}{\omega'^2} Im\epsilon(q,\omega') \tag{1.13}$$

Parallel process in material

$$\chi(\omega) \equiv [\varepsilon(\omega) - \varepsilon_\infty]/\varepsilon_0 = \chi'(\omega) - i\chi''(\omega) \tag{1.14}$$

$\chi(\omega)$ present susceptibility of the materials which influenced by the complex permittivity $\varepsilon(\omega)$ and ε_∞ is a suitable high-frequency permittivity.

Series process in materials

$$M(\omega) = M'(\omega) + iM''(\omega) = \frac{1}{\varepsilon(\omega)} = \frac{\varepsilon'(\omega) + i\varepsilon''(\omega)}{[\varepsilon'(\omega)]^2 + [\varepsilon''(\omega)]^2} \tag{1.15}$$

The dielectric modulus, which is the reciprocal of $\varepsilon(\omega)$ is emphasized in this process [35].

The dielectric behavior of materials in frequency range can be categorized based on polarization can be divided into the two main areas; relaxation and resonance.

Dielectric respond by device

Lets get look at how the permittivity calculated in devices:

$$V(t) = V_0 cos(\omega t) = Re[V^* exp(i\omega t)] \tag{1.16}$$

$$I(t) = I_0 cos(\omega t + \phi) = Re[I^* exp(i\omega t)] \tag{1.17}$$

$$Z^*(\omega) = Z' + iZ'' = \frac{V^*}{I^*} = \frac{V_0}{I_0}(cos\phi - isin\phi) \tag{1.18}$$

$$\epsilon^*(\omega) = \epsilon' - i\epsilon'' = \frac{1}{i\omega C_0}\frac{1}{Z^*(\omega)} = \frac{I_0}{i\omega C_0 V_0}(cos\phi + isin\phi) \tag{1.19}$$

Permittivity becomes negative while $\phi > \pi$ and sinϕ becomes negative. There are many reports that this condition meet when the conductivity increases [60].

1.1.3 Dielectric relaxations

Dielectric relaxation is one of the scientific terms in physics which research on it goes back to 18th centuries. The term relaxations are applied when by remove of stress, the strain has to recover. So, relaxation is time-dependent phenomena and its dependent on angular frequency, which can represent by Fourier transformation [35]:

$$f(t) = (2/\pi) \int_0^\infty x'(\omega) cos(\omega t) d\omega \tag{1.20}$$

$$= (2/\pi) \int_0^\infty x''(\omega) sin(\omega t) d\omega \tag{1.21}$$

As it can be seen from above formula, the time-domain response is related to the real and imaginary components which mathematically correspond to the Kramers-Kronig transformation. Many materials properties like dielectric, chemical, mechanical and so on, has the relaxation responds. Besides that, some properties like the dielectric relaxation of materials, can be influenced by many aspects of the material, like electrical, chemical and physics. Furthermore, in the systems that contain interfacial process like metal-insulator, semiconductor-insulator, electrode-electrolyte the relaxation process plays an important role. Consequently, many research conduct in materials that posses this nonlinear behavior to give a better explanation of their behaviors. As been noted, dielectric relaxation applied to a different system which makes variable functions suited for them and in following there be defined [35].

1.1.4 Maxwell-Wagner relaxation

In system consist of elements which has a significant difference in their conductivity, the interface plays essential role and charges accumulate in those regions due to hinder the

flow of current lead to nanocapacitor response of the interface. By applying AC loading, the charges can cross the interface by hopping and generate the additional conductivity in the system. By growing the difference in conductivity of two elements of the system, the electron is hopping and charge accumulation raises which drive to increase in both conductivity and permittivity; However, by increasing frequency, the charge hopping increases lead to decrease in permittivity [86].

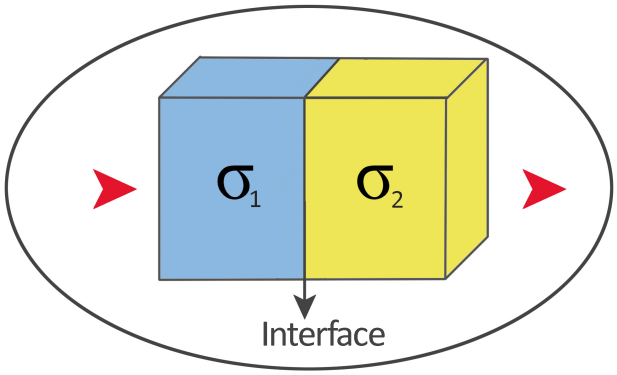

Figure 1.4: Maxwell-Wagner interface [86].

The variation in dielectric behavior by applied bias voltage may result from interface impact and space charge polarization. The dielectric affected more under a bias voltage at a low frequency since the charges can follow electrical field more freely [86] [17].

1.1.5 Hopping carrier systems

In the system that the conduction is result of moving charge carriers its works oppose the dipolar systems. In other words, based on Jonscher postule the charge carries like hopping electrons in such a systems, can move relatively free between electrods which contribute to giantic polarizations. This behavior of hopping electrons can be consider as DC conductivity [35].

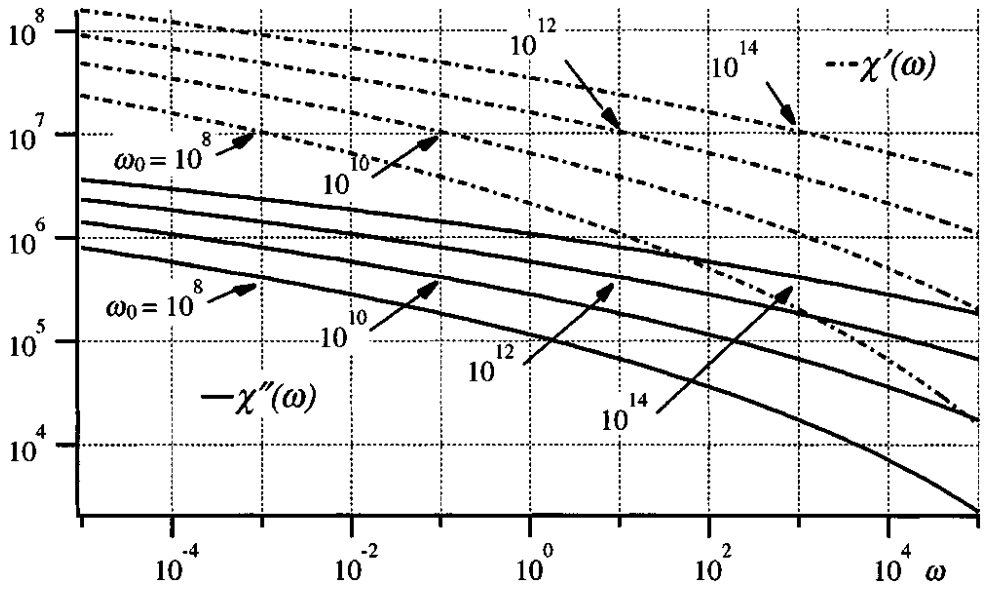

Figure 1.5: The hopping electronic systems [35].

1.1.6 Low frequency dispersion

The analysis of dielectric behavior in low frequency wasn't conventional till the late 1980s. It was shown that the power law is very close to the one (1-n). In this dispersion, the conductivity is weakly depend on frequency ($\omega^{n_{LFD}}$) which has a small difference compared to horizontal DC responds. The imaginary part doesn't show any peak in this range and follows as below equation:

$$\chi'' = cot(n\pi/2)\chi' \propto \omega^{n-1} \tag{1.22}$$

The importance of distinguishing such behavior from DC conductivity lies on high dielectric response. It is known that by DC conductivity the charge carriers cannot be stores, but in this case they can be finite and reversibly stored in interfaces.

The electronic hopping conduction can completely fit this extension of power-law and can utterly related to the interfacial. The following pics can illustrate such behavior in both dielectric and conductive response in the very low-frequency range [35]:

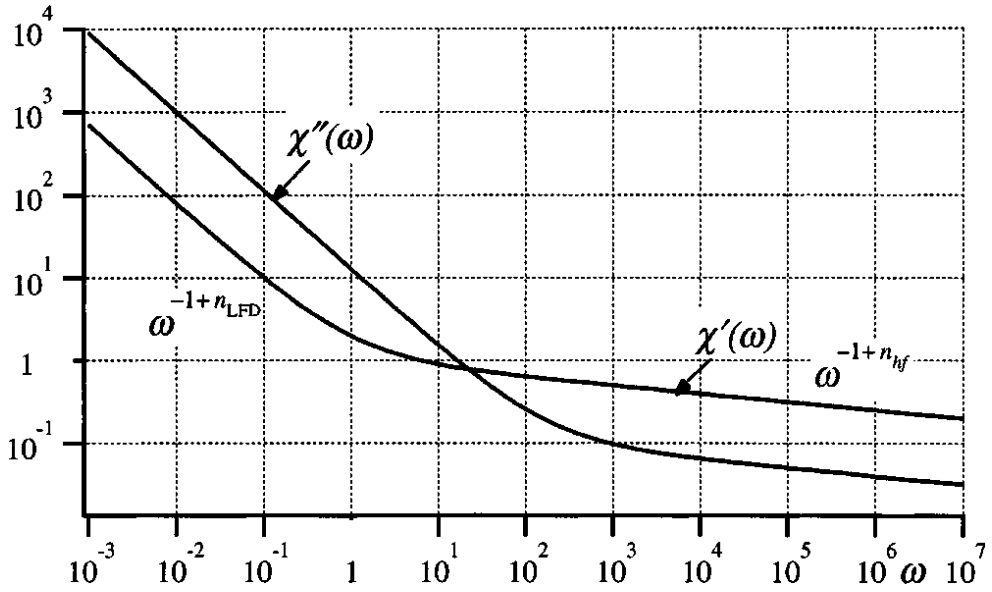

Figure 1.6: The dielectric behavior of a material hopping electrons dominated [35].

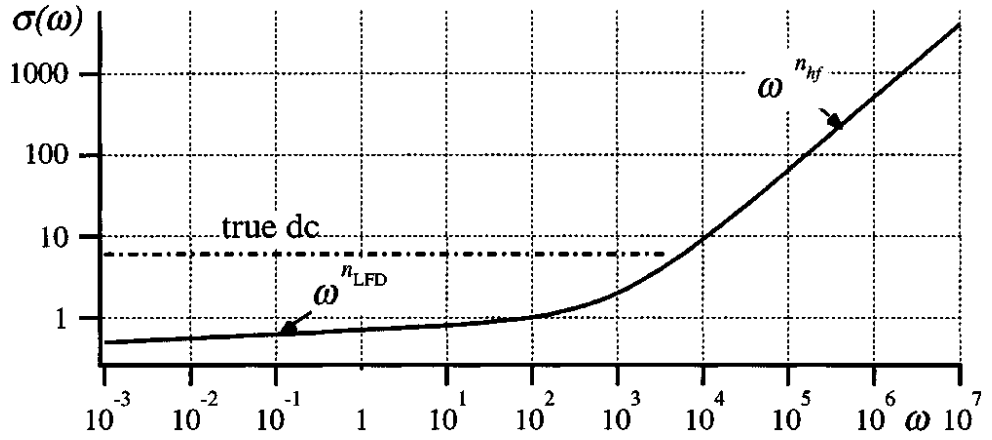

Figure 1.7: The frequency dependence of electrical conductivity of a material hopping electrons dominated [35].

1.2 Sign of dielectric function

Based on Kramers-Kronig relation, when the momentum is zero, it will lead to confronting to negative permittivity sign. However, only the external field is controlled, and there is no control on an entire electrical field inside the medium [18] [15].

The sign of permittivity in dielectric and semiconductor materials should be positive at zero

momentum situation. However, the presence of negative sign proposed that the finite momentum exists and dominate the inner system [18].

The dielectric response which origin in polarization is mechanical shifting the masses by an electrical field. All polarizations can be divided into the two main polarization of relaxation and resonance. On resonance, there is restoring force to pull the chargers back to the original place, and in relaxation, the driving force can be affected by the influence of the electrical field. There are three possibilities that medium can possess negative permittivity:

a) Relaxation by including mass: The relaxation is the delay in changing the direction by the dipole in the alternative electrical filed. This mechanical response of dipoles is usually considering to ignore the mass of them. However, in exceptional cases when the mass of dipoles cannot be excluded the relaxation can contribute to the negative permittivity in a short range of frequency.

b) Resonance with damping: When small damping force applied to the charge carriers, they can oscillate in short range without external force. This reaction contributes to the negative permittivity in a small period of frequency.

C) Free electrons: At very high frequency, there is no damping force applied to charge carriers, and they can move freely which can contribute to negative permittivity.

The complete explanation of the mentioned mechanism comes in following.

1.2.1 Drude model-Plasma oscillation

For the metals, the contribution of positive charges (ions) is negligible due to the much small mass of the electrons compare to them which has only the effect of movement of electrons on polarization is considered. So, in this case, the plasma like resonance of electrons is responsible for its dielectric permittivity behavior [28]. The following formula is used for conductors with free electrons which there is no restoring force applied to electrons [21]. Based on the Drude model, the following equation can be used for dielectric behavior of metals near plasma frequency [108] [9].

$$\epsilon(\omega) = 1 - \frac{\frac{Ne^2}{(\epsilon_0 m)}}{\omega(\omega + i\gamma)} = 1 - \frac{\omega_p^2}{\omega(\omega + i\gamma)} = (1 - \frac{\omega_p^2}{\omega^2 + \gamma^2}) + [\frac{\omega_p^2 \gamma}{\omega(\omega^2 + \gamma^2)}]i \tag{1.23}$$

$$\epsilon' = \epsilon_\infty - \frac{\omega_p^2}{\omega^2 + \gamma^2} \tag{1.24}$$

$$\omega_p = (\frac{Ne^2}{\epsilon_0 m})^{0.5} \tag{1.25}$$

Where ϵ' is the relative dielectric permittivity, N is the concentration of charge carriers contributing to oscillation, e is the charge of a carrier, m is the carrier mass, ϵ_0 is the absolute dielectric permittivity of vacuum.

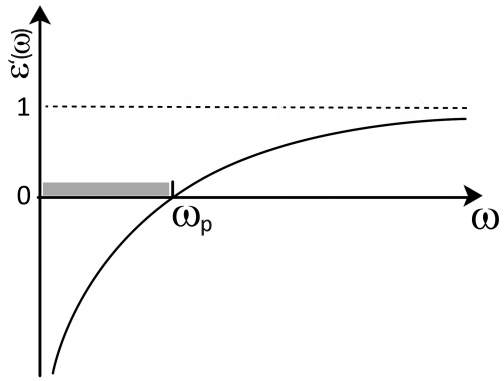

Figure 1.8: Free electron plasma frequency based on Drude model [34].

When the frequencies are below plasma frequency, the charges can move quickly to shield the interior of the medium from the electromagnetic radiation. When the frequency passes the ω_p, the medium acts like a regular dielectric medium [28] [38]. The dielectric relaxation of composites may affect the experimental result of plasma frequency and show lower values of ω_p than obtained fitting values [21].

Intraband transitions: Charge localize-delocalize mechanism

Based on the Drude model, the delocalized electrons in the conduction band is responsible for low plasma frequency; meanwhile, moving of this delocalized electrons are control by

phonon backscatter [36]. It is known that this type of moving originated from an electron-electron collision which is named as an intraband transition [21].

The low plasma frequency shows that mostly delocalized electron in conduction band participate in the mechanism [36]. In the case of the localization-delocalization boundary, the DC conductivity is weak dependence to the temperature, and the permittivity is very high [81].

1.2.2 Drude-Lorentz model - Electron oscillation (Lorentz correction)

In this model, instead of atoms and molecules, it estimated theoretically a set of harmonically bond electron which has the same frequency for oscillator resonant [28]. As for the following equation, the Lorenz force applied to the electron which is based on an elastic restoring force that bond electron to its equilibrium position in atom and molecule [28]. The dielectric permittivity can be presented by Drude-Lorentz relation [47] [36] [77] [8]:

$$\epsilon^* = 1 + \frac{\omega_p^2(\omega_0^2 - \omega^2)\tau^2}{\omega^2 + (\omega_0^2 - \omega^2)\tau^2} + i\frac{\omega_p^2\omega\tau}{\omega^2 + (\omega_0^2 - \omega^2)^2\tau^2} \tag{1.26}$$

$$\epsilon' = \epsilon_\infty + \frac{\omega_p^2(\omega_0^2 - \omega^2)}{\omega^2\tau^2 + (\omega_0^2 - \omega^2)^2} \tag{1.27}$$

In these equations ω_0 is the circular resonance frequency defining the elastic restoring force, and τ is the relaxation (decay) time [47]. For the electron dielectric function, we can consider the rigid lattice which includes ions with significant large ions [18].

The study of negative permittivity sign in low-frequency range is conducted by Lorentz correction which applied to conduction electron that is controlled by the local field [47]. The plasma frequency is the same in both transitions and depends on the number of delocalized electrons [108].

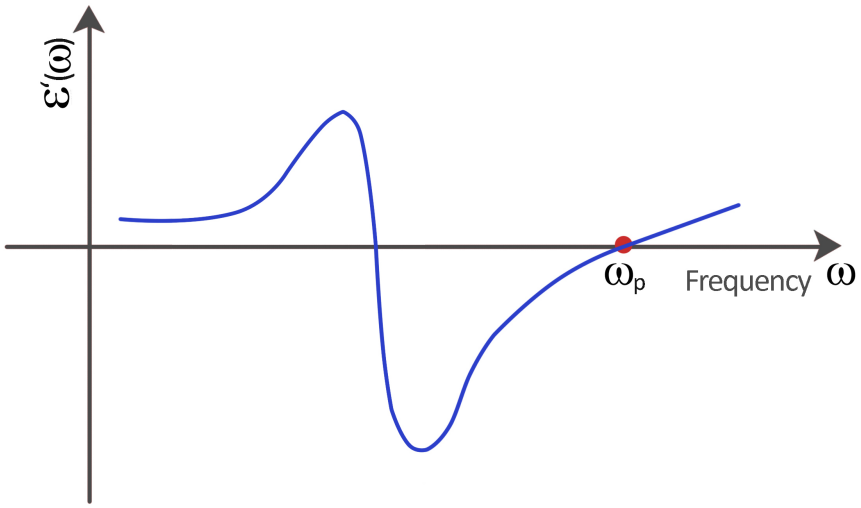

Figure 1.9: Lorentz oscillation of dielectric medium [72].

Interband transitions: bound electron

In some system, the permittivity switch is from positive to negative and very similar to metallic materials. In these materials the instead of intraband transition by Drude model, the transition occurs by electron transfer from bound level to conduction band which is an interband transition [72].

Furthermore the positive to a negative frequency in interband transition is attributed to the delocalized electrons. This phenomenon usually reported for the wavelength shorter than 550 nm which Drude model cannot work ultimately. In interband transition low layer bands, electrons are promoted by high energy photons [108].

It is believed that the interband transition of electrons originated from induced electric dipoles in insulated areas which make them cover plasmonic behavior because the majority of electrons are localized. Increasing in temperature, improve the scattering rate of electron-electron and electron-phonon interaction [21].

1.2.3 Resonance dispersion law: Relaxation and resonance behavior of fiber composites

The following discussion has corresponded to the system that contains a low concentration of conductive fillers in an insulative matrix. The following formula is to being used to describe the dielectric properties of such composites systems. This law can be applied when the filler concentration is not high because its capacitance and inductance have been negligible [41].

$$\epsilon(f) = \epsilon_m + \frac{A}{1 - i\frac{f}{f_{rel}} - (\frac{f}{f_{res}})^2} \tag{1.28}$$

ϵ_m is matrix permittivity and factor A depends on a load of filler. By using this equation, we can categorize the composites into three different states. The first one is applied when the conductivity is minimal which make relaxation dominate on dielectric behavior ($f_{rel} < f_{res}$). For the average case that has high conductive filler, both resonance and relaxation effected the dielectric spectrum ($f_{rel} \sim f_{res}$).

For very high conductive fillers, only resonance dispersion can be seen. The resonance

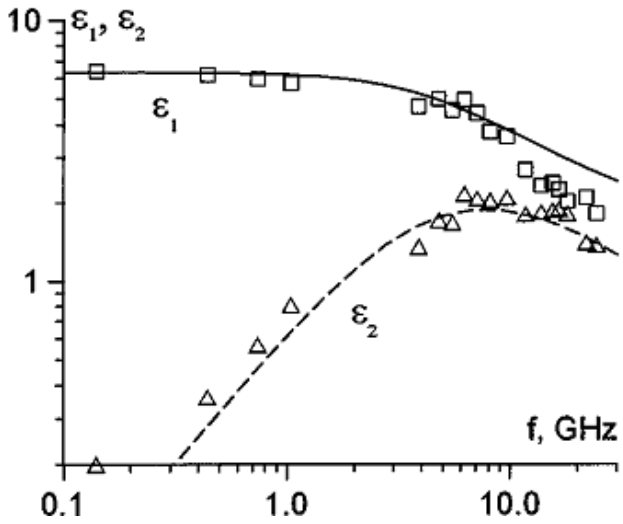

Figure 1.10: Relaxation like dielectric behavior of composites [41].

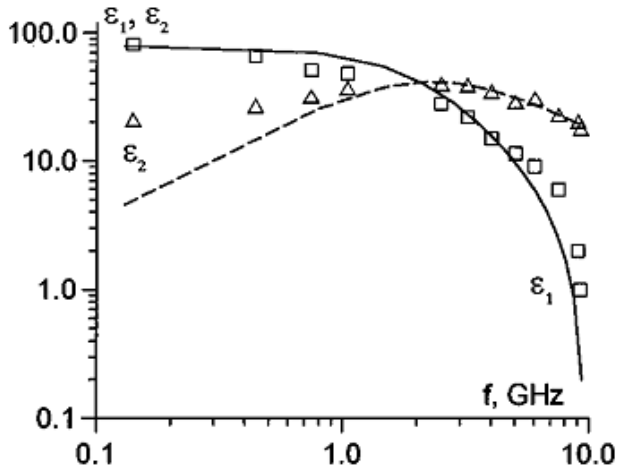

Figure 1.11: Mixed responds dielectric behavior of composites [41].

frequency of such composites can be determind by followed formula [41]:

$$f_{res} = f_0\sqrt{\epsilon_{eff}} \tag{1.29}$$

In above formula the f_{res} coresponded to the resonance frequency of filler and composites, respectfully and ϵ_0 is represent the dielectric of effective medium.

It should mention that all of this condition is only applied when the concentration of the

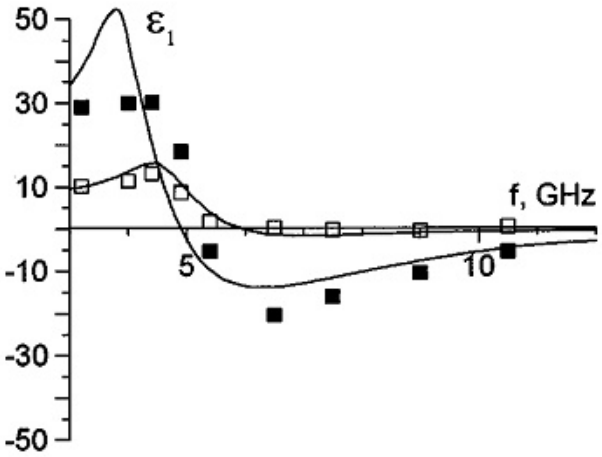

Figure 1.12: Resonance like dielectric behavior of composites [41].

filler is lower than percolation threshold and near to that the top equation cannot be used because of formation of conducting cluster [41].

1.3 Dielectric materials classifications

Based on the relationship between polarization and applied electric field, the dielectric materials can be categorized. These categories also can be divided to the smaller groups based on their mechanism [64].

1.3.1 Linear dielectric materials

On this kind of dielectric materials, the medium can be polarized linearly by applied electric field. By electrical removal field these dielectrics be depolarized which can be divided into 3 following groups:

Non-polar materials

In this materials, the electron cloud of valance electrons just can have elastic displacement by applying electrical field.

Polar materials

In polar dielectric materials, both electrons clouds and ions have elastic displacement. In this materials, the total polarization is included both electronic and ionic polarizations. However, this material does not possess permanent dipole moment.

Dipolar materials

When the materials posses orientation polarization beside electronic and ionic polarization included in this class. Those materials with permanent dipole moment are included in this group.

1.3.2 Nonlinear dielectric materials

This material possess spontaneous polarization without applying electrical field due to their crystal structure. 21 class amoung 32 crystal structure do not have a center of symmetry which essential for posses spontaneous polarization. The piezoelectric, pyroelectric and ferroelectric materials are in this category [7].

1.3.3 Ferroelectric materials

The ferroelectric materials are the type of piezoelectric materials that their remanent dipoles can change their direction by applying electrical field. The lining up the dipoles in ferroelectric materials by applying an electric field, and remaining at their direction even after removing electric field make hysteresis behavior in this materials. There is saturation polarization which all dipole are aligned with an electrical field and when electrical field completely removed its called remanent polarization. The coercive field is called to the reverse electrical field which makes the polarization to the net zero [5].
The ferroelectric materials are also type of pyroelectric materials which their properties depend on the temperature. This behavior is due to change in the symmetric centro of unit cell by increasing temperature to above Curie temperature.

1.4 NIMs, Negative index materials

Negative index materials are also known as left handed materials, exhibit both negative permittivity and negative permeability which are recognized as a new class of electromagnetic. Drude entirely explained metals with negative permittivity, but it was in 1967, which for the first time that Veselago proposes that the medium with a negative refractive index. However, there was significant uncertainty about this theory for a long time [33].

Followed up the Veselago proposition some experiments exhibits such behavior, but it was Pendry in 1996 that explained to get negative index properties artificially. These types of materials have a periodic structure artificially designed are known as metamaterials [55].

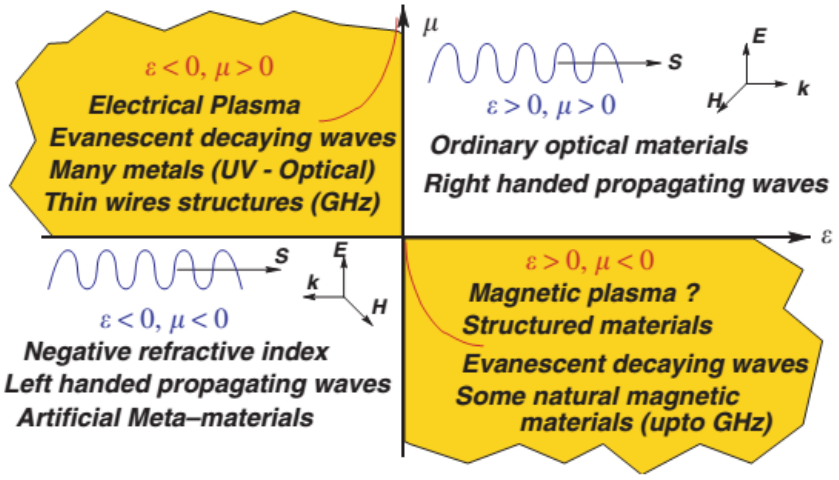

Figure 1.13: Materials classification based on their reflective index [61].

Moreover, It was in 2001 that Shelby experimentally approved this model [68].

The negative index materials can be used in application such as lightweight, compact RF

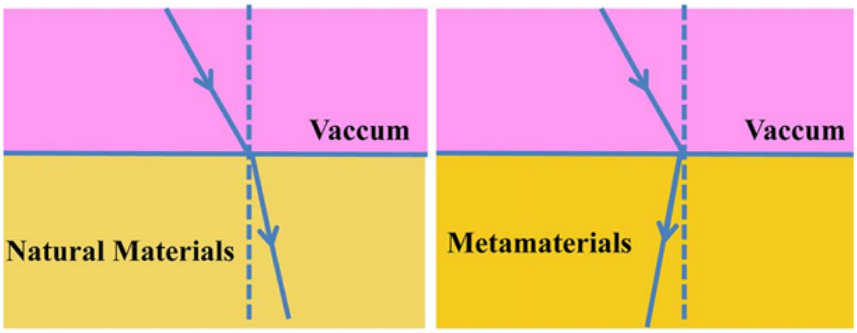

Figure 1.14: Metamaterial refraction comparison [61].

or microwave structures, as improved optics for imaging systems, wireless antenna suits, reduction of energy/power beam dispersion, and also as EM cloaking devices, in which the material is used to render a volume effectively invisible to incident radiation [26] or unique cavity resonator, and microwave attenuation [80].

Moreover, Application for single negative materials can also be used as a band-pass filter, small-size microstrip antenna [80].

1.5 Negative permittivity materials

It is known to get a negative refraction index; it is essential to have negative permittivity. There are no individual materials that show this property so to reach this purpose fabrication has been used [82]. The importance of negative dielectric materials is originated from the fact that if we can fabricate the materials with tunable frequency for negative permittivity, it will be much easier to achieve implementing negative permeability to it [26]. Epsilon-negative materials (ENG) are the term to be used for materials which have only negative permittivity and not negative permeability [95].

It is known that based on the Drude model, the negative permittivity can obtain in metals with free electrons. However, It was suggested that in some systems the negative permittivity might due to high plasmon resonance conductivity at a relatively low frequency [28]. In 1995, Wang [81] and Joo [36] reported negative permittivity in PAN (polyaniline) polymer. Moreover,It was reported the plasma oscillation of the delocalized electron may lead to the negative permittivity of some polymer composites with conductive fillers [38]. Negative permittivity behavior can also be found in doped semiconductor [49] and this materials can show plasmonic response [66].

Gavrilova tried to explain the negative permittivity, by the two primary mechanisms. First

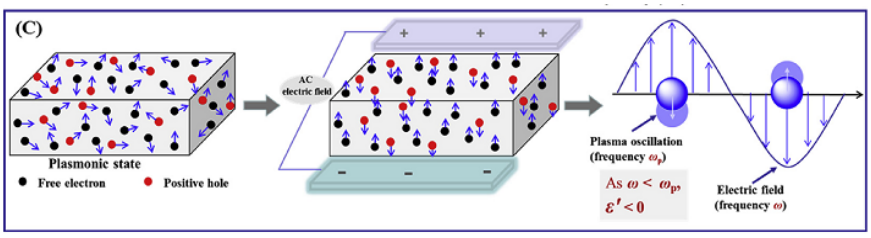

Figure 1.15: Behavior of epsilon negative materials under AC electrical field [38] .

is the effect of out-of-phase conductivity on permittivity which is usually known as induced conductivity. And in the second mechanism, there are some charge carriers which can cause dielectric polarization; these carriers can actively oppose the restoring force, this one also be known by metal-like conductivity [23].

In another words, the frequency that the samples show negative dielectric in which the structural elements have delay response to electric field lead to antiphase of displacement (orientation). The negative dielectric is possible when this out of phase displacement has a comparable contribution to other polarize mechanism [23]. At normal condition, the charges bond at their equilibrium position with restoring force. However, when the specific condition applied, the charges are left their positions and can move based on their mass under an electrical field. Under this condition, no restoring force applying to the charge carriers and their phase shift up to 180 respect to the electrical field causes negative dielectric [23]. So it can be concluded that any composites comprise an element that is no restoring force applying to them could display negative dielectric despite component mechanism. The outer magnetic field can alter the mobility of this charge [23].

Materials with negative permittivity are achievable by two main approaches [82]. The first one is artificially made a structure like wire and split ring resonators which have a periodic structure that alternate the response of high pass filters [33]. The other method known as random composites, which reports of these materials till now shows such a behavior under formation 3D hopping conductivity in their structure [95].

This type of materiasl are interested in the field of high dielectric materials, having high loss can be a disadvantage, but lossy materials also can be used in many applications like microwave absorbing, electromagnetic attenuation and shielding fields [72]. Materials like polymer composites with high loss have a potential application like cloaking, superlens, wave filters and superconductors [108].The epsilon-negative materials have vast potentials to be used in applications like a band-pass filter, ultra-thins waveguides and electromagnetic interference shielding field [11].

1.6 Artificial structure (Metallic mesostructures - Metamaterial)

Composites based on metal fillers and dielectric matrix are most used in an electromagnetic application [61]. There are reports of negative permittivity at low frequency in such

a composite. The terms, metamaterials are known for the materials that artificially made and has negative index properties. Furthermore, the epsilon-negative materials which has such a structure also known as electrical metamaterials. In this method, it was attempted to reduced plasma frequency based on Drude theory by intensified the effective electron mass. It makes the average concentration of electron decrease by assembling the periodic structure of very thin layer while causes the self-induction of them [55] [83].

Pendrys Model

Based on this model, the negative permittivity can be obtained by a 3D network of thin metallic wires which indeed depends on the radius of the wire.

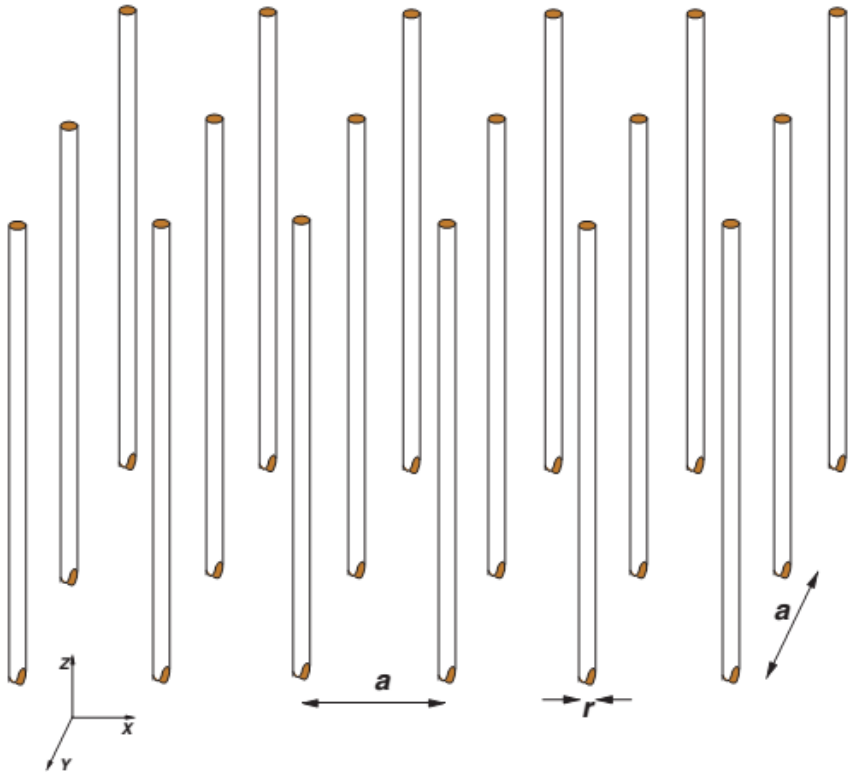

Figure 1.16: Arrays with radius of "r" made by metal wires and distance of lattice period of "a" [38] .

$$n_{eff} = n\frac{\pi r^2}{a^2} \tag{1.30}$$

$$m_{eff} = \frac{\mu_0 \pi r^2 e^2 n}{2\pi} Ln(a/r) \tag{1.31}$$

In this assemble the dominant effect will be the restoring force that applied to self-inductance and will not just limit to the mass of electrons. Moreover, to know an effective number of electrons, the electrons in the wire should be considered [55].

Besides these, we should also consider the stability of plasmon which is determined by electron-hole pairs creation and phonons in the wire. So, it cannot ignore the effect of conductivity in the wires which lead to the following formula for dielectric [55]:

$$\epsilon_{eff} = 1 - \frac{\omega_P^2}{\omega(\omega + i\epsilon_0 a^2 \omega_P^2 / \pi r^2 \sigma)} \tag{1.32}$$

There are many designs including on the structure of the materials to reach negative index by applying the Drude model. Some of these models are double-split-ring resonators, S-shaped resonators, multilevel dendritic structures, nano/small apertures, metallic nanoclusters [42]. It is also reported the use of BST ceramic in these structures which poses high permittivity [56]. It was believed the negative permittivity of PEI/CNF obtained by this method [42].

1.7 Macroscopic induction effect

A composite that has conductive rod-filler in a dielectric matrix can present the negative permittivity by the cause of the induction effect. The dielectric response can be changed from relaxation type to resonance type which the conductivity of fillers plays a vital role which more conductive fillers make more influence [26] [27] [38]. The mentioned system can be explained by considering the inner surface of fillers as a capacitor plate and the dielectric matrix as an inductor which leads to the following equation:

$$Z_C + Z_L = \frac{1}{i\omega C_1} + i\omega L \approx \frac{1}{i\omega C_1} + \frac{1}{i\omega C_2}, \omega \sim \omega_p \tag{1.33}$$

Thus, a capacitor (C_2) with a negative-dielectric filling appears to be an inductor, and

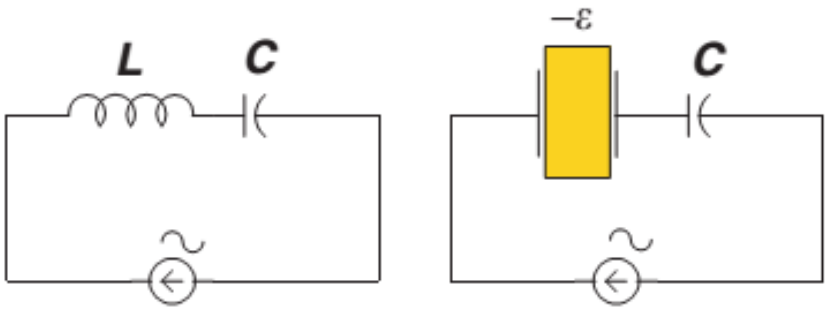

Figure 1.17: Capacitor-inductor system [61].

the circuit is resonant at a particular frequency [91]. The temperature plays an essential role as affecting the conductivity which conductivity higher than specified value make the dielectric relaxation change to the resonance spectrum. This system is very similar to a Colpitts oscillator circuit that set up of inductance and capacitance [26] [27] [82].

As it was said, in the systems that contain conductive fillers, when the content reach and pass percolation threshold the conductivity change to metal-like behavior which reactance corresponded the inductive characterization by showing positive (Z0) in the frequency range. This behavior is originated from the formation of a continuous conductive network with the electrons in fillers [84] [72].In this system the resonance frequency can be calculated as a [80]:

$$f = \frac{1}{2\pi(LC)^{0.5}} \tag{1.34}$$

1.8 Random composites

In the last decades, many researchers report negative permittivity without the use of artificial arrays which depend on intrinsic properties of random composites [87]. This group

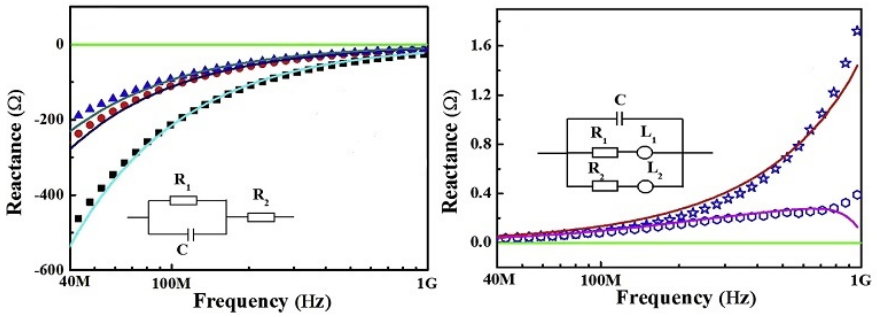

Figure 1.18: Conductive and inductive system [80].

is also known as intrinsic metamaterials whose performance is depended on the concentration of the conductive fillers and their shapes [38]. In most cases, these composites contain a large number of metals or conductive fillers in matrix of an insulator or some conductive polymers [26]. The delocalized charge proceeds negative permittivity in nano-composites which is comparable to the periodic structure has well scattered [96] [87].

In this type of system, that forming a continuous network of conductivity is essential for possessing negative permittivity. It is believed the metal-like conductivity is the origin of such behavior in these composites. To better study of these composites, they become categorized based on their matrix materials types.

1.8.1 Random composites with polymer matrix

Conductive polymer due to their properties are very common on these field of studies which PANI is most known polymer among them. PANI is one of the most interesting materials in the field of negative index materials which is reported to has negative permittivity behavior for a wide range of frequency. The reason behind this behavior is suggested of delocalize charges from inhomogeneous regions which can be increased by crystallization areas [36] [81]. There are many reports of PANI as a matrix with the use of other fillers in it which their behavior can be tunable by filler concentration and can get to negative permittivity in a different frequency range. These fillers can be conductive like a MWCNT/PANI [92] [93], or some oxide such as Fe_3O_4/PANI [95], BTO/PANI [107], Al_2O_3/Polyanilline Composite [96]

and CSA/PANI [20]. Its also can seen small percentage of PANI in PANI/DBSA [33] composites can get negative permittivity and higher concentration increase conductivity since the nanoparticles can form a pseudo-continues conductivity pathway [96]. Such behavior also can be seen by combination of mostly conductive fillers in other conductive polymer matrix like PPy/WO_3 [110] [28], MWCNT/PPy [38], PPy/YIG [9].

Making random composites are not just limited to the conductive polymers but nonconductive polymers can also possess such behavior when an adequate amount of conductive fillers added to the matrix. Some example of these composites are graphene/acrylic polyurethane [84], PP/CNT [108], Fe-Si-Ni/epoxy [32], MWCNT/polydimethylsiloxane [77], CNT/YIG [8] and bilayer polymer Graphine/PVDF [78] the negative dielectric emerge when the conductivity reaches to percolation threshold and after that the mechanism of conductivity will be changed.

In these random composites which contain insulator parts, at a low content of fillers, the composites show the hopping conductivity is dominated mechanism, and AC conductivity follows Jonscher power law ($\sim \omega^n$). However, when the amount of filler exceeds the percolation threshold, the conductivity behavior will be changed and became metal-like behavior [84]. In this mechanism, the conductivity decreases at high frequency which can be explained by skin effect [84]. It can understand that by forming a conductive path and produce polarization by making composites the generation of plasma oscillation in low frequency can occur.

In composites with non-plasma materials, the plasma frequency cannot be obtained by individual dipole but by natural collective oscillation frequency of many electrons [8]. Based on Lorentz oscillator mode, the resonance behavior can be described by Drude-Lorentz formula which corresponded for isolated conducting clusters associate by bonded electrons [21]. The fundamental of this Lorentz correction is coming from the polarization of electrons bound to impurity centers. It means that the effect of impurity conductivity in the Lorentz factor is much stronger than the total conductivity [47]. Increasing the conductivity will decrease

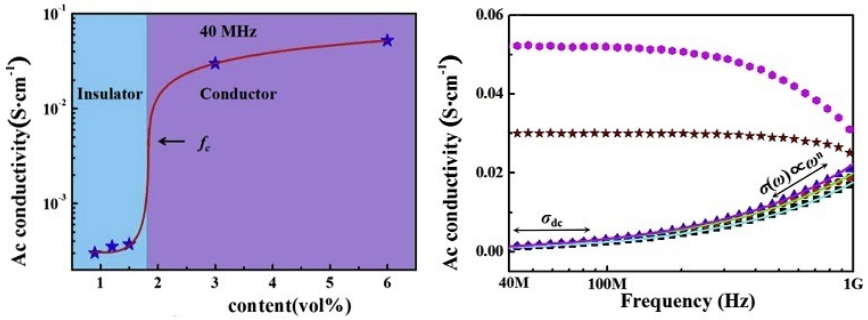

Figure 1.19: Effect of filler concentration on AC conductivity of composite [80].

the damping effect which makes the transition from Lorentz to Drude [8]. For metal-like conductivity the conductivity follows following formula [59].

$$\sigma_{ac} = \frac{\sigma_{dc}\omega_\tau^2}{\omega^2 + \omega_\tau^2} \tag{1.35}$$

$$\sigma_{dc} = \frac{Ne^2\tau}{m} = \frac{\omega_P^2\tau}{4\pi} \tag{1.36}$$

It was believed that the conduction loss play dominated roll on the dielectric loss of composites which make the imaginary part on inverse relation to the frequency in low frequency. However, by increasing the frequency of the relaxation loss generated by defect dipole and interfacial polarization rule the dielectric loss of materials [10] [59]. At high frequency, the polarized dipole dominated the dielectric loss which makes the relaxation at high frequency [77]. At high Frequency, the long-range migration of weakly bond electrons decreases, so dielectric loss also decreases in this range [95].

1.8.2 Ceramic materials

Making ceramic composites are one of the most common methods to reduce the plasma frequency obtained by the metals. In most of these composites, the structure contains an insulative matrix like the most oxide, and the fillers are metals like Fe-Fe_3O_4-Al_2O_3 [109], Ag/ZrNiO [24] [25], Ag/Al_2O_3 [72], Co/Al_2O_3 [80]. In all of this type of composites, the

Table 1.1: Random composites with conductive polymer matrix

Matrix	Filler	Frequency (Hz)	Mechanism	Reason	Factor	Year	Ref.
Conductive Polymer							
PANI	CSA	2 THz	Drude (Inductor)	Crystalline	Delocalized region	1995	[36] [81]
PANI	Fillers Review	Varies	Drude	Interchain interaction	Filler Conc.	2013	[28]
PANI	MWCNT 80% Pure	150 MHz 23 KHz	Drude (Inductor)	Inductor Field Induced	Filler Conc.	2016	[93]
PANI	MWCNT 5% Pure	5 kHz 23 KHz	Drude (Inductor)	Inductor Field Induced	Filler Conc.	2016	[92]
PANI	Fe_3O_4 Pure	4 kHz 30 kHz	Drude	Crystal Nanowire	Filler Conc.	2018	[95]
PANI	Al2O3 (μ m) Pure	5 kHz 23 KHz	Drude (Inductor)	Inductor Field Induced	Filler Conc./Type	2016	[95]
PANI	Al2O3 (nm) Pure	30 KHz 23 KHz	Drude (Inductor)	Inductor Field Induced	Filler Conc.	2016	[94]
PANI	BTO 20% <20%	110 No Positive	Drude (Inductor)	PANI metallic state	Filler Conc.	2012	[107]
DBSA/ PAA	PANI (>6%)	No Positive	Drude	Metal-like Conductivity	Filler Conc.	2012	[33]
PPy	YIG F.M. Pure	8 GHz 101 GHz	Drude (Inductor)	Metal like Inductor	Filler Conc.	2019	[9]
PPy	MWCNT 80% Pure	200 MHz No Positive	Drude (Inductor)	Metal like	Filler Conc.	2016	[38]
PPy	WO3(2%) Pure	100 Hz 5.3 kHz	Drude	Metal like	Filler Conc.	2010	[110]
PI	MWCNT BTO	50 kHz	Drude (Lorentz)	Delocalized electron	DC bias Polarizat.	2018	[100]
PEI/PI	CNF	10 kHz	Drude 100 range	Nano structure	Filler Conc. size	2009	[42]

Table 1.2: Random composites with insulative polymer matrix

Matrix	Filler	Frequency (Hz)	Mechanism	Reason	Factor	Year	Ref.
Insulator Polymer							
Silicone resin	CoFeSiB CNT/GO coated	10 GHz	Drude/Inter Lorentz/Intra	Metal like Metallic Wire	Filler type Filler Size	2019	[21]
PDMS	MWCNT	1 GHz	Lorentz	Metal like conductivity	Filler Conc.	2017	[77]
APU	Graphene	1G	Drude (Inductor)	Inductor Field Induced	Filler Conc.	2017	[84]
Phenolic	MWCNT	1G	Drude (Inductor)	Inductor Field Induced	Filler Conc.	2016	[58]
Phenolic	graphine	1G	Drude (Inductor)	Inductor Field Induced	Filler Conc.	2017	[85]
Epoxy	Fe-Si-Ni	1.61 GHz	Drude (Inductor)	Interface Polarization	Filler Conc.	2016	[32]
Epoxy	FeSiB SiO_2 Coat	80 MHz f_p 1 GHz	Drude	Metal like Inductor	Filler Con. Coating	2017	[87]
PVDF	Graphite	100 MHz	Drude	Metal like	Filler Con. Layer	2017	[78]
PP	CNT	200	Drude/Inter Lorentz/Intra	Metal like Metallic Wire	Filler Con. Temp	2015	[108]

plasma frequency of composites shows much lower values compare to its filler plasma frequency which can be predicted based on dispersion law.

Recently, carbon nanotubes are mostly used due to their excellent conductive properties, and this behavior makes them as a candidate to be used in ceramic composites to get negative permittivity. In this regards, an example of ceramic composites which poses negative permittivity are C/Si_3N_4 composites [10], CCTO/CNT [59]. In this composites, the structure is porous and carbon thin layer cover grains which easily can form the conductive network for electron transfer. Changing conductivity behavior from an insulator to conductor form

plasma oscillations in this composite [11].

Moreover, there are many reports of systems contains multiferroic composites with properties of showing negative permittivity. Wang reported the negative permittivity by Lorentz model in the system of BTO/$Y_3Fe_5O_12$ multiferroic composites at high frequencies [82]. In the system that contains BTO, the dielectric resonance might originate from the potential movement of Ti ion to equilibrium position which generates resonance of charge. The relocation of Ti^{4+} from the center of the unit cell in octahedral sites makes appear of negative permittivity at high-frequency [82]. Bartkowska reported negative permittivity only at a temperature higher than 600 ^oC in Mn-doped multiferroic ceramics which cannot reach in undoped ceramics or at room temperature of doped ones [6].

The most important parameter among the negative epsilon materials is the transition frequency or technically speaking, the plasma frequency. So for these materials, their advantages and disadvantages can be classified based on this parameter. Moreover, based on the application these materials will be used the highest negative permittivity and the highest positive permittivity after transition frequency. The other parameters like the damping frequency and plasmon material concentration can be critical base on the application uses. In following pictures some of these parameters are plotted against plasma frequency for a different type of negative epsilon materials.

1.8.3 Effect of different parameter on tune the plasma frequency of random composites

Temperature dependence Conductivity

The electronic conductivity can describe as a basic conductivity by the tunneling between the localized state, and the ionic one is barrier crossing process [19]. The parameter that can affect the permittivity behavior and negative spectrum are interfacial conditions, defects, temperature and roughness which control the mechanism by influenced scattering

Table 1.3: Random composites with ceramic matrix

Matrix	Filler	Frequency (Hz)	Mechanism	Reason	Factor	Year	Ref.
Ceramics							
Al_2O_3	Iron Pure Fe	208 GHz 3660 THz	Drude	Metal like Inductor	Efec. Mass Elec. Dens.	2012	[70]
Al_2O_3	Nickle Pure Ni	26 GHz 1600 THz	Drude	Metal like Inductor	Efec. Mass Elec. Dens.	2012	[71]
ZrNiO	Ag	10 GHz	Drude (Inductor)	Inductor	Metal Wire	2016 2017	[24] [25]
CCTO	CNTs/CB	9.2 GHz	Drude (Inductor)	Metal like Inductor	Filler Conc.	2018	[59]
YIG	CNT	9.5 GHz	Lorentz	Metal like Inductor	Filler Conc.	2018	[8]
Si_3N_4	Carbon Low conc.	9.4 GHz 12.5%	Drude (Inductor)	Metal like Inductor	Filler Conc.	2017	[10]
Si_3N_4	Carbon High conc.	4.4 GHz 13%	Drude (Inductor)	Metal like Inductor	Filler Conc.	2016	[11]
BTO	$Y_3Fe_5O_{12}$	1 GHz	Lorentz Ti-O	Metal like Inductor	Filler Conc.	2017	[82]
Fe_3O_4	Al_2O_3	400 MHz	Drude (Inductor)	Metal-like Conductivity	Filler Conc.	2013	[109]
Al_2O_3	Ag	>100 MHz	Lorentz Interband	Metal like Inductor	Filler Con. Elec. Dens.	2015	[72]
Al_2O_3	Cobalt	40 MHz	Drude (Inductor)	Metal like Inductor	Filler Conc.	2014	[80]
BiFeMnxTiO	Manganese Ions (0.9)	1 MHz	———	Polarization Direction	Temp (600) Mn	2018	[6]

rates. One more parameter that can affect the plasma frequency by increasing temperature is the reduction of effective mass with that [21].

At low temperature, the conductivity weakly depends on temperature and depends on the frequency which is used for impurity conduction. At high temperature, the conductivity mostly depends on DC conductivity and become almost frequency independent [47]. The decrease in conductivity and increase on activation energy of high-temperature conductivity which leads to shifting the boundary to higher temperature [47].

Variable range hopping is model to understand better the electron transportation and its

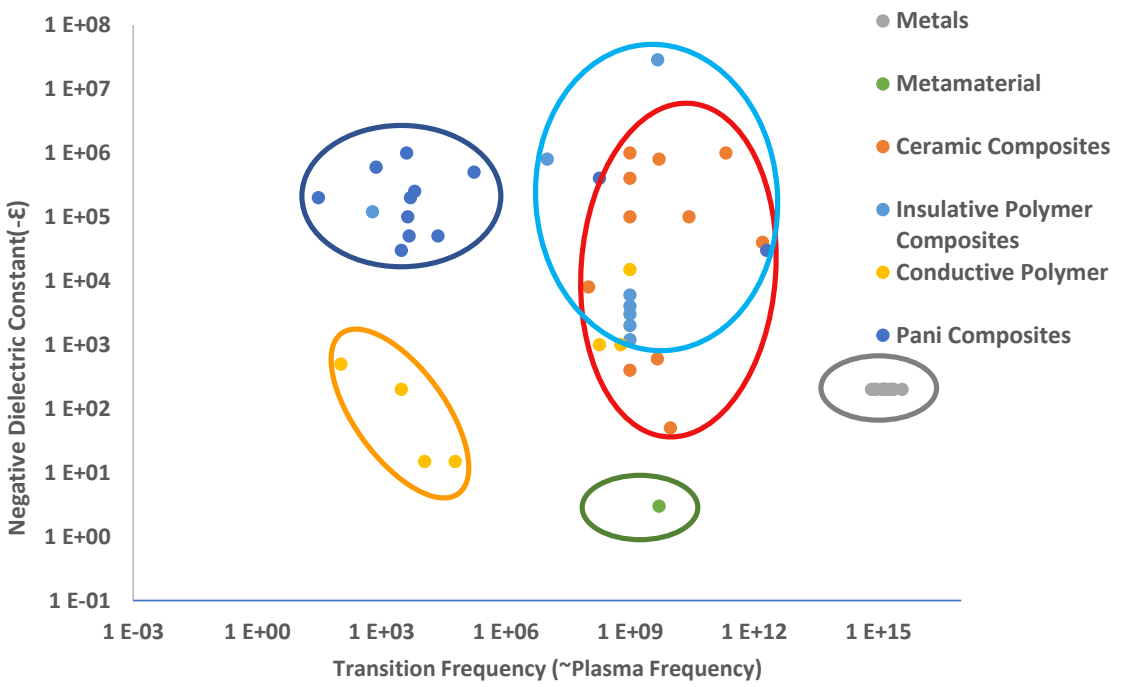

Figure 1.20: Highest negative permittivity vs transition frequency of different epsilon negative materials

dependence on temperature. The following equation is used to determined the electron conductivity dimension and parameter to find out localization of charge carriers [110].

$$\sigma = \sigma_0 exp[-(\frac{T_0}{T})^{1/n}] \tag{1.37}$$

In this equation, T_0 indicate localization of the charge carriers [108]. The hopping process can be activated by DC conductivity due to the migration of the carrier through the whole sample, and AC conductivity is a result of polarization in a short area. This behavior makes the AC conductivity weaker dependence on temperature than DC conductivity which is strongly changed by increasing temperature [76].

Usually at low temperature, the DC conductivity rise by increasing temperature, meanwhile at high temperature, the difference becomes smaller, and activation energy becomes bigger. This behavior can be originated from two possible process: One, at high temperature the charge carrier may be scattered by phonons due to lattice vibration. Moreover, the second

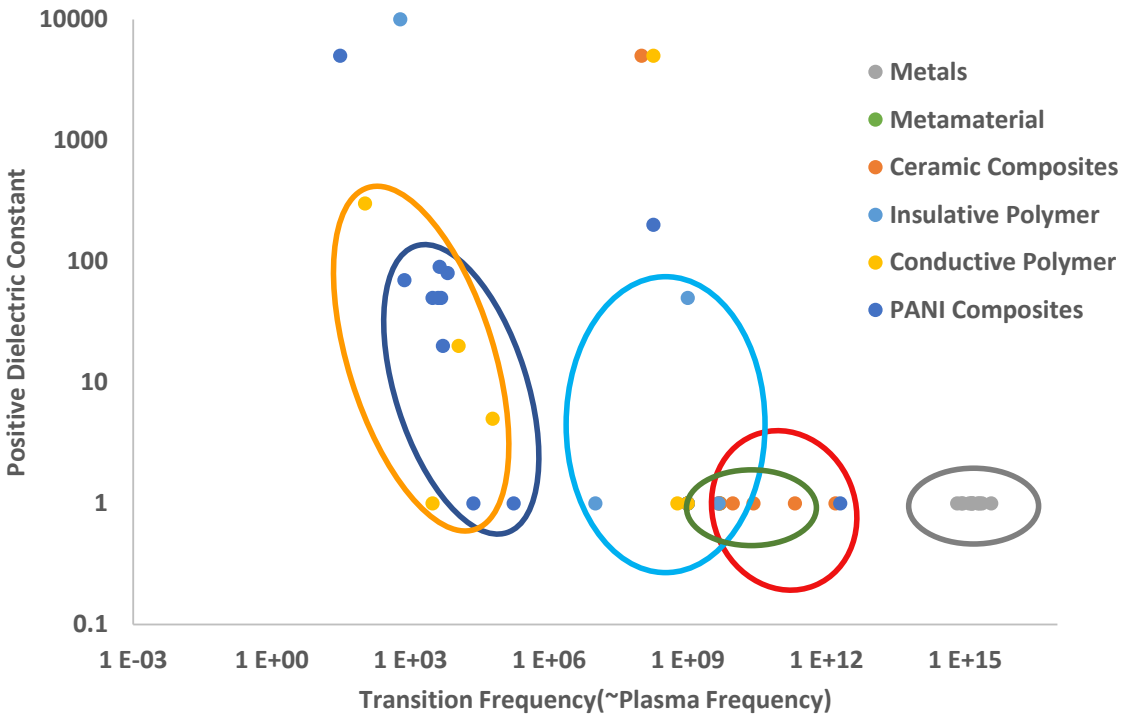

Figure 1.21: Highest positive permittivity vs transition frequency of different epsilon negative materials

reason may come up from the crystallographic phase transition. The originated this conductivity comes from the hopping of charge from one site to another one which due to the trap of charges in defects. This mechanism which leads to polarization is thermally activated [90].

Conductive path of fillers

One method to control and tune the negative permittivity in polymeric composites is to control the conductivity of fillers. In such a percolative system by coating, some of the fillers with insulative materials like SiO_2 can control fillers conductivity which can tune permittivity value and also plasma frequency [87]. In a system with coated and uncoated FeSiB in epoxy polymers, dual percolative behavior can be seen. By paying attention to the insulative SiO_2 layer, it can recognize that the conductivity path is cut off which make the properties based on the carrier concentration. By localized the free electron inside the insulative layer, the active charge carriers reduced. This behavior makes the plasmon

frequency reduced and the negative value decreases [87].

The other way to change the conductive path of composites is how it was fabricated. It was reported that in PANI/BTO composites that the sign of permittivity can be altered by the synthesized method. The negative permittivity can only be found in composites polymerized in a chemical process, while the composite fabricated by physical mixture, only presented the positive sign which is believed due to ferroelectric nature of BTO can provide storage of charges [107].

Microscopic effect- ionic plasma frequency

As we know, the Drude model theoretical works for metals with conductive bulk, lead to negative dielectric permittivity below the plasma frequency. However, if the system contains ions instead of an electron, the plasma frequency becomes lower due to more massive charge carriers. By consideration of ion oscillation for the dielectric function, we can reach to ion plasma frequency as the following equation [18]:

$$\omega_p = (\frac{4\pi N Z^2 e^2}{M})^{0.5} \tag{1.38}$$

In the nonpolar dielectric, the relative contribution of ions is small due to limited electron effect on the dielectric. However, in the polar dielectric, the contribution from optic mode is negative like the metals, which lead to surpass the electron contributions and total dielectric becomes negative. Such behavior is very likely to the semiconductors with narrow forbidden bands [18].

The difference on charge carriers is related to mass, and furthermore, there is more interaction between these ions and electrons compare to system contain just by electrons which make more reduction in oscillation frequency due to lower the density of charge carriers. In mentioned formula $m_e = -9.11 * 10^{-31}$ kg is the effective mass of electron and m_i, is the effective mass of the ion [26] [27].

$$\omega_p^* = \omega_p(\frac{m_e}{m_i})^{0.5} \tag{1.39}$$

$$\sigma_{ion} = \frac{N_{ion}e^2D_0}{k_BT}exp[-(\frac{Q}{k_BT})] \tag{1.40}$$

The results indicate that the conductivity plays a primary role to get negative permittivity which is caused by the higher mobility of ions. The results of this study show the effect of temperature and also the concentration of filler on conductivity which leads to change on the sign of permittivity. One of the influences of the highly conductivite fillers is that their induction affects the resonance frequency of material[26] [27].

Furthermore, we can find the US patent about phosphoric acid in PBI matrix shows negative dielectric with elevated temperature. This behavior is the result of resonance of high mobility ions in high temperature and high frequency [27]. The conductivity PBI doped with phosphoric acid is dominated by proton conductivity which $H_2PO_4^-$ anions in the membrane has both proton acceptor and donor site which play the leading role for conductivity. The high permittivity in the low-frequency range is originated from interfacial polarization resulted from a large number of ions. The emerging of this polarization at low frequency is due to its large dipole relaxation time. In this case, the induced dipole moment increases because of field distortion of polarization. The result shows that higher ions mobility can be reached at a higher temperature; so the constant dielectric increases in a result of polarization at low frequency [26].

Effect of Electrical Field on sample

In the inhomogeneous system, the Maxwell-Wagner has dominated mechanism for interface polarization. It can be said that in such a system, the conductivity can be changed by applying voltage because the charge carrier is accumulated at the boundary of less conducting regions which is initially are interfacial polarization. The polarization can also affect

the conductivity dependence on frequency. In this mechanism, the doping concentration, interface state density, and insulator layer thickness play an important role. We can also add the influence of oxygen ions to a space charge effect at low frequency [97]. The space charge concentration can be increased at low frequency in systems contains oxygen ions [97]. The interface will dominate the behavior of conductivity and permittivity, which in the case of Maxwell Wagner there will be a big difference between the conductivity of two regions. In the result, the current cannot flow through this region which leads to charge accumulation at the interface. The amount of charge accumulation is directly proportioned to the difference between the conductivity of the two regions. When the Ac electrical field applied, the electrons can pass through the interface by hopping which can cause an increase in conductivity and decrease in permittivity by frequency.

The reason for this behavior is due to reduce in charge accumulation at the interface and increase in the number of electrons pass through the interface [86]. Based on this model any system contains phases with different conductivity are frequency dependence. That means by increasing the frequency the motion of localizing charge which is responsible at high frequency is possible [19]. This system is consist of the capacitor-resistor network which has debye like relaxation in medium frequency, and the universal dielectric response is applied to it lead to high permittivity at low frequency. This system that usually consists of nano-defect the induced electrical field is very high [15].

On material with the crystal structure, the space charge can be accumulated in grain boundary which is the origin of polarization and conductivity part of the dielectric loss in such material. In such a system the electrons and oxygen vacancies can make the path for conductivity and electrons in oxygen vacancies can be ionized by the thermal or optical process. By applying DC voltage, the ionized oxygen vacancies can be separated from positive space charge near to it which lead to decrease the ionized energy and increase in the number of free electrons [62]. In the sample with this behavior, it was reported that the conductivity

could be originated from oxygen vacancies and the calculated activation energy shows a similar range for this mechanism. Furthermore, the electron capturing process occurs while its exposure to the air. The active area created by oxygen will cause a reduction in conductivity [47].

In the composites systems, both an induced electrical field and electrical polarization field has been exposed in the alternating electrical field so to get the negative dielectric the sum of this two should be higher than the original electrical field. This inequality just valid at low frequency because the resistivity of filler is a small and induced field is high, but by increasing the frequency the induced electrical field becomes small and will disappear which make positive permittivity. In low-frequency range, the dipoles and alternating currents can pass through the barrier caused by the resistivity of the matrix which at high frequency this condition is not fulfilled [93].

Yao. [94] reported Nano-Al_2O_3/PANI composites with large negative permittivity ($-2.24 * 10^{-6}$) which achieved by adding $5\% Al_2O_3$. Low-frequency Loss can be affected more since the migration of weakly bond electron reduced by increasing frequency. By applying an electrical field, the fillers lead to positive due to polarization which makes inner negative charges accumulated opposite site. This effect followed up by increasing internal current which produces an internal electrical field. The negative permittivity occurs when the sum of the induced electrical field and polarization become more significant than the applied electrical field. In such systems, two effect of Maxwell-Wagner-Sillars and micro-capacitors are responsible for increasing of permittivity due to interfacial polarization [84] [94].

Regarding the top system [15]: 1) No magnetic field greater than 10^-6 can be found which rule out inductive properties. 2) the conductivity spectrum shows simple hopping conductivity which rules out the possible formation percolative path and metal-like conductivity. 3) particle size affect the result. 4) higher temperature shift to higher frequency. 5) collective excitation of large effective mass in interface induced by an electrical field.

The above system contains Magnetic iron oxide Nanofluid in oil, which presents negative

permittivity by applying electrical field at very low frequency. The reason behind is the conductive path formation with aggregation nanoparticles and also dipole-dipole polarization. At low temperature, the frequency is stable when permittivity gets to negative and increasing voltage do not make much difference. However, higher temperature moves plasma frequency to the higher range but applying higher voltage fluctuate the plasma frequency. The higher temperature is suitable for free charge mobility and decreasing viscosity. It should be mentioned that the system shows no negative permittivity without DC bias even high temperature and low frequency [60].

There are many reports in the literature regarding large negative permittivity in the microwave frequency range. Among these reports, we can mention negative dielectric permittivity reported by and also nanoparticles of BRTCO in silicon oil reported by the Chu which is alternate by DC bias and temperature [15].

1.9 The nonlinearity of I-V curve

To analysis, the electrical response of devices ohms laws can be used as a simple method to explain the behavior of materials. Based on this law, the plot between current and voltage has a straight line which mathematically called linear. It means the resistance of materials is constant by applying all range of voltages.

$$R = \left(\frac{V}{I}\right) \tag{1.41}$$

However, ohmic laws are not applying for all materials, and their $I - V$ plot is not nonlinear. In this materials, the conductivity change by applying voltage. This materials also can call the nonohmic which make many manufacturers use this advantages.

The varistor is one of the famous circuits which is designed to express nonlinear conductivity by applying voltage. As it comes from its name, Varistor (variable resistor), the resistivity is very small for a wide range of electric field, but in certain point which called the breakdown

the conductivity raises dramatically and current reach to a certain value. Not similar to the insulators breakdown, this is not a failure for the device, and it can perform again for this range of voltage [16].

The first varistors were made in the 1930s by using SiC, and in 1970s ZnO based materials become most famous in varistor industry. The $figure1$ present the current density change for the overall applied field of ZnO based varistor. The varistors technology needs growth with Zener diode due to their need to protect from voltage breakdown [48, 53].

To show the behavior of materials in the nonlinear region, the power law can be used

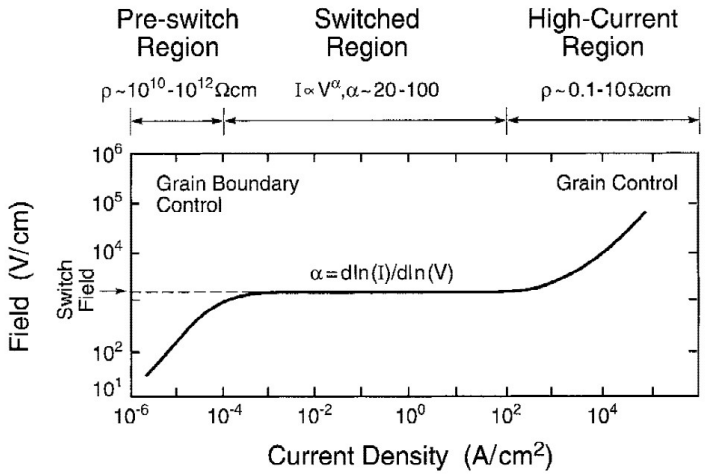

Figure 1.22: The nonlinearity of ZnO in different electrical field [16].

between current and voltage. The nonlinear coefficient, α, that presents heterogeneous electrical property of the material, can be calculated from [46]:

$$\alpha = \frac{log(\frac{I_1}{I_{0.1}})}{log(\frac{V_1}{V_{0.1}})} \tag{1.42}$$

In this equation, V_1 and $V_{0.1}$ correspond to the voltage at I=1 mA and I=0.1 mA. Although the nonlinear coefficient is calculated from the $I-V$ test, it has a direct relationship to the breakdown field of the composites which cannot precisely indicate the materials properties.

To understand the varistor concept, it should be looking to the materials microstructures. The origin of the current-voltage behavior of this materials comes from the potential barrier exist in grain boundaries. In this model resistive grain boundaries surrounded by semiconductive grains, which make the Fermi energy of this two-state become different. The flow of electrons to get equilibrium are hindered by defects and impurities; This negative electrons act like a sheet on grainboundaries which has a positive side for each grain. Although the nonlinear coefficient is calculated from the I-V test, it has a direct relation with the breakdown field of the composites which cannot precisely indicate the materials properties. To understand the effect of temperature and electrical field on the material the double Schottky barrier model can be used. The information about the material's electrical properties and microstructure effects can be obtained by fitting the I-V result with the Richardson empirical equation [22]:

$$J = AT^2 exp\left(-\frac{\Phi_B - \beta E^{1/2}}{kT}\right) \tag{1.43}$$

where J is the current density, E is the applied electrical field, T is the temperature, k is the Boltzmann constant, A is the Richardson constant for materials ($1200 mA mm^{-2} k^{-2}$), and Φ_B and β are materials properties which are corresponding to the potential barrier height and width, respectively [50].

1.10 Energy storage density

The energy storage density can be defined as it is, which the amount of stored energy in specific space in a unit volume [29]. The dynamic method which the energy density can be calculated by using above equation and physics fundamental that instead of charge density, the electric displacement can be used for dielectrics:

$$J = \frac{W}{Ad} = \frac{\int_0^Q V dq}{Ad} = \int_0^{E_{max}} D dE \tag{1.44}$$

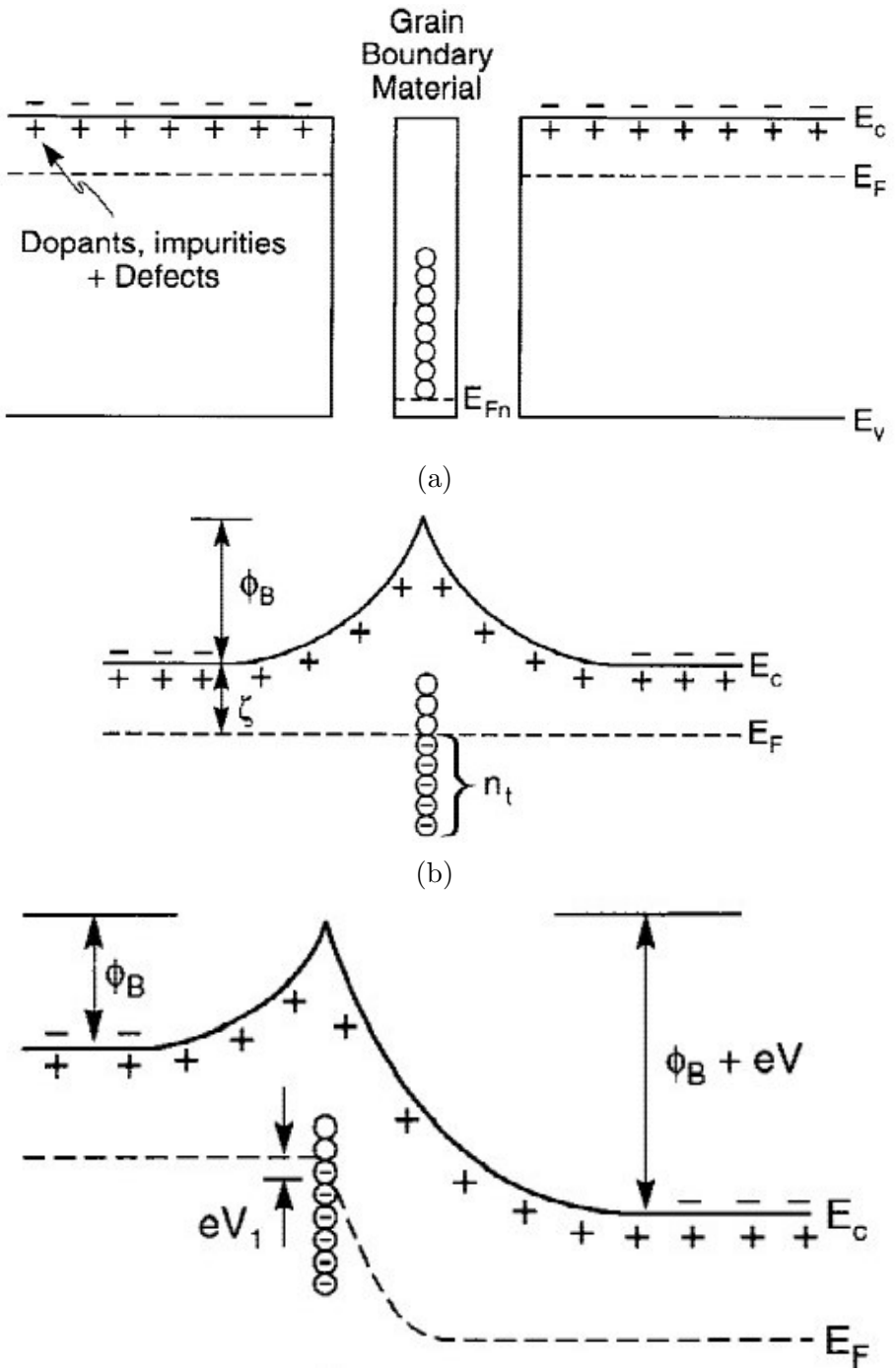

Figure 1.23: Effect of grain boundary on nonlinearity of materials. (a) Charge Build-up around grainboundaries. (b) Fermi energy near grainboundaries. (c) Overcome Fermi energy by applying electrical field [16].

In above formula, V/d has been considered to be an external electrical field. Also for media, with a high permittivity, it can consider the polarization as the same amount of displacement [106]:

$$J = \int_0^{E_{max}} PdE . J = \int_0^{E_{max}} \varepsilon_0 \varepsilon_r E dE \tag{1.45}$$

The above equation can simplify when the materials are linear dielectric which the permittivity does not depend on the applied external field:

$$J = \int_0^{E_{max}} PdE = \frac{1}{2} \varepsilon_0 \varepsilon_r E^2 \tag{1.46}$$

This formula shows that the energy density is proportional to the permittivity and also the square of the external electrical field. In the P-E loop figure (Polarization-Electrical field) the area between the graph and polarization axe in the first quarter is showing the energy density. It can be obviously seen by below figures that for nonlinear dielectric the above equation does not completely represent the stored energy due to energy loss inside the graph.

1.11 Materials for electric applications

Base on the P-E loop figures, there is four type of materials that can be used as energy storage. This four type consists of first linear dielectric like glass, ferroelectric that has spontaneous polarization like BTO, relaxor ferroelectric with nanosize domains and antiferroelectric with net zero polarization. As energy density analysis shows suitable materials for energy storage applications should have both high polarization and high breakdown field, meanwhile kept the energy loss low. Each of this group individually has faced some limitation like small polarization for linear dielectric or moderate breakdown field for relaxor ferroelectric and antiferroelectric. Meanwhile, the high energy loss of ferroelectric make some

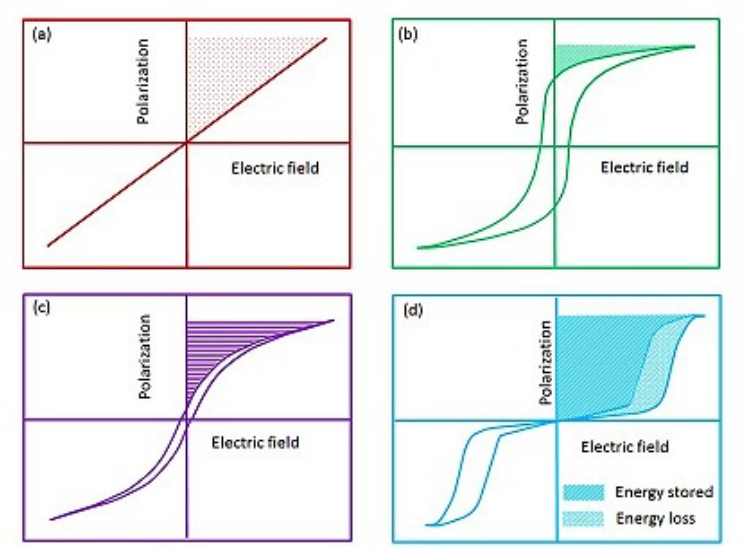

Figure 1.24: Figure represents the typical polarization versus electric field (P-E) hysteresis loops and energy storage characteristics of the four classes of solid dielectric materials namely (a) linear; (b) ferroelectric; (c) relaxor ferroelectric; (d) anti-ferroelectric (demonstration only; not to scale) [7].

researcher develop a new manufacturing process to make materials fulfill the energy storage needs. Making composites of two or more materials for developing glass-ceramic and polymer-based ferroelectric are promising technics to reach to materials with high permittivity and high breakdown field [29].

1.11.1 $CCTO$ ($CaCu_3Ti_4O_{12}$)

In the case of dielectric materials, new materials with extraordinary dielectric properties were reported by Subramanian in 2000. $CCTO$ with perovskite structure shows permittivity more than 10^5 depend on the preparation process. This material does not show any ferroelectric behavior, and its dielectric response is almost independent of temperature for wide range of 100 K to 600 K. In the form of single crystal, $CCTO$ even shows higher permittivity, but the large dielectric loss is presented in all cases [65].

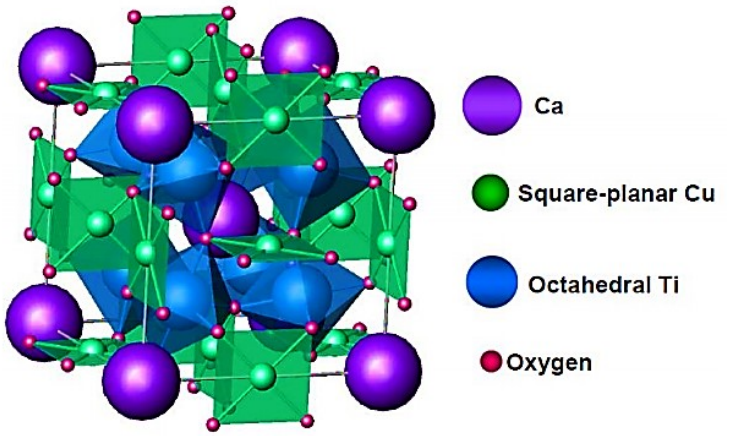

Figure 1.25: *CCTO* Crystal (pervoskite) structure [65].

CCTO structure and properties origin

The $ACu_3Ti_4O_{12}$ family is famous due to poses permittivity higher than 1000, but among them, *CCTO* shows unique dielectric behavior. Its cubic structure is originated from $CaTiO_3$ perovskite structure, but Cu^{2+} square planar was made by tilting the TiO_6 octahedra site [65].

(A) $O_o^{2-} + 2Ti^{4+} \rightarrow V_0^{"} + 2Ti^{3+} + 1/2O_2 : Ca(Cu_3)Ti_{4-u}^{4+}Ti_u^{3+}O_{12-u/2}$

(B) $3Cu^{2+} \rightarrow 2Cu^{1+} + Ti_{Cu}^{4+} + Cu \uparrow : Ca(Cu_{3-3V}^{2+}Cu_{2V}^{+}Ti_v^{4+})Ti_4O_{12}$

(C) $Cu^{+} + Ti^{4+} \rightarrow Cu^{2+} + Ti^{3+} : Ca(Cu_{3-V}^{2+}Ti_v^{4+})Ti_{4-2v}^{4+}Ti_{2v}^{3+}O_{12}$

(D) $3Cu^{2+} \rightarrow V_{Cu}^{"} + 2Cu^{2+} + Cu \uparrow : Ca(Cu_{3-3y}^{2+}Cu_{2y}^{+}V_y^{"})Ti_4O_{12}$

(E) $O_o^{2-} + Ti^{4+} \rightarrow V_0^{"} + Cu_{Ti}^{2+} + 1/2O_2 \uparrow : Ca(Cu_3^{2+})Ti_{4-w}^{4+}Cu_w^{2+}O_{12-w}$

To explain the extraordinary dielectric behavior of *CCTO*, many researchers conduct a various test like impedance spectroscopy, x-ray diffraction, *SEM*, and *TEM*. The experimental results indicate that just intrinsic properties cannot explain its dielectric properties. One of the most acceptable model to explain the dielectric respond of *CCTO* is internal barrier layer capacitors (*IBLC*) which first was reported by Subramanian. In this model,

consider the parallel capacitor form in the microstructure of $CCTO$ which rise the high permittivity. In $CCTO$ sample with polycrystalline structure, grains play as a semiconductor and grainboundaries are insulators that form the circuit of capacitors. Base on this model smaller grain size improves the dielectric behavior of sample. For single crystal $CCTO$, researchers tried to illustrate the behavior of sample by point out the twin boundaries in the single grain structure. This structure rises from dislocation, and planar defects have been introducing due to lattice disorder and displacement. To explain the grain and grainboundaries specific properties, sintering effect was investigated. The process like limited reoxidation or grains oxygen loss in high temperature is used to understand the semiconducting properties of grains and also insulative behavior of grainboundaries [5].

Some researcher also suggested that the interface between the sample and the electrode

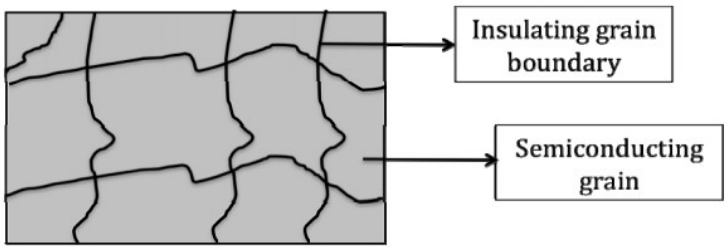

Figure 1.26: General schematic of the $IBLC$ theory associated with $CCTO$ giant dielectric constant [5].

rise the Maxwell-Wagner relaxation which may raise the permittivity in the interfacial layer. Besides all of these explanations, recently the new model of nano barrier layer capacitors has been rise up to try an explanation of $CCTO$ behavior. This model which work parallel to the IBLC model proposes that the gigantic permittivity cannot only rise from barrier layer between semiconductor grains. In this model, inside the grains there many nanosize capacitors which are formed during the heating process in shape of dislocations and other disorders. This structure makes many small capacitors inside the grains and results in huge permittivity depends on the distance between them [73, 75].

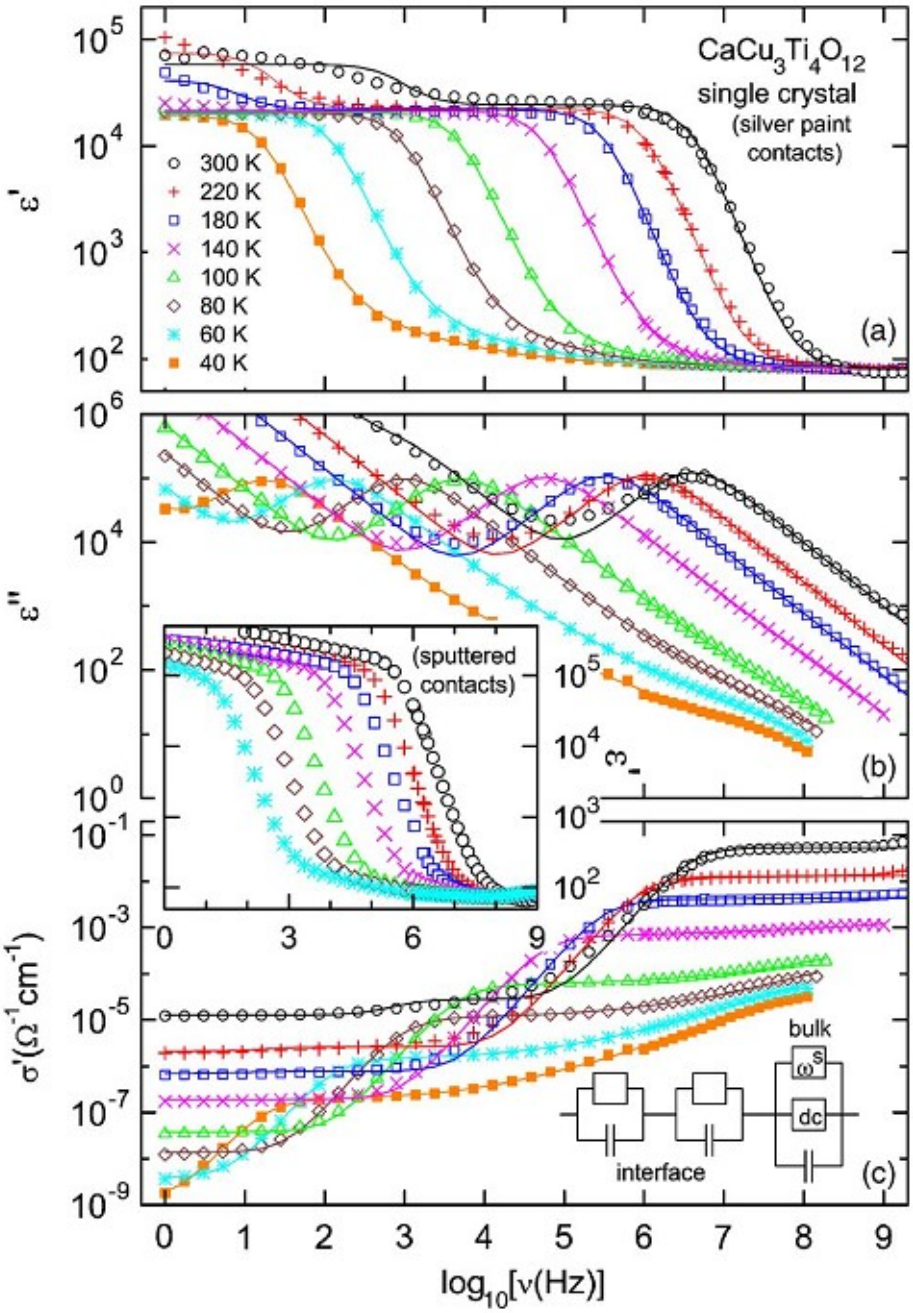

Figure 1.27: Frequency-dependent permittivity [75].

1.11.2 Glass-ceramic materials

In order to make composites with high energy storage, combine two phase that has a high permittivity and high breakdown field is a good suggestion which making glass-ceramic

Table 1.4: Ceramic composites with $CTTO$

Ceramic	Fillers	Fillers Content	Permittivity (* 10^4)	Loss	Breakdown (kV/cm)	α	Ref
$CCTO$	SiO_2	1 wt%	12.78	0.005			[79]
$CaCu_{3-X}Sr_XTi_4O_{12}$	Sr	X= 0.4	0.4	0.3	0.8		[52]
$CCTO$	SiO_2	2 wt%	0.3	0.5			[37]
$CCTO$	NiO	1 wt%	6.9833	0.073	0.3169	3.66	[45]
$CCTO$	SnO_2	1 wt%	5.1443	0.061	0.4857	3.77	[45]
$CCTO$	SiO_2	1 wt%	5.5240	0.136	0.2966	2.75	[45]
$CCTO$	Al_2O_3	1 wt%	3.0226	0.100	1.3907	3.74	[45]
$CaCu_{3+X}Ti_4O_{12}$	Cu		0.05				[67]
$CaCu_XTi_YO_{12}$	Cu	X=2.94	1.24	0.092			[40]
$CaCu_XTi_YO_{12}$	Cu	X=3.06	1.01	0.170			[40]
$CaCu_XTi_YO_{12}$	Ti	Y=3.92	1.48	0.0 67			[40]
$CaCu_XTi_YO_{12}$	Ti	Y=4.08	1.07	0.280			[40]
$CCTO$	TeO_2	1.5 wt%	0.3000	0.13			[1]
$CCTO$	TiO_2		5.2000	0.2			[54]
$CCTO$	GeO_2	4 wt%	0.5000				[2]
$Ca_{1-X}Sr_XCu_3-$ $-Ti_4O_{12}$	Sr	X=0.2	1.5000	0.1	0.400	5.02	[89]
$Ca_{1-11*X/6}Pr_XCu_3-$ $-Ti_4O_{12}$	Pr_6O_{11}	X=0.2	0.3000	0.1			[88]

composites that consist of an amorphous phase and crystalline is a practical way to reach this purpose. There are two widely use method to make such a composites, the first one is consist of mixing the glass, and ceramic powders and heat treat them after pressed in a certain shape. This method is not ideal, due to development of some of porous, so in the advanced method, it was tried to remove this porous by partially crystalized the amorphous phase. In this composites, the interfacial layer between an amorphous phase and crystalline phase plays an important rule in the final properties and performance of medium [29, 3].

1.11.3 Dielectric-dielectric composites

The growing interest in making the composites of two dielectric its essential to choose the dielectric with high permittivity. Materials like ferroelectrics and relaxor are a good candidate to be used for this purpose, but $CCTO$ due to its temperature independence

dielectric behavior provide interesting opportunely. Due to weak flexibility in the ceramic dielectric, the polymer has been used as a matrix in dielectric composites. Despite their low permittivity, high breakdown field made them suitable to be mixed with high permittivity fillers, but it may reduce flexibility in higher fillers load.

In the fundamental of research, it is important to understand the dielectric response of composites. To theoretically calculated the effective permittivity the volume fraction-fraction is a simple method to be used for composites:

$$\varepsilon_{eff} = \phi_1 \varepsilon_1 + \phi_2 \varepsilon_2 \tag{1.47}$$

Where phi is the volume fraction of each phase and epsilon is the permittivity. Despite the simple approach of this formula, the lack of accuracy makes many researcher approach new model to be used for this purpose. In this path, models based on field theory are more realistic.

One of the theoretical models based on mean field approximation is Maxwell equation. In this equation, it was assumed that the filler has a spherical shape and also its fraction is close to zero.

$$\varepsilon_{eff} = \varepsilon_1 \frac{\varepsilon_2 + 2\varepsilon_1 - 2(1-\phi_1)(\varepsilon_1 - \varepsilon_2)}{\varepsilon_2 + 2\varepsilon_1 + (1-\phi_1)(\varepsilon_1 - \varepsilon_2)} \tag{1.48}$$

For the binary mixing of spherical fillers, Bruggeman model has been suggested. All of this model it was supposed that inorganic fillers were mixed within the polymer matrix. In below figure the difference between all this model can be shown. It was assumed that inorganic fillers have permittivity around 1000 and polymer with permittivity around 3.

All of this models can be used if the size of fillers is very small and in the small volume fractions to calculate effective permittivity. However, in experimental, the other factors can be influenced the dielectric respond of the composite. The interfacial layer between fillers

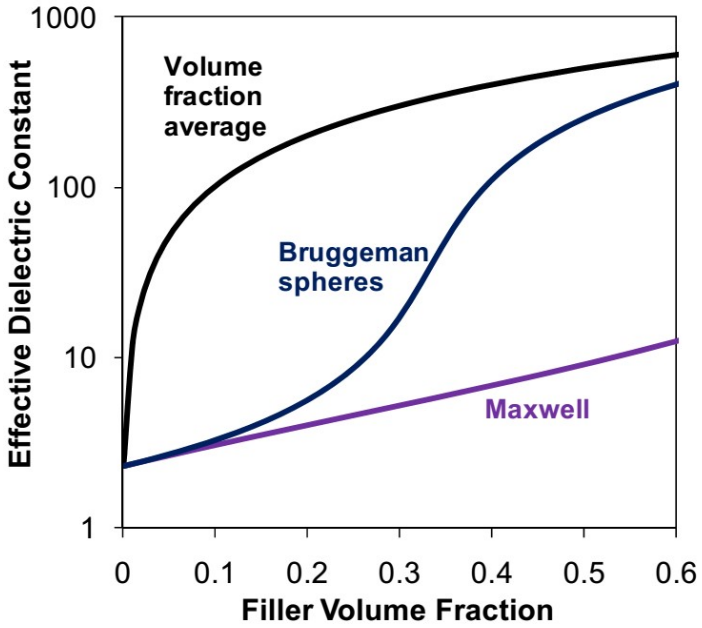

Figure 1.28: Effective permittivity for different volume fraction by using 3 composites models [5].

and matrix can change the dielectric respond significantly which made many models like numerical calculation develop to explain this behavior. The other parameters like conductivity of fillers, molecular polarizability can also be considered to develop a model to explain the dielectric behavior of polymer-ceramic composites [5].

1.11.4 Conductive fillers composites

One of the interesting composites in the category of dielectric materials is conductive-dielectric composites. In these composites, the percolation threshold determines the properties of composites. Before certain amount of fillers the composites act as an insulator but bypassing that amount, the composite shows conductive behavior which filler content percentage is known as percolation threshold [101].

In the range of insulator, the composites permittivity increase rapidly by increasing the filler content which provides the opportunity to make composites with gigantic permittivity. In order to make these composites, fillers with various size from macro to nanosize and

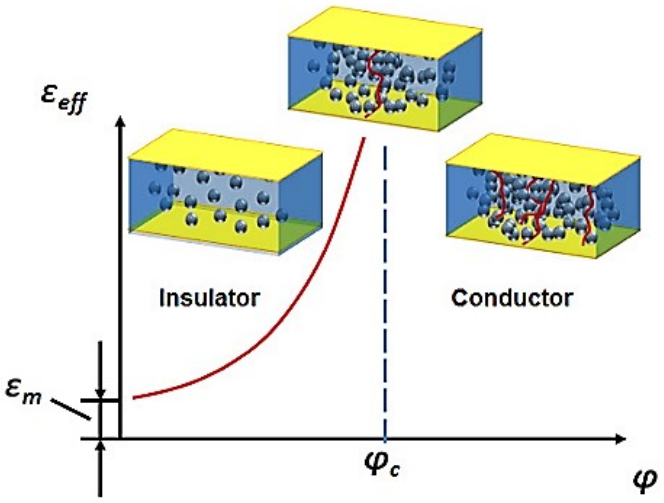

Figure 1.29: Composition dependence (i.e., volume fraction of conducting filler,) of the effective permittivity (ϵ"eff) of 0-3 CDCs, where c is the percolation threshold (dashed blue line) [103] .

also shaped like a tube, core/shell, spherical or fiber can be used to get higher permittivity. That factor can also affect the amount of percolation threshold which can make composites with better flexibility. It was found for the binary system the effective permittivity can be calculated by below equation:

$$\begin{aligned} &\varepsilon_{eff} \propto \varepsilon_m(\rho_c - \rho)^{-s}, \\ &\varepsilon_{eff} = \varepsilon_m(\frac{\rho_c - \rho}{\rho_c})^{-s} \\ &(\rho < \rho_c) \end{aligned} \tag{1.49}$$

Where is volume fraction of conductive fillers and is the percolation threshold. Due to the simplicity of this equation, many researchers try to use and fit experimental data to it [102, 104].

1.11.5 Interface contribution

In composites that fillers size is the range of nano size, the interface between fillers and matrix plays dominated role to determine dielectric respond. It should be mentioned that

decreasing the filler size cause in increasing surface area which can improve some properties. Due to this fact, many researchers tried to modify the surface of nanosize fillers to improve the interface between particles and matrix and get desired results [5].

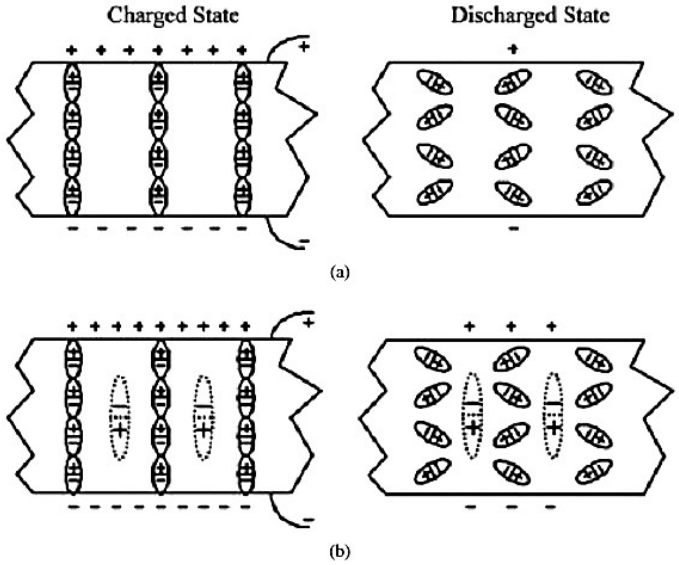

Figure 1.30: The Schematic of the charge and discharge mechanism in a dielectric capacitor: (a) without interfacial polarization and (b) with interfacial polarization [29].

As it was mentioned, there are many models try to explain the effect of an interfacial layer between fillers and matrix. On of famous model proposed to explain these layers by dividing them into three main three distinct regions. In this multi-core layer of polymer matrix composite, the first interface bound layer of inorganic fillers is contact layer between it and matrix. The second layer which also called as a bound layer is an interfacial layer which contributes to the dipoles motion. The loose layer which is called as a third layer usually responds to the matrix properties, and like second layer the properties of the composite originated from this two interfacial layers. So in order to affect the dielectric response of composites, the surface of inorganic fillers has been modified with the organic group which can change the region in the aspect of polarity, polarizability, mobility, and size [103].

Chapter 2

Preparation and characterization methods

The illustration of the step by step preparation of the samples and performing various characterization on the samples have been discussed in this chapter. The first subject has been discussed here, was the raw materials information and preparation if it is applied to them. For both ceramic composites and polymer composites, the filler and matrix preparation and mixing methods have been talked in details. This information contains the details about how to mix ceramic, polymer and conductive fillers and optimization of the methods and finally preparation to get final product ready to be tested. All characterization method that been used to test properties of samples and also their structure observation has been explained here. Furthermore, the data analysis if it is applied in characterization was included.

2.1 Raw material introduction

2.1.1 Calcium copper titanate $CaCu_3Ti_4O_{12}$

$CCTO$ is the famous ceramic with perovskite structure posses gigantic permittivity. The growing demand for miniaturization of electronic devices and energy storage make this ceramic to be a good candidate to be used. The properties of $CCTO$ is strongly depended on the preparation steps like calculations and also to the sintering temperature which small change on that make a big change on the behavior of ceramic. Beside it dielectric properties, the nonlinear I-V behavior with nonlinear coefficient around 4 and higher make this ceramic also to be used as a varistor [75, 73, 99, 30].

Despite large permittivity, the low breakdown field and high dielectric loss open a wide field of study to make $CCTO$ suitable for being used in the electronics industry. In this regards,

many researchers try to control the dielectric loss by using some additive like TiO, SiO_2, GeO, etc. Making ceramic composites is one of the ways to control dielectric loss and try to improve breaking down the field of these ceramics and also enhancing the permittivity of ceramic. The reason that the ceramic composite makes it work is due to the fact that the $CCTO$ properties are not only intrinsic but also extrinsic. In conclusion, making the ceramic composites, it can change the microstructure of $CCTO$ which determines the electrical response of the composite [74, 65].

In this study, high purity $CCTO$ (99.0%, Electronic, and Advanced Materials Department CO.) particles with the average size of 500 nm have been used. The glass-ceramic composites was made by mixing and heating the $CCTO$ particles with SiO_2. The composites respond strongly dependent on the sintering temperature and also the SiO_2 volume fractions. The SiO_2 is coated with the $CCTO$ particles by the conventional sol-gel method.

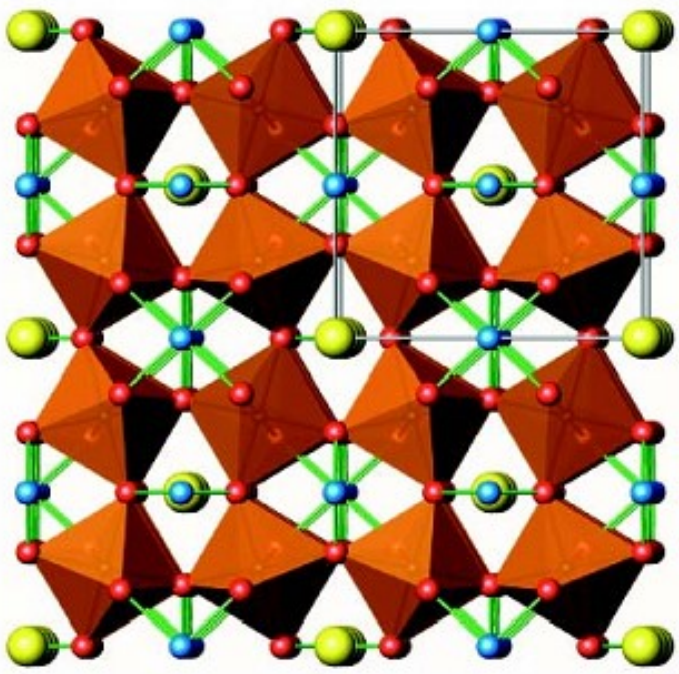

Figure 2.1: The structure of $CaCu_3Ti_4O_{12}$ (Cu-blue, Oxygen-red, Ca-yellow) [75]

2.2 Ceramic-glass composite fabrication

2.2.1 Experimental procedure

The glass-ceramic composites prepared to study dielectric properties which composite formed by $CCTO$ and SiO_2. The $CCTO$ powders with an average size of 500 nm and purity of 99.99 percent were purchased from Smart Metal Limited Company (Electronic and Advanced Materials Department). In this study, two common sol-gel methods have been used to make a SiO_2 layer on $CCTO$ particles. The purpose of the reaction is to produce core/shell structure by SiO_2 and $CCTO$ particles by the Stber process.

2.2.2 Sol-gel process

$CCTO$ powders were mixed with deionized water, and then the acetic acid was added to the solution for adjusting the acidity to 3.6 pH while being stirred at room temperature to form a suspended solution. In the final steps of synthesizing process, different calculated amount of tetraethylorthosilicate ($TEOS(Si(OC_2H_5)_4)$) has been added to obtain different SiO_2 concentration (10 $V\%$, 20 $V\%$, and 30 $V\%$). So it can form a coating layer of SiO_2 with an approximate thickness of 18, 39 and 50 nm, respectively. The final solution was stirred for 3 hours at 90 $^{\circ}C$ to form a gel coating and followed by washed six times with deionized water and methanol to remove other reaction products. In this work, this method has been named as acetic method due to SiO_2 formation in acetic environment. The chemical reaction to form SiO_2 gel:

$$TEOS(Si(OC_2H_5)_4) + H_2O \rightarrow SiO_2 + C_2H_5OH \tag{2.1}$$

The second method which we called it as ammonia method is a sol-gel process in an environment with pH equal to 9. In this process instead of water the powder suspended in the ammonia and followed by adjusting the PH of the solution. The calculated amount of TEOS has been added to the final mixture and heated at 40 $^{\circ}C$ for 7 hours. The washing

process was the same in the methyl alcohol. The $SiO_2/CCTO$ coated particles dried at 120 $^{\circ}C$ to make sure all the water or any remaining product of chemical process beside the composite powders have been evaporated.

2.2.3 Sintering process

Composite powders were obtained by drying the solution at 120 $^{\circ}C$ is ceramic green bodies which followed by the hand granulation method to make sure there will be no aglumaration on the particles. The water solution PVA as a binder has been used to prepare the sample green body followed by hand grandualtion and sieving to get uniform particle size. A pallet with a diameter of 1 cm was made by pressing the PVA added powders by the force of 100 Mpa for 5 min, with controlled in thichness about 1 mm.

The setup for sintering the green bodies is using four pallets on the top of each other in

Figure 2.2: Image of 46100 Barnstead Thermolyne furnace.

a closed crucible which put some $CCTO$ pure powder between them. The sintering takes placed by slowly increasing temperature by the rate of 2 $^{\circ}C$/min to get 600 $^{\circ}C$ and hold it for 1 hour for complete removal of PVA. The process was followed by increasing temperature to get sintering temperature which is between 1000 $^{\circ}C$ to 1100 $^{\circ}C$. In this study three temperature of 1040, 1050 and 1060 $^{\circ}C$ were used to sinter the pallets. After holding the pallets

for four hours in sintering temperature, they have been cooled down to room temperature as slow cooling rate. The furnace has been used in this study was the Barnstead Thermolyne furnace that is shown in the picture. It also the sintering steps can be seen the following figure.

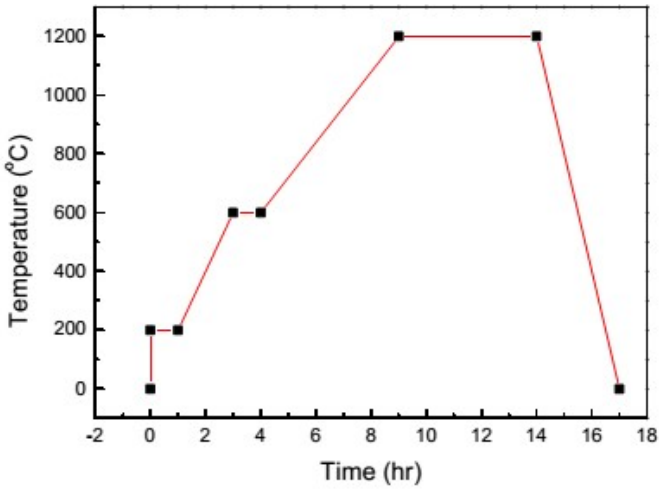

Figure 2.3: The sintering steps of composite samples.

2.3 Characterization methods

2.3.1 Crystalline structure determination

To study and characterized the structure and phases of ceramic and polymers the widely accepted method X-ray diffraction (XRD) method has been used. This characterization method can provide the information regarding as phases, crystallinity, orientation, etc. In order to investigate the microstructure of composites, the XRD was used between 10 to 80 angles. The scanned was performed at 40 kV and 40 mA with the scanning speed of 5/min and a sampling interval of 0.01. The obtained pattern was analysed with the special software for matching the peaks and determining the background. The sample orientation

for 2D composites was investigated by changing Chi angle from 0 to 20 angle by each 5 degree and Phi angle between -40 to 40 in every ten degrees.

2.3.2 Microstructure analysis

One of a most used method to observed the samples microstructure is using electron microscopy. The scanning electron microscopy (SEM) give the images from sample surfaces by applying high-energy electron beam to it. The images were produced by collecting scattered electron form sample surface which has interaction with the atoms of the sample. By using a different type of electrons like secondary electrons, backscattered electrons, characteristic X-ray, cathodoluminescence, and transmitted electrons some information such a surface morphology and composition distribution and also grain size and phase distribution can also be recorded. he free and fracture surface of samples was analyzed by using scanning electron

Figure 2.4: The JEOL JSM 7000F FE-SEM Scanning Electron Microscopy (SEM) used in the microstructure determination of composites.

microscopy (SEM). To make better images and avoid the electron buildup on the surface of the sample for SEM, the samples should be conductive or make them conductive. In our

research, for both ceramic and polymer samples, the gold coating had been used to make a thin conductive layer for applying a voltage to it. The sputter coating machine of Pelco SC-6 sputter coater used in this purpose and the plasma applied two times on the surface of the specimen for 30 sec. The FE-SEM microscope with the model of JEOL JSM 7000F FE-SEM performed the image processing at 20 kV. The compositional analysis was performed by using Oxford Instruments Electron Dispersive X-ray Spectroscopy (EDS) system which gives information on the elemental weight percentage on a different part of samples and also a mapping of surface elements. The following pictures show the gold sputtering and also SEM-EDS instrument.

Figure 2.5: The Pelco SC-6 sputter used for gold coating.

2.3.3 Impedance analysis

To study the impedance behavior of the composites samples, the permittivity and dielectric loss was measured by using Agilent 4294A impedance analyzer. The permittivity of composites samples was calculated by the capacitance obtained in the range frequency between 100 Hz to 1 MHz. For polymer film samples, making a parallel electrode on both sides is sufficient. However, for ceramic samples, the thickness should be reduced to around 300 micrometers and also surface should be smooth by polishing and then gold electrode

applied to it. To avoid any environmental and systematic noises on the measured result, the device was calibrated. To analysis the dielectric behavior of composite in different working temperature, samples placed into the handmade probe inside the Fisher Isotemp 800 Series Programmable oven, and connected to the impedance analyzer by cable to out of the oven. The following pictures show the impedance analyzer and oven used in this study.

Figure 2.6: he image of Agilent 4294A impedance analyzer.

2.3.4 Nonlinearity and energy storage calculation

In the case of ceramic composites, the nonlinear behavior of samples has been measured by applying a voltage to the samples and measuring the responds current. The Precision-LC100 system with $H.V.$ Supply Amplifier/Controller was used to applied this voltage and measured the current which also can provide the breakdown field of samples. The sample prepared for impedance analysis is used in soaked silicon oil and voltage continuously applied to the sample in the frequency of 10 Hz.

The vision software has been used to work parallel to the device and perform the applying voltage to the samples. Beside the $I-V$ measurement, it can provide the $P-E$ loop which is shows polarization over the different electrical field. Polymer composites due to their

matrix ferroelectric behavior show hysteresis loop on this test device and the energy density of samples can be measured.

Chapter 3

Dielectric and non-ohmic behavior of $CCTO/SiO_2$ composites

In this study, the electrical properties and microstructure of $CCTO/SiO_2$ composites have been studied. The ceramic composites were made of $CCTO$ coated with SiO_2 by sol-gel method. The composites were made of in various SiO_2 concentration and sintered in different temperature. The effect of SiO_2 concentration and sintering temperature on the microstructure and non-ohmic behavior of composites were investigated. The breakdown electrical field for the composite of $CCTO$ can improve from 1.96 kV/cm to 40 kV/cm by adding SiO_2 due to the formation of a resistive layer in grainboundaries. The nonlinear coefficient of the sample is influenced by changing the Schottky barrier parameters to reach 3.8, which is improved the CCTO nonlinearity by 30 percent. Moreover, composites made of with SiO_2 concentration more than 25 percent, exhibit gigantic permittivity when ceramics sistered at temperatures higher than 1060 ^0C. It is believed that, the emerge of the eutectic liquid phase can form a new phase and defects in the structure. The SEM pictures and XRD results were conducted to evaluate the microstructure change by sintering of these composites.

3.1 Introduction

The demand for miniaturization and increased usage of electronic devices for many applications require materials with high permittivity. $CaCu_3Ti_4O_{12}$ ($CCTO$) with perovskite structure shows a gigantic permittivity (up to 10^5), which is stable in a wide range of temperatures [75, 39]. Besides the permittivity, the remarkable nonlinear behavior of $CCTO$ made it a candidate to use in electronic devices. The limits in using material like ZnO or SnO_2 as a varistor raises a demand to look for substitutional material with special properties.

The lack of ability to control circuits in varistors made of these materials and requirements to adjust the breakdown field for different usage, attracted many researchers into utilizing $CCTO$ [57, 45, 105]. To explain the unusual electrical behavior of $CCTO$, many models suggested base on intrinsic and extrinsic properties of $CCTO$. The internal barrier layer capacitors model (IBLC) is one of the accepted models used to explain the observed properties of $CCTO$ [89, 73, 43]. Besides that, the nano barrier layer capacitor (NBLC) is a new model that recently used to describe the gigantic permittivity of CCTO. In this model, grainboundary plays an important role in dielectric properties of the composite.

Despite $CCTO$s extraordinary permittivity and high nonlinear coefficients, its low breakdown field, limits its applications. To overcome this limit, composites of $CCTO$, with a suitable insulator was used to change $CCTO$ properties. These composites posses lower dielectric loss, and higher breakdown field can be obtained. Based on Maxwell-Wager relaxation, conductivity in grainboundaries cause the dielectric loss that leads to a lower breakdown field [74]. To get a higher breakdown field and nonlinear coefficient, researchers use additives like TiO_2, CuO, ZrO_2, SnO_2, and SiO_2 to change the composites microstructure to reach the desired properties. It was reported the breakdown field could be improved by adding a different kind of additive to reach 1.4 kV/cm while the nonlinear coefficient can reach 3.66 [74, 54, 40]. The SiO_2 is one of the most used additive materials in this area due to the excellent insulated properties, which leads to a decrease in the dielectric loss [52, 37]. Moreover, SiO_2 layer makes the grainboundary more insulated due to resistive properties [45, 51].

In this work, we try better understanding the fundamental and get better breakdown field we use a higher range of SiO_2 percentage to the composites. Moreover, The most work on CCTO was on its dielectric performance. We try to improve this material for varistor applications.

3.2 Experimental

High purity $CCTO$ (99.0 %, Electronic and Advanced Materials Department CO.) particles with the average size of 500 nm and $TEOS$ (Aldrich Chemistry CO.) were used to make composites by the conventional sol-gel method. $CCTO$ powders were mixed with deionized water, and then the acetic acid was added to the solution for adjusting the acidity to 3.6 pH while being stirred at room temperature to form a suspended solution. In the final steps of synthesizing process, different calculated amount of $TEOS(Si(OC_2H_5)_4)$ has been added to obtain different SiO_2 concentration (10 $V\%$, 20 $V\%$, 25 $V\%$, 30 $V\%$ and 35 $V\%$), so it can form a coating layer of SiO_2 with an approximate thickness of 18, 39, 50, 64 and 93 nm, respectively. The final solution was stirred for 3 hours at 90 $^{\circ}C$ to form a gel coating and followed by washed six times with deionized water and methanol to remove other reaction products. Composite powders were obtained by drying the solution at 120 $^{\circ}C$ and mixing with PVA (Polyvinyl alcohol) as a binder. A pallet with a diameter of 1 cm was made by pressing the silica-coated powders, and then, It was sintered in the air at different temperature (1040 $^{\circ}C$-1080 $^{\circ}C$) for 4 hours.

Scanning electron microscopy of different composition and sintered condition was carried out due to the investigation of the microstructure. The X-ray diffraction was used in room temperature in the range of 20 to 80 degree and to examine the phase characterization of sintered ceramic samples. The sintered pellets were polished to around 300 micrometer thickness and followed by coating on both sides with gold sputtering as an electrode. The I-V test was conducted by using a P-E loop device for each sample to investigate the nonlinear behavior of samples.

3.3 Result and discussion

3.3.1 X-Ray diffraction

The XRD pattern presented in Fig. 3.1 and Fig. 3.2, was obtained from CCTO ceramics contains various percent of SiO_2 sintered at different temperatures. The XRD result shows the sharp characterized peaks of $CCTO$ in composites sintered at temperature lower than 1060 ^0C and there is no secondary phase detected. There is a small peak related to SiO_2 also appeared in the XRD pattern, which suggests the crystallization change in morphology of the composite by different preparation conditions.

The XRD Fig. 3.1 shows the main peak of $CCTO$ for the composites prepared by 25

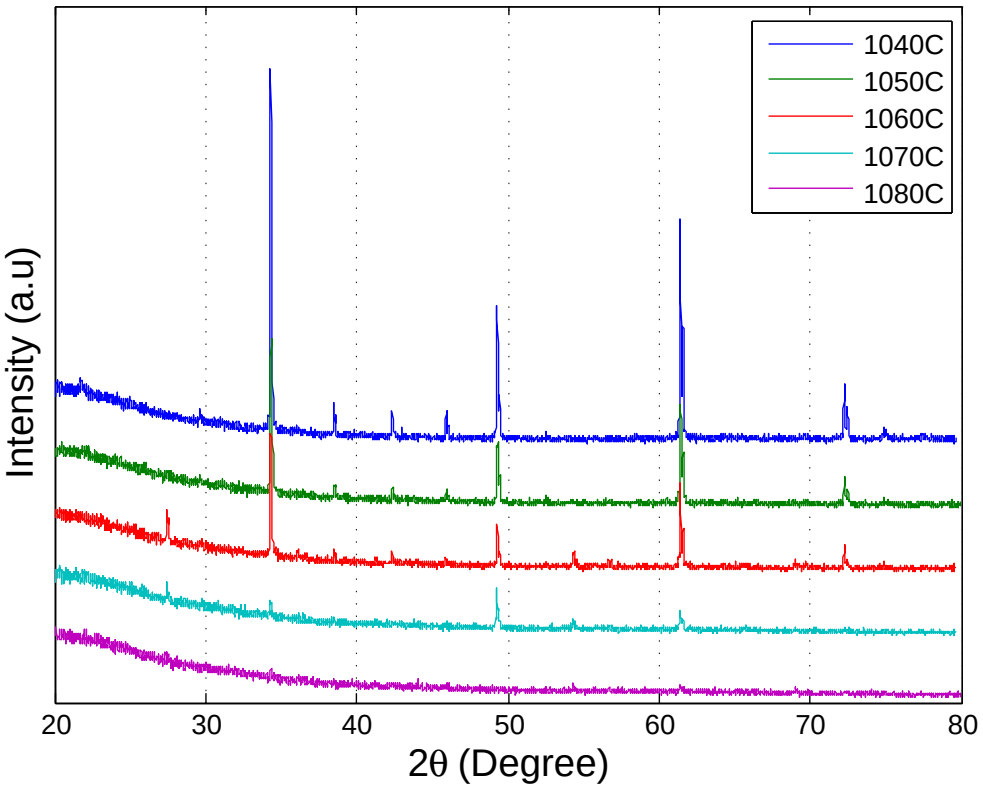

Figure 3.1: XRD pattern of ceramic of 25% SiO_2/ $CCTO$ composite in different sintering temperature.

percent SiO_2 at sintering temperature of 1040 $^\circ C$ without any other impurity. Increasing

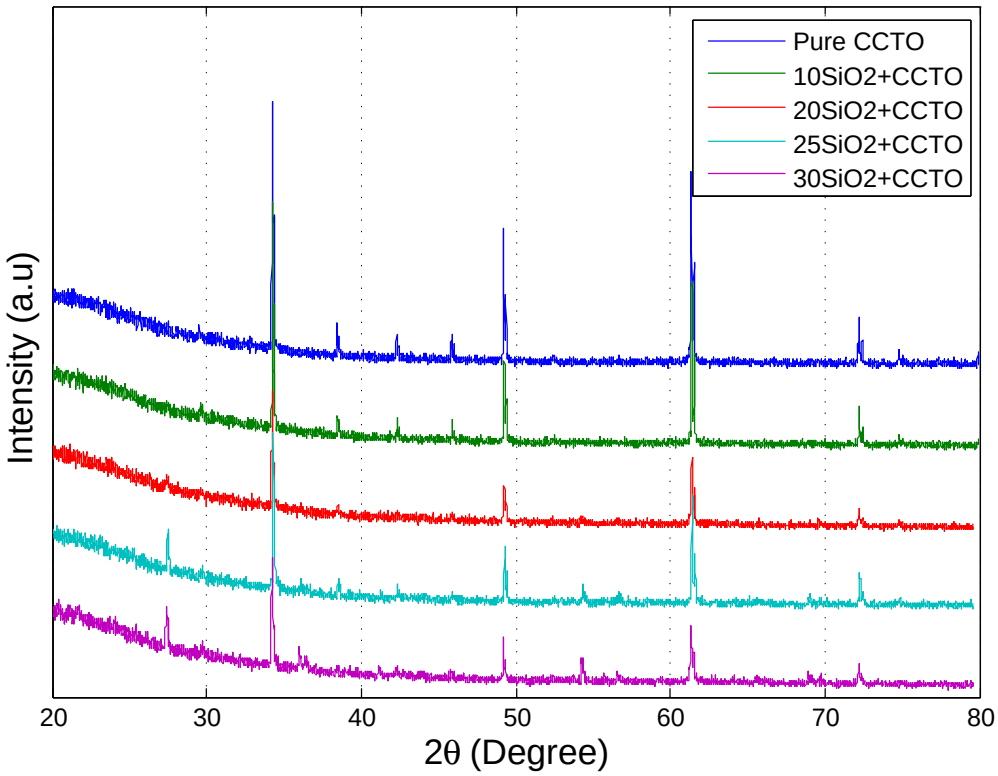

Figure 3.2: XRD pattern of ceramic of SiO_2/ $CCTO$ composite at 1070 sintering temperature.

the sintering temperature reduce the peak intensity but the main peaks of $CCTO$ exist. When sintering temperature reach to 1060 $^{\circ}C$ the peak intensity reduced more and also new peaks appear. The new peaks are corresponded to the formation of new phase which is fitted to the $CaSiTiO_5$ peaks. It is known from the literature that the CuO move from grain to grainboundary in sintering higher than 1060 $^{\circ}C$. It also reported that the eutectic could form between SiO_2 and CuO almost around 1050-1060 $^{\circ}C$. It can conclude that the liquid phase formation results in an amorphous structure which is reduced the peak intensity. Furthermore, the CuO extraction from $CCTO$ causes it to lose it a structure which can result of formation of new phases. The further increase in the temperature cause more reduction in peaks intensity.

3.3.2 Scanning electron microscopy

The morphology of $SiO_2/CCTO$ composites were investigated using SEM images on the fracture surface of the samples.The pure $CCTO$ powders can be seen in Fig. 3.3a, before sintering. In Fig. 3.3b, you can see a significant increase in the average grain size by increasing sintering temperature.

In Fig. 3.3b and Fig. 3.3c, it can be seen that the average grain size of composites increased by increasing sintering temperature. Fig. 3.3d, illustrates the change in the microstructure by increasing the concentration of SiO_2 from 10 percent to 30 percent. The results suggest formation of the liquid phase in grainboundary with SiO_2 helps the movement of ion diffusion in grainboundary. Improvement in diffusion makes the grainboundary move easier and cause grain growth. Moreover, by increasing the temperature, more pores can be formed in the sample. The SEM picture indicated that, the microstructure is strongly dependent to the sintering temperature and SiO_2 concentration.

3.3.3 Dielectric properties

The permittivity of pure $CCTO$ measured in the frequency range of $10^2 - 10^6 Hz$ has been plotted in Fig. 3.4a. The Fig. 3.4b shows the effect of SiO_2 concentration on the permittivity of composites. The result shows the high permittivity of pure $CCTO$ for a broad range of frequency that can be altered by the composites process. By adding an additive to $CCTO$, it alters the resistivity of grainboundary.

Based on the IBLC model, the permittivity of the composite determined by the properties of grainboundary which result in a decrease in grainboundary by getting resistive grainboundary. As it was discussed before, by adding adequate amount of SiO_2 to the composite, liquid can be formed in grainboundary which leads to grain growth. Increasing grain size that is suitable as an IBLC model, it makes an increase in the permittivity of composite [89].

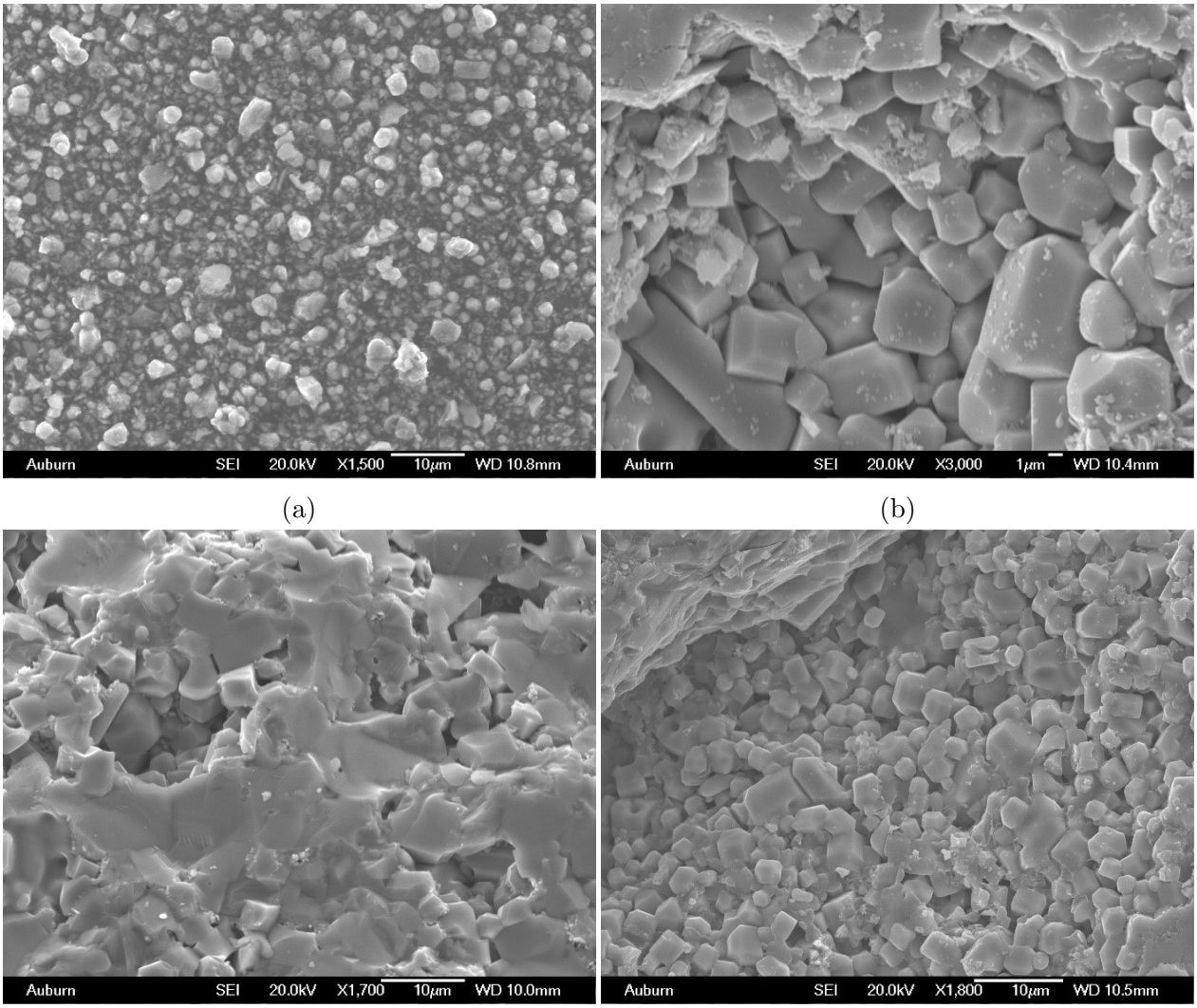

Figure 3.3: SEM images of(a) Pure $CCTO$ particles. (b) 10% $SiO_2/CCTO$ composites sintered at 1060 $^{\circ}C$.(c)10% $SiO_2/CCTO$ composites sintered at 1070 $^{\circ}C$. (d)30% $SiO_2/CCTO$ composites sintered at 1060 $^{\circ}C$.

Fig. 3.5 present the permittivity and Fig. 3.6 dielectric loss of $CCTO$ for different SiO_2 composition. The plots consist of different sintering conditions and for 10 percent SiO_2 concentration. By using dielectric loss and permittivity, the other parameter like imaginary part and conductivity was calculated and plotted.

In temperature below 1060 $^{\circ}C$ by increasing SiO_2 concentration both permittivity and dielectric loss will be reduced. The composites permittivity can be explained by using mixing rules. Based on this model, the total permittivity will be reduced by adding a resistive

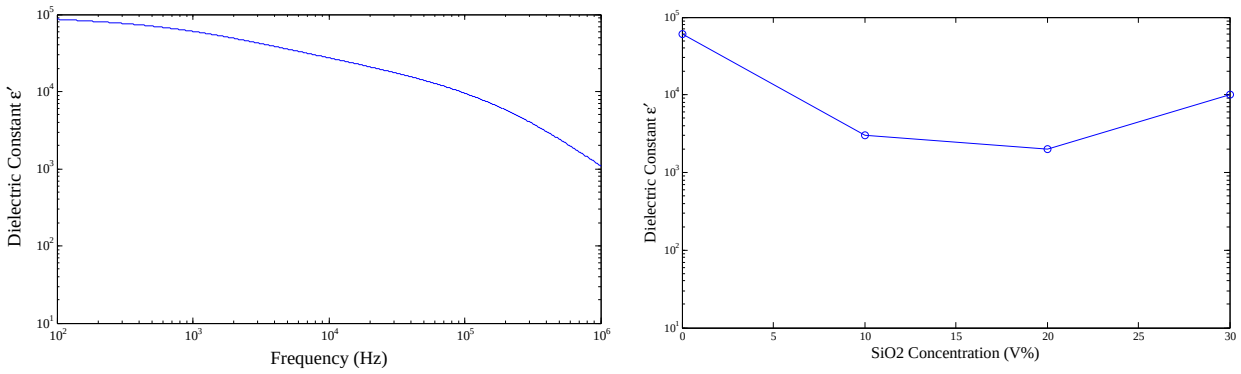

(a) (b)

Figure 3.4: (a) The permittivity of pure $CCTO$ as a function of frequency. (b) The permittivity of $SiO_2/CCTO$ composites as a function of different SiO_2 concentration.

component to the dielectric material.

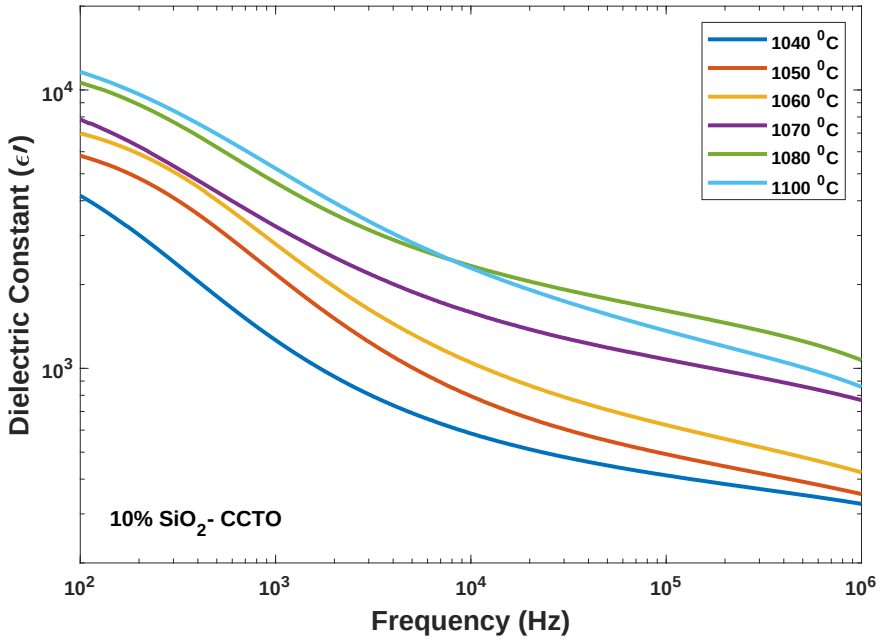

Figure 3.5: Permittivity response of 10 % $SiO_2/CCTO$ composite.

SiO_2 and the $CCTO$ in the composites. So by increasing SiO_2 concentration, the total permittivity dropped significantly. It also can explain by using $IBLC$ model which effective

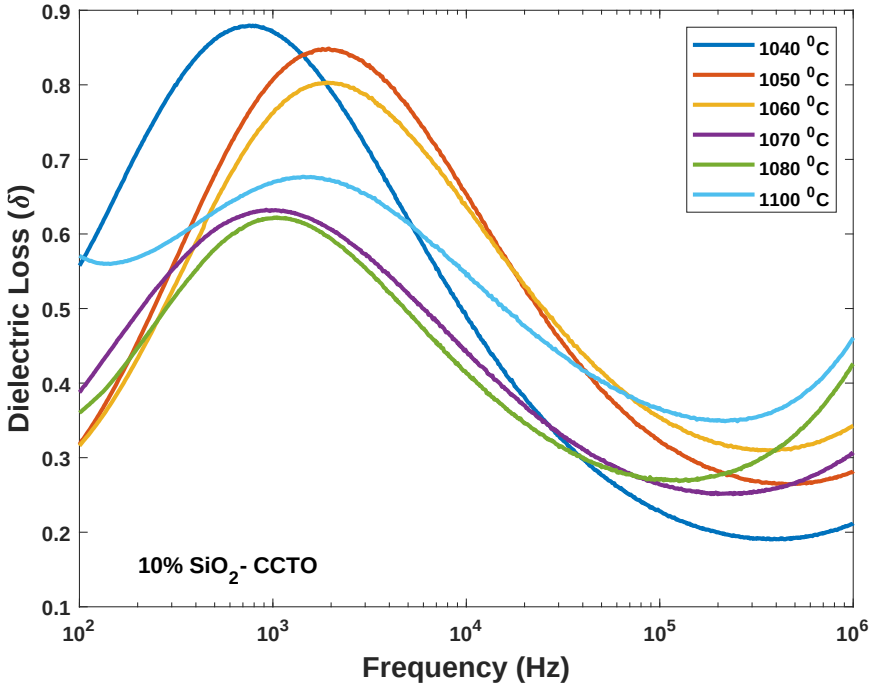

Figure 3.6: Dielectric loss of 10 % $SiO_2/CCTO$ composite.

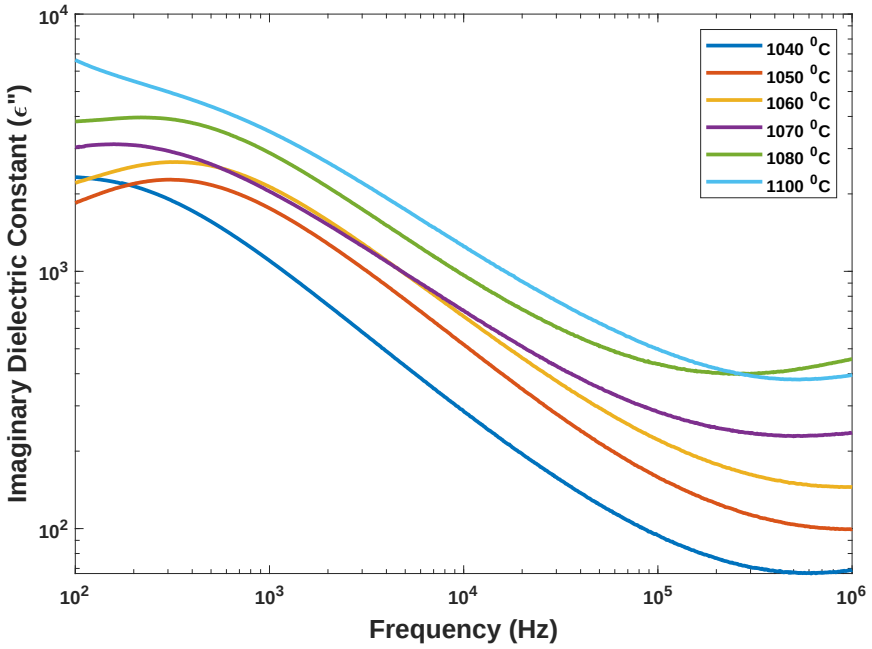

Figure 3.7: Imaginary part dielectric of 10 % $SiO_2/CCTO$ composite.

dielectric depend on grain boundary capacitance and also its thickness. The effective permittivity in this model calculated by:

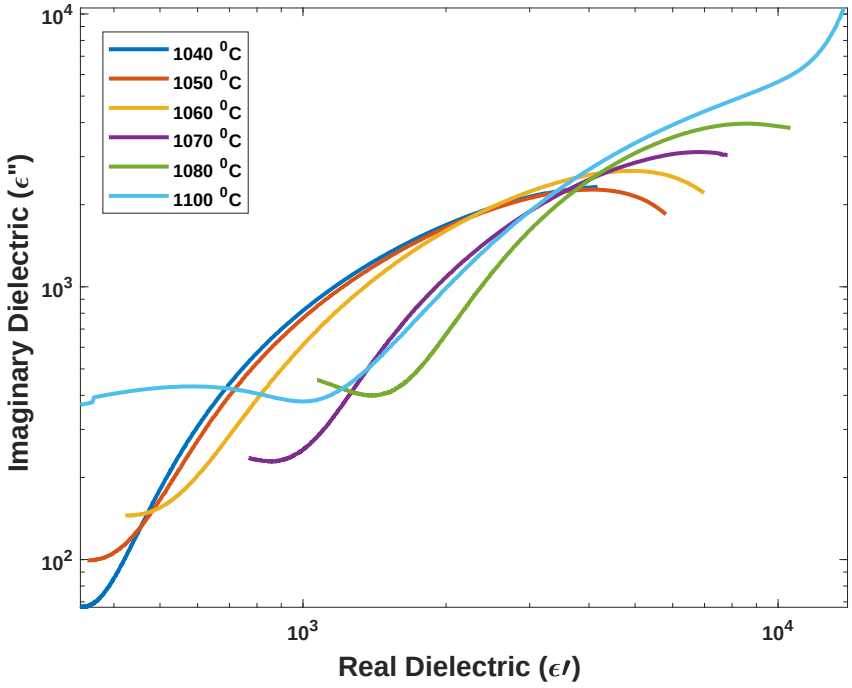

Figure 3.8: Cole-Cole of 10 % $SiO_2/CCTO$ composite.

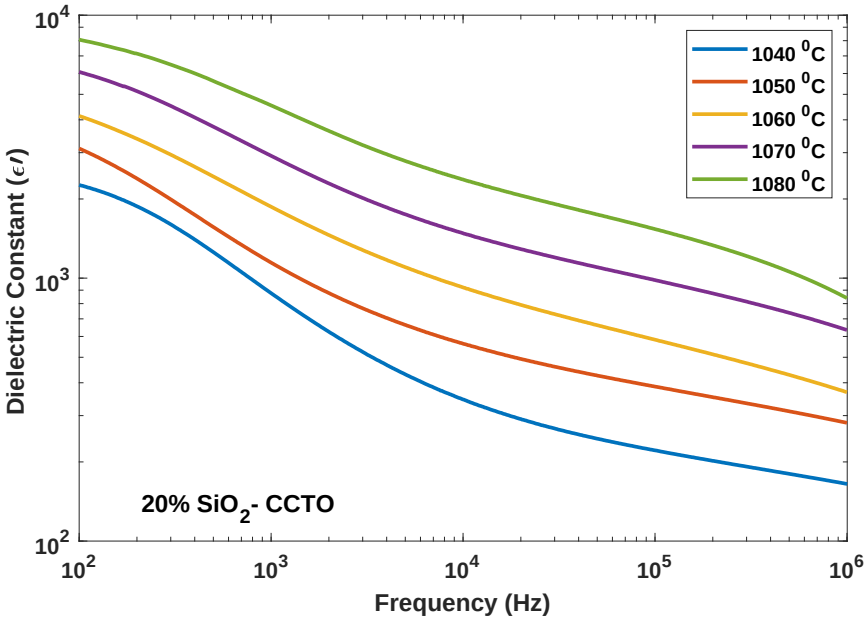

Figure 3.9: Permittivity response of 20 % $SiO_2/CCTO$ composite.

$$\varepsilon_{eff} = \varepsilon_{gb}\frac{D}{d} \tag{3.1}$$

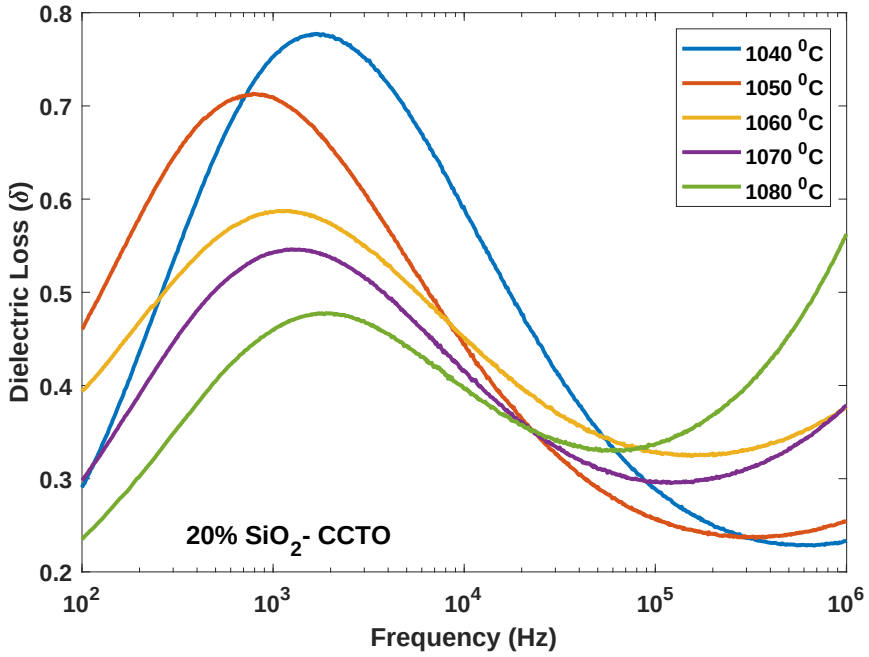

Figure 3.10: Dielectric loss of 20 % $SiO_2/CCTO$ composite.

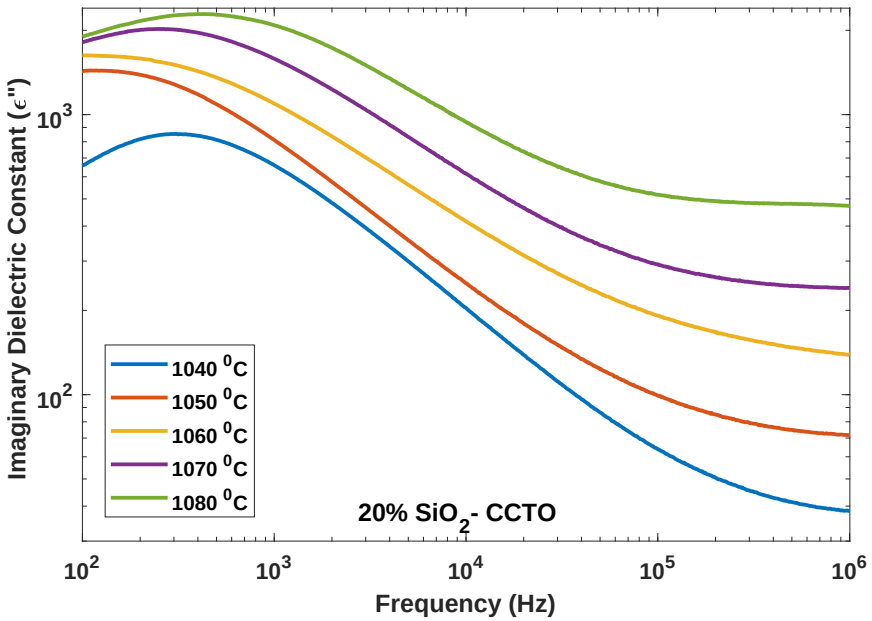

Figure 3.11: Imaginary part dielectric of 20 % $SiO_2/CCTO$ composite.

Where D and d are grain size and average grainboundary thickness, respectively. In our experiment, Because of the almost homogeneous coating of SiO_2 by making core/shell structure around $CCTO$ particle, form $CCTO$ grain with SiO_2 in grainboundaries during

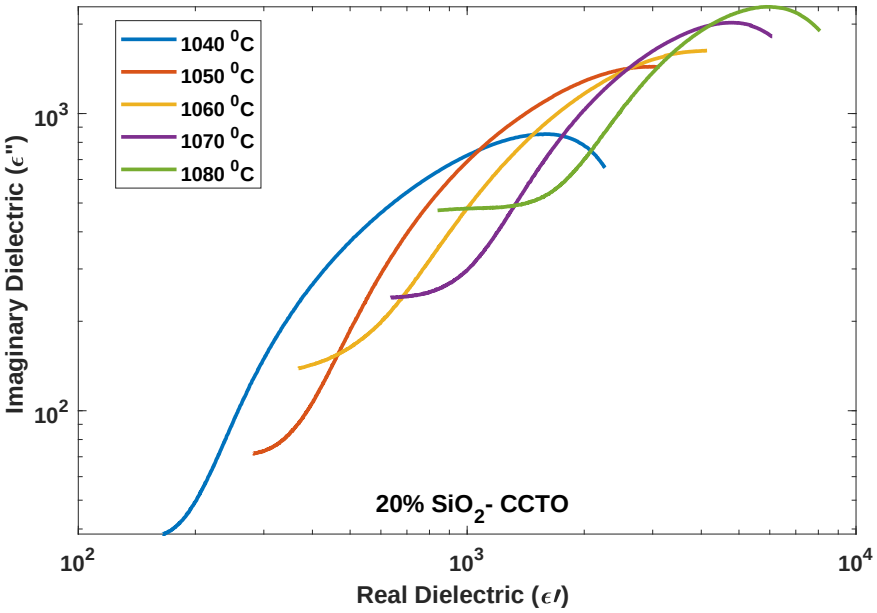

Figure 3.12: Cole-Cole of 20 % $SiO_2/CCTO$ composite.

sintering. Therefore, grainboundary thickness and also its resistivity increased, which both has a negative effect on the permittivity of composites by considering $IBLC$ model.
We have an impedance of different concentration which illustrates the increase in resistivity of grainboundary by increasing SiO_2 concentration for sintering temperature lower than 1060 $^{\circ}C$. $CCTO$ powders were coated with SiO_2 lead to grainboundary become more resistive by increasing the amount of SiO_2, and this will also be increased grainboundary thickness. So as $IBLC$ model we have resistive barrier layers and semiconductive grains.

Sintering temp lower than 1060 $^{\circ}C$

In our composites system, when sintering temperature lower than 1060 $^{\circ}C$, due to core/shell structure, we have a semiconductor grains and resistance grainboundary. The interfacial region in grainboundary contributes to Maxwell-Wagner relaxation which emerges a peak in frequency dependence of loss. This relaxation which originates from the conductivity of insulator region can be surpassed by adding more insulator materials. The frequency dependence of dielectric loss of composites shows a reduction in the peak height by increasing

SiO_2 concentration.

The internal barrier layer capacitor ($IBLC$) model is favorable with Debye model because it is also based on system consist of semiconductor grains and insulator grain boundaries. Base on $IBLC$ model, the permittivity of composites depends on the permittivity of grain-boundaries. In result of this model by increasing the insulator to the grainboundaries, the permittivity should be reduced to lower values. This behavior can be seen on all composites made by sintering with the temperature lower than 1060 $^{\circ}C$.

The Fig. 3.5 shows the permittivity and loss of composites with 10 percent SiO_2 concentration. The results imply that making core-shell structure reduced the permittivity significantly by making resistive layers in grainboundaries which is the main origin of electron conductivity in $IBLC$ model. The loss of each material comes from charge carrier conductivity and second from relaxation made by dipoles. The SiO_2 layer almost controls electron conductivity through the grainboundaries, but When the sintering temperature is higher than 1060 $^{\circ}C$ for the composites with 10 and 20 percent SiO_2 composition, the Debye relaxation still rules the behavior of dielectric loss. Besides that, increasing temperature caused grain growth and densified the structure, and the resistivity of grain boundary improved which lead to decrease in the dielectric loss. The reduction in the defects in grain boundary leads to improving the effect of insulator layer which is a decrease in conductivity and having smaller dielectric loss peak.

The $IBLC$ model also can be used to describe the effect of sintering temperature on the permittivity of composites with a concentration lower than 25 percent. Base on this model, besides the permittivity of grainboundary, the size of grains and grainboundary will affect directly on composite permittivity. As the grain growth by increasing sintering temperature and getting smaller grain boundary, it will be favorable to the $IBLC$ model which lead to increase in the permittivity of bulk.

Sintering temp higher than 1060$^{\circ}C$

At high sintering temperature, some oxygen loss can follow by Ti reduction. The reduction of Cu^{2+} to Cu^{1+} can also make Cu loss. In conclusion, the $CCTO$ structure will be distorted due to radii change of Cu, so in the result, by substitution of Ti_{4+} to the copper sites; the reduction will be overcome and also some oxygen vacancy may be formed in reduction conditions. In result of this process, some CuO leaves grains and move to grainboundaries.

$O_o^{2-} + 2Ti^{4+} \rightarrow V_0^{"} + 2Ti^{3+} + 1/2O_2 : Ca(Cu_3)Ti_{4-u}^{4+}Ti_u^{3+}O_{12-u/2}$

$3Cu^{2+} \rightarrow 2Cu^{1+} + Ti_{Cu}^{4+} + Cu \uparrow : Ca(Cu_{3-3V}^{2+}Cu_{2V}^{+}Ti_v^{4+})Ti_4O_{12}$

$Ca^{2+}Cu_3^{2+}Ti_4^{4+}O_2^{-12} \rightarrow Ca(Cu_{3-3V}^{2+}Cu_{2V}^{+}Ti_v^{4+})Ti_{4-u}^{4+}Ti_u^{3+}O_{12-u/2}$

$\rightarrow Ca^{2+}Cu_3^{2+}Ti_4^{4+}O_2^{-12} + CuO$

In pure $CCTO$ ceramics, the CuO move out of grains and make the resistive grainboundary. In $CCTO/SiO_2$ composites, by increasing temperature to more that 1060 $^{\circ}C$, the CuO move to grainboundary which filled with SiO_2. The CuO and SiO_2 have a eutectic point around 1060 $^{\circ}C$ the liquid phase will be formed in grainboundaries.

It should mention that the CuO has a melting point around 1300 $^{\circ}C$ so without an adequate amount of SiO_2 the movement of CuO into grainboundary hindered with SiO_2 layer around grains.

For lower concentration, the surface of $CCTO$ particles coated by SiO_2 will limit the surface conductivity which can be surpassed by the formation of the liquid phase in grainboundaries. Now there is two dominant mechanism leads to the conductivity of system. First, increasing in diffusion pass by liquid phase at the interface of grains create more oxygen vacancies. This defects state lead to the possibility of hopping between Cu sites which result in electron hopping between $Cu^{2+} - V^O$ and $Cu^{1+} - V^O$.

$Ca^{2+}(Cu_{1-3X}^{2+}Cu_{2X}^{1+}Ti_X^{4+})_3Ti_4O_{12} + Cu^{2+}O \rightarrow Ca^{2+}Cu_3^{1+}Ti^{4+}4O_{12-x}^{2-}$,

$Cu^{1+} \leftrightarrow O^{2-} \leftrightarrow Cu^{2+}$

The other mechanism activated by exchange electrons from Cu^{+} to the Ti^{4+} sites due to the unstable stage of Cu sites in the liquid form and forming Cu^{2+} and Ti^{3+} by cooling down. This behavior results in high conductivity by polaron relaxation and leads to change in relaxation process and get higher permittivity and dielectric loss.

$Ca^{2+}(Cu^{2+}_{1-3X}Cu^{1+}_{2X}Ti^{4+}_{X})_3Ti_4O_{12} + Cu^{2+}O \rightarrow Ca^{2+}(Cu^{2+}_{1-X}Ti^{4+}_{X})_3(Ti^{4+}_{4-6X}Ti^{3+}_{6})O_{12}$

$Ca^{2+}Cu^{2+}_{3}Ti^{3+}_{4}O^{2-}_{12-x}\ Ti^{4+} \leftrightarrow O^{2-} \leftrightarrow Cu^{+}$

This process shows why the $CCTO$ ceramics shows the ultrahigh permittivity even compare to the other perovskite materials. The reason is the capacitive barrier not limited to the grainboundaries, but actually, it has barriers in atomic size in the grains which increase the electronic charge storage.

The grains also become bigger by forming liquid phase due to high ion diffusion pass in grainboundaries result in a reduction in grainboundary resistance and get to the higher dielectric loss and constant.

At lower SiO_2 concentration, by increasing temperature, the amount of CuO comes to grainboundary is limited due to a small formation of eutectic compositions. In this cases, the increasing sintering temperature causes a small change in dielectric response of materials. However, when the amount of SiO_2 reach to 25 volume percent, the CuO can completely merge with it and form liquid phase by reaching the eutectic point.

By improving sintering temperature to higher than 1060 $^{\circ}C$ for 10 and 20 percent SiO_2 concentration, grains slightly growth, and because this growth will be in solid phase, the structure becomes denser so reduce the conductivity of resistive part. This will be reduced the dielectric loss of material, and as Maxwell relaxation, the peak which originated from the conductivity of grainboundary will move to a lower frequency. On the other hand, grain growth is good for $IBLC$ model and improve permittivity. This change can be seen from the cole-cole plot that by improving temperature there will be a large increase in permittivity of both grains and grain boundary. However, due to grain growth, the thickness of grain

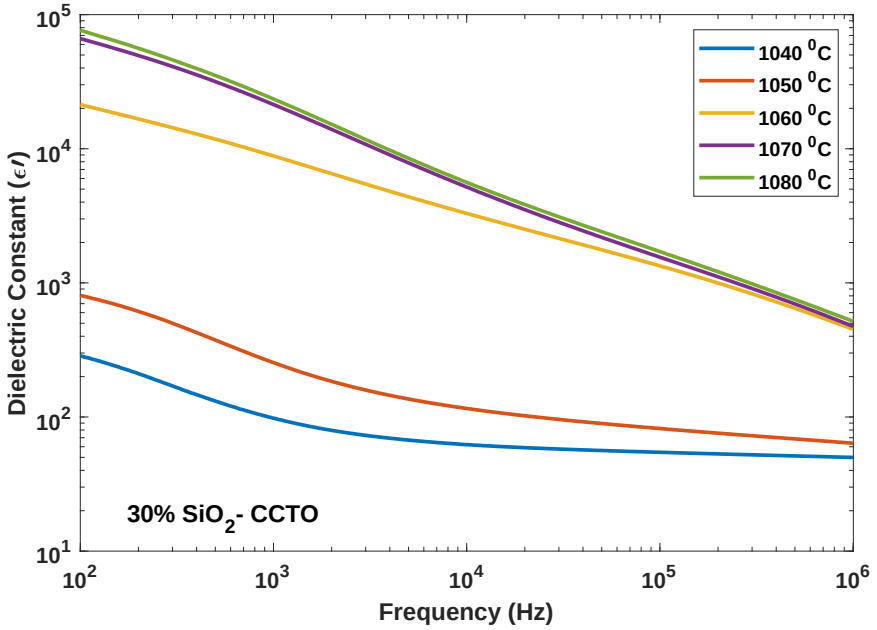

Figure 3.13: Permittivity response of 30 % $SiO_2/CCTO$ composite.

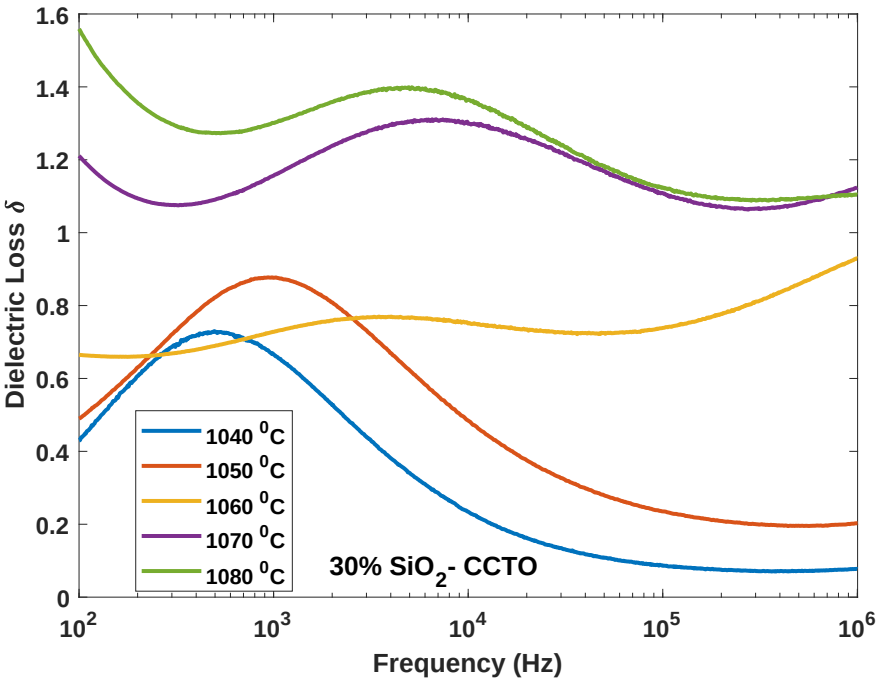

Figure 3.14: Dielectric loss of 30 % $SiO_2/CCTO$ composite.

boundary will be reduced which cause a reduction in the impedance of the composite by increasing sintering temperature.

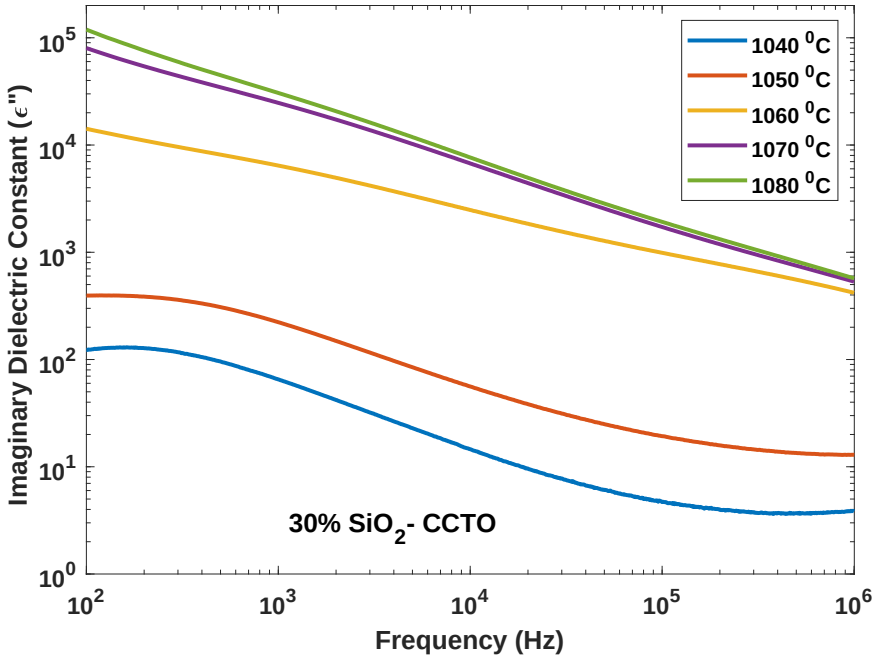

Figure 3.15: Imaginary part dielectric of 30 % $SiO_2/CCTO$ composite.

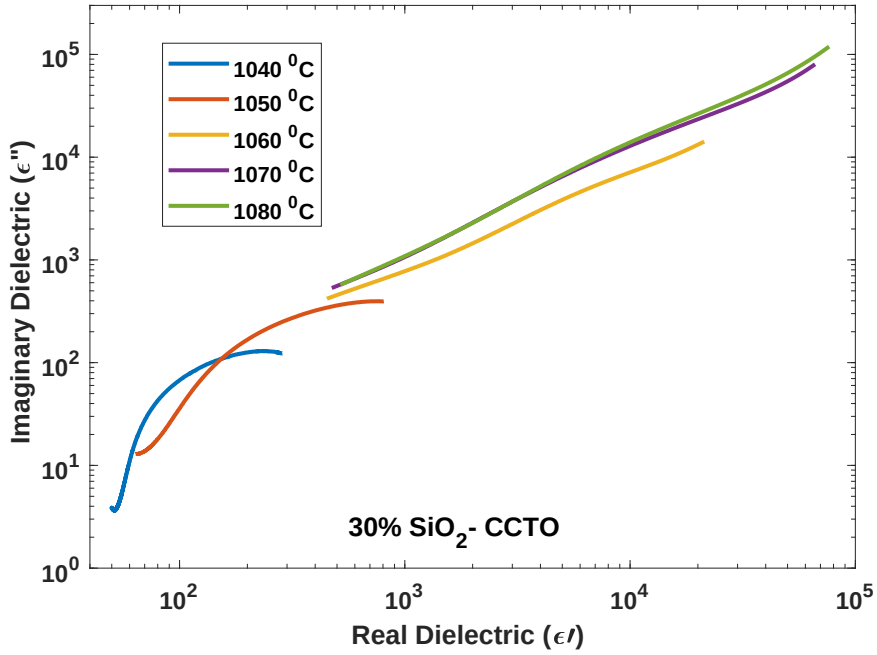

Figure 3.16: Cole-Cole of 30 % $SiO_2/CCTO$ composite.

3.3.4 Temperature dependency

The following pictures show the temperature dependence of impedance analysis of composites with different concentration. The dielectric loss shows that the process is moving

from low frequency to high frequency by increasing temperature. This is the result of the temperature-activated process. Moreover, at high temperature, the conductivity results in a higher dielectric loss in the low-frequency region.

In the case of composites contains more than 30 percent SiO_2, the dielectric loss is more dominated to the conductivity. Start from zero ^0C, the low-frequency region of dielectric loss is moved up by increasing temperature.

3.3.5 DC Bias

The DC bias applied to the sample while it was tested for dielectric behavior by the impedance analyzer. The fig. 3.19 present the effect of DC bias to the 25% SiO_2-$CCTO$-1100 $^\circ C$ ceramic composite permittivity. It is clearly can be seen the permittivity start to decreases by DC bias and become negative when sufficient DC bias applied. By increasing the DC bias, the transition frequency increases and lead to higher plasma frequency. The DC bias effect is mostly on low frequency, and frequency higher than 10^6 has remained unchanged.

The dielectric loss change by the DC bias of 25% SiO_2-$CCTO$-1100 $^\circ C$ ceramic composite is presented in fig. 3.20. The dielectric loss jumped up in the low-frequency range, and the sharp peaks related to the negative permittivity emerge in this frequency range. Similar to the permittivity, the high-frequency dielectric loss is almost unchanged by DC bias.

The ceramic shows very small DC conductivity at low frequency rang, but by applying DC bias the strait horizental line appear which result of high DC bias. By influence of DC bias, the conductivity increases sharply and move up by applying more of it. This behavior is the sign of hopping conductivity which is essential to get negative permittivity. Its suggested that the DC bias influence the number of electrons can freely move in medium and formation of drude like negative permittivity.

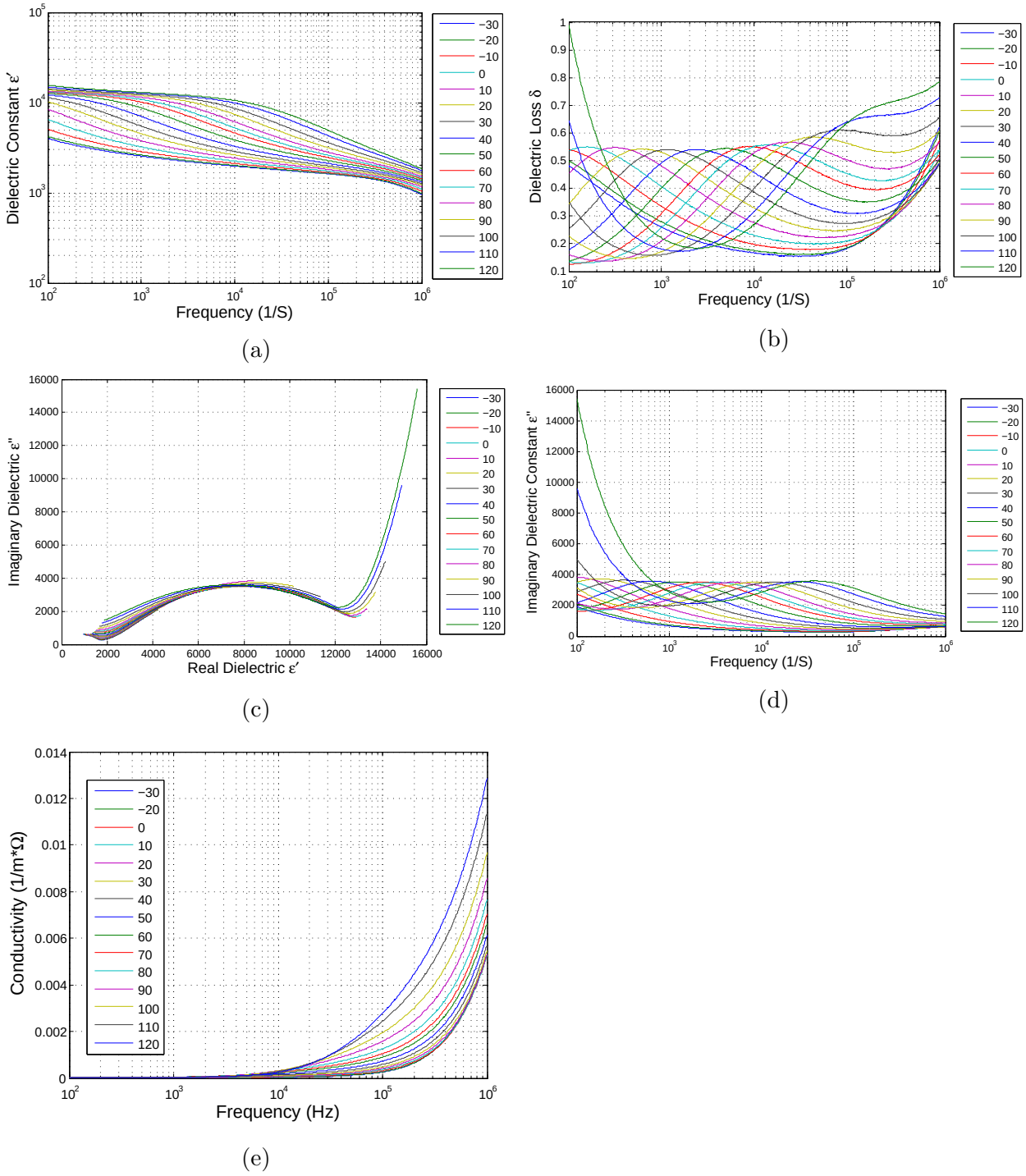

Figure 3.17: 10 %(a) Real part dielectric. (b) dielectric loss. (c) Cole-Cole.(d) Imaginary part dielectric.(e) Conductivity.

3.3.6 I-V curve

Fig. 3.22a shows the current density (J) of different SiO_2 concentration composites in different electric fields (E). The nonlinear characterization of material was obtained from an

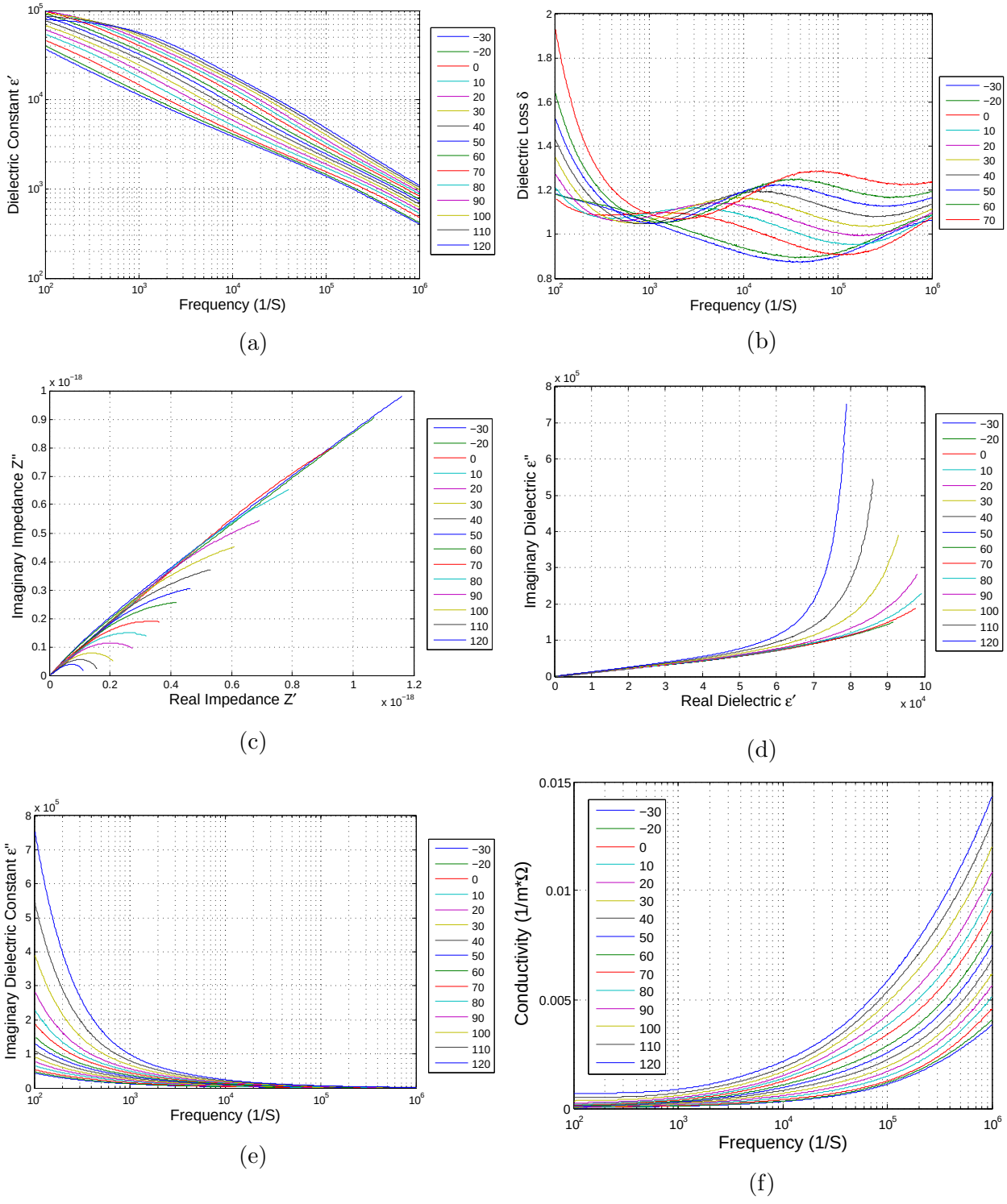

Figure 3.18: 30 %(a) Real part dielectric. (b) dielectric loss.(c) Impedance plot. (d) Cole-Cole.(e) Imaginary part dielectric.(f) Conductivity.

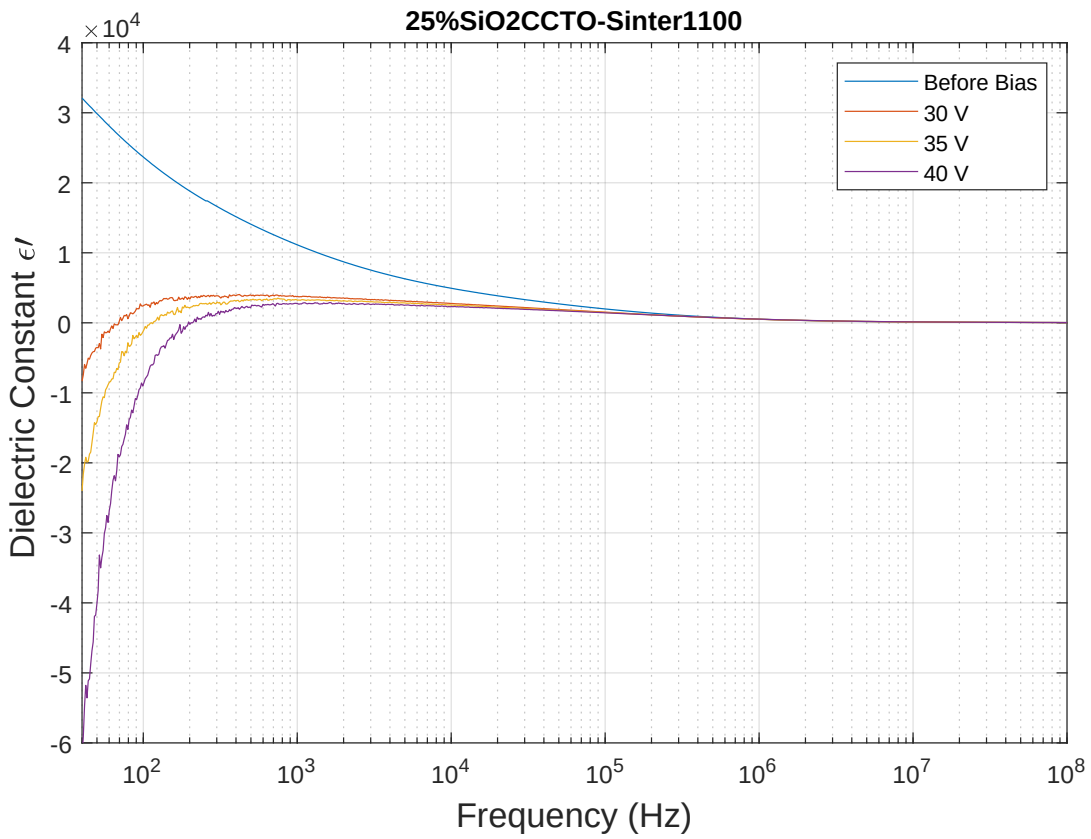

Figure 3.19: DC bias effect on Dielectric constant of 25% SiO_2-$CCTO$-1100 $^{\circ}C$ ceramic composite.

$I-V$ test, where the breakdown field considered to be at the current density of 27 mA/cm^2. It is well known that the nonlinearity coefficient can be altered by the additive. For the pure $CCTO$, the value of the nonlinear coefficient, α, is 2.9, but it can increase to 3.5, 3.8, 3.56 by adding 10 $V\%$, 20 $V\%$ and 30 $V\%$ of SiO_2 in $CCTO$. The change in the conductivity of composites by applying electrical field for different sintering temperature can be seen in Fig. 4(b). The results show the relationship between conductivity and breakdown field. The nonlinear coefficient for samples with 10 $V\%$ concentration changes the to 3.4 and 3.3 for 1070 $^{\circ}C$ and 1080 $^{\circ}C$ sintering temperature respectively.

Breakdown field of $CCTO$ can increase drastically from 2 kV/cm to 37 kV/cm and 42 kV/cm for 10 and 20 composites. However, for 30 V concentration of SiO_2, the breakdown

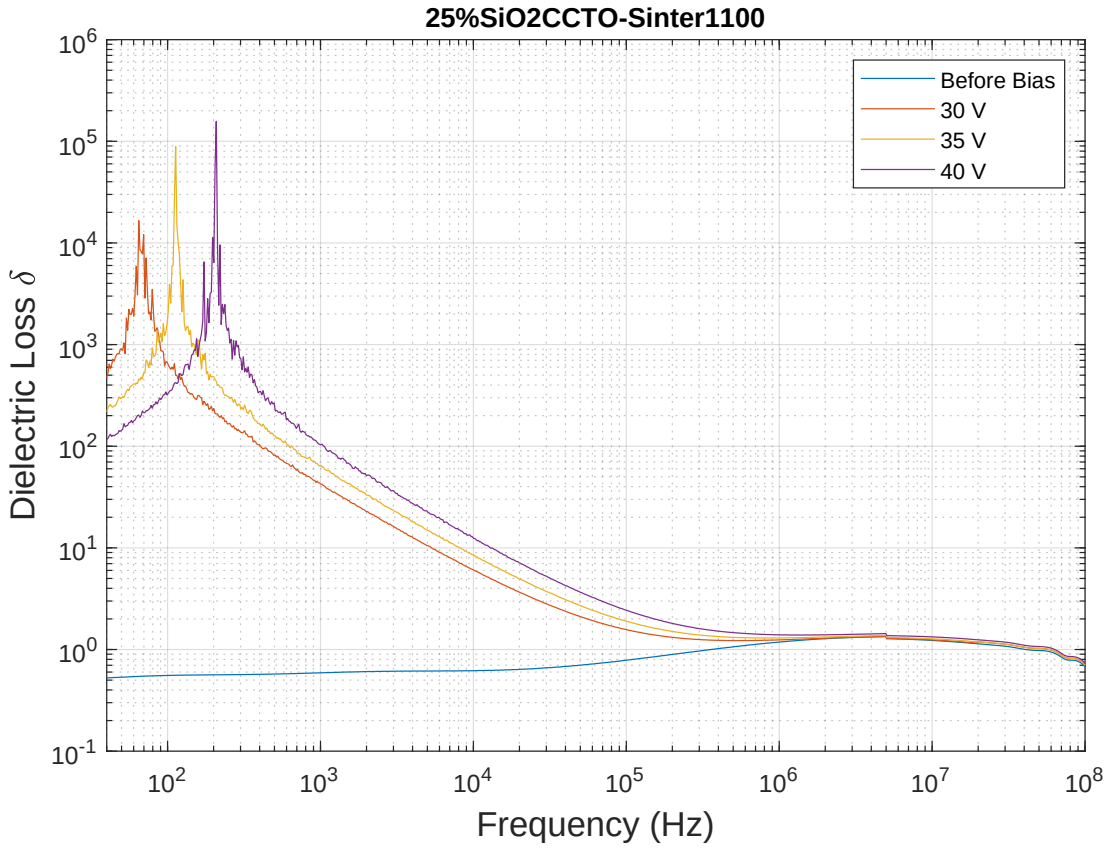

Figure 3.20: DC bias effect on Dielectric loss of 25% SiO_2-$CCTO$-1100 $°C$ ceramic composite.

field of $CCTO$ composite decreases to 19.4 kV/cm. This trend also can be seen for composites sintered at 1070 $°C$ and 1080 $°C$ sintering temperature, which the breakdown field decreases to 22 kV/cm and 6 kV/cm respectively. This result is much bigger than the breakdown field reported by Liu. which by adding different additive to $CCTO$ and get breakdown field in range of 0.2 kV/cm to 1.39 kV/cm [45].

Composites make in core/shell structure causes grainboundary to become more insulator and reduce conductivity. Adding SiO_2 to $CCTO$ by 10 and 20 can reduce conductivity and results with an increase in the electrical field and nonlinear coefficient. The Schottky barrier model explains the change in conductivity by considering the charge trap layer as a potential barrier in grainboundary. Fig. 3.22b shows a linear match between $ln(J/AT^2)$ and E with

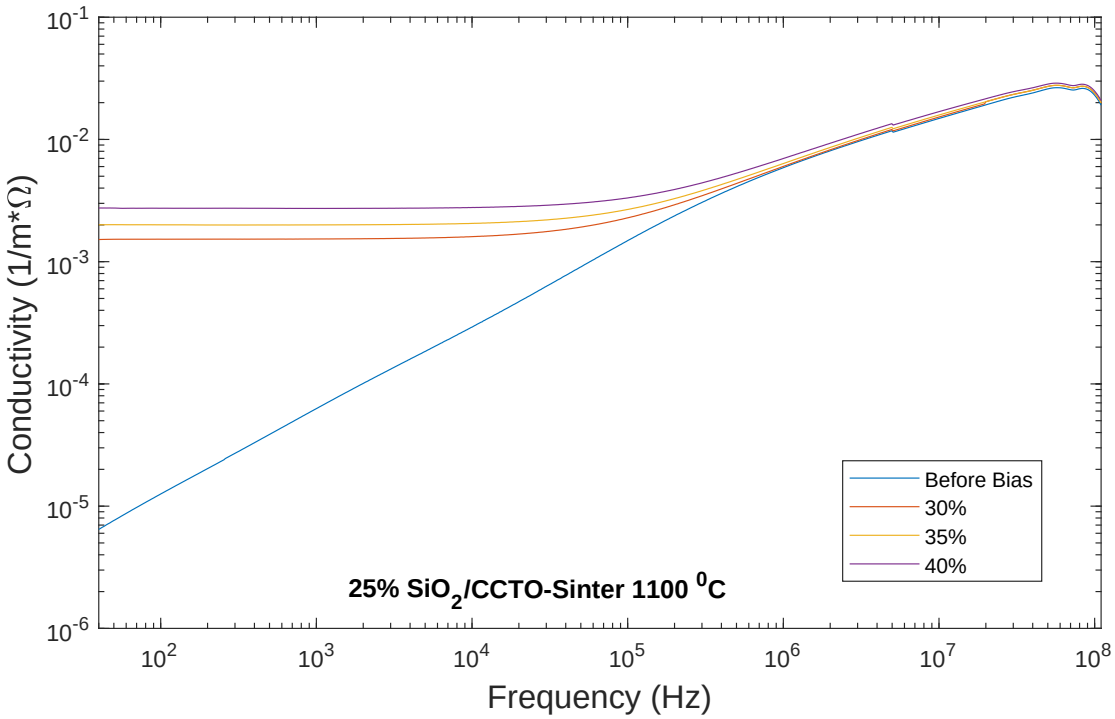

Figure 3.21: DC bias effect on AC conductivity of 25% SiO_2-$CCTO$-1100 $^{\circ}C$ ceramic composite.

composites at different levels of the SiO_2 concentration. The plots are based on the Poole-Frenkel equation [22] confirm the effects of sintering temperature and the electrical field on the emission of the electron. The effect of sintering the temperature on the Poole-Frenkel equation, also, can be seen in Fig. 3.22b. In both Fig. 3.22a, the slope of the plots, represent the width of the potential barrier, which is an intrinsic material property that relates to the grain size and the number of grains.

The materials properties obtained from the fitting result is presented in Table. 3.1, which shows the height and width of the potential barrier in a depletion layer in grainboundaries. The height of the potential barrier is improved by adding an insulator additive which results in a decrease in conductivity. In the Schottky barrier model, grain size can directly affect the barrier width which is inversely proportional to the breakdown field. Same as $IBLC$ model [89], in Schottky emission model [22], the grains act as a semiconductor, and the

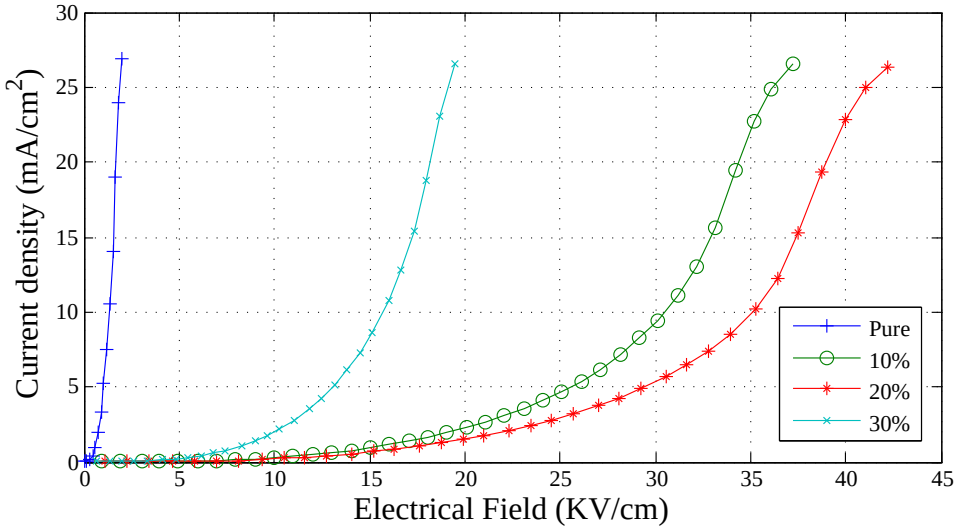

(a)

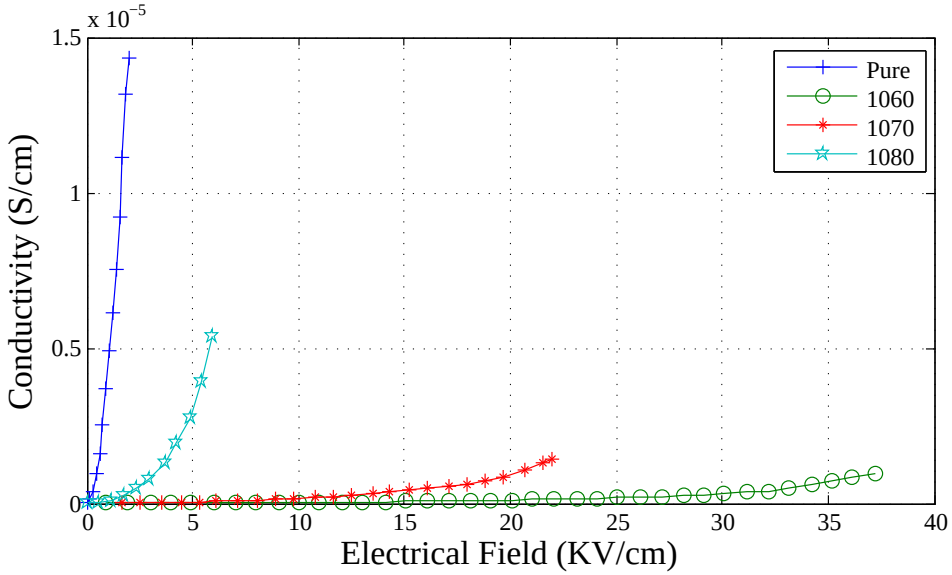

(b)

Figure 3.22: The I-V test results. (a)) The J-E curve for different SiO_2 concentration sintered at 1060 ^0C. (b) The $\sigma - E$ Curve for 10% SiO_2 concentration sintered at different temperatures.

grainboundary acts as an insulator between the grains. The property of Schottky barrier can be influenced by changing the microstructure of the sample. By forming a suitable amount of liquid phase in grainboundary, makes the grains to growth and consequently decreases the size of grainboundary and increase conductivity. Therefore, by sintering at

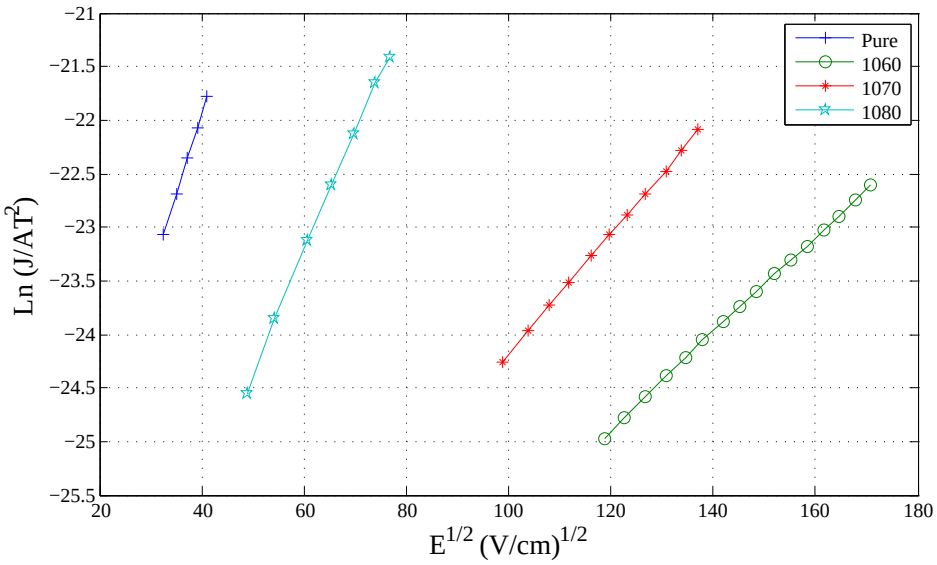

(a)

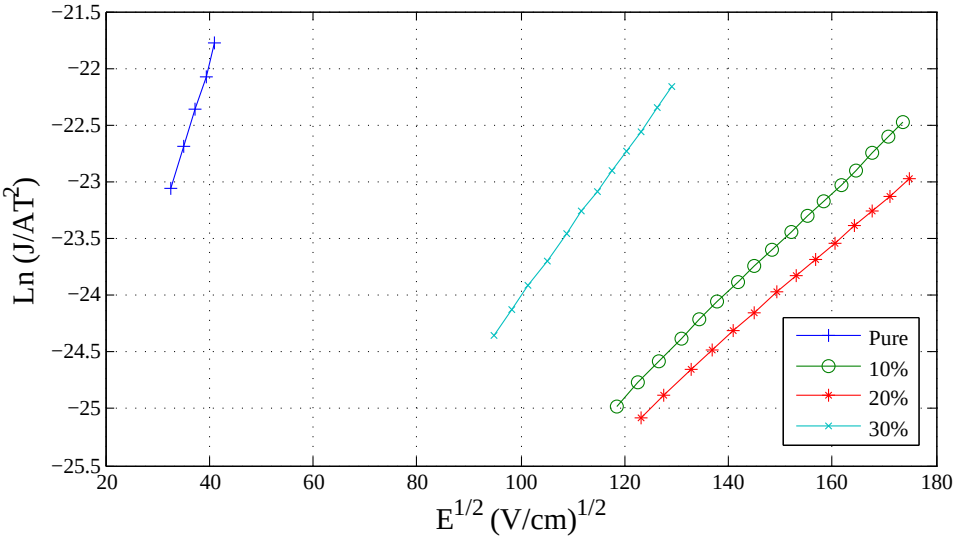

(b)

Figure 3.23: The I-V test results. (a)) The $J-E$ curve for different SiO_2 concentration sintered at 1060 ^0C. (b) The $\Sigma - E$ Curve for 10% SiO_2 concentration sintered at different temperatures.

a higher temperature or adding SiO_2 more than 20, the height of potential barrier will be decreased due to the change in resistivity of grainboundary. The barrier height in the range of 1.2 to 3.6 is smaller than Felixs report which is in the range of 5.68 to 9.23 and makes it suitable for improving the nonlinear coefficient and breakdown field [22]. The change on

Table 3.1: Nonlinearity coefficient by fitting data

Composites	Nonlinear Coefficient (α)	Barrier Height (ϕ_B)(eV)	Barrier Width (1000β) ($eVV^{-1/2}cm^{1/2}$)	Breakdown Field (E_B) (kV/cm)
0% SiO_2- 1060 $^\circ C$	2.9	0.65	3.6	1.96
10% SiO_2- 1060 $^\circ C$	3.5	0.743	1.29	37.2
20% SiO_2- 1060 $^\circ C$	3.8	0.745	1.22	42
30% SiO_2- 1060 $^\circ C$	3.51	0.73	1.74	19.4
10% SiO_2- 1070 $^\circ C$	3.4	0.71	1.5	22
10% SiO_2- 1080 $^\circ C$	3.3	0.72	3	6

grainboundary properties causes a reduction in the breakdown field and nonlinear coefficient, which make the composite a suitable material for use as a varistor.

3.4 Conclusion

The sintering temperature can alter the microstructure drastically, which changes the results in the electrical behavior of composites in ceramics. By increasing sintering temperature, the grain size increases and more pores might emerge which results in reducing the conductivity in grainboundary. Based on experimental result, the Schottky potential barrier suggests the proportional effect of barrier height on the breakdown field of samples. The results obtained from this method confirm the improvement of barrier in grain boundaries which leads to a decrease in conductivity by increasing the concentration of SiO_2 in $CCTO$ grain boundaries. Forming the SiO_2 layer can increase the resistivity in grainboundary, which increases the breakdown field and nonohmic characterization. At a certain concentration level, the liquid phase level increases, which results in drastic increases of the diffusion. The increase diffusion rate results in an increase of the grain size and consequently decreases

and increases the height and width of the potential barrier size respectively. The SEM pictures prove the change in structure by changing sintering conditions.

Chapter 4

SPS BTO-SiO_2 composites, dielectric properties and structure study

The 50 nm and 140 nm powders of $BaTiO_3$ were used to prepare ceramic composites. The powder was vacuum treated at 850 ^0C to get better properties. The treated powder was coated by 10 nm SiO_2 by the conventional sol-gel method. The SPS was used to make ceramics with coated or uncoated powders. The ceramic was then cut to small pieces and polished to get a uniform surface. The samples shows a large permittivity up to 10^6 at 100 Hz frequency and dielectric loss is about 10. The first analysis of these composites shows the permittivity can change to negative by applying the DC bias, and the DC bias size can determine the plasma frequency. The temperature dependence of dielectric shows almost no phase transformation which was also in agreement with the DSC result.

4.1 Introduction

$BaTiO_3$ (BTO) is one of the promising powders in the field of dielectric materials due to its perovskite structure. In addition, its high permittivity and low dielectric loss makes it a right candidate for energy storage purposes. Our previous works show that vacuum treating the powder can improve the permittivity significantly. Emerging oxygen vacancies in treated powder are suggested as the reason behind their enhanced performance. Many researchers attend to lower the dielectric loss and increase their ceramic breakdown field by making composites with other insulative fillers like TiO, CuO, etc. SiO_2 is one of these insulative materials which is mostly used in dielectric materials due to its close to zero dielectric loss. The chemical sol-gel method is the most widely used method that can be used in ceramics studies for getting a uniform coating layer around ceramic powder.

The mostly used ceramic composites in electrical applications are fabricated by the conventional sintering method. However, spark plasma sintering has been used and in some studies due to the fast preparation process. The rapid heating rates make it much quicker than the conventional method, and by applying the electrical field to the sample, it generates heat inside the samples and omits the need of preparing grain bodies. This process beside its time-saving benefits, results in ceramics with extraordinary properties as dielectrics. The gigantic permittivity while proportionally low dielectric loss is beneficial for the dielectric application.

The increasing interest in materials with negative permittivity has engaged many researchers to look for materials with such properties. The artificial structure of metamaterials makes random composites more favarable for this application due to their easy process fabrication and tunable properties. Random composites show much lower plasma frequency compared to the metals, and the filler concentration can be used as a tunning factor. These composites are mostly made by insulative and conduction parts mostly shows negative permittivity after formation of a conductive path by reaching a percolation threshold. Random composites made by ceramic are filled mainly by some metals or conductive materials like carbon nanotubes and have plasma frequencies in the range of GHz-THz spectrum. There are some reports of negative permittivity by applying an electrical field in a range lower than 100 Hz in systems consisting of liquid phases. It has been show that the temperature can be used to tune the results, but it can not be used as an only driving force to generate negative permittivity in those materials. The origin of such a behavior still is a debate, but many researchers try to explain it by considering the formation inductor inside composites or emerge of internal electrical field.

In this research, the vacuum treated powder was coated by SiO_2 to get composites with a high permittivity and low dielectric loss. The SPS method was used to process ceramic samples with extraordinary properties. The color of SPS sample is close to dark blue which is a sign of high conductivity of those samples which can be present in the permittivity up to

10^6 and dielectric loss of 20 at a frequency of 100 Hz. The permittivity can become negative by applying DC bias. Moreover, the very low frequency region shows negative permittivity without DC bias. The temperature dependence shows no phase transformation in the permittivity responds. The result obtained at low frequency shows negative permittivity in a frequency range lower than 10 Hz while temperature change from -150 ^0C to 150 ^0C. The Ac conductivity shows that there are two different region with different activation energy.

4.2 Experimental

The pure BTO sample with a size of 50 and 140 nm was prepared by the NASA (Marshall Space Flight Center, located in Huntsville) named as BT50 and BT14, respectively. The 50 nm BTO powder was milled and then reduced in forming gas (25% H2, 75% N2) at 900 ^0C for 60 minutes prior to being coated with SiO_2 by the industrial method in NASA center. While the 140 nm powders were first vacuum treated at 850 ^0C and then sol-gel coated by the conventional method.

$TEOS$ (Aldrich Chemistry CO.) were used to make a coating by the sol-gel method. BTO powders were mixed with ethanol, and then acetic acid was added to the solution for adjusting the pH and increasing the surface reactivity while being stirred at room temperature to form a suspended solution. In the final steps of synthesizing process, calculated amount of $TEOS(Si(OC_2H_5)_4)$ has been added to obtain SiO_2 concentration of 9.1 $wt\%$. This concentration, can form a coating layer of SiO_2 with an approximate thickness of 5 nm. The solution was then stirred and sonicated for 4 times. The ammonia was added to the final solution to reach a pH of 9 and then was stirred for 5 hours at 40 $^\circ C$ to form a gel coating. The final composites was washed six times by the ethanol to remove other reaction products. Composite powders were obtained by drying the solution at 120 $^\circ C$ to be ensure the complete ethanol evaporation.

The ceramic sample was fabricated by the spark plasma sintering (SPS) method. In this method, the powder was placed between graphite plates without the needs of green body

preparation. The SPS process starts with heating the powder by the rate of 100 ^0C/min to 950^0C and holding at that temperature for 2 min. Ramping the temperature with the rate of 50 ^0C/min to 1050 ^0C and holding for 5 minutes. Soak temperature was 1050 ^0C, and a direct current of about 1850 amps was applied to the sample at 1050 ^0C and at the end the current was turned off and the pressure released to zero.

The SPS samples were cut through their cross section and each half was divided into smaller pieces. The cutted samples were polished from outside surface to about 300 μm thickness, and they were coated with the gold electrode with a diameter of 2 mm. For the DSC test, the sample was broke to the powder. The impedance test was conducted by applying DC bias in a range of 40 Hz to 110 MHz. The temperature dependence of the sample was evaluated in the range of 0.01 Hz to 10 MHz by the temperature of -150 ^0C to 200 ^0C.

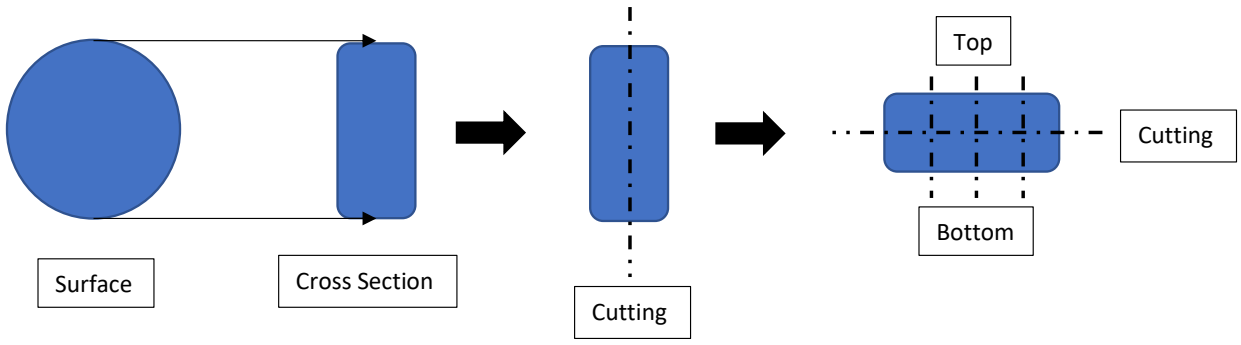

Figure 4.1: Schematic of SPS sample cutting.

4.3 Result and discussion

4.3.1 DSC

The following picture presents the DSC behavior of BT50 in range of -90 ^0C to 200 ^0C (Fig. 4.2). Two small peaks in heating and cooling pattern can be seen with a temperature of 116 ^0C and 108 ^0C, respectively. The peaks temperature is close to 120 ^0C is suggested to be as a phase transition of BTO which is altered by the coating and sintering process.

The sign of change in the structure of composites can be seen in the change in dielectric behavior of the sample and also the activation energy obtained by the conductivity. For temperatures lower than -50 ^0C the DSC result is not validated because they are close the minimum working temperature of the device.

On the other hand, the DSC pattern of BT14-SolGel-SPS sample shows no peaks (Fig. 4.3).

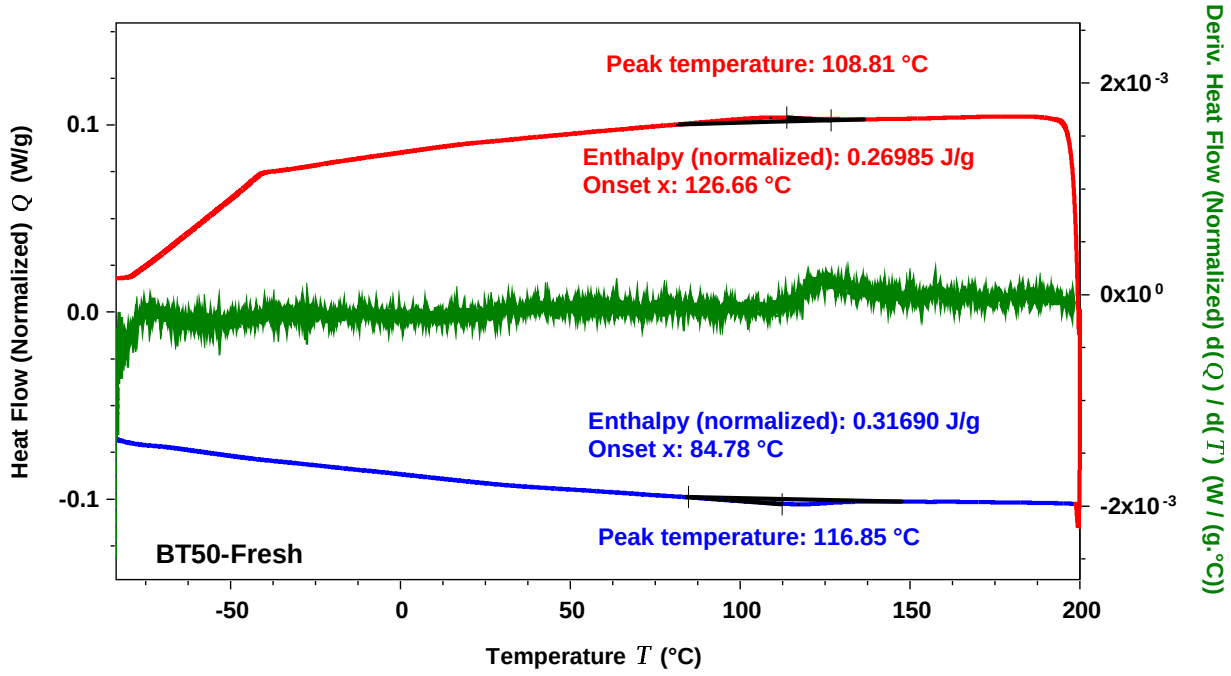

Figure 4.2: DSC pattern of BT50 Composite.

The derivation of heat flow by the temperature, proves that the there isn't any sudden change in the DSC pattern of the sample. The permittivity of BT14 is also validating this result because unlike BT50, the BT14SG sample shows no change in their permittivity behavior by increasing temperature. The increasing temperature even to 400 ^0C for this sample also has no sign of a peak in the pattern. The reason behind the difference between these two composites might be originated from fabrication and pretreatment process. First of all, the size of the powder is different, and the second difference comes from a pretreatment process which was performed at different environment and temperature. However, the most critical difference between these two composites comes from the thickness of SiO_2 which for BT14

is more than two times bigger than BT50 powder. This difference might result in hinder and cover the phase transition in the DSC pattern.

To better study and understanding the effect of SiO_2 on SPS sample properties and

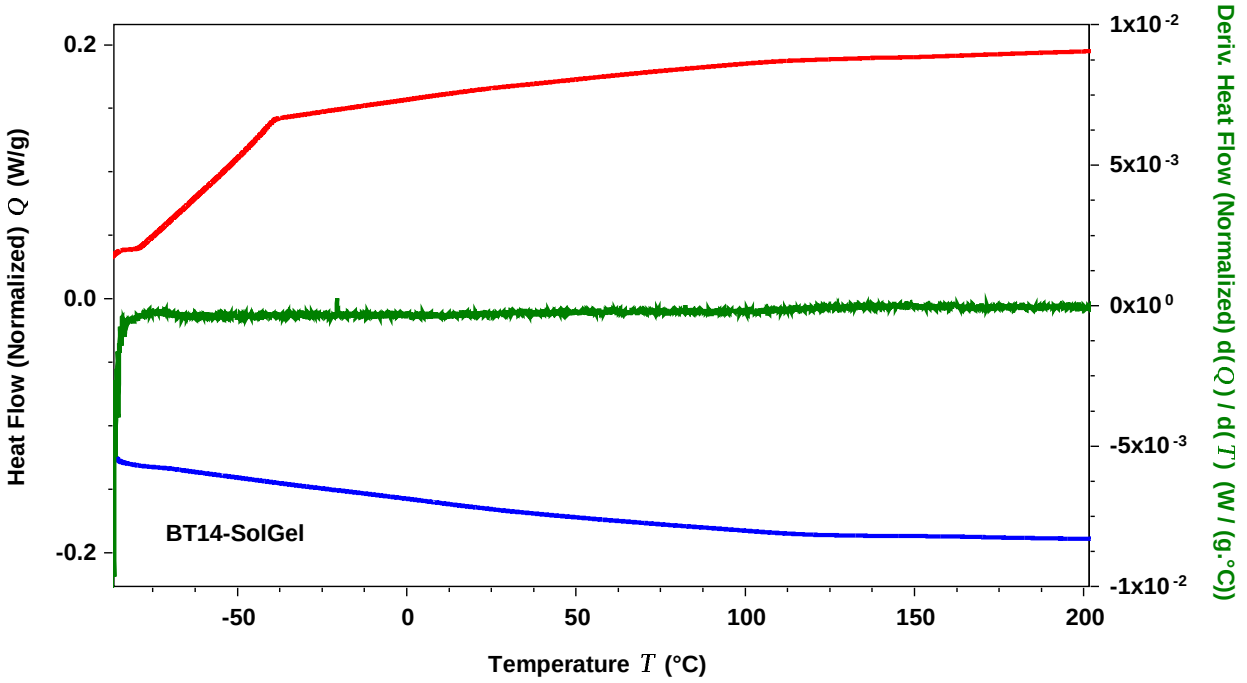

Figure 4.3: DSC pattern of BT14SG SPS Composite.

behavior, the DSC pattern of BT14 NC SPS sample was tested and showed in Fig. 4.4. It clearly can be seen that there is a peak around 110 ^0C which can easily be linked to the phase transition of BTO. The only difference between this sample and BT14 SG is the SiO_2 coating layer. It can be concluded that the SiO_2 layer causes the absent of phase transformation in the DSC result.

4.3.2 Dielectric properties

The dielectric behavior of SPS sample of BT50 is shown in the following Fig. 4.5 which presents the dielectric of $7*10^5$ in a frequency of 100 Hz. The effect of DC bias on the sample was tested in a range of 40 to 110 MHz. The applying voltage starts from a small voltage of 0.2 V to the high voltage of 1.5 V which affected the permittivity behavior. At the low

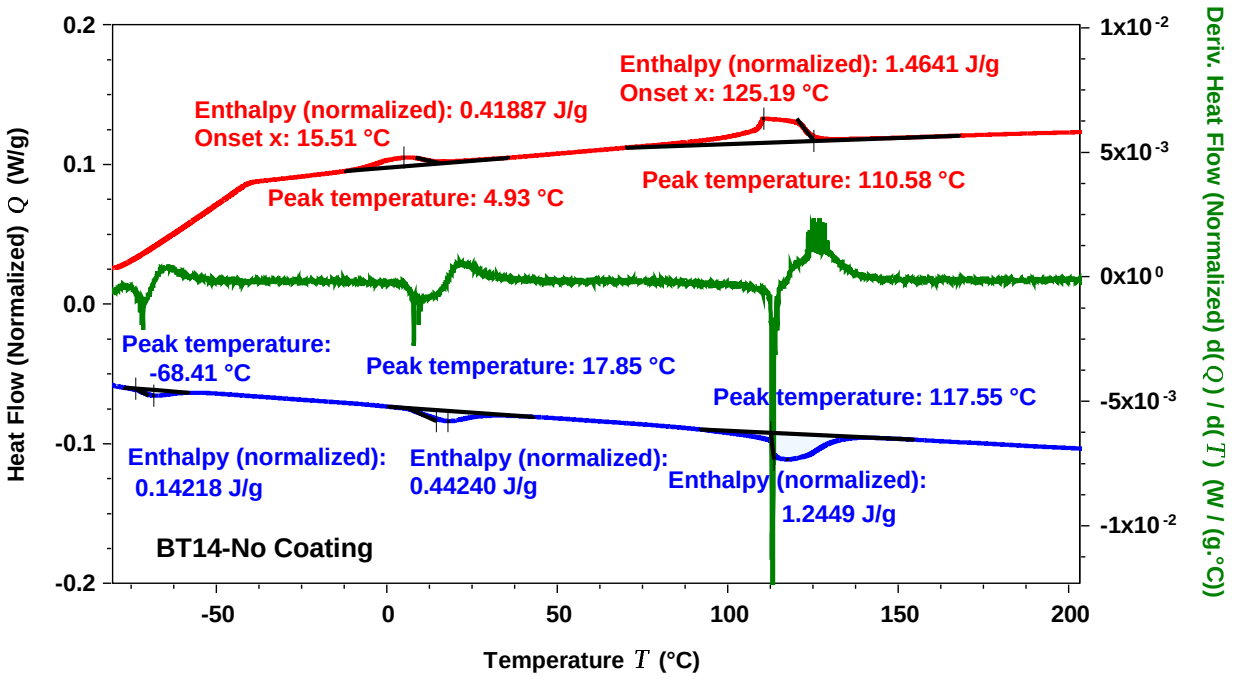

Figure 4.4: DSC pattern of BT14NC SPS Composite.

applied voltage, there is a slight rise in the dielectric spectrum at the low-frequency range. However, by increasing the value of applied DC voltage, the dielectric spectrum shifted to the downside, and more of the frequency range is being affected. After using 1.2 volts, the dielectric spectrum starts from a negative value at 40 Hz, and this behavior continues and gets to more negative by applying higher voltage to the sample.

The Fig. 4.6 shows the dielectric loss of the BT50 sample. At zero bias, the dielectric loss is about 20 at 40 Hz frequency, but it decreases by the frequency and gets to the minimum of value of 0.3 at 10^4 frequency. The spectrum shows a relaxation type peak in a frequency range between 10^6 to 10^7. By applying the DC voltage, the dielectric loss slightly decreases but start to increase by further increasing the voltage. When the voltage reached 1.2 volts the dielectric loss pass, 1000 and the peak corresponded to negative dielectric shows up. The peak starts to shift to a higher frequency by adding more DC bias to the sample. It should be mentioned that the effect of DC bias is more on the low-frequency range than the high range. When the frequency is higher than 10^5, the DC bias has no influence on the dielectric

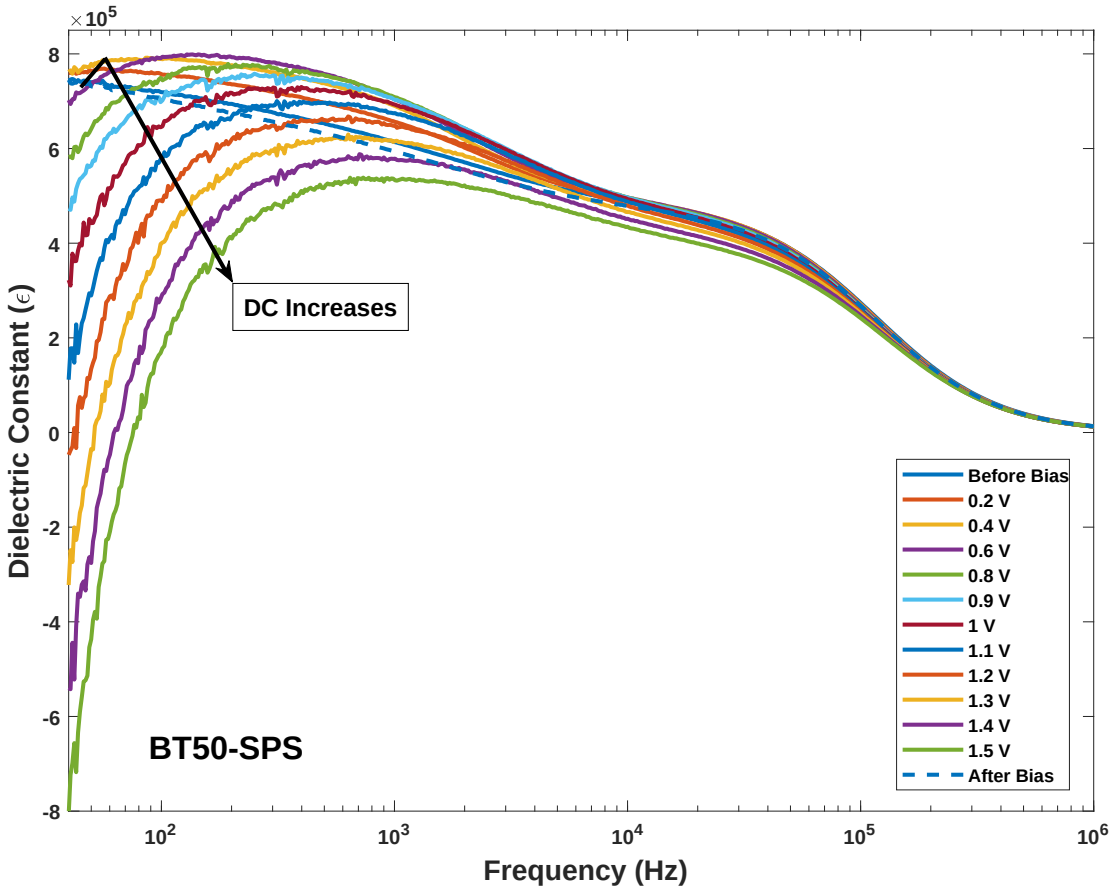

Figure 4.5: Effect of DC bias on permittivity of BT50 SPS sample.

loss.

The Fig. 4.7 and 4.8 shows the detailed effect of DC bias on the value of permittivity and loss of sample BT50 for each frequency. It shows a decrease in the dielectric loss by shifting the plasma frequency to a higher frequencies. On the other side, the peak on a permittivity of each frequency moves to a higher voltage by increasing the frequency.

The change of conductivity of sample BT50 can be seen in Fig. 4.9. The AC conductivity of sample starts by a vertical line which can count as a DC conductivity. The AC conductivity hold the value of $7 * 10^{-3}$ until about 500 Hz. The AC conductivity follows the universal power law (Aw^n) exhibit in increase in the conductivity by the increasing frequency. By applying the DC bias the DC conductivity to a higher value and reach to 10 times bigger than without bias conductivity. The change in DC conductivity is not only on the amount

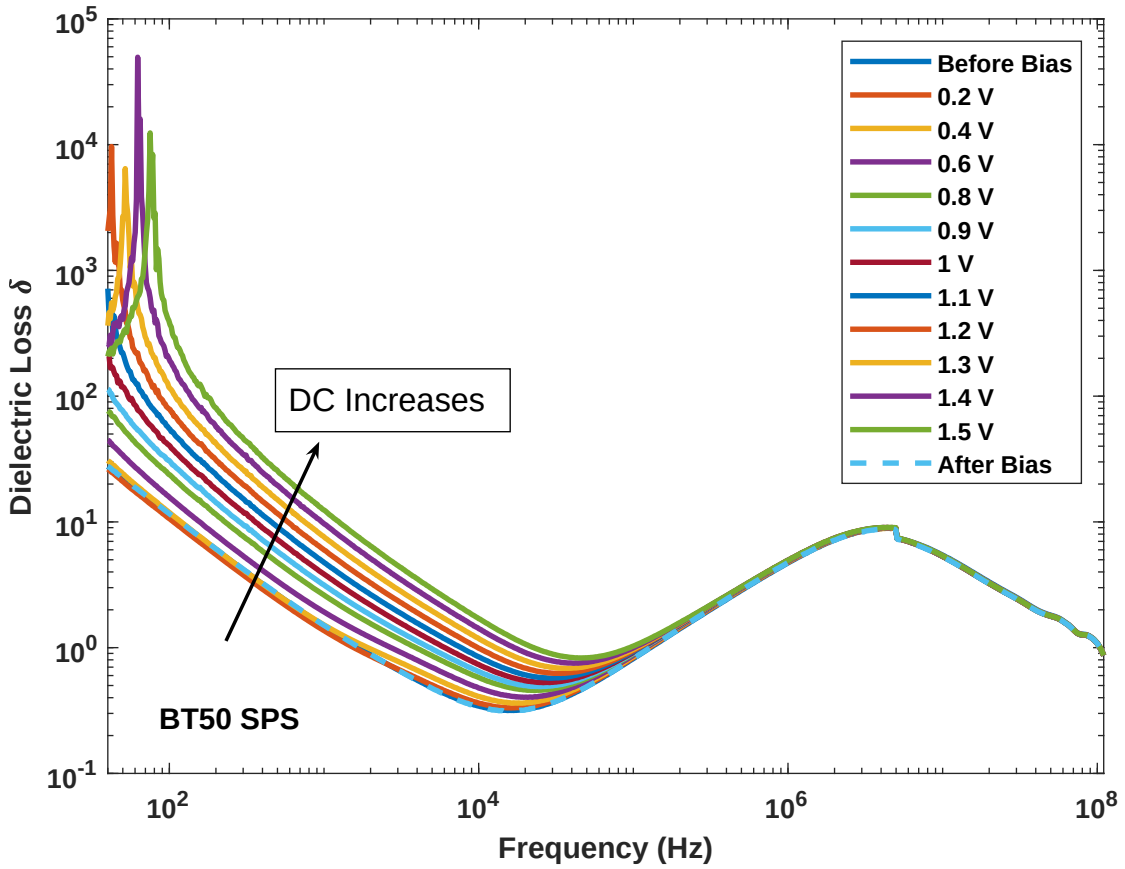

Figure 4.6: Effect of DC bias on dielectric loss of BT50 SPS sample.

of it, but also the frequency range shifted to a higher frequency and reach to more than 10^4. The Imaginary dielectric constant show two different regions separated by the peak related to relaxation (Fig. 4.10). The low-frequency part affected by increasing the DC bias and the imaginary part jumped to a higher value but kept the behavior of it. Meanwhile, the peak and after the peak part of the imaginary dielectric constant is unchanged by DC bias.

Plasma Frequency: Effect of DC bias

The negative permittivity obtained by applying the DC bias has Drude like behavior. It is known the frequency which permittivity change from negative values to positive values known as plasma frequency. The result shows the dependence of plasma frequency to the magnitude of DC bias. To better understand the result and the behavior of the sample lets

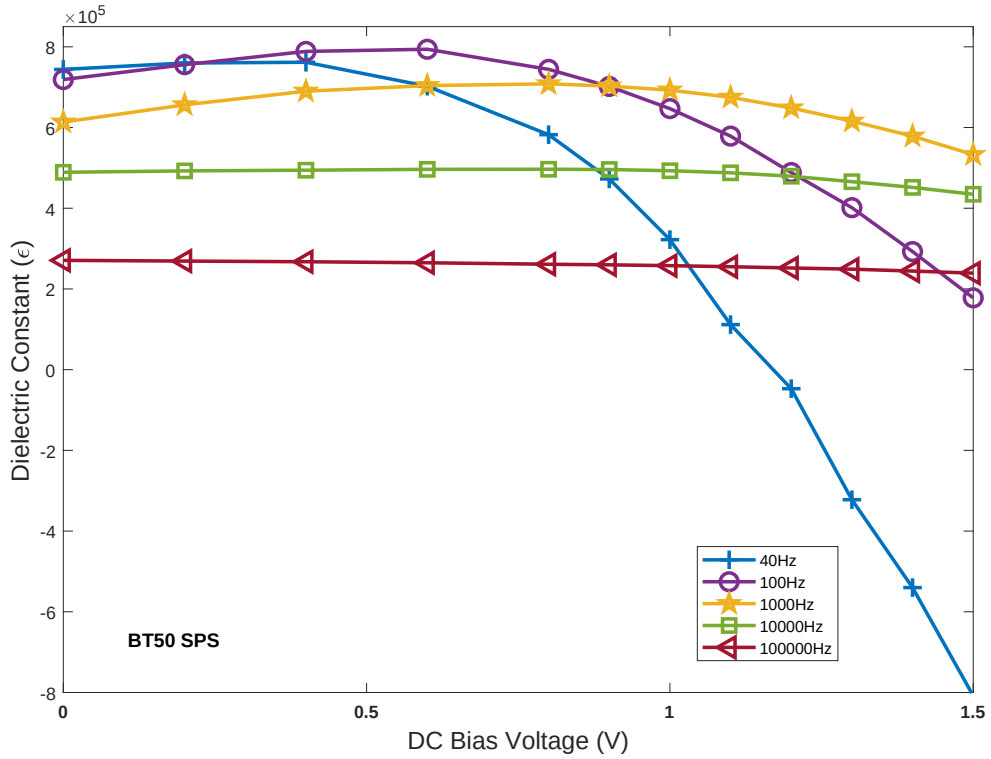

Figure 4.7: Effect of DC bias on dielectric Constant of each frequency of BT50 SPS sample.

have a close look at the Drude equation for plasma frequency and try to fit the data by this formula. The Drude equation for the composites can be affected by the other mechanism permittivity and rewrite as follows:

$$\varepsilon' = 1 - \frac{\omega_p^2}{\omega^2 + \gamma^2} \rightarrow \varepsilon' = Const - \frac{\omega_p^2}{\omega^2 + \gamma^2} \rightarrow \tag{4.1}$$

For fitting the above equation with the data, the following assumptions should be used:

$$1) Y = C + a * X^b \rightarrow C = Const, a = -\omega_p^2, b = -2, \gamma^2 << \omega, Y = \varepsilon', X = \omega \tag{4.2}$$

As it can see from follow fitting pictures (Fig. 4.11, Fig. 4.12), the fitting has very good match with the data. By this method, the constant can be calculated which is present the positive value of permittivity. Moreover, the plasma frequency obtained by the fitting has a value much bigger than the actual frequency that the permittivity shifted from negative to

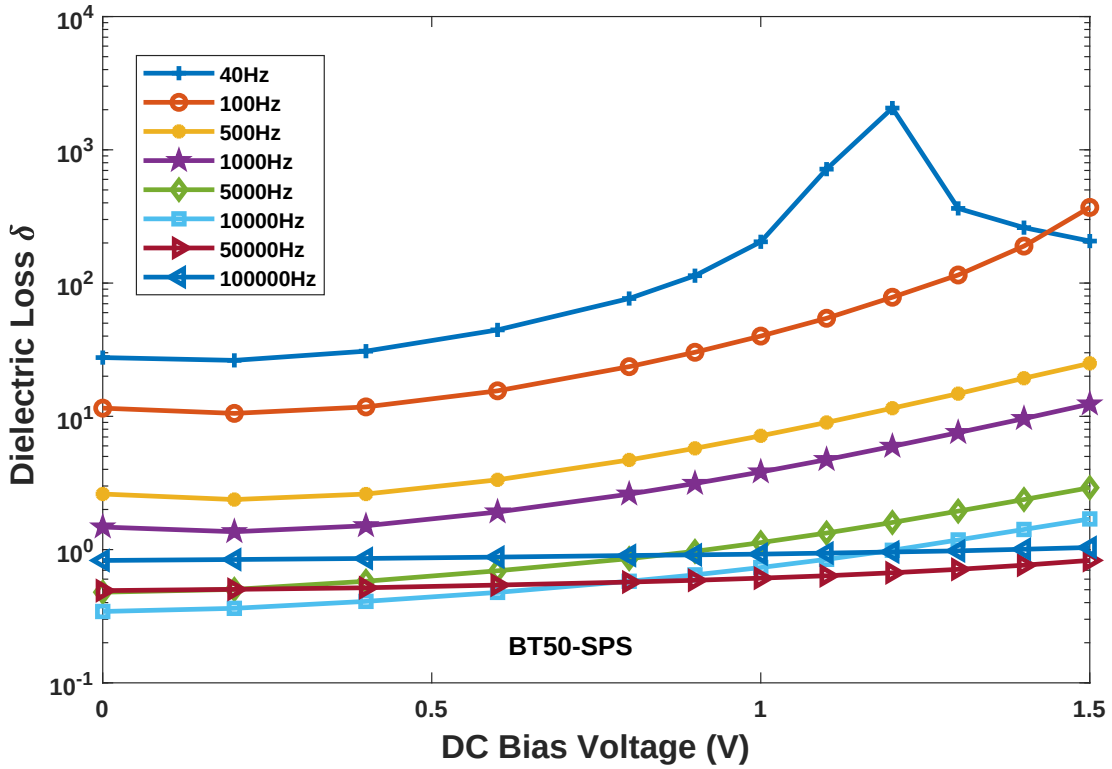

Figure 4.8: Effect of DC bias on dielectric loss of each frequency of BT50 SPS sample.

positive. This behavior is because of the influence of other mechanisms on the behavior of permittivity.

Although the above figures show proper fitting, the assumption was made base on that the damping frequency should be much smaller than frequency. Moreover, the fitting data shows different value for frequency power than what is suppose to be. These uncertainties can be take over by rewriting the equation in another shape as it comes in the following formula:

$$Const - \varepsilon' = \frac{\omega_p^2}{\omega^2 + \gamma^2} \rightarrow \frac{1}{Const - \varepsilon'} = \frac{\omega^2 + \gamma^2}{\omega_p^2} \rightarrow \frac{1}{Const - \varepsilon'} = \frac{1}{\omega_p^2} * \omega^2 + \frac{\gamma^2}{\omega_p^2} \rightarrow \quad (4.3)$$

The new fitting has been attempted by use of the new formula base in the following parameter:

$$2) Y = aX + b \rightarrow a = \frac{1}{\omega_p^2}, b = \frac{\gamma^2}{\omega_p^2}, X = \omega^2, Y = \frac{1}{Const - \varepsilon'} \quad (4.4)$$

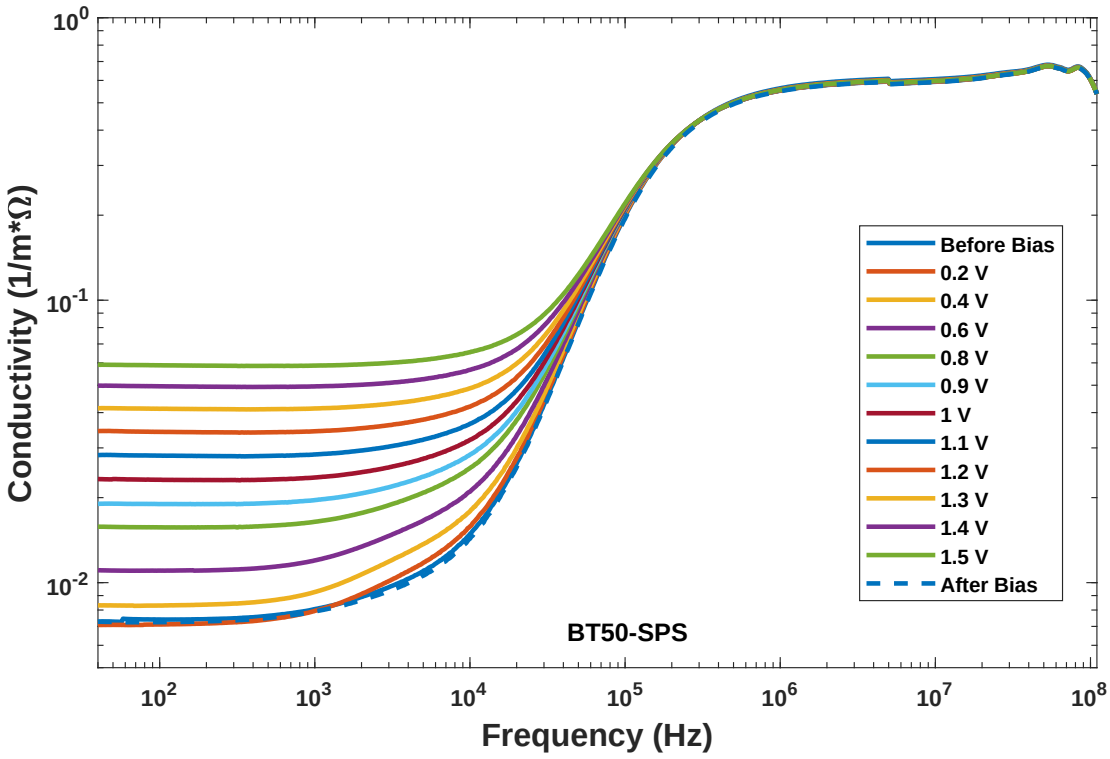

Figure 4.9: Effect of DC bias on Conductivity of BT50 SPS sample.

The fitting of the permittivity of BT50 sample on the influence of DC bias based on a new formula is showed in Fig. 4.14 and Fig. 4.13. The fitting shows a perfect match to the data for the frequencies near to zero permittivity plus the constant and the plasma frequency are almost similar to the previous fitting. By this formula, the damping frequency can be calculated and complete the fittings. It should be mentioned that the small mismatch in high frequency is due to affected other mechanisms on the behavior of permittivity.

The Drude like behavior not only present the equation for permittivity but also the imaginary part of dielectric constant has a relationship with plasma frequency and damping frequency. The imaginary part can be fitted perfectly by the power factor as the following equation.

$$1) Y = a * X^b, Y = \varepsilon'', X = \omega, b = -1, a = \gamma?! \tag{4.5}$$

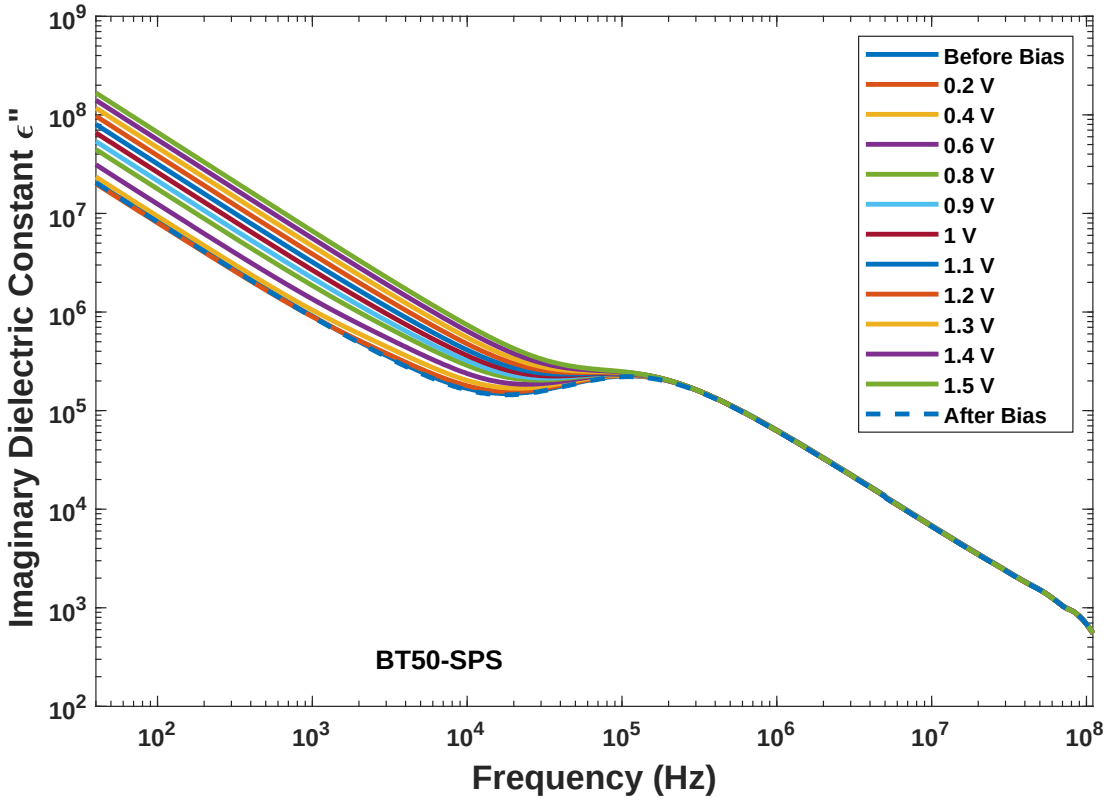

Figure 4.10: Effect of DC bias on imaginary dielectric constant for each frequency of BT50 SPS sample.

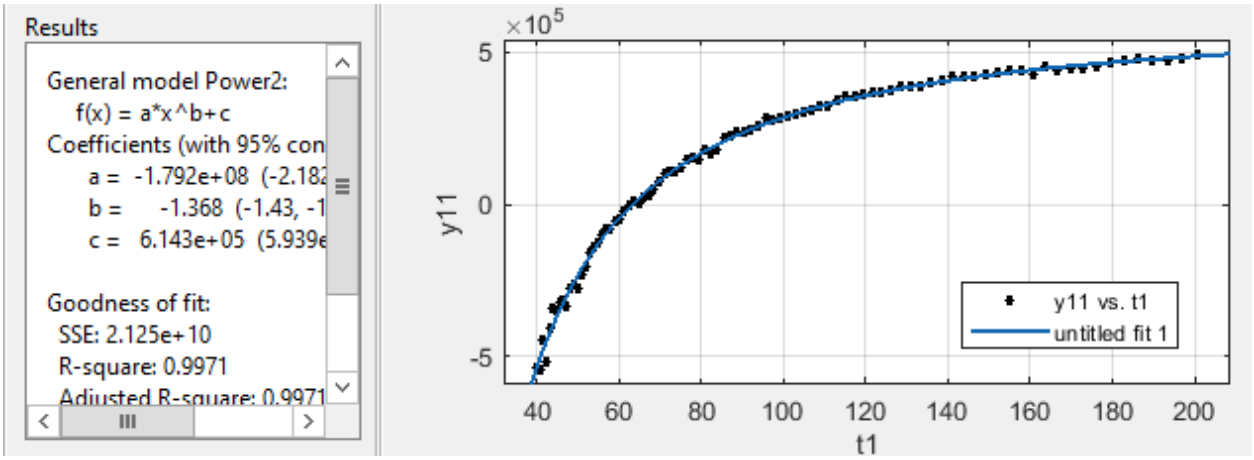

Figure 4.11: Fitting model 1 of negative permittivity with DC bias of 1.4 V.

It can clearly be seen the model fit the data with perfect match in following pictures (Fig. 4.16, Fig. 4.15). However, there is uncertainty about the model and parameter of this

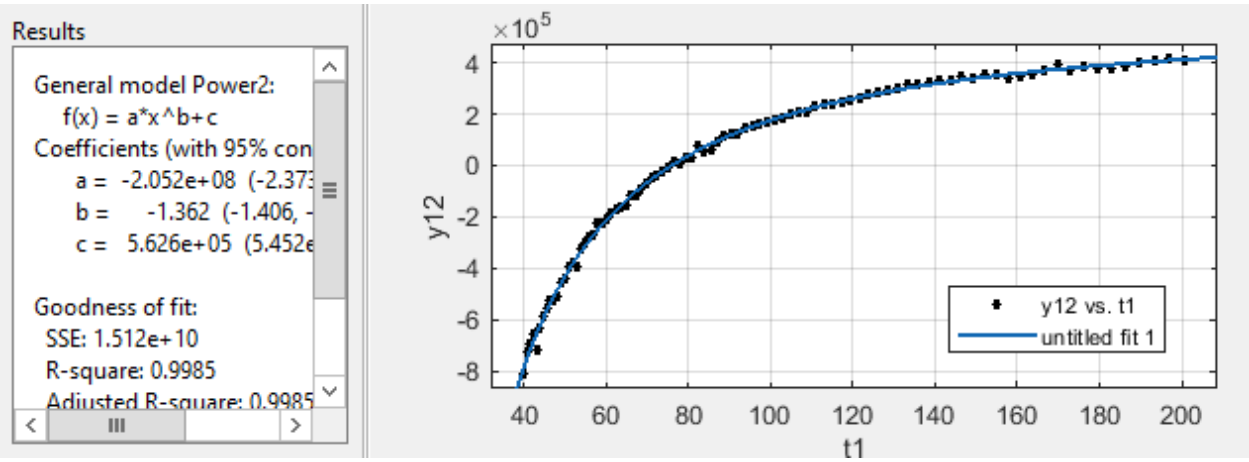

Figure 4.12: Fitting model 1 of negative permittivity with DC bias of 1.5 V.

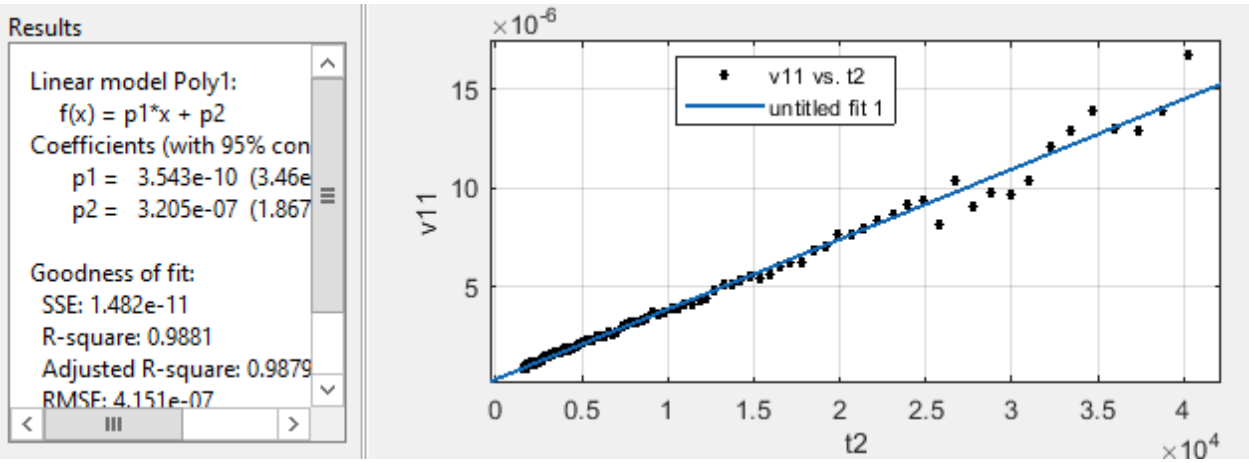

Figure 4.13: Fitting model 2 of negative permittivity with DC bias of 1.4 V.

fitting which makes use of other system and models.

The following equations are tried to find a better model to describe and fit the imaginary part data. To do so the imaginary part of the Drude model has been rewritten again in the following equations:

$$\varepsilon'' = \frac{\gamma}{\omega} * \frac{\omega_p^2}{\omega^2 + \gamma^2} \rightarrow \frac{1}{\varepsilon''\omega} = \frac{\omega^2 + \gamma^2}{\gamma\omega_p^2} \rightarrow \frac{1}{\varepsilon''\omega} = \frac{1}{\gamma\omega_p^2} * \omega^2 + \frac{\gamma}{\omega_p^2} \tag{4.6}$$

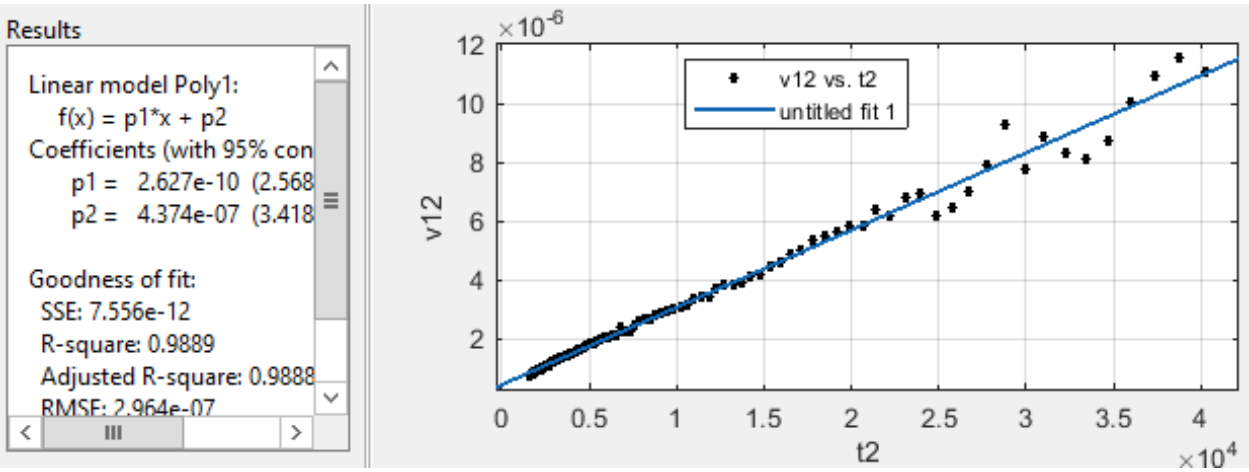

Figure 4.14: Fitting model 2 of negative permittivity with DC bias of 1.5 V.

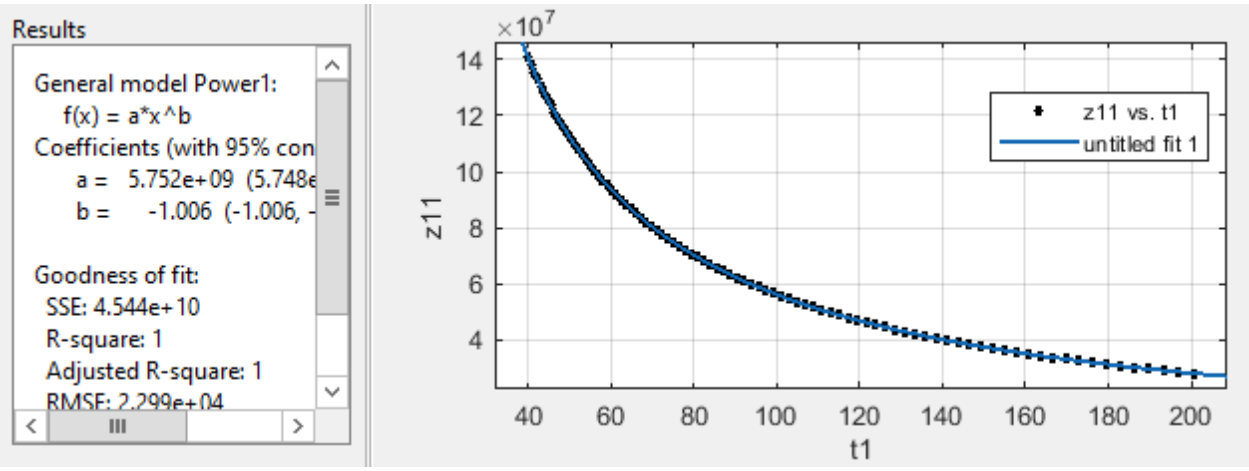

Figure 4.15: Fitting data 1 of Drude like imaginary dielectric constant with DC bias of 1.4 V.

$$2) Y = aX + b, a = \frac{1}{\gamma\omega_p^2}, b = \frac{\gamma}{\omega_p^2}, X = \omega^2 \tag{4.7}$$

The fitting result of above equation comes in following pictures (Fig. 4.18, Fig. 4.17). The fitting is just accurate in the low-frequency range, especially before plasma frequency. However, the fitting is not perfect compared to the first model.

To overcome the obstacle with the first two models, the new look at the Drude equations and rewrite them is needed.

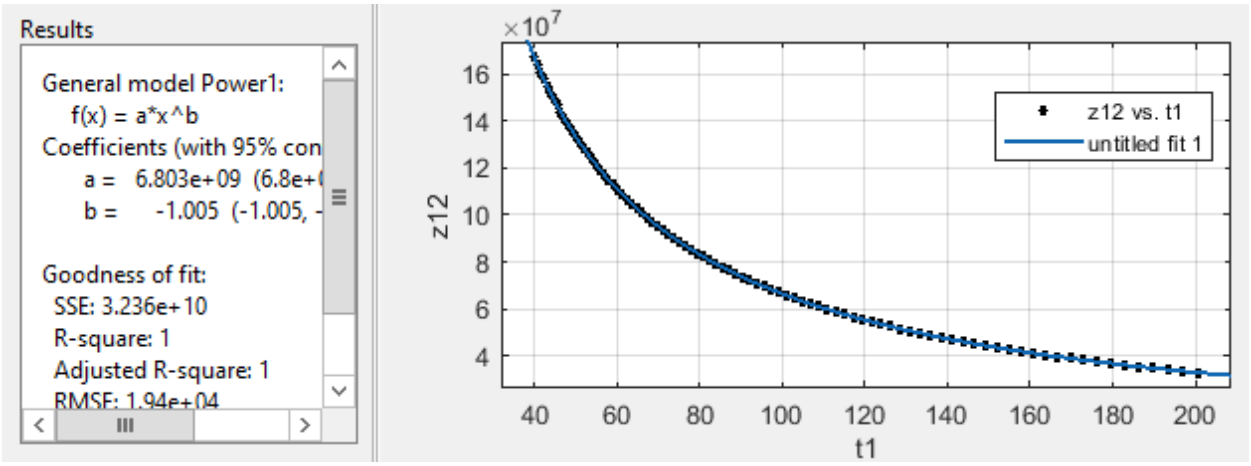

Figure 4.16: Fitting model 1 of Drude like imaginary dielectric constant with DC bias of 1.5 V.

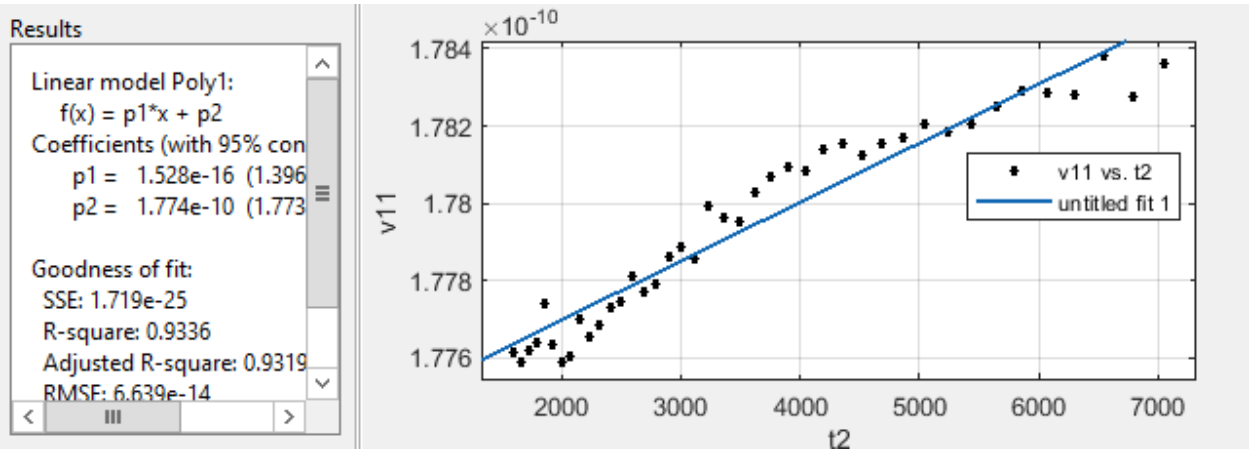

Figure 4.17: Fitting model 2 of Drude like imaginary dielectric constant with DC bias of 1.4 V.

$$\frac{1}{\varepsilon''} = \frac{1}{\gamma\omega_p^2} * \omega^3 + \frac{\gamma}{\omega_p^2} * \omega \tag{4.8}$$

$$3) Y = aX^3 + bX, a = \frac{1}{\gamma\omega_p^2}, b = \frac{\gamma}{\omega_p^2}, X = \omega \tag{4.9}$$

The new model fitted the imaginary dielectric data but it is valid if it was assumed the a value is close to zero. The following picture (Fig. 4.20, Fig. 4.19) which shows the fitting

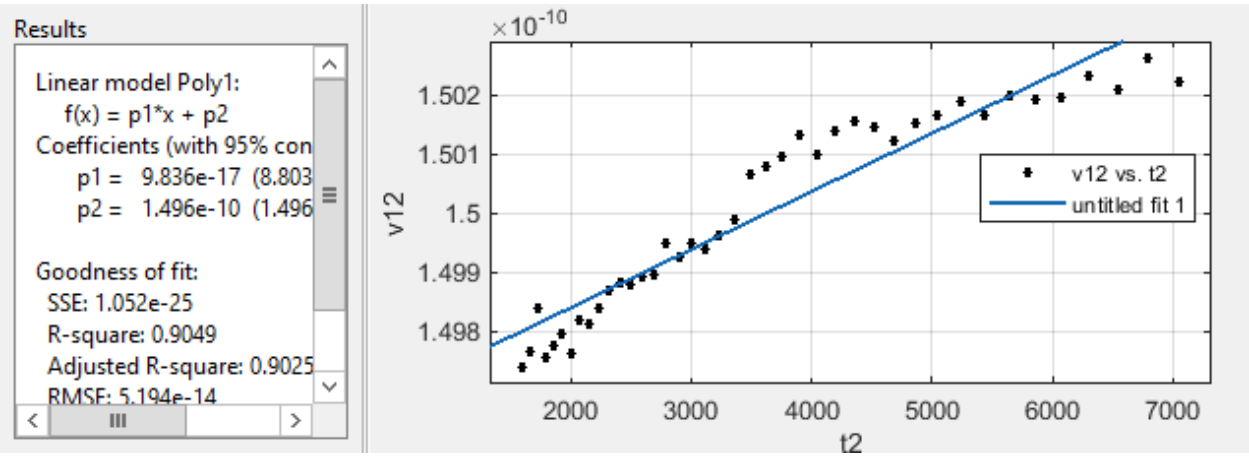

Figure 4.18: Fitting model 2 of Drude like imaginary dielectric constant with DC bias of 1.5 V.

parameter of this model shows a perfect match if we could consider this assumption.

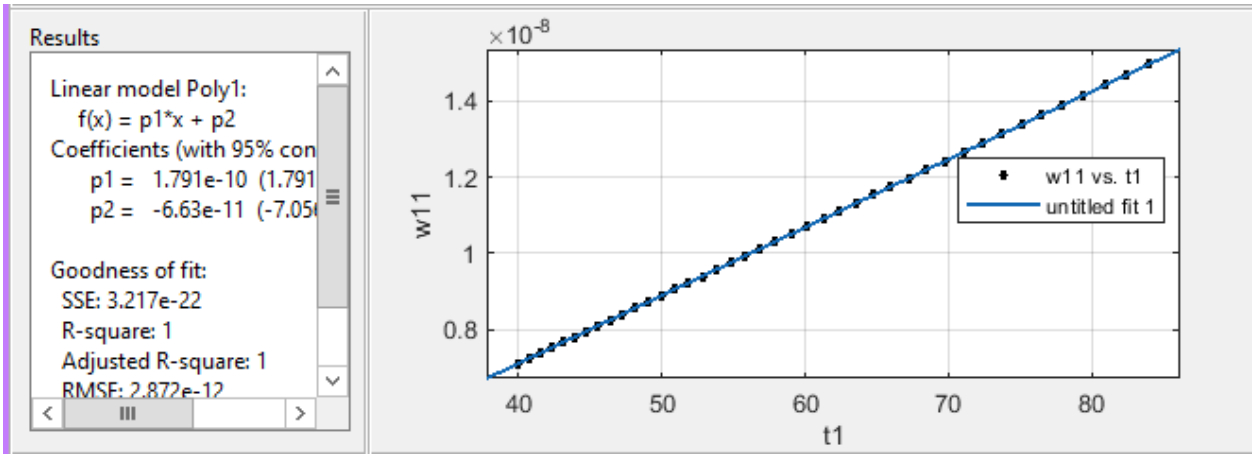

Figure 4.19: Fitting model 3 of Drude like imaginary dielectric constant with DC bias of 1.4 V.

The data fitting reported in the above equations and pictures for imaginary dielectric constant make to look at the Drude model in another way. The conductivity results show that for this sample, the relationship between current density J and electrical field E is not linear. So the conductivity is not constant and is a function of the applied electrical field.

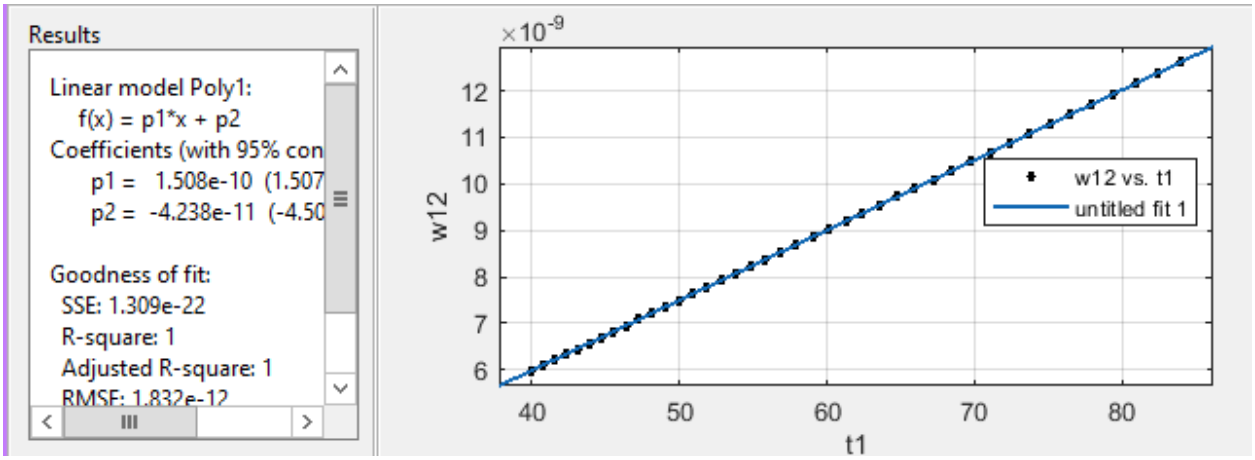

Figure 4.20: Fitting model 3 of Drude like imaginary dielectric constant with DC bias of 1.5 V.

It means that, similar to the tunable composite which its conductivity can be alter and significantly increases by the microstructure and filler content, in our system this phenomenon can be reached by applying DC bias to the sample. On the other hand, based on the Drude model, the damping frequency is dependent on DC conductivity:

$$\gamma = \frac{\varepsilon_0 \omega_P^2}{\sigma_{dc}} \tag{4.10}$$

That means by changing conductivity the value of plasma frequency and damping frequency will be altered significantly. It can be estimated that by increasing conductivity both plasma and damping frequency increases which this behavior can be explained the emerging zero permittivity behavior and shifting to a higher frequency by applying higher DC bias.

Previously was mentioned that the imaginary dielectric constant dominated by two-part, one correspond two the polarization mechanism and the other one is related to the conductivity. As it was known that in low frequency the conductivity would rule the imaginary part and especially in this system which the applied DC bias make the DC conductivity much bigger value so the imaginary part can rewrite as the following equation:

$$\varepsilon'' = \frac{\sigma_{dc}}{\omega\varepsilon_0} \rightarrow \varepsilon'' = \frac{\varepsilon_0\omega_P^2/\gamma}{\omega\varepsilon_0} \tag{4.11}$$

$$\varepsilon'' = \frac{\omega_P^2}{\omega\gamma} \rightarrow \frac{1}{\varepsilon''} = \frac{\gamma}{\omega_P^2}\omega \tag{4.12}$$

This model can thoroughly explain the behavior of the imaginary part and also totally match with first and third fitting parameters.

4.3.3 Temperature dependence

The behavior of permittivity of sample BT50 in temperature range between -150 $°C$ to 200 $°C$ can be seen in Fig. 4.21 and Fig. 4.22. The frequency range starts from a low frequency of 0.01 Hz to a high frequency of 10^7 shows a wide spectrum of permittivity. It can be seen in both figures for all temperature range from -150 $°C$ to -70 $°C$ the permittivity shows just positive value. The negative value of permittivity start from -50 $°C$ and continued till temperature reach to 150 $°C$. The logarithmic scale of permittivity presented in Fig. 4.22 can illustrate the behavior of sample whole frequency range. The Dude like behavior of permittivity shows the plasma frequency as low as $4 * 10^{-2}$. By increasing temperature to a higher one, the plasma frequency shifted to a higher value. When the temperature passes the 100 ^{0}C and reaches to 110 ^{0}C, the dielectric behavior change and Drude like behavior change to Lorentz like behavior. For 110 ^{0}C, the positive to negative change start at $8 * 10^{-2}$ and plasma frequency reach more than 10. The same response can be seen in 130 ^{0}C, permittivity spectrum by a significant shift in positive to negative frequency $6 * 10^{-1}$ but a small change in plasma frequency. The next figures (4.23, 4.24) represent how the logarithmic scale of permittivity for each frequency change by the temperature. The spectrum of each frequency shows almost 3 or 4 types of machines in the temperature range. For low frequencies which included 0.01 Hz to 10 Hz, the permittivity increases to a higher value and then shifted to a negative value and at the end of range moved up again to positive and increase for higher

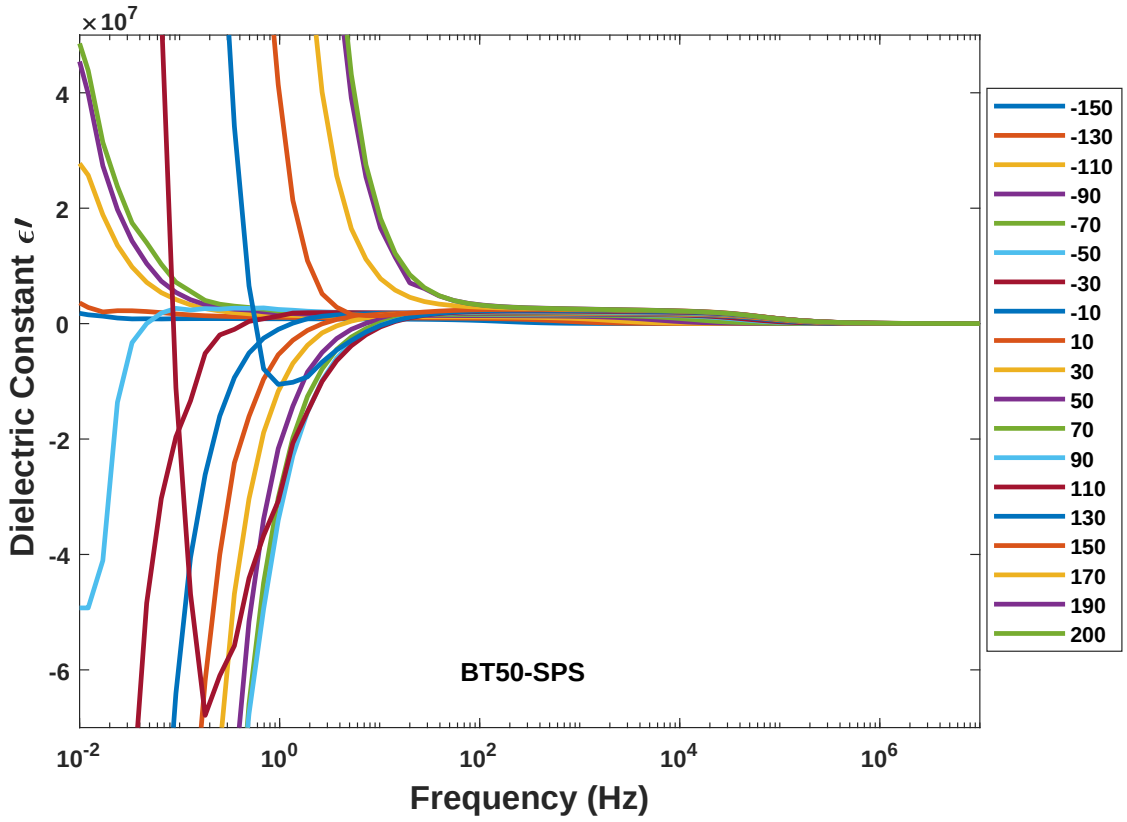

Figure 4.21: Effect of temperature on permittivity of BT50 SPS sample.

temperature. When the frequency increases, the negative range moved to a higher temperature; while, the temperature period becomes smaller. By increasing the temperature, the permittivity value becomes smaller for both positive and negative range. The Fig. 4.24 is used to better present the dielectric behavior of higher frequencies more than 10. For low temperature, the permittivity sharply increase by temperature, but for the medium temperature range, the permittivity slightly increases. At high temperature, the permittivity has another jump at very high temperature, but such behavior is gone for frequency bigger than 1000 Hz. The sharply decrease in whole temperature change for the frequency higher than 10^4. The dielectric loss of the sample at a different temperature can be seen in Fig. 4.25. The debye like relaxation peak at high frequency can be clearly be seen, and it is moving to a higher frequency by increasing temperature. The magnitude this peak start to rise at -70 ^0C and reach to the maximum at 30 ^0C and decreases by further increasing temperature. On

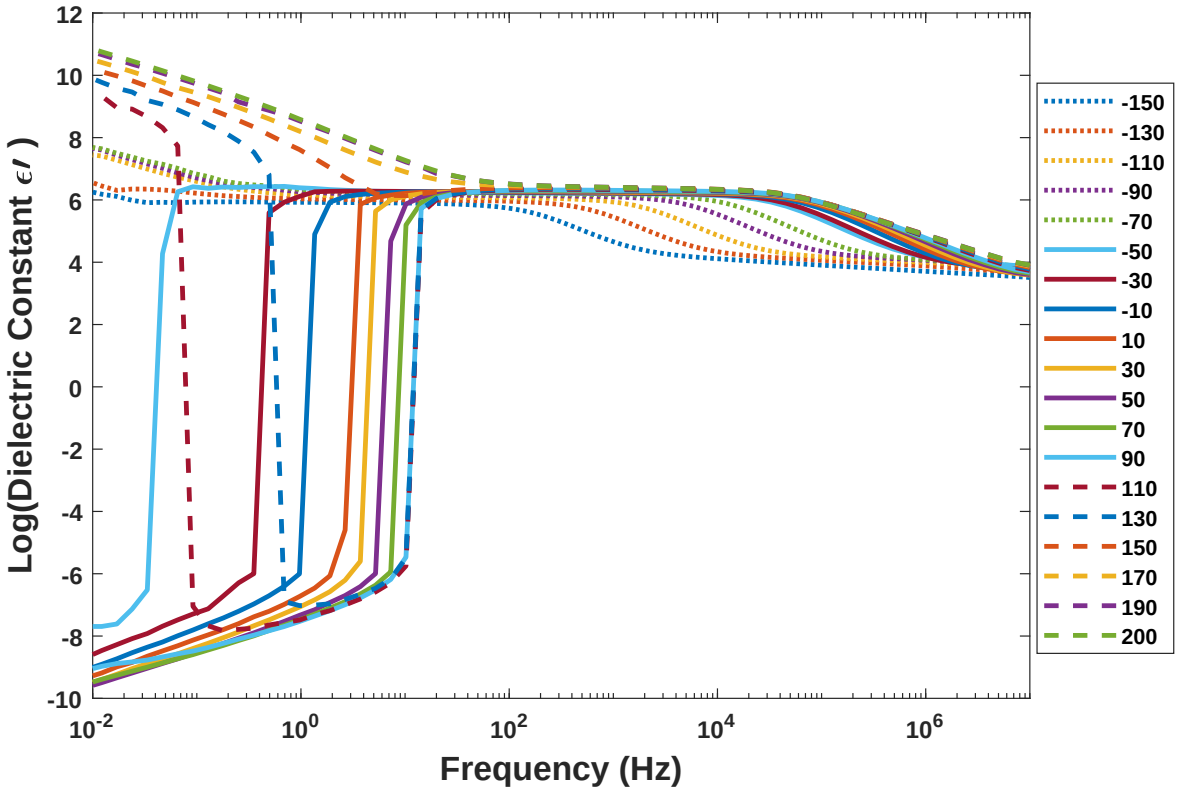

Figure 4.22: Effect of temperature on permittivity of BT50 SPS sample in logarithmic scale.

low-frequency region, there is another peak like mechanism start at low temperature. The smooth peak shapes change to the sharp peaks by emerging negative behavior and continued to shift to a higher frequency by increasing temperature. Finally, at a temperature of 170 ^0C and above the smooth like peak showed up again.

It can be seen a better effect of temperature on each frequency in Fig. 4.26. For all frequencies the behavior has two peaks around -70 ^0C and 120 ^0C which presents the temperature which Drude like behavior started and ended. By increasing the frequency value, the size of those two peaks reduced and at 100 Hz it can rarely be seen in the plot.

The universal power law is dominated by the conductivity of the sample for each temperature (Fig. 4.27). For each temperature, the conductivity spectrum starts with almost constant DC conductivity and continued by the increase by a power of frequency. It is like

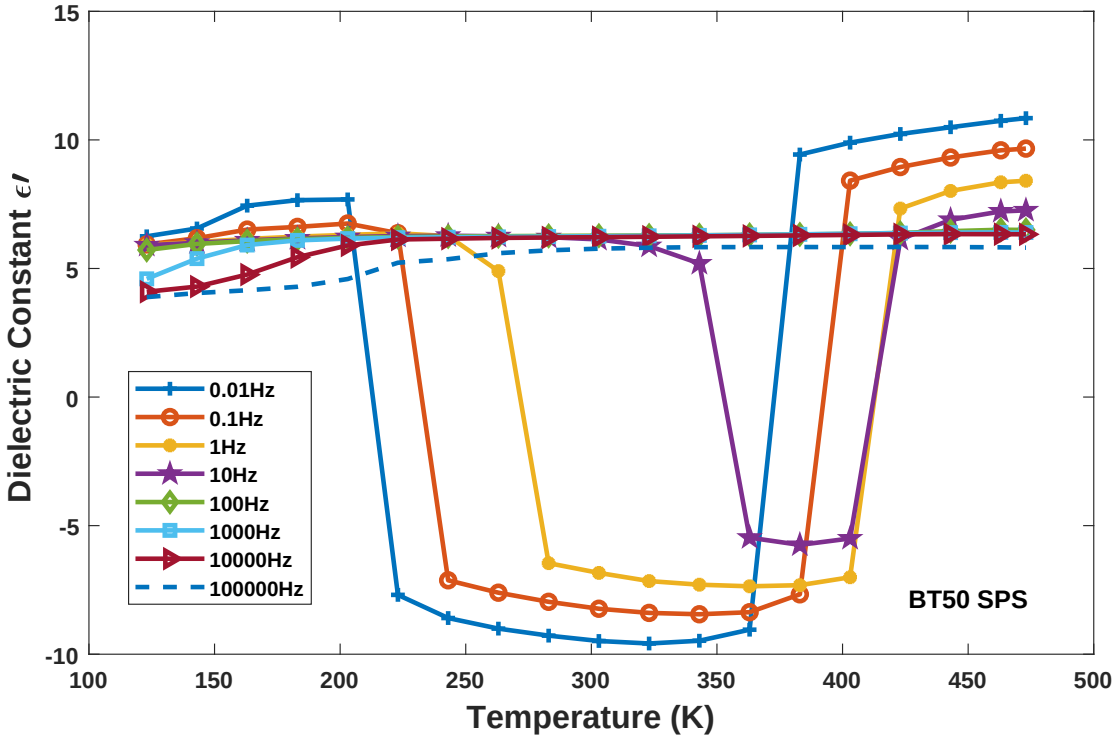

Figure 4.23: Effect of temperature on permittivity for each frequency of BT50 SPS sample in logarithmic scale.

the frequency of start of power behavior is corresponded to Debye-like relaxation in a dielectric loss which moves to a higher frequency by increasing temperature. Not only the shift in mechanism but also the magnitude of conductivity increases significantly by the temperature.

By plotting the magnitude of conductivity for each frequency at different temperature the Fig. 4.28 can be obtained. It can clearly show the behavior of conductivity and also its value is almost similar for the low-frequency range. The higher frequency shows different behavior due to response to the relaxation process.

To investigate mechanism ruled the conductivity, the conductivity of 0.1 and 100 Hz frequencies plotted based on reciprocal order of temperature. The figures (4.23, 4.24) shows the trend of conductivity can be slipped in two lines with different slop which corresponds

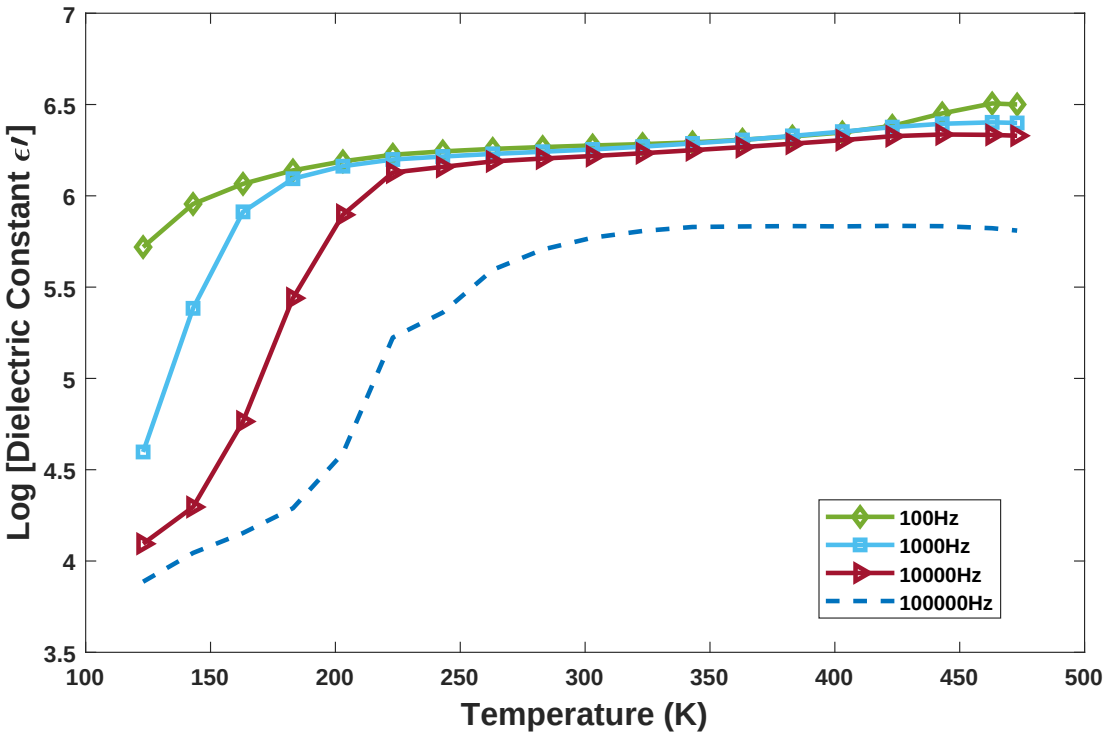

Figure 4.24: Effect of temperature on permittivity for each frequency of BT50 SPS sample in logarithmic scale.

to DC conductivity of the sample. Such a behavior suggested the domination of two mechanisms which at low to medium temperature with the activation energy of 0.08 eV and at a temperature higher than 120 ^0C with the activation energy of 0.2 eV.

$$\sigma_{dc} = \sigma_0 exp(\frac{-E_a}{kT}) \tag{4.13}$$

$$ln(\sigma_{dc}) = ln(\sigma_0) + \frac{-E_a}{kT} \tag{4.14}$$

The imaginary part of dielectric constant in different temperature shows in the following picture (Fig. 4.31). The relaxation like a peak in medium range frequency can be seen in all temperature and move to higher on by rising in the temperature. In low-frequency range, the imaginary part of dielectric constant has linear behavior by the logarithmic scale. This

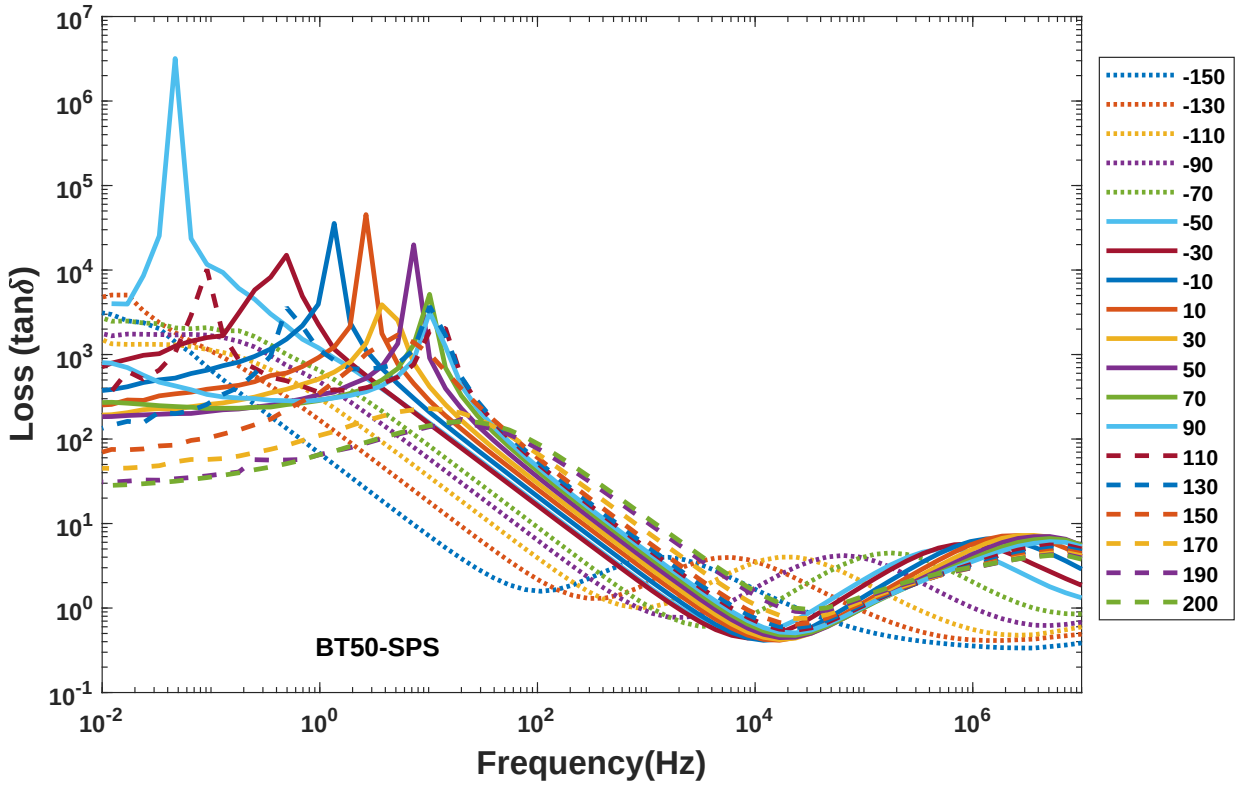

Figure 4.25: Effect of temperature on dielectric loss of BT50 SPS sample in logarithmic scale.

Table 4.1: Activation energy of conductivity of BT50 sample.

	0.1 Hz	
Temperature	**Activation Energy E_a (eV)**	σ_0
150 ^0C to 200 ^0C	0.422	712.37
-150 ^0C to 130 ^0C	0.186	1.43
	100 Hz	
Temperature	**Activation Energy E_a (eV)**	σ_0
150 ^0C to 200 ^0C	0.539	23458
-150 ^0C to 130 ^0C	0.175	0.884

behavior suggests the linear relationship with the reciprocal of frequency. Such a behavior suggested the conductivity related part of the imaginary dielectric constant ($\sigma_{dc}/\omega\epsilon_0$) is dominated in the low-frequency range.

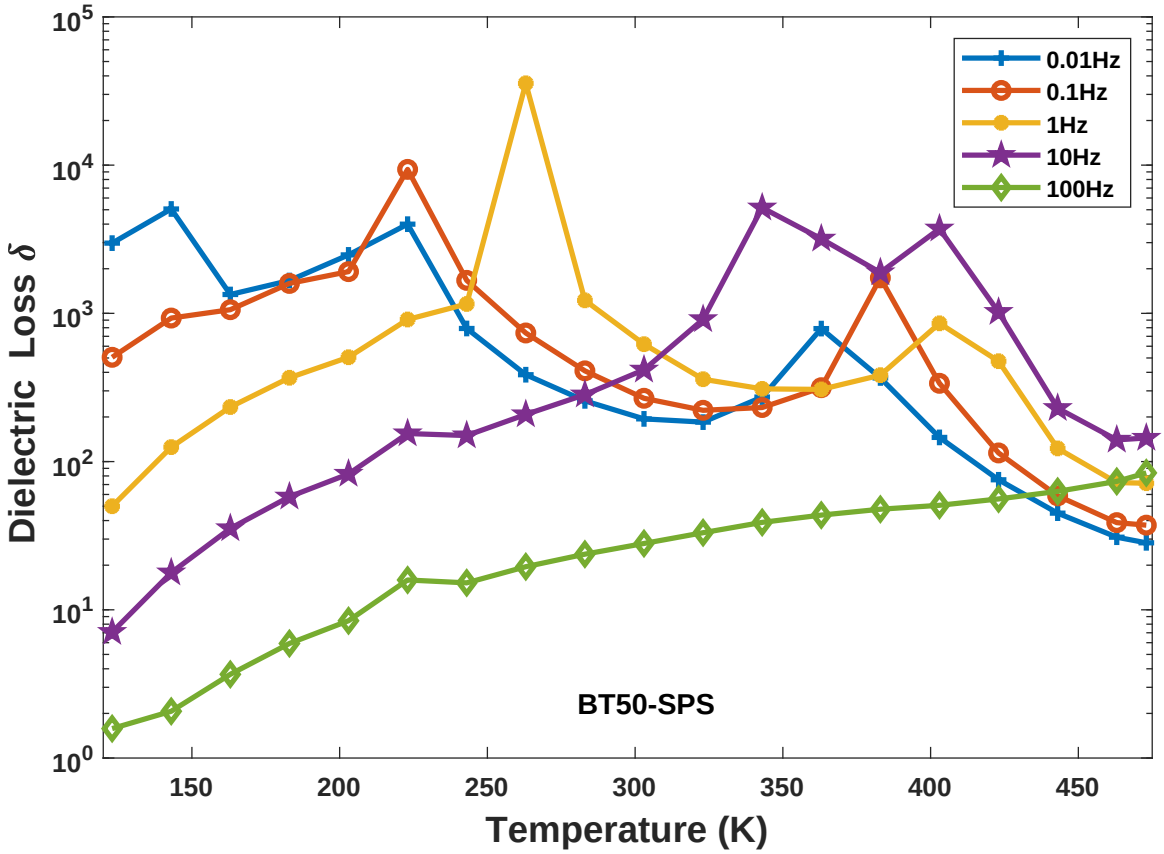

Figure 4.26: Effect of temperature on dielectric loss of each frequency of BT50 SPS sample in logarithmic scale

Drude model fitting in different Temperature

In the previous section, the negative behavior of the dielectric was fitted based on the Drude model. The negative response was posses by applying external DC Bias to the sample. However, in frequency range low to 10^{-2} sample shows negative permittivity in different temperatures. The behavior of the sample is analyzed by fitting those data by Drude models and the plasma frequency, damping frequency, and transition frequency.

Based on this fitting, the plasma frequency and damping frequency can be calculated. The following table presents the fitting parameter for all temperature range and their fitting with R^2 bigger than 0.996 which is obeying the Drude model and fitting formula. The transition

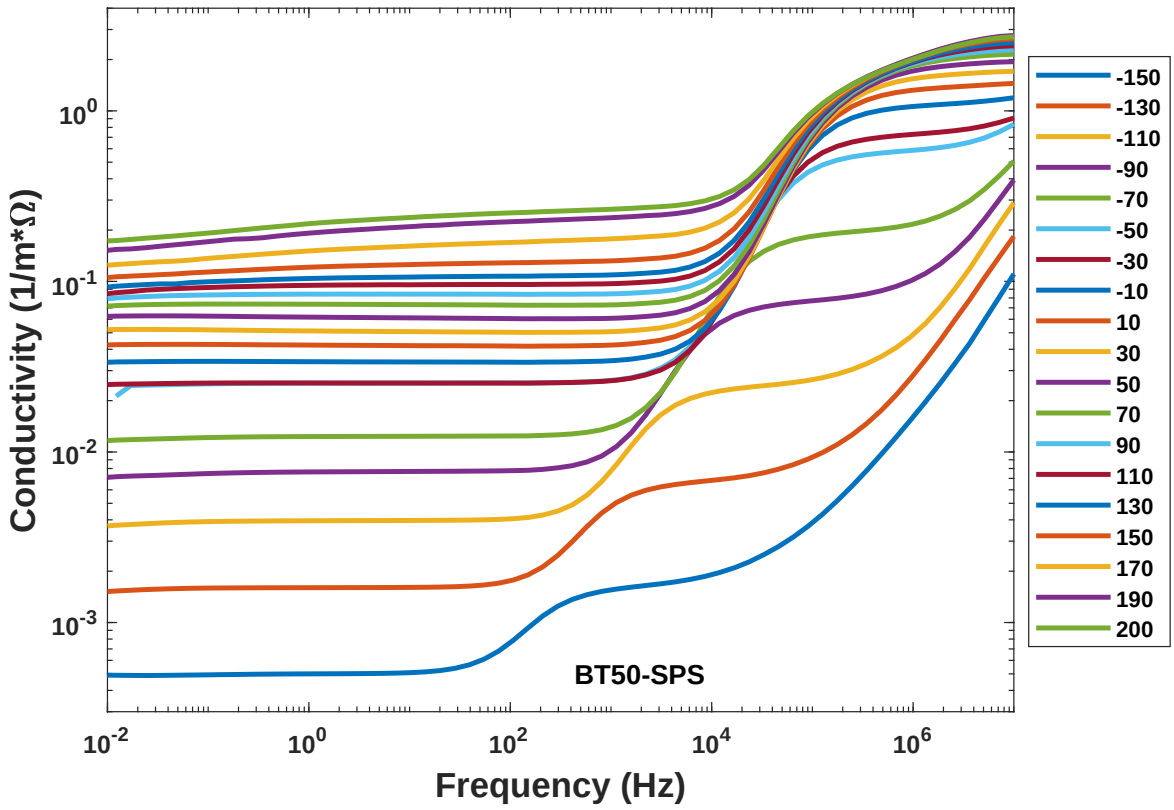

Figure 4.27: Effect of temperature on conductivity of BT50 SPS sample.

frequency is read from the permittivity figure and presented in the table.

Table 4.2: Fitting parameter of Drude model.

	a	**b**	**c**	p_1	p_2	c_2	ω_T	ω_P	γ
223	-279.4	-2.938	2.61E6	1.1E-4	3.65E-7	2.65E6	0.04	95	0.0573
243	-1.02E6	-1.267	2.95E6	3.78E-6	1.17E-8	1.40E6	0.42	515	0.0557
263	-3.81E6	-1.214	3.97E6	3.00E-7	2.29E-8	1.75E6	1.2	1827	0.277
283	-9.32E6	-1.147	4.38E6	4.63E-8	6.25E-8	1.85E6	3	4646	1.16
303	-2.01E7	-1.078	7.67E6	2.13E-8	4.76E-8	1.80E6	4.3	6852	1.50
323	-3.01E7	-1.056	7.22E6	1.01E-8	2.85E-8	1.70E6	6	9966	1.68
343	-4.43E7	-0.9173	1.01E7	4.97E-9	2.91E-8	1.80E6	9	14190	2.42
363	-4.04E7	-0.8573	6.04E6	3.36E-9	4.25E-8	1.85E6	12	17246	3.56
383	-3.13E7	-0.8064	3.83E6	2.51E-9	6.40E-8	1.98E6	12	19944	5.05

It is interesting that DSC and conductivity show any sign of phase transition in zero, but in fitting the plasma frequency there is different in behavior by passing this temperature.

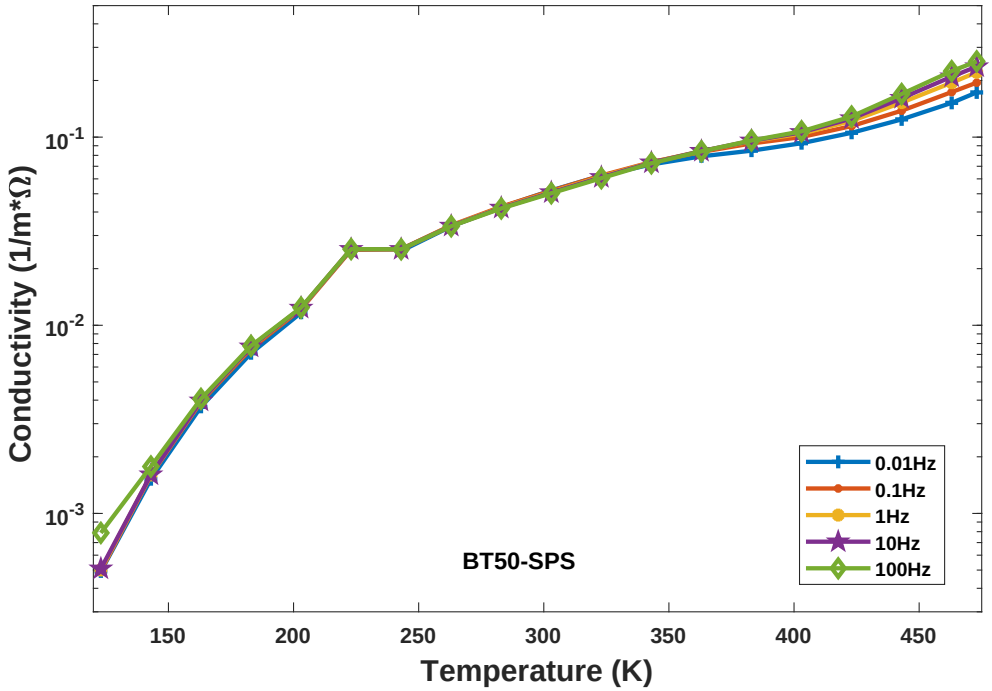

Figure 4.28: Effect of temperature on conductivity for each frequency of BT50 SPS sample.

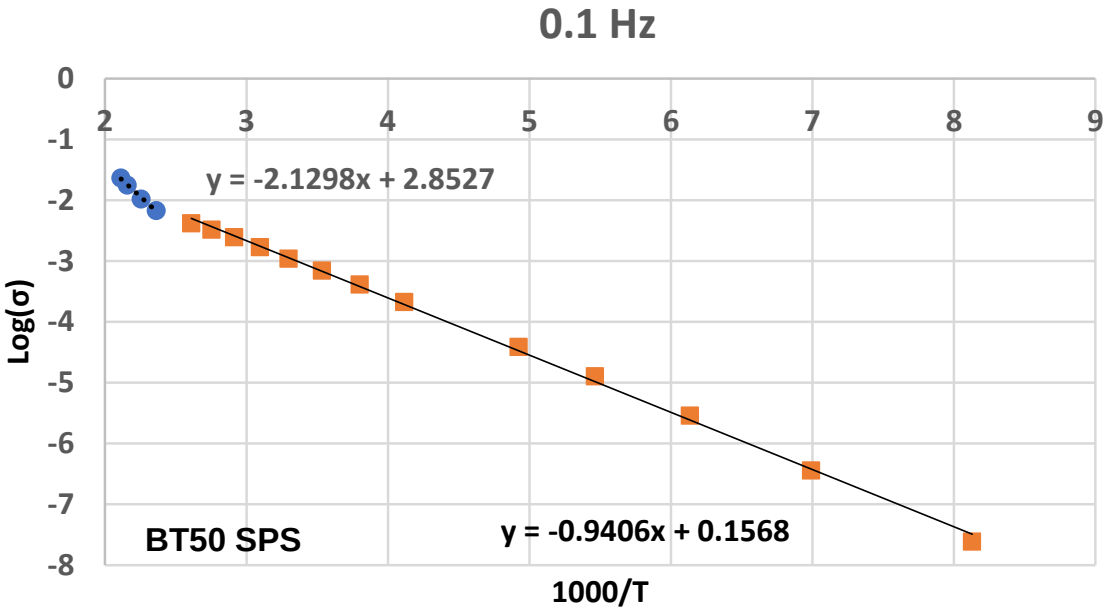

Figure 4.29: Reciprocal temperature dependence of conductivity of BT50 SPS sample at 0.1 Hz.

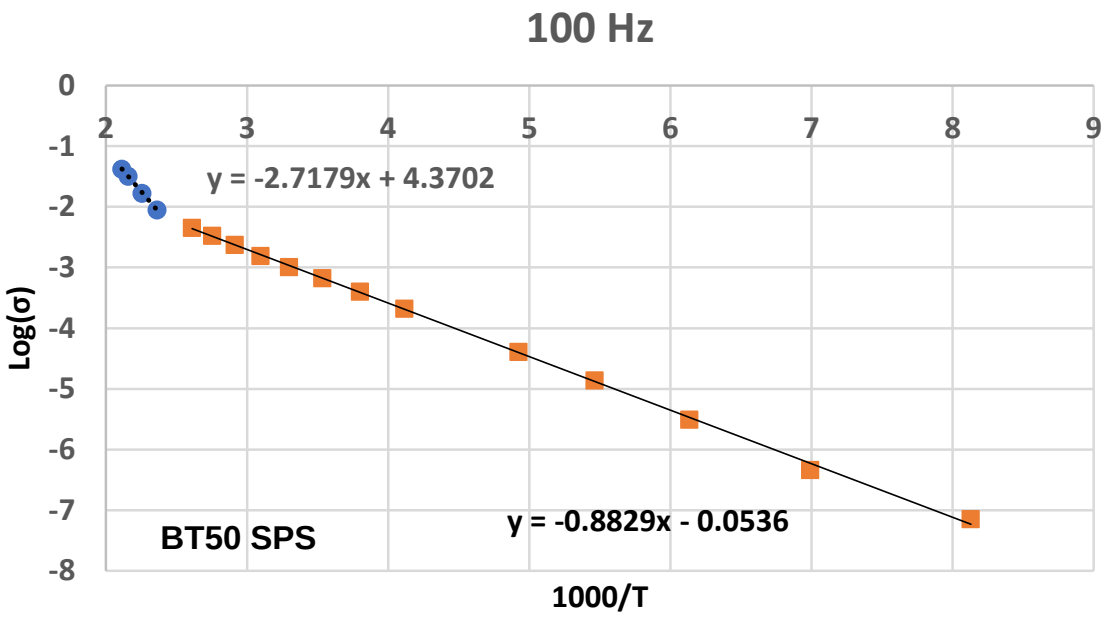

Figure 4.30: Reciprocal temperature dependence of conductivity of BT50 SPS sample at 100 Hz.

It is a sign that the BTO structure still influences the negative behavior of ceramic. The following picture shows different slop of fitted Parameter in a varied range of temperature.

In our system, the reason behind of negative permittivity comes from the localized and delocalized electrons. In the mentioned composites, there are many vacancies in the system in which electron can hopping and trap on them. To surpass these potential barriers, electrons needed the energy to pass them which can be generated by many external fields like the electrical field or temperature. Following our thought, the high permittivity of ceramics originated from the polarization of electrons and dipole polarization. In our system due to the existence of SiO_2, Maxwell -Wagner system formed and we have the polarization of localized electrons. At low frequency, electrons can have time and energy to migrates to other traps and polarized. Temperature can be as driving energy of some of the localized electrons to pass activation energy and become delocalized. By increasing the temperature, both the number of localized and delocalized electrons increases which make an increase in polarization of localized electrons and also plasma oscillation of delocalized electrons.

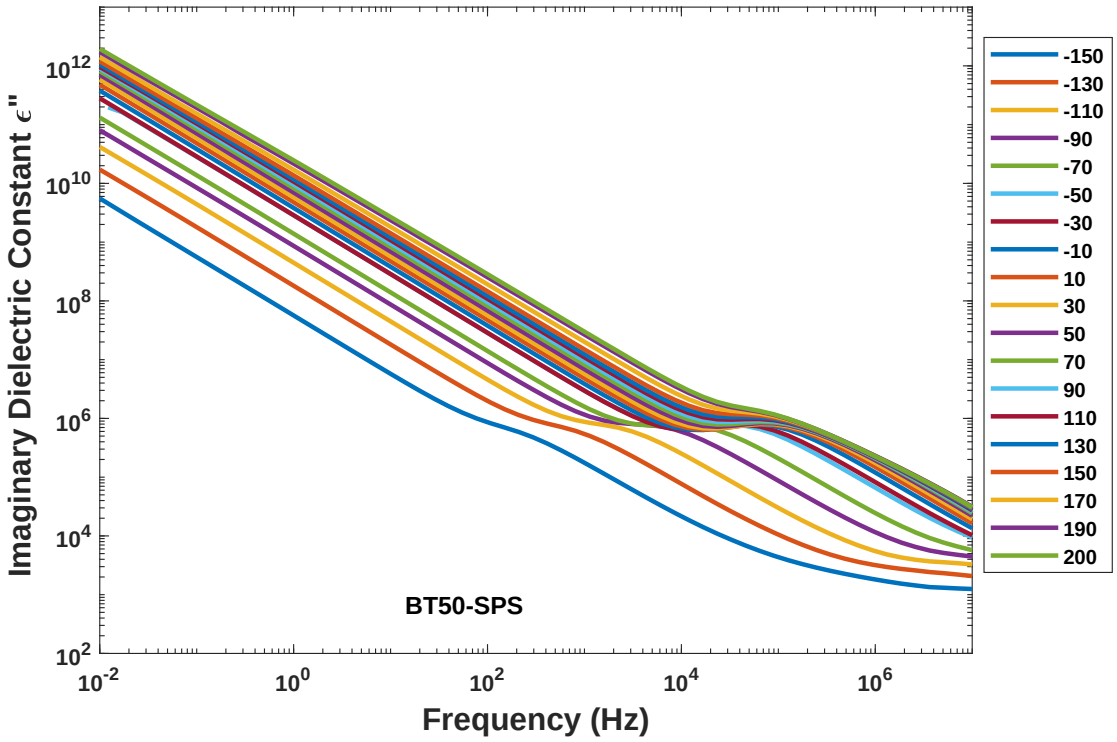

Figure 4.31: Effect of temperature on imaginary dielectric constant for each frequency of BT50 SPS sample.

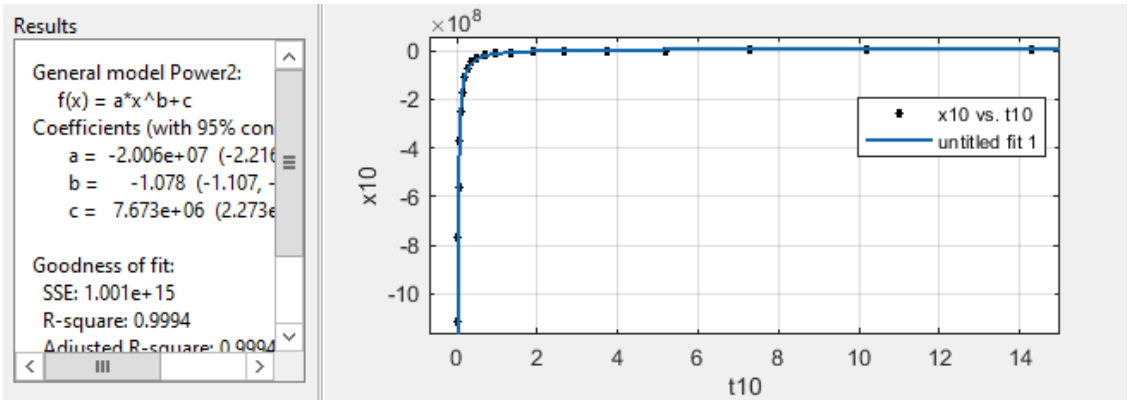

Figure 4.32: Effect of temperature on imaginary dielectric constant for each frequency of BT50 SPS sample.

At low frequency due to easily migration of electrons the number of them contributed to plasma oscillation by delocalization increases which reduced the number of electrons make polarization in sample generate positive and negative sign of permittivity. By reaching

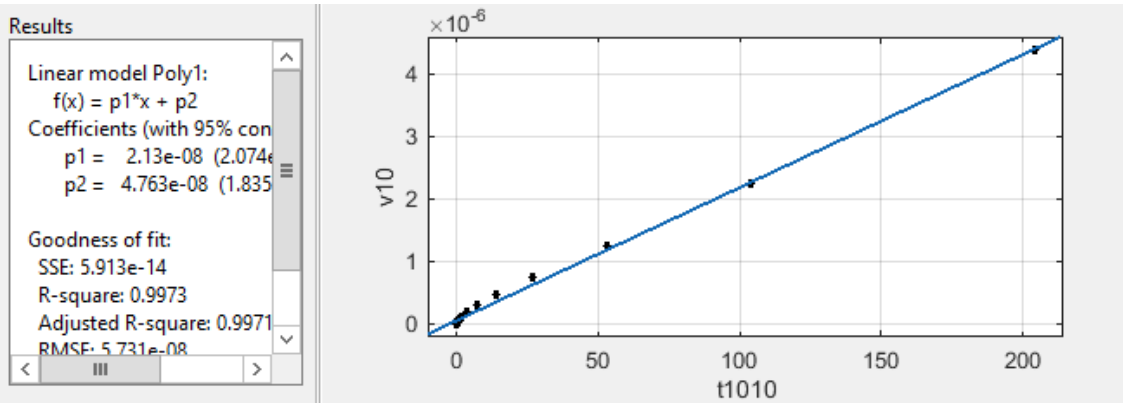

Figure 4.33: Effect of temperature on imaginary dielectric constant for each frequency of BT50 SPS sample.

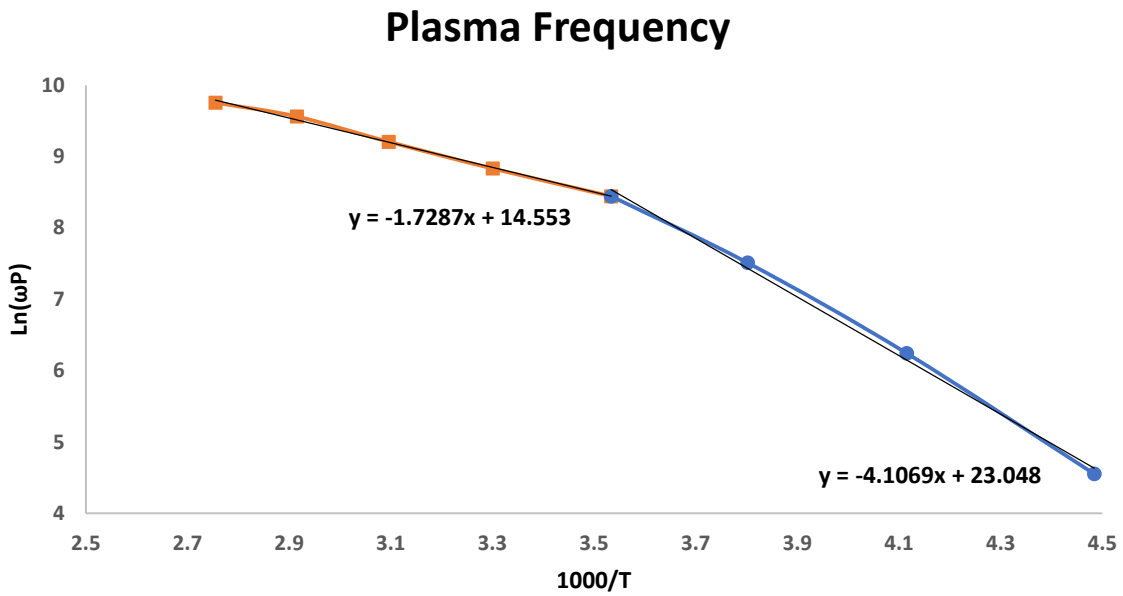

Figure 4.34: Effect of temperature on imaginary dielectric constant for each frequency of BT50 SPS sample.

a specific temperature, the energy is enough to make so many delocalize electrons which can make oscillation bigger than localized polarized electrons and negative permittivity. When the temperature increases, more number of electrons can be delocalized so a more comprehensive range of frequency the dielectric sign is negative. Moreover, the formation of thin SiO_2 network can cause an increase in effective mass and reduction the number of electrons.

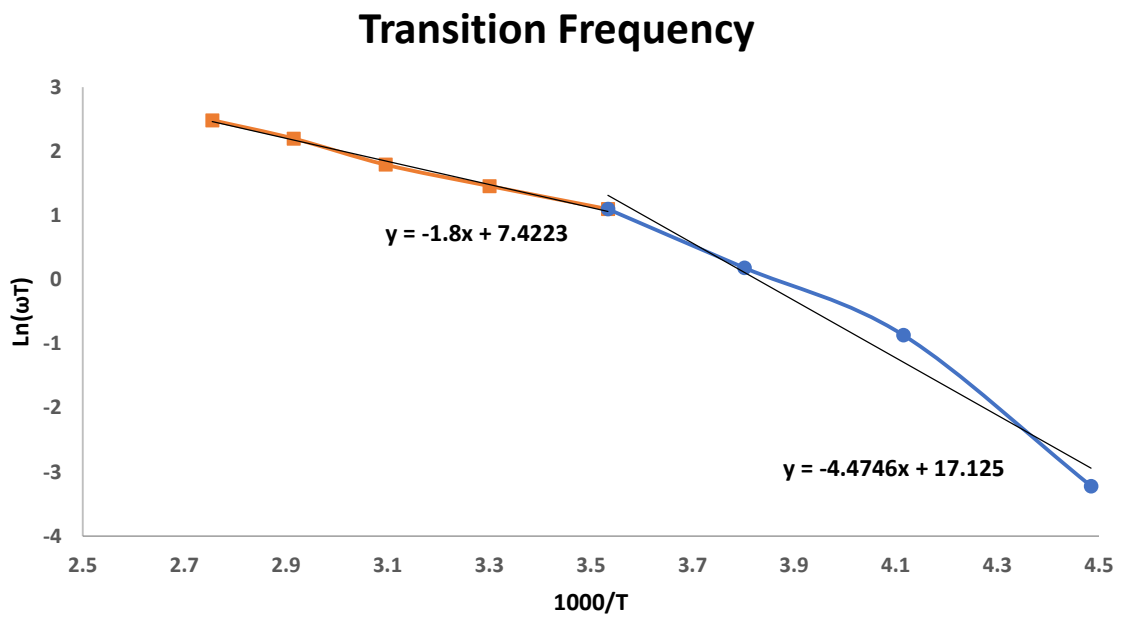

Figure 4.35: Effect of temperature on imaginary dielectric constant for each frequency of BT50 SPS sample.

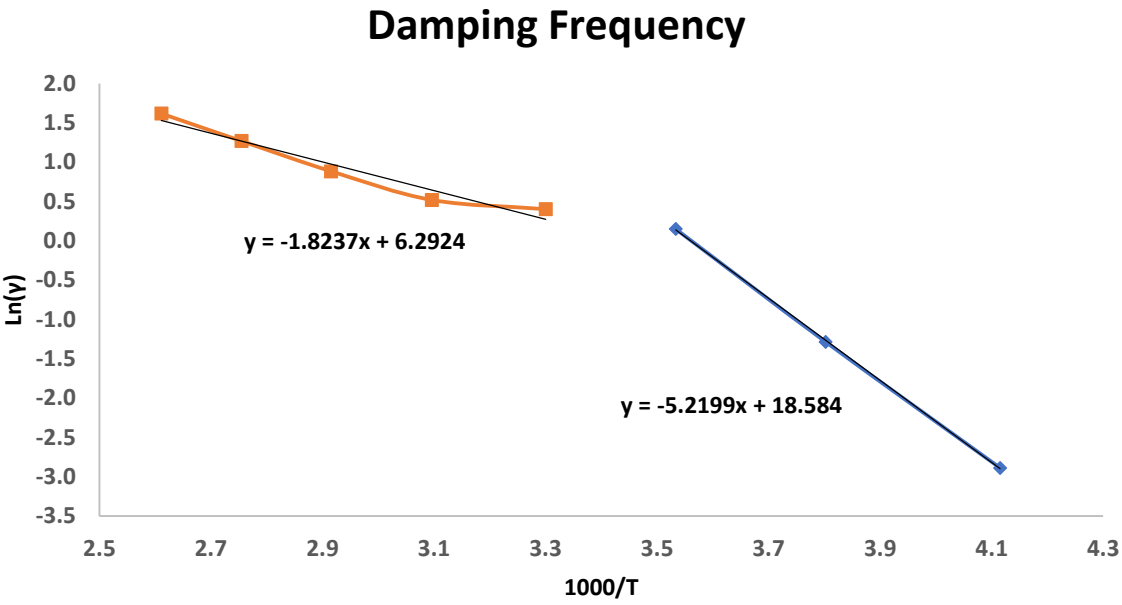

Figure 4.36: Effect of temperature on imaginary dielectric constant for each frequency of BT50 SPS sample.

By applying an electrical field, the number of electrons contributed to polarization increase which shows by increasing the permittivity. However, when the electrical field passes specific

values, there is enough energy to delocalized electrons from their initial position and move through vacancies. This delocalized electrons oscillated at a higher frequency which can not be reached at that temperature. Further increases the DC bias, increased the delocalized electrons and reduced the number of localized electrons which reduced polarization and the absolute value of negative permittivity increases.

At high temperature, the energy is that high that we have a lot of polarized electron witch make plasma resonance of localized electrons added to our mechanism, but by the further increase in temperature all of this mechanism is overcome by polarization process and positive permittivity. At high temperature, the activation energy increases while phonon-electron and electron-electron interaction increases. Increase in activation energy makes it harder for an electron to pass the potential barrier and become delocalized but due to rise to their interaction make it possible for the interband transition.

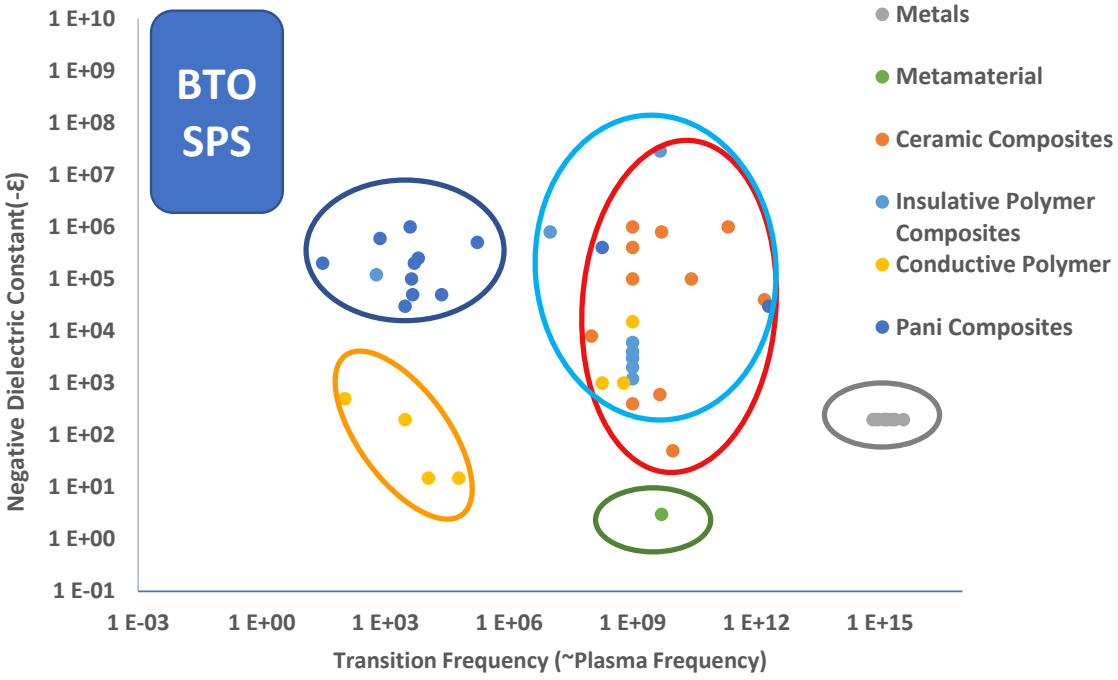

Figure 4.37: Effect of temperature on imaginary dielectric constant for each frequency of BT50 SPS sample.

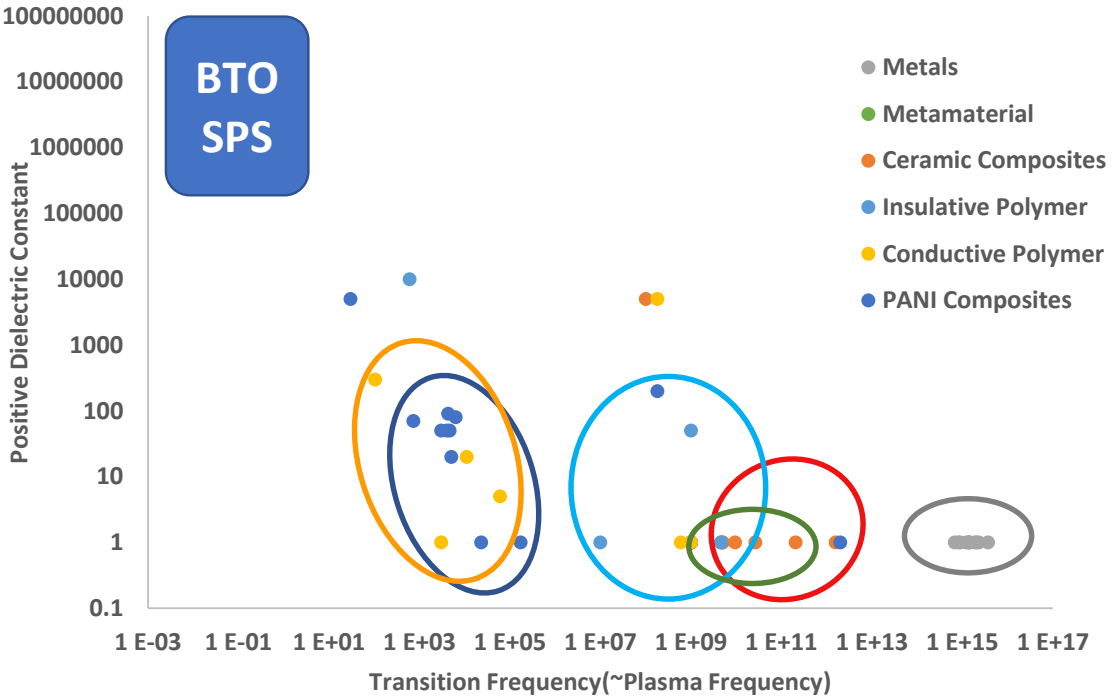

Figure 4.38: Effect of temperature on imaginary dielectric constant for each frequency of BT50 SPS sample.

4.4 Conclusion

In this chapter, the dielectric behavior of SPS ceramics was analyzed. The ceramic poses a gigantic permittivity up to 10^6 and a dielectric loss of 20 at 40 Hz. The reason behind this high permittivity and imaginary part may lie under the fabrication process. The pre-sintering treatment and fast plasma sintering make oxygen vacancies in the ceramic which can be resulting in the hopping process by an alternative electrical field. The Ac conductivity of sample shows Jonscher power law behavior in low-frequency dispersion.

By applying the electrical field to the sample, the negative permittivity emerges in the low-frequency spectrum which obeys the Drude model by the fitting. The reason behind such behavior is the increasing the number of the electron in the interfacial region and increase the moveability of electrons by an alternative electrical field.

The temperature dependence of samples was conducted from -150 ^0C to 200 ^0C to analysis the dielectric behavior in a range of 10^{-2} to 10^7 frequency. The negative permittivity emerges

in range of -60 ^0C to 130 ^0C in low-frequency dispersion. The reason behind is the freely hopping of electrons in the low-frequency range in tetragonal structure. When the structure change to the cubic, the activation energy sharply increases, and the permittivity spectrum become entirely positive.

Chapter 5

Effect of annealing on dielectric properties of SPS BTO-SiO_2 composites

The SPS samples made by BTO/SiO_2 composite posses very high permittivity and dielectric loss Moreover, the electrical field range is very limited to the low voltage. These ceramic properties are much different from composites fabricated by a conventional sintering process. In order to rpove the responsibility of oxygen vacancies for SPS smaple properties, they were annealed in different temperature an time. The surface color of the annealed samples has been changed to white which is known as the original color of BTO samples. As it expected the dielectric loss of samples can be reduced to some extent and also the ceramics still possess high permittivity. The sample annealed at 1100 ^0C for 4 hours, has become complete in whole volume. However, the DSC results and permittivity temperature-dependence just shows small phase transformation behavior and still shows different properties compare to conventional sintered BTO samples.

5.1 Introduction

Ceramics with perovskite structure are famous for their unique properties. In field of dielectric materials and energy storages, BTO is one of most promising materials. The BTO has a high permittivity (up to 4000), and with acceptable low dielectric loss which make it right candidate for a dielectric application. Coating with some insulative materials like SiO_2 and also vacuum treated sample could improve dielectric behavior of BTO. It is believed that the treating BTO powder generates oxygen vacancies and the ceramics can be polarized at low-frequency range due to polaron electrons. Meanwhile, the SiO_2 coating can reduce the conductive loss in sample which can improve the breakdown field and also make the PE loop slimmer.

The samples fabricated by the SPS process shows unique properties in dielectric field. The large permittivity posses by this method are suggested to be originated by the oxygen vacancies formed in this method. According to the literature, the oxygen vacancies concentration can be change by annealing which is kinetic process. It can be implied that the properties of annealed sample can be different from fresh sample due to change in structure. It is the hypothesis that the structural change could drive into a shift in the relaxation process of the samples.

The energy density of materials are depend on both permittivity and dielectric loss. Polymers are known as material with high breakdown field but their low permittivity limited their application. Materials which poses high permittivity can be better candidate for energy storage application. However, their dielectric loss should be control. The SPS sample with gigantic dielectric properties are a good candidate in this field, but their dielectric loss limits the use of them. Managing dielectric loss of such material and improving the working electrical field make it top candidate for energy storages.

As it is known for random composites the negative permittivity can be formed in wide range of conductivity. Changing the conductivity properties of material may tune the plasma frequency and also change the value of permittivity and negative value. Optimizing the negative and positive of permittivity can be favorable in many application especially in transistors. Change in microstructure and oxygen vacancies not only can affect the polarization and positive spectrum of dielectric but also may change in negative behavior of materials.

As presented in the previous chapter, the SPS sample shows a dark blue color which is a sign of high conductivity. This properties can be alter by annealing of ceramics at different temperature from 800 to 1100 ^0C for 1 to 4 hours. The color change to white is depend on both temperature and duration of annealing but sample thickness shouldn't be forgotten. The dielectric studies of annealed sample less than 1000 shows high permittivity up to 10^5 and dielectric loss near to 0.5. The dielectric spectrum shows negative values in low frequency range for wide range of temperature and also they can alter by electrical field.

The color of samples annealed at 1100 ^0C for 4 hours has completely changed to the white and the dielectric behavior is very similar to conventional sintered samples. Moreover, The annealing effect one side more than others which make the examples shows inhomogeneous properties like different conductivity in each side.

5.2 Experimental

The BT50 and BT14 ceramic sample were used to be annealed after cutting. The annealed sample has a typical thickness of 1500 μm. Samples usually have a rectangular shape with a size of about 5 mm on each side. The samples placed inside the crucible ceramic with a lead on the top of it. The crucible inserted inside the oven and The heating process undergoes by the below steps (Fig. 5.1):

It can be clearly be seen all samples heated up almost in the same trend and the primary

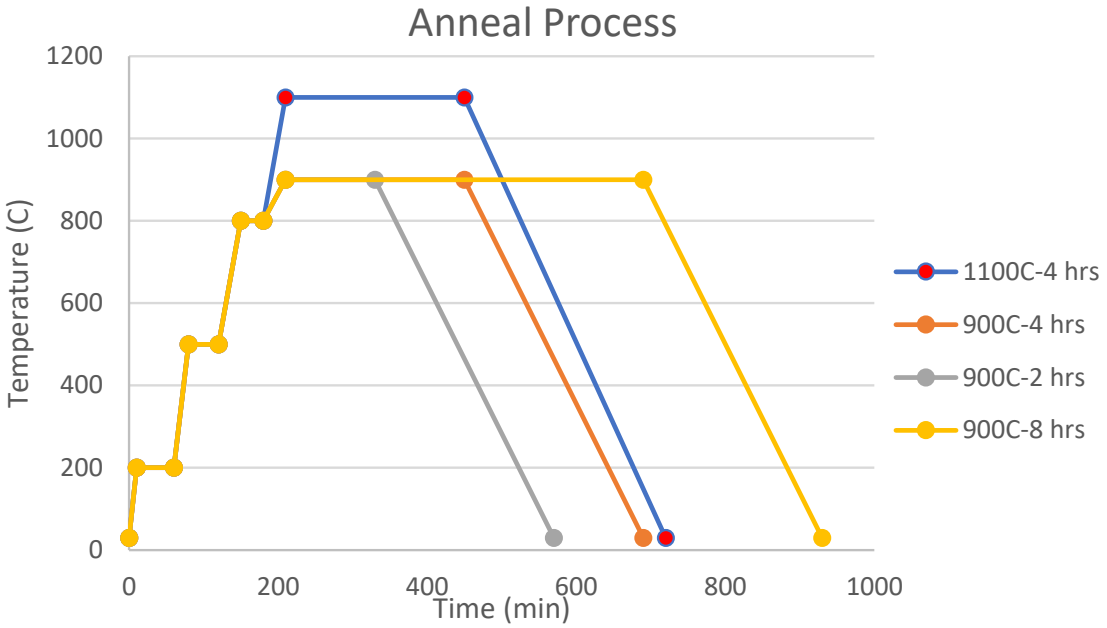

Figure 5.1: Annealing process steps of SPS sample.

annealing process start 900 ^0C. At this temperature three annealing time of 2, 4 and 8 hours been used for samples. It can be assumed that the annealing process has direction from top to down and the top surface of sample affected more than other areas.

The sample shows a change in color through the annealing process. The longer process transformed the sample to become more white by this process. To reduced the effect of the annealing process direction, the sample was polished on both sides to the thickness about 300 um. Although the polishing process completely fades the white side of the samples, thin lines with the white color can be seen in sample macrostructure by naked eyes which mixed by the original blue color of the sample.

For the sample undergoes annealing process at 1100 ^0C after four hours sample completely become white. The emerging color is very similar to the composites of BTO with SiO_2, and it can assume that the sample entirely affected by the annealing process and lose its properties obtained by the SPS process. The schematic can explain the effect of annealing on the microstructure of SPS sample in the below picture (Fig. 5.2):

It should be mentioned that the annealing process has almost the same effects on BT50 and BT14SG samples which has a mixed color by annealing at 900 ^0C temperature. However, BT14NC samples color completely change even by annealing at low temperature for a short period.

The polished sample obtained by annealing sample was gold sputtered as an electrode to prepared for a dielectric test. The impedance analyzer was used to measure the dielectric behavior of sample and DC bias applied to the samples to test their negative dielectric properties. The effect of working temperature on the sample was examined in a range of -100 ^0C to 180 ^0C temperature. A small part of annealed samples was cut and broken to a small particle to be used for DSC testing. At the last step, the well-annealed samples at 1100 ^0C were tested by PE loop measurements.

5.3 Result and discussion

5.3.1 DSC

The DSC results of annealing samples come in the following pictures (Fig. 5.4, Fig. 5.3, Fig. 5.5, Fig. 5.6). Unlike to the SPS fresh sample, the anneal samples shows an almost

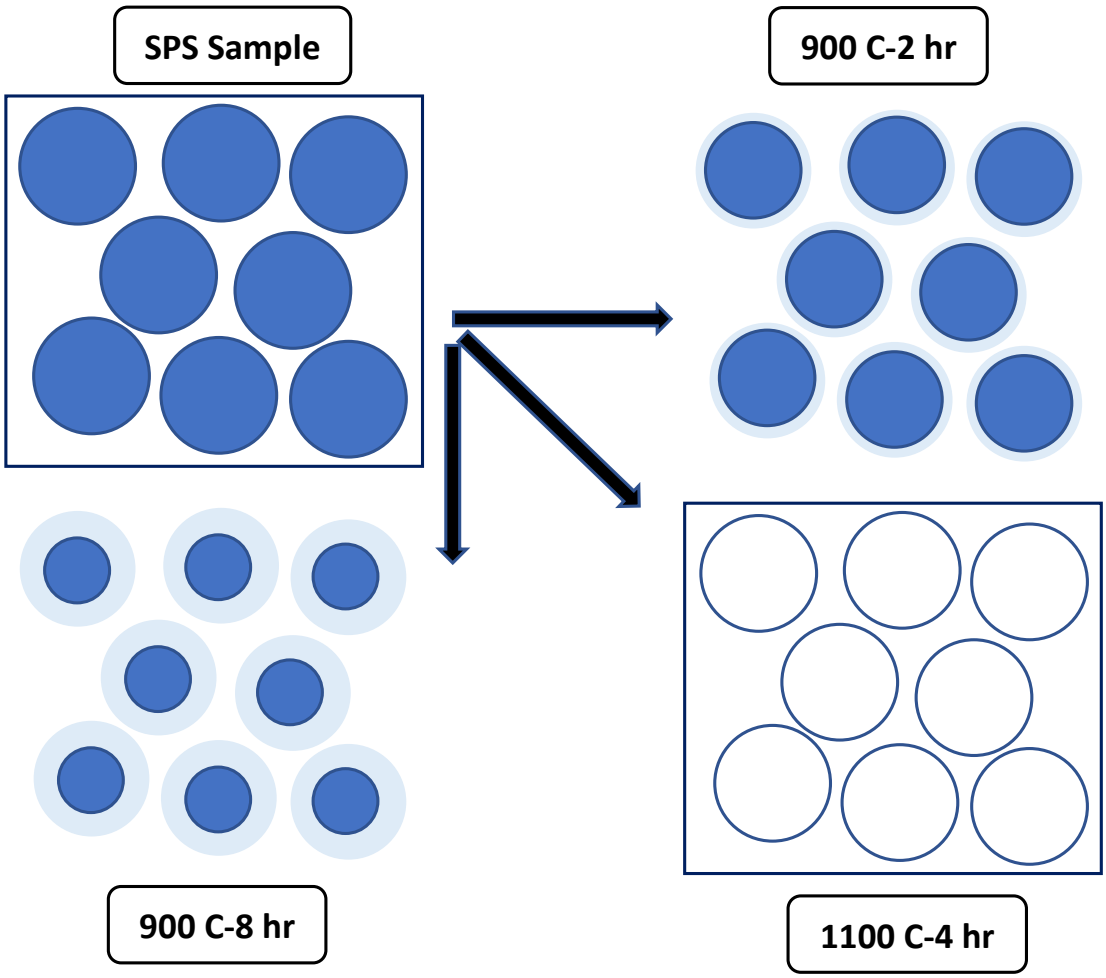

Figure 5.2: Schematic of effect of annealing process on microstructure of SPS sample.

sharp peak for the phase transformation process. The annealing effect on the enthalpy value of phase transformation which increases by improving the annealing process. Moreover, in heating process, the peak temperature is increases to 120 ^0C even for 2 hours annealed sample and pass this value by increasing the annealing time.

It is fascinating that the annealing makes the composites transformation peak move to 124 ^0C when its kept for 8 hours at 900 ^0C. This sample shows the highest enthalpy among all other annealed ones at 900 ^0C.

For the sample annealed at 1100 ^0C for four hours, the peak temperature becomes normalized and get to 122 ^0C. On the other hand; the DSC results indicate the highest enthalpy

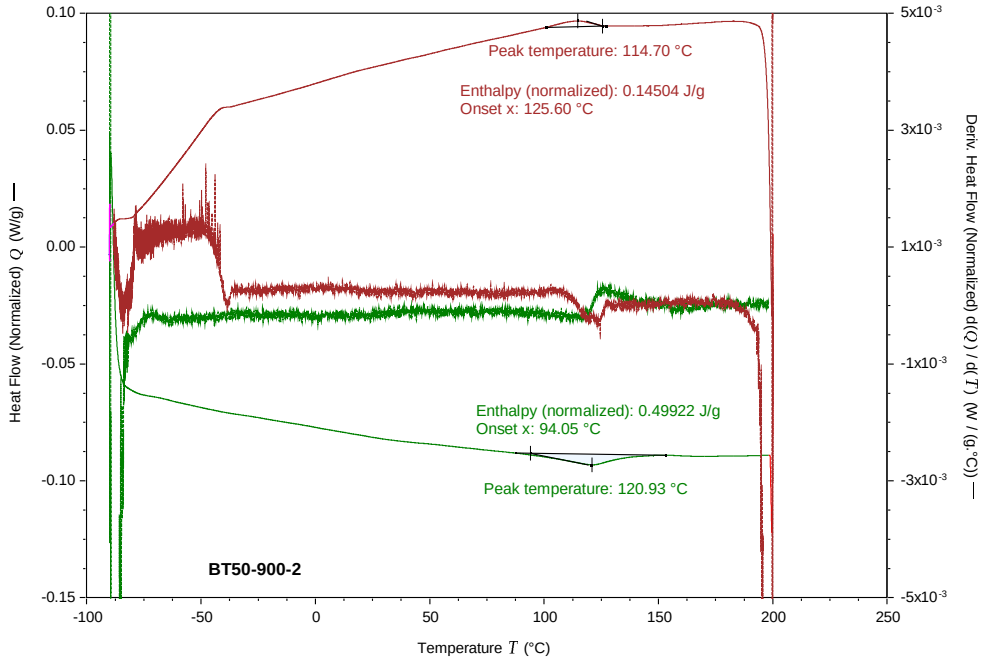

Figure 5.3: DSC pattern of BT50 composite, annealed for 2 hours at 900 ^0C.

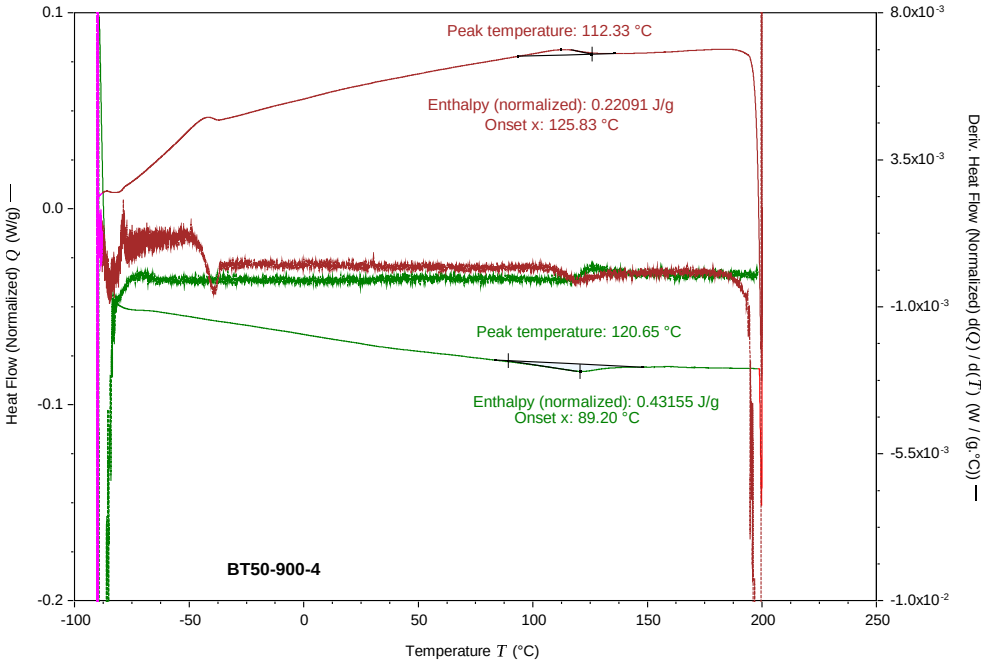

Figure 5.4: DSC pattern of BT50 composite, annealed for 4 hours at 900 ^0C.

among annealed and fresh samples is presented in wholly annealed sample. However, there is no sign of transformation peaks in the range of 0 ^0C or -60 ^0C. This concludes that

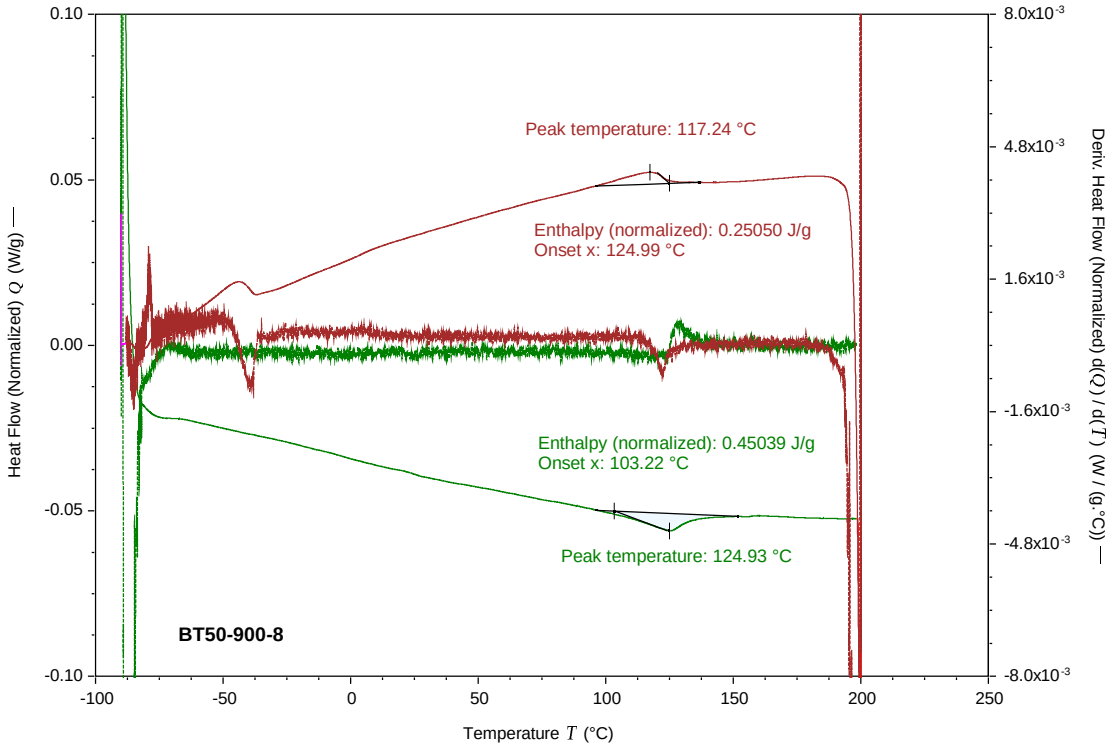

Figure 5.5: DSC pattern of BT50 composite, annealed for 8 hours at 900 ^0C.

the coating process and pretreated process affect the microstructure of BTO and composite cannot behave like the pure BTO.

The DSC result of 1100 ^0C annealed BT14 sample has been shown in the following picture (Fig. 5.7). It's interesting that even after wholly annealed sample to the regular composites, there is no peak sign related to phase transformation can be seen in the cooling process. On the other hand, the heating process is almost the same, but there is very small peak can be noticed around 120 ^0C. This peak is close to BTO phase transformation peak which has very small enthalpy.

On the other hand, the DSC results related to BT14-NC sample is entirely different from others. There phase transformation in temperature about -60 ^0C, 10 ^0C, 120 ^0C is presented clearly in all annealed samples. The peak related to -60 ^0C is very small and close to start point which can not be seen in the cooling process. By comparing this result with BT14, it can conclude that the change in structure is completely related to the coating process and

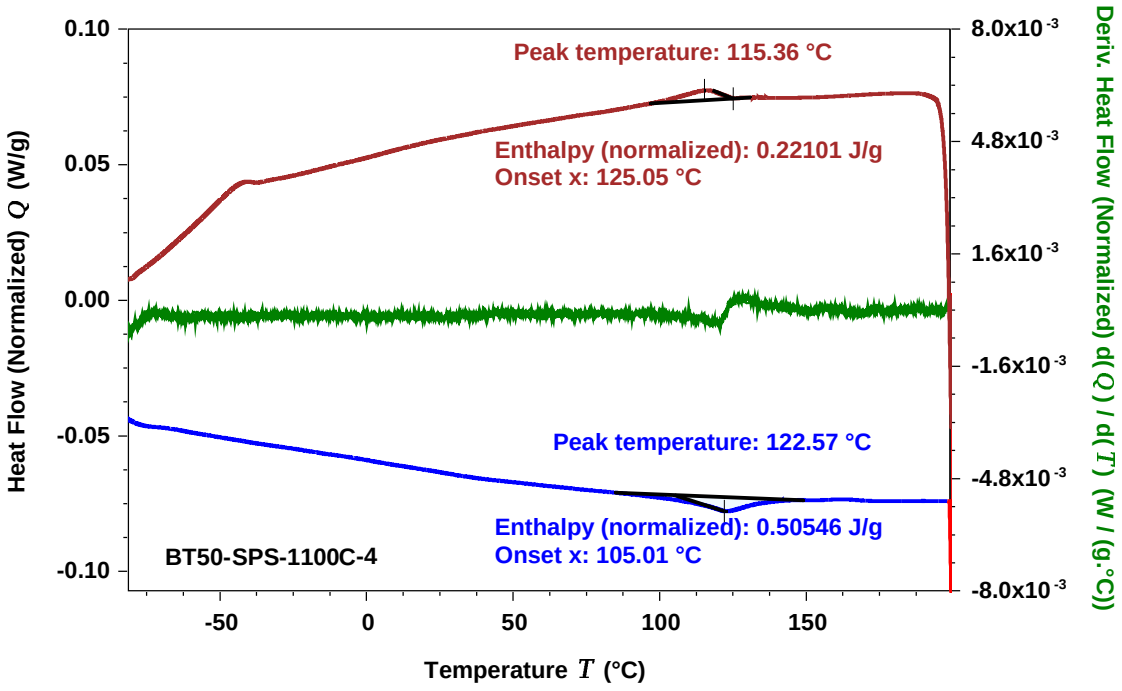

Figure 5.6: DSC pattern of BT50 composite, annealed for 4 hours at 1100 ^0C.

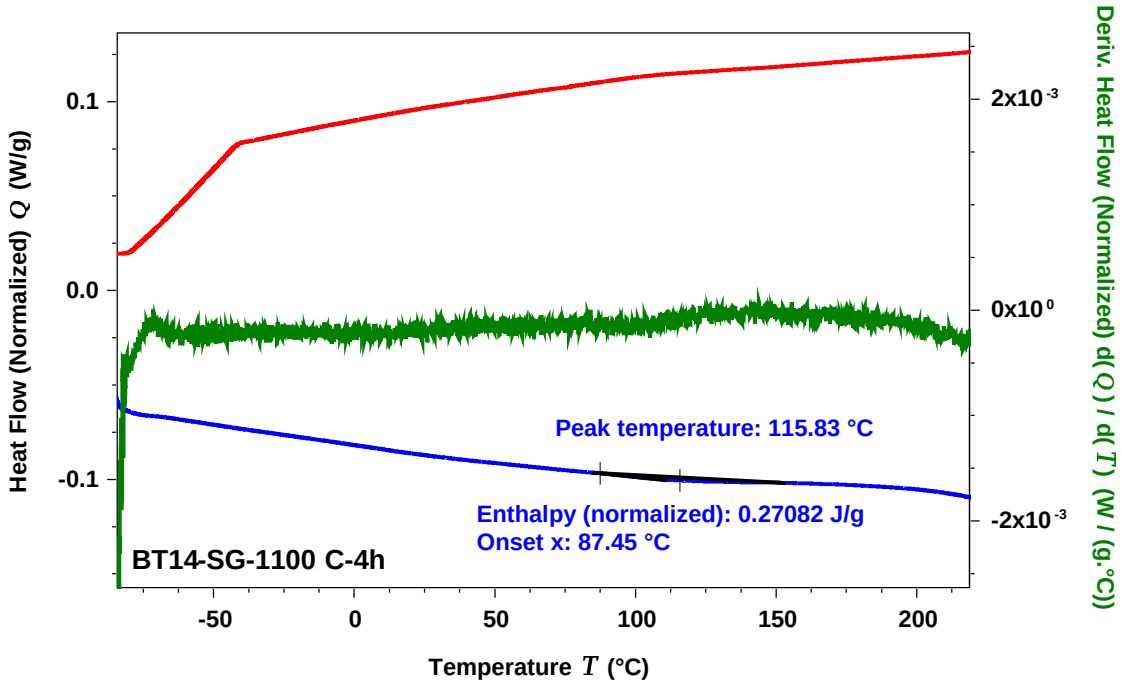

Figure 5.7: DSC pattern of BT14-SG composite, annealed for 4 hours at 1100 ^0C.

SiO_2 layer and SPS process on its own has not much influence in this regards. However, it should be mentioned that the annealing process has a small effect on the size of 2-5 ^0C on peak temperature and change peaks enthalpy.

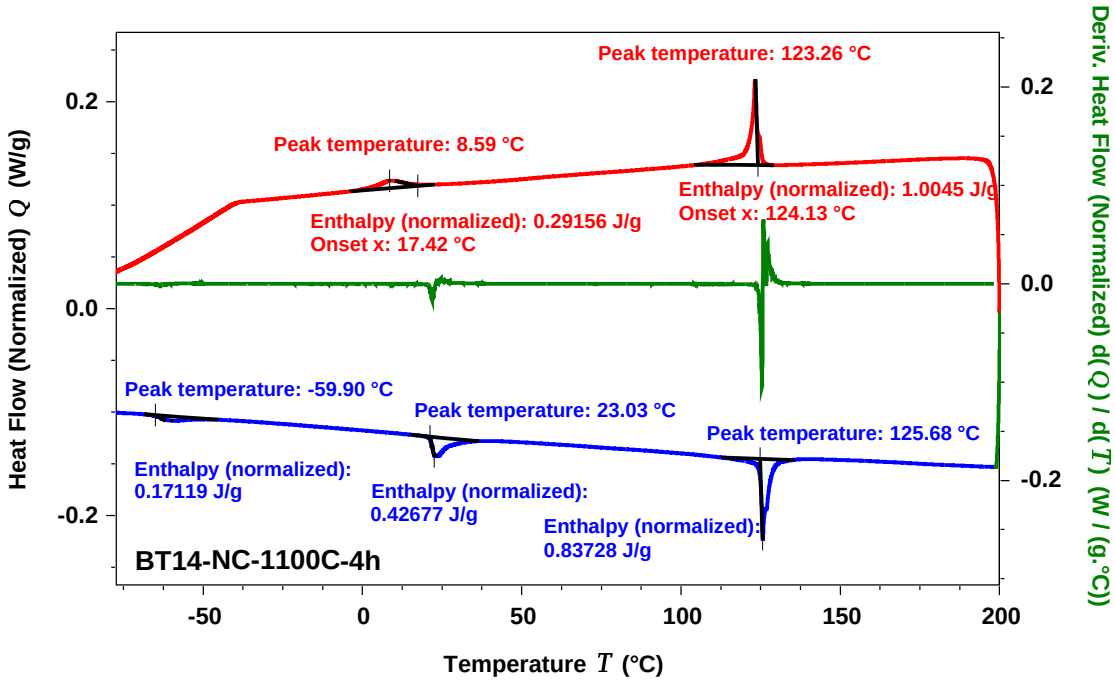

Figure 5.8: DSC pattern of BT14-NC composite, annealed for 4 hours at 1100 ^0C.

5.3.2 Dielectric properties

The permittivity of the annealed sample showed in the following picture (Fig. 5.9). The result indicates that the reduction on the magnitude of permittivity occurs in the range of low to 10^6Hz frequency by the annealing process. The permittivity value is going down by increasing the annealing time. The annealing time effect is not only on the amount but also the step-like reduction of permittivity behavior at low frequency become entirely flattened by this process. Moreover, the big step on permittivity which happens in frequency range about 10^5 also moves to lower frequency. For frequency, more than $5 * 10^6$ the permittivity has different behavior and rise by annealing. Annealing at the 1100 ^0C for 4 hours make the permittivity behavior totally different and shifted to the original BTO behavior which

is flattened for the whole frequency range.

The dielectric loss also altered significantly by the annealing process (Fig. 5.10). It can be

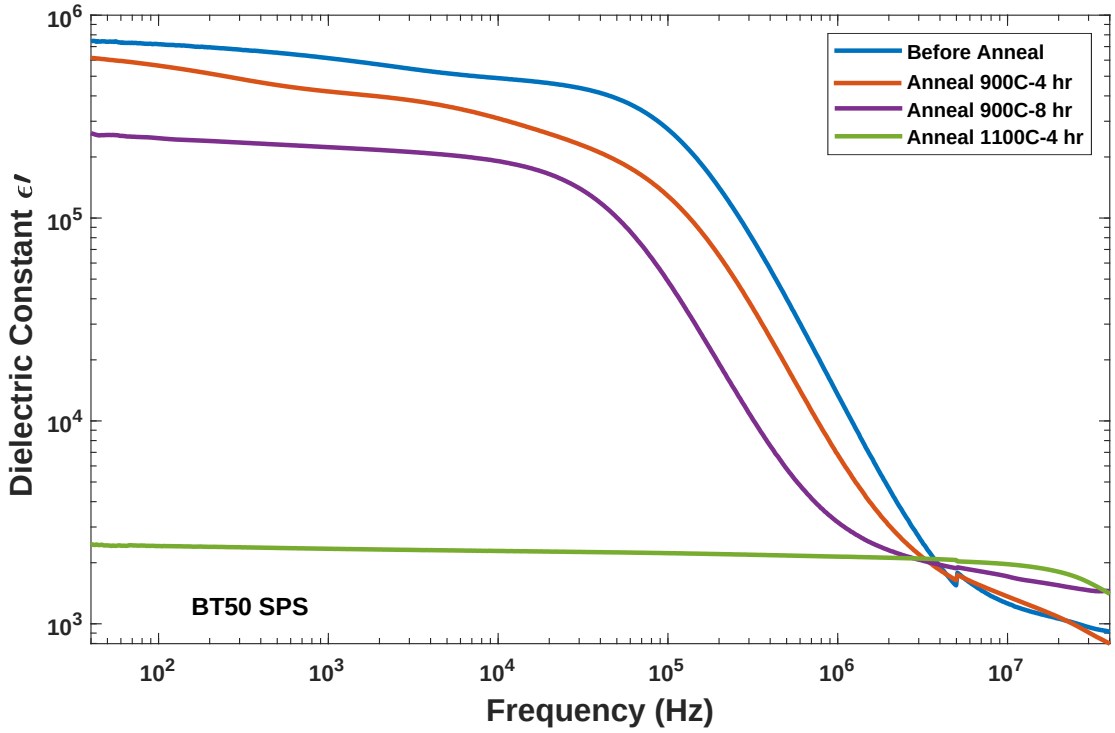

Figure 5.9: Effect of annealing on permittivity of BT50 SPS sample.

seen the sharp decrease in low-frequency dielectric loss values which lower the dielectric loss to more than ten times smaller just by annealing for 2 hours. The debye like relaxation can be seen about 10^7 frequency for a fresh sample, but annealed samples show shifted in the frequency of this peak and increasing the time make it emerge for lower frequency. Same as the permittivity, the dielectric loss of the annealed sample shows completely different behavior compare to fresh sample by possessing the dielectric loss in magnitude less than 0.03 with no sign of any relaxation peak.

The effect of sintering time on the conductivity can be seen in the following picture (Fig. **??**). The conductivity sharpy decreases for low frequencies. For the fresh sample, the conductivity started with a straight line (σ_{dc}) and continued with a step-like jump which correspond to a universal power law. On the other hand, the annealed sample shows the step-like behavior

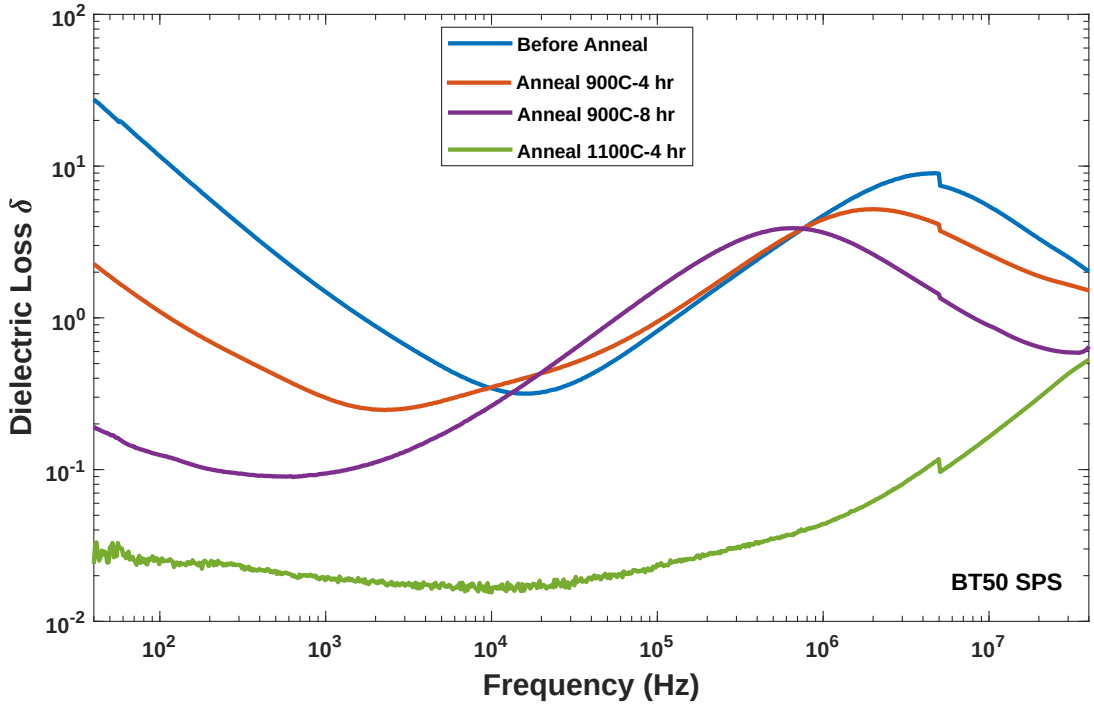

Figure 5.10: Effect of annealing on dielectric loss of BT50 SPS sample.

in lower frequency and also the start line is not completely vertical which means much lower conductivity. In the end, the conductivity of the 1100 ^0C annealed sample becomes more than five orders of the magnitude smaller than a fresh sample at low frequency and has no strait horizontal line.

The imaginary part shows very similar behavior to the dielectric loss by the effect of annealing. The main difference is the relaxation peak which emerges at a lower frequency of 10^5Hz. It can see the reduction in low-frequency values and also the spectrum behavior become different from the straight line. The relaxation moves to a lower frequency by increasing the annealing time.

As we understand from the previous chapter, the original of high permittivity and high conductivity is on formation defects as oxygen vacancies in the sample. The charge carriers such as electrons can move along the sample by these traps and results in dielectric behavior as we found in those samples. The annealing cause reduction in a number of these vacancies especially at interfaces and grainboundaries. In consequence of this process, the relaxation

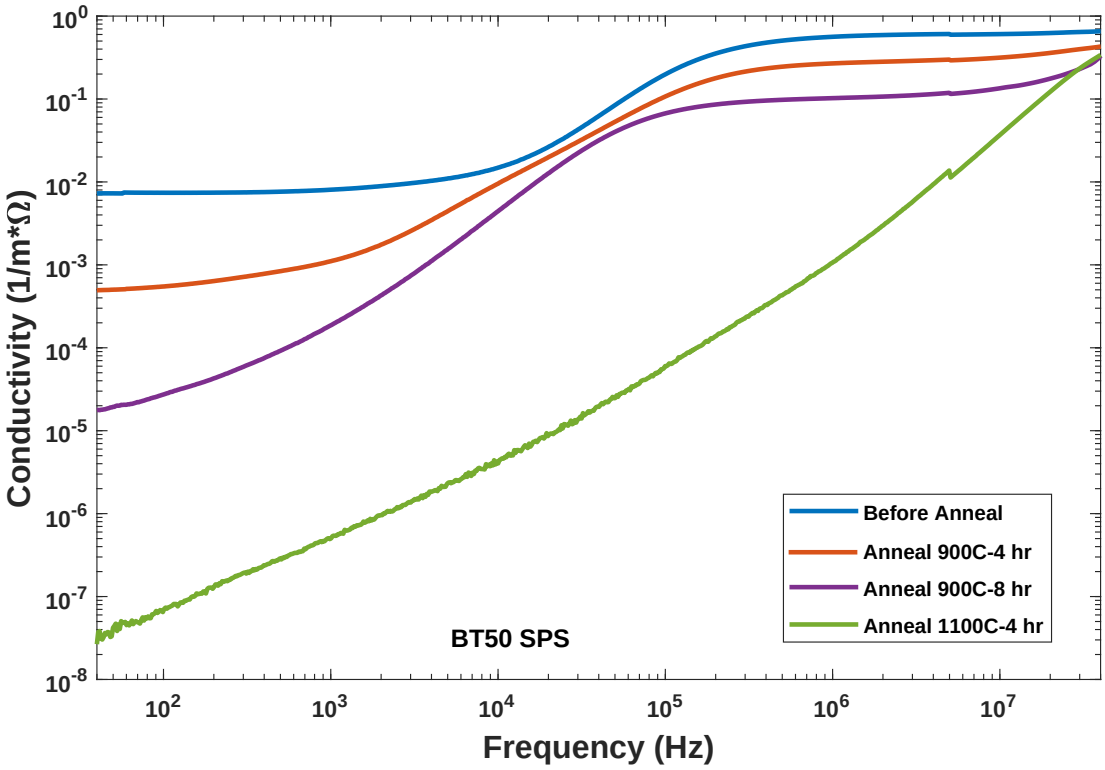

Figure 5.11: Effect of annealing on dielectric loss of BT50 SPS sample.

peak decreases to lower frequency region which is due to an increase in charge transfer time in the sample [14] [111] [31]. By increasing the annealing time or temperature, the effect improves and more reduction of oxygen vacancies.

The effect of annealing process on electrical behavior of BT14 samples is very similar to BT50 sample.

5.3.3 Effect of DC bias on dielectric properties of annealed sample

The Annealed sample shows a smaller permittivity and loss compare to fresh samples. However, the effect of DC bias is almost similar in the annealing samples. The following pictures present the outcome of DC bias on Dielectric behavior of annealed samples. In Fig. 5.13 the permittivity of annealed sample for four hours at 900 ^0C can become negative by applying high voltage to the sample. The bias voltage or in a better way to say it, the

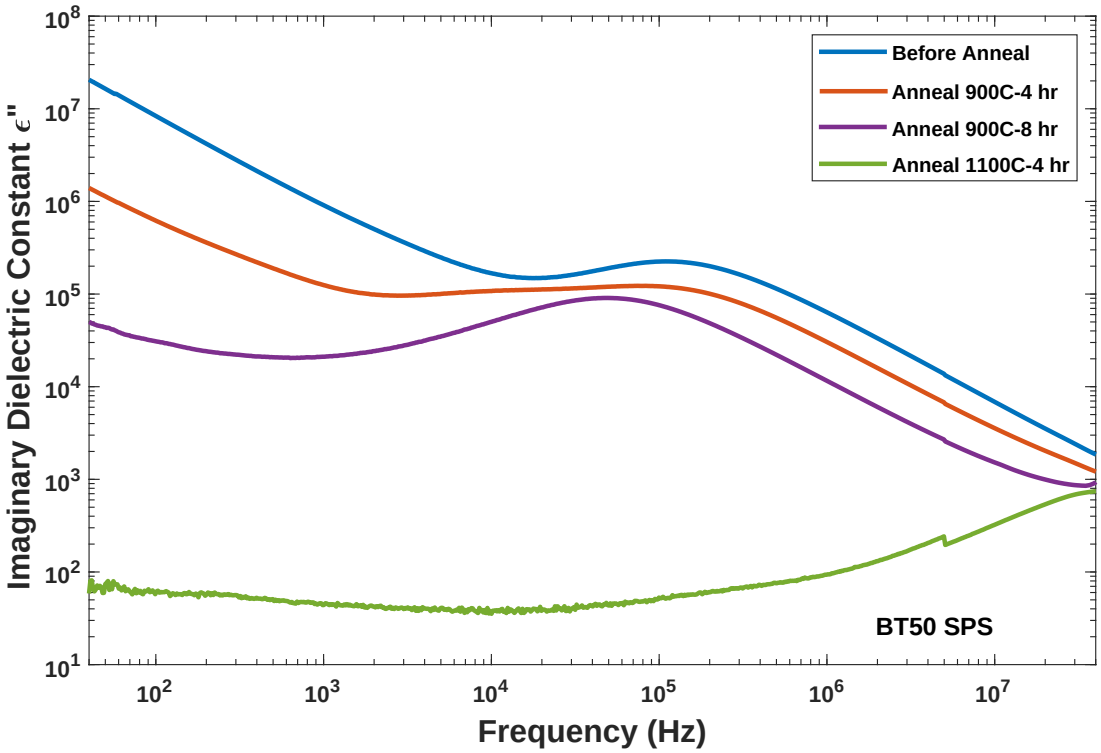

Figure 5.12: Effect of annealing on Imaginary dielectric constant of BT50 SPS sample.

external electric field applied to sample cause the permittivity get to a negative value. It should be mentioned that the highest DC bias can be applied to the sample is larger for the annealed sample compares to the fresh samples.

The DC bias effect on the dielectric loss of the annealed sample is very similar to the fresh sample. Although, the dielectric loss shows smaller values for low frequency, by applying DC bias the dielectric loss rise sharply in this range and the peak correspond to the negative permittivity shows up at high DC bias. The frequency range of DC bias effect on dielectric loss is limited to the low frequency which increases by increasing the amount of DC bias, but for the frequency larger than 10^6 it remains unchanged.

Although the conductivity of the annealed sample shows much smaller values especially at low frequencies, the final conductivity value after applying DC bias is similar to the fresh sample. Previously it was mentioned the importance of DC conductivity in the presence of negative permittivity in the particular frequency range, and by analyzing the data obtained

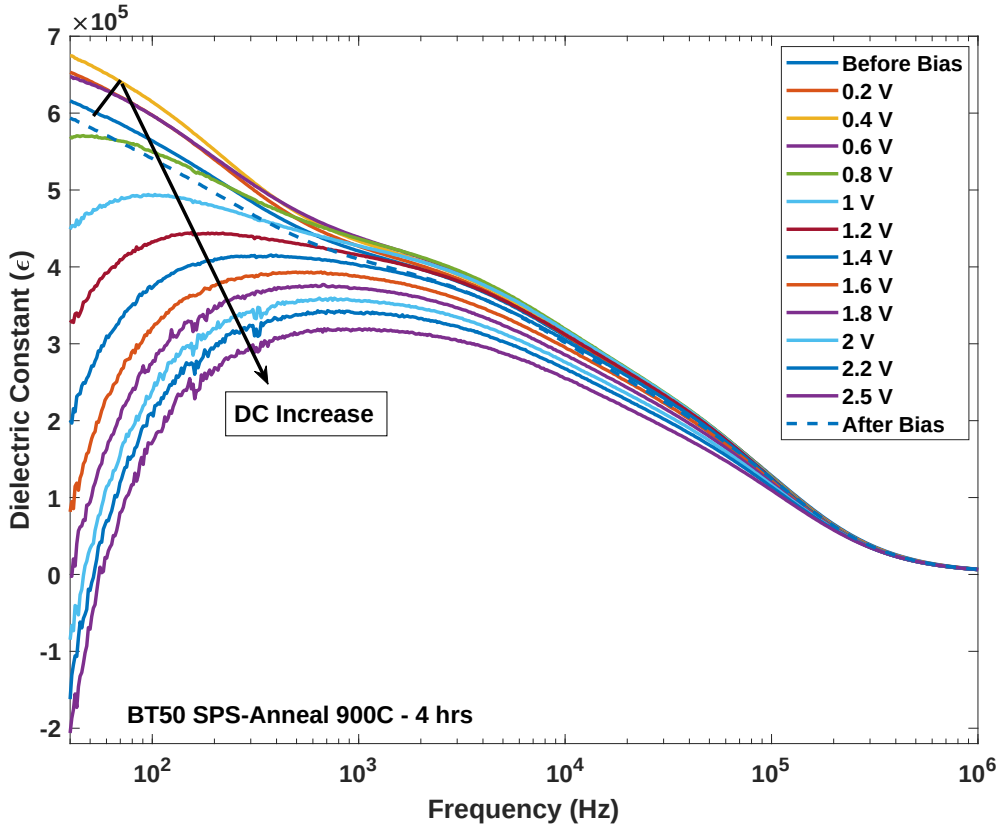

Figure 5.13: Effect of DC bias on permittivity of BT50 SPS sample annealed at 900 ^0C for four hours.

from the fresh and annealed sample, it can validate.

5.3.4 Effect of temperature on dielectric properties of annealed sample

The dielectric behavior of annealed sample was tested in different temperature from -100 ^0C to 180 ^0C. The frequency range of this test was from 10^{-2} to 10^7 Hz. The following picture (Fig. 5.16) demonstrate the permittivity response in different frequency and temperature. The annealed sample shows negative dielectric in frequency range smaller than one like the fresh sample. The temperature range that the annealed sample poses negative permittivity is starting from -40 ^0C to 160 ^0C which has small differences compare to fresh sample.

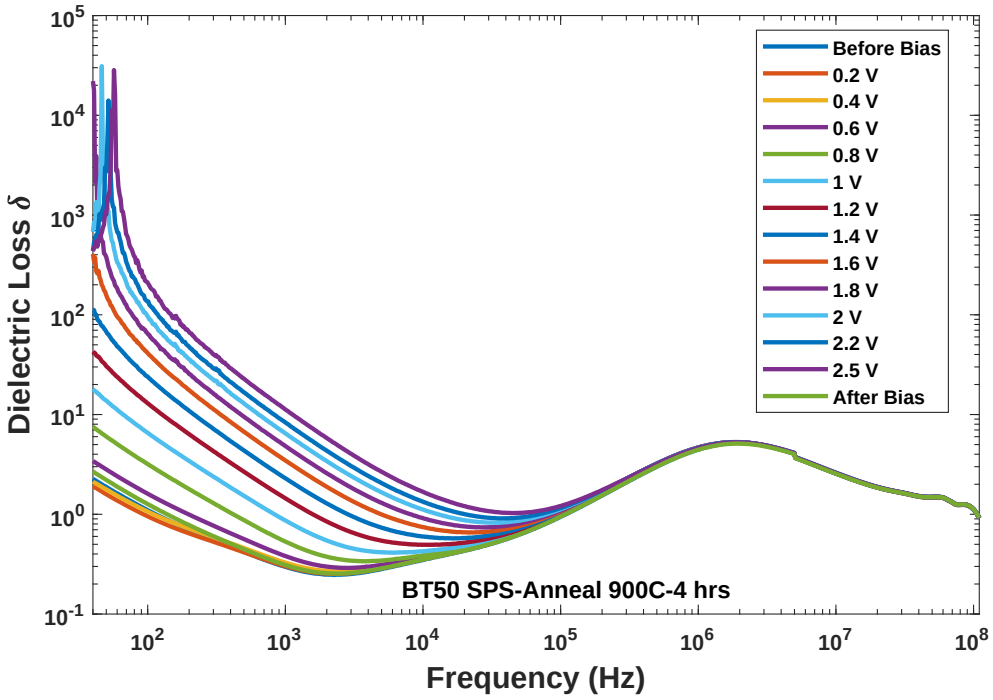

Figure 5.14: Effect of DC bias on dielectric loss of BT50 SPS sample annealed at 900 ^0C for four hours.

The logarithmic scale of permittivity behavior can be seen in Fig. 5.17. Under this scale, the permittivity response in different temperature can be clearly be seen in the whole frequency range. It can be seen that the dielectric process moves to a higher frequency by increasing the temperature. It is also indicated that the permittivity increases by temperature for the range of frequency larger than 10 Hz. The most top negative dielectric in order of $10^7 - 10^8$ can be obtained in most negative dielectric cases, and it increases by the temperature. The negative to positive transition frequency also affected by temperature and shifted to a higher frequency by increasing the temperature.

The change of permittivity by the temperature for each frequency is presented in Fig. 5.18. It is undeniable that the process moves to a higher temperature by increasing the frequency. The negative permittivity range also become shorter by an increasing frequency and it's wholly gone for 10 Hz frequency.

The dielectric loss shows two processes in low and high frequency presented in Fig. 5.19.

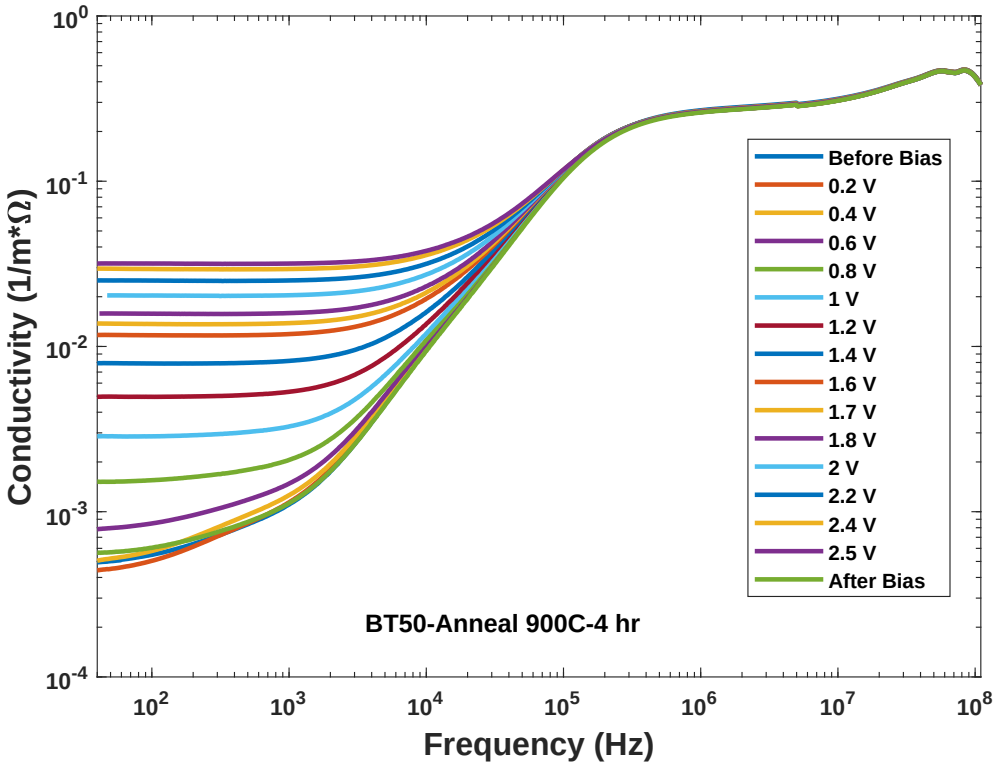

Figure 5.15: Effect of DC bias on conductivity of BT50 SPS sample annealed at 900 ^0C for four hours.

The low-frequency process change to the sharp peak at -40 ^0C corresponded to negative permittivity and shifted to a higher frequency by increasing temperature. When the temperature reaches to 180 ^0C, the sharp peak completely has gone, and the Debye-like peak will emerge. The process at higher frequency has similar behavior, its start at 10^4 Hz and its move to a higher frequency by increasing temperature. The peak values are constant for most temperature range but when it got to more than 100 ^0C its start to increase slightly.

The dielectric loss of sample increases by increasing the temperature except peaks corresponds to negative permittivity. Besides, the sharp peaks there is two small peak at -10 ^0C and 140 ^0C which is can be seen in the frequency of 1, 10 and 100 Hz.

The effect of temperature on the AC conductivity of the annealed sample presented in Fig. 5.21. The conductivity starts with a horizontal straight line which is related to dc conductivity of sample and increases by increasing the temperature. At high frequency, the

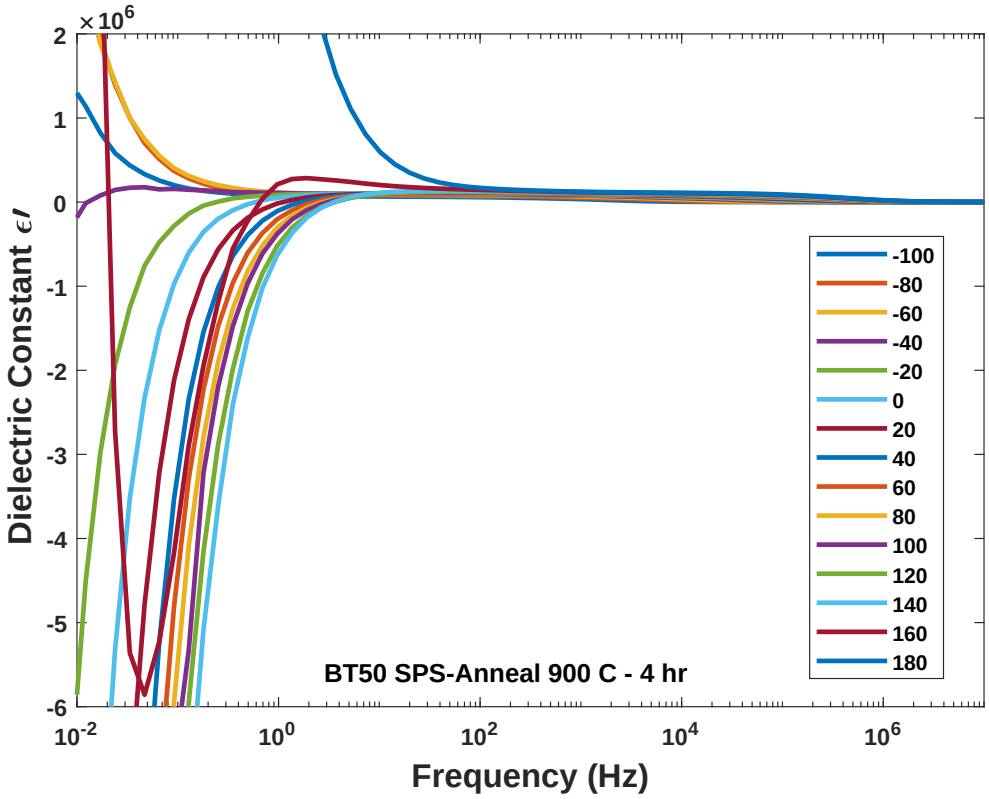

Figure 5.16: Effect of temperature on permittivity of BT50 SPS sample annealed at 900 ^0C for four hours.

conductivity obeys the universal law and rising by the factor of Aw^n. By increasing the temperature the dc conductivity range increases to a higher frequency and the process shifted by it. A better view on the effect of temperature on DC conductivity can be seen by plotting conductivity against the temperature for each frequency. It seems that the conductivity is increasing with different rate by low and high frequency. The Fig. 5.22 indicates that for the frequency range from 10^{-2} to 10^2 the conductivity almost has a similar pattern. As we explained in the previous chapter, the low-frequency conductivity can be considered as a DC conductivity because based on universal power law the straight vertical is known for it. The above figure validates this theory and shows for a long range of frequency; the conductivity shows almost the same values. Based on this consideration, the different process in the system can be recognized, and the activation of each of them can be calculated. The following two figures (Fig. 5.23, Fig. 5.24), plotted Logarithm of DC conductivity versus the

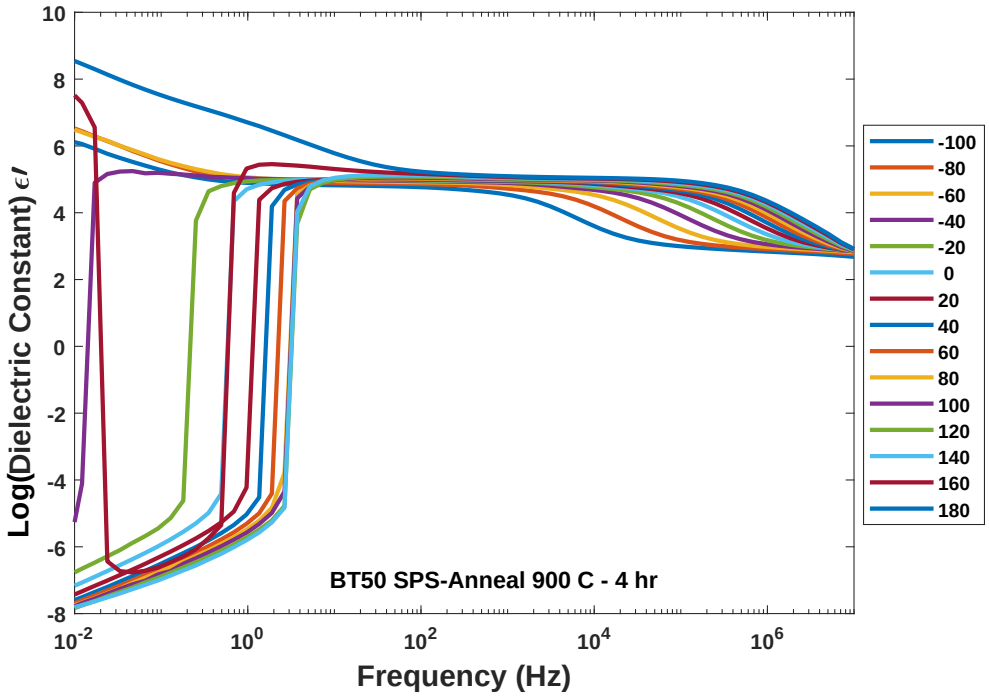

Figure 5.17: Effect of temperature on permittivity of BT50 SPS sample annealed at 900 ^0C for four hours.

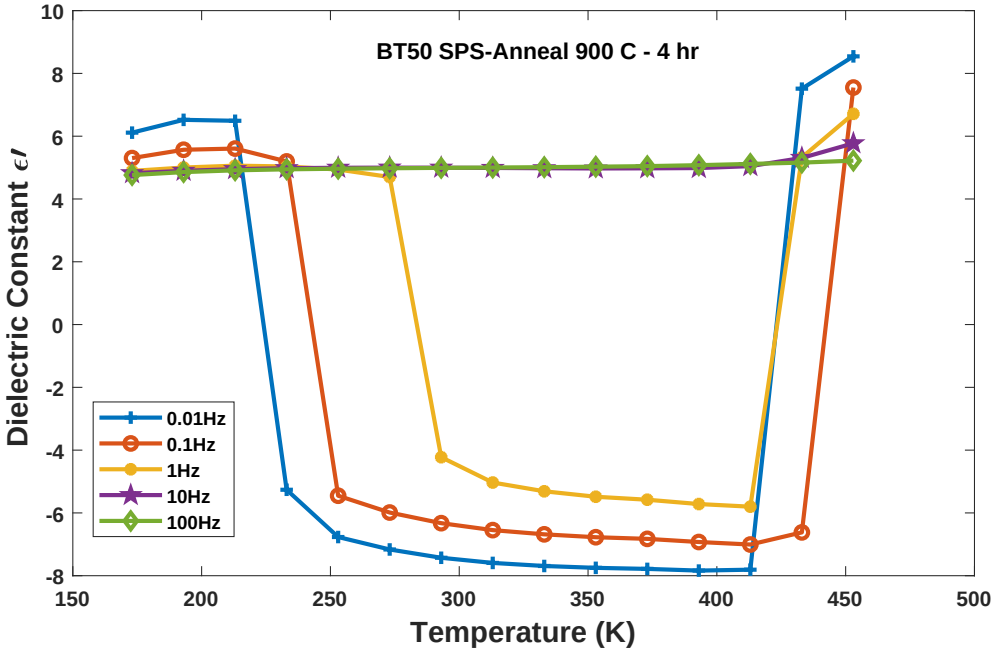

Figure 5.18: Effect of temperature on permittivity of BT50 SPS sample annealed at 900 ^0C for four hours.

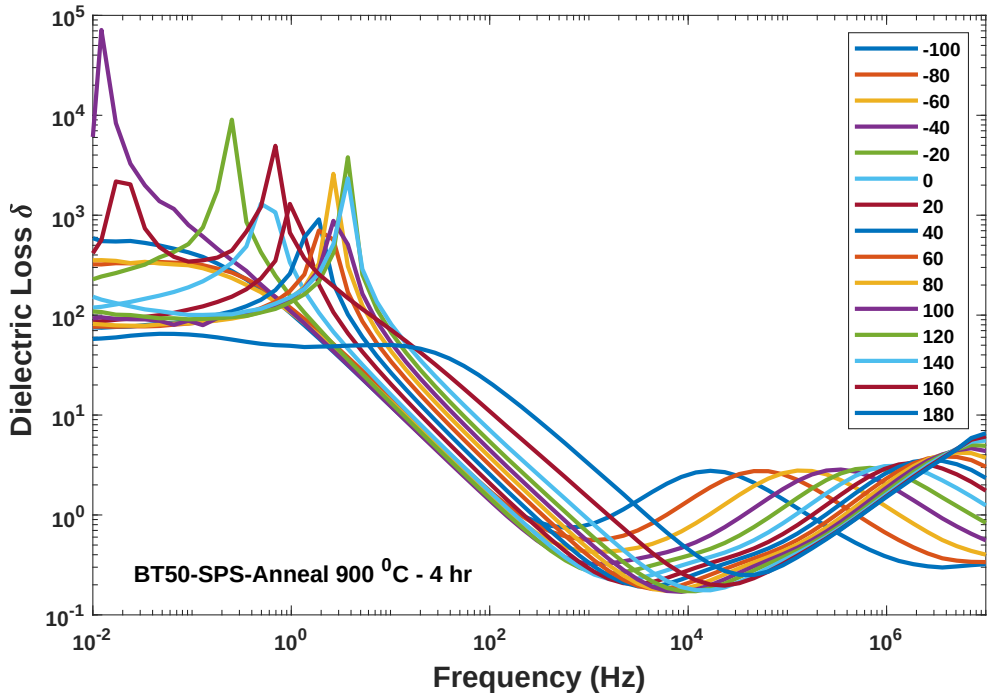

Figure 5.19: Effect of temperature on dielectric loss of BT50 SPS sample annealed at 900 ^0C for four hours.

inverse of the temperature. By calculating the slope of each mechanism, their activation energy can be calculated. The three conductivity is connected to the behavior of permittivity on the different temperature range. The first one is related to the positive permittivity in low temperature at analyzed frequency. The second one starts around -60 ^0C and negative permittivity start at this temperature. The last mechanism corresponds to the temperature bigger than 140 ^0C which can consider as phase transition temperature and the negative permittivity begin to vanish.

Dielectric temperature dependency of 1100 ^{0}C annealed sample

In the previous section, the temperature dependence of the annealed sample was studied. As mentioned, the annealed sample behaves as a fresh SPS sample and keep its temperature dependence as same as before annealing. In those samples, the annealing temperature or time is not large enough which make the annealing not affect all sample and mostly more

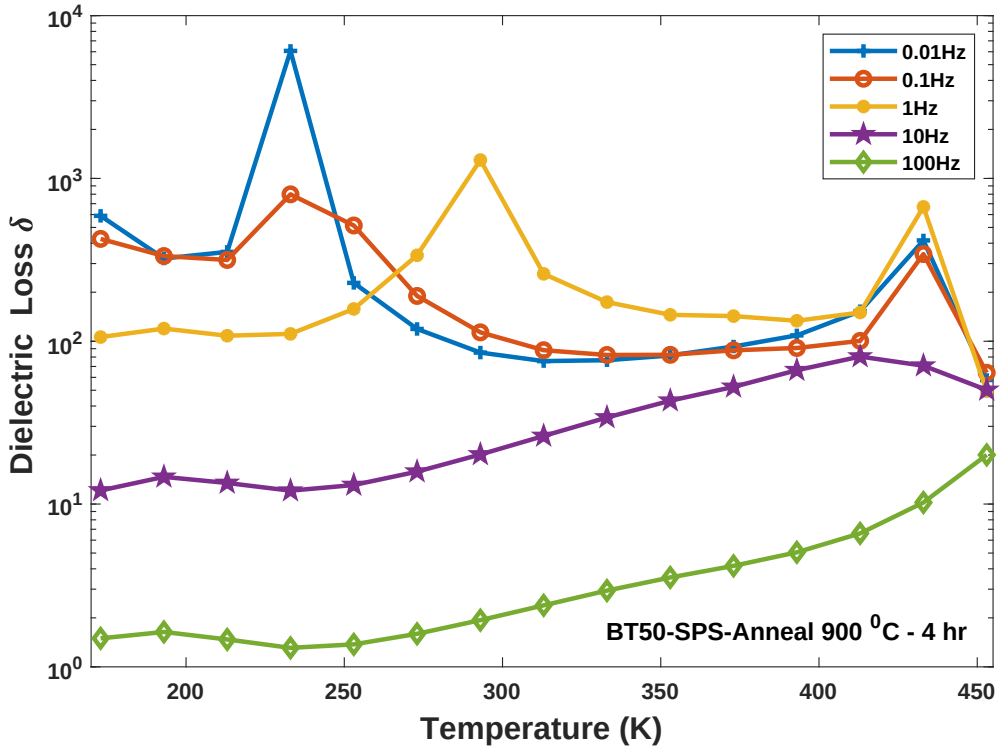

Figure 5.20: Effect of temperature on dielectric loss of BT50 SPS sample annealed at 900 ^0C for four hours.

Table 5.1: Activation energy of conductivity of BT50 Annealed at 900 ^0C for four hours sample.

	0.01 Hz	
Temperature	**Activation Energy E_a (eV)**	σ_0
120 ^0C to 180 ^0C	0.252	1.097
-20 ^0C to 100 ^0C	0.098	0.0102
-100 ^0C to -40 ^0C	0.0209	0.00029
	100 Hz	
Temperature	**Activation Energy E_a (eV)**	σ_0
120 ^0C to 180 ^0C	0.386	46.81
-20 ^0C to 100 ^0C	0.09268	0.00754
-100 ^0C to -40 ^0C	0.0209	0.000324

exposed areas like surface and grainboundaries effected. However, when the annealing took place at 1100 ^{0}C for adequate time, the color sample changes entirely from dark blue to close to white color. These means that the defects such as oxygen vacancies generated by the SPS process are eliminated by the annealing completely. In result, the sample behaves

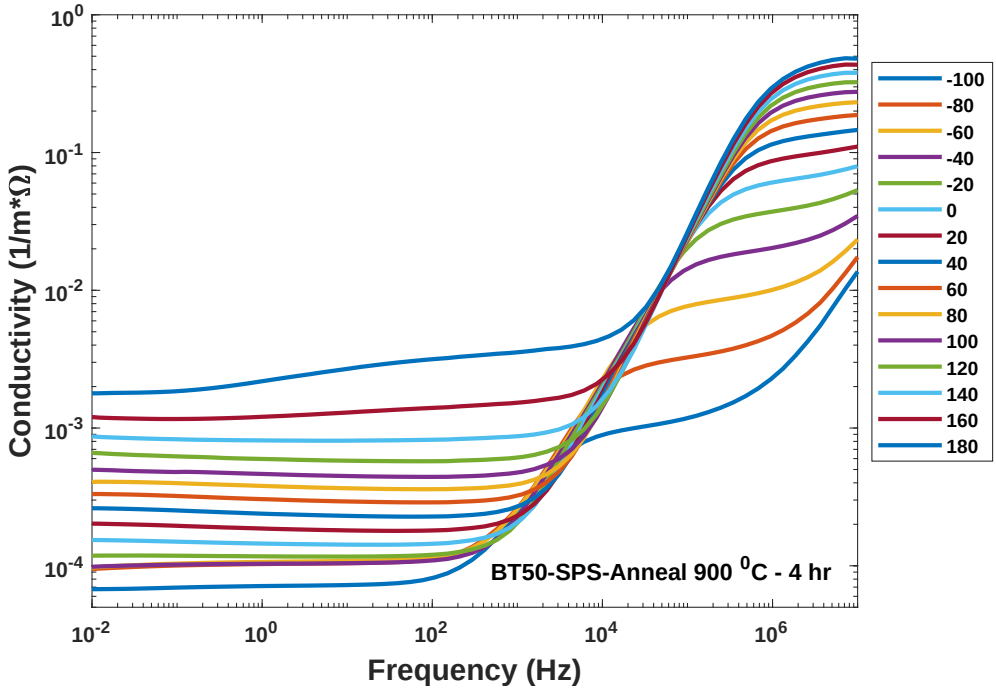

Figure 5.21: Effect of temperature on conductivity of BT50 SPS sample annealed at 900 ^0C for four hours.

very similarly to a composite made by conventional sintering.

The following picture presents the permittivity of BT50 SPS sample annealed at 1100 ^0C for four hours (BT50-11-4) in different temperature for various frequency (Fig. 5.25). The relaxor-like dependency can be seen around 120 ^0C, and there is a smooth peak close to 0 ^0C. Totally the permittivity value doesn't affect much by the temperature. Such behavior is almost the same for all frequency.

The dielectric loss of the sample is less than three percent at low-frequency range. The dielectric loss mostly shows decreasing by the increasing temperature. The dielectric loss change of various frequency by the temperature is shown in Fig. 5.25. It seems by increasing the frequency, and there is a process which move to a higher temperature. At 10^5 frequency, the dielectric loss shows two peaks at -10 ^0C and 105 ^0C. Although, these process is not very clear in a lower frequency, but they might due to phase transformation of BTO.

The permittivity of BT14 SPS-SG sample annealed at 1100 ^0C for four hours (BT14-SG-

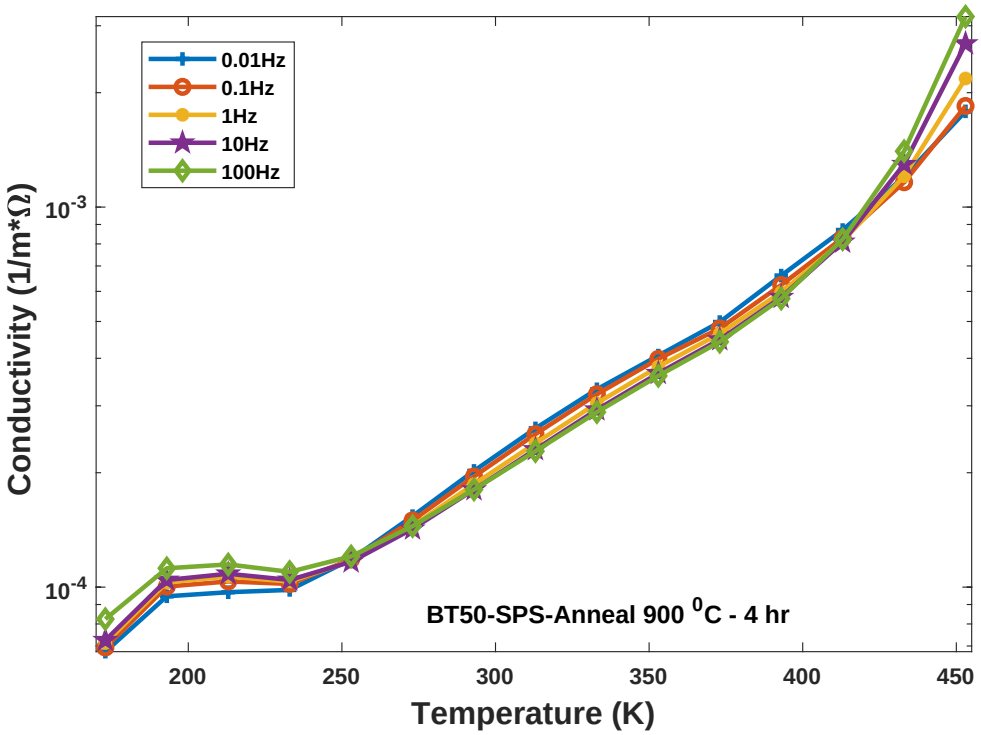

Figure 5.22: Effect of temperature on conductivity of BT50 SPS sample annealed at 900 ^0C for four hours.

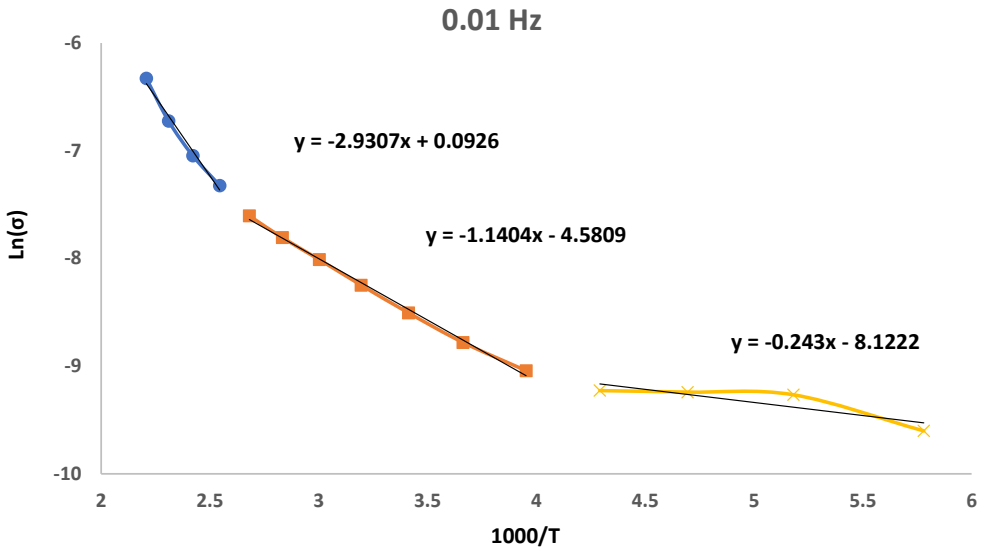

Figure 5.23: Effect of temperature on dielectric loss of BT50 SPS sample annealed at 900 ^0C for four hours.

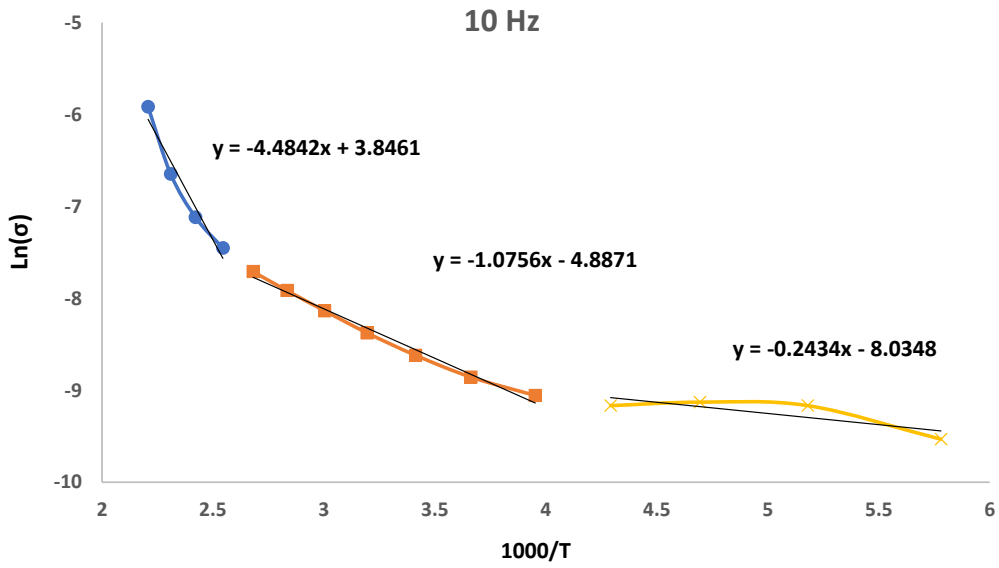

Figure 5.24: Effect of temperature on dielectric loss of BT50 SPS sample annealed at 900 ^0C for four hours.

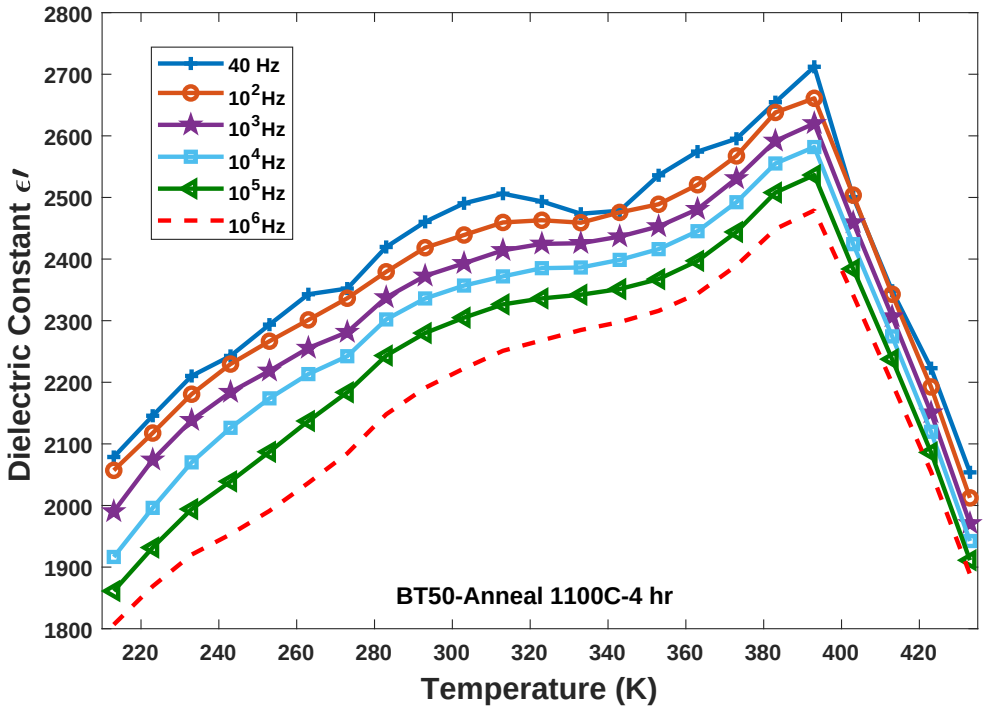

Figure 5.25: Effect of temperature on permittivity of BT50 SPS sample annealed at 1100 ^0C for four hours.

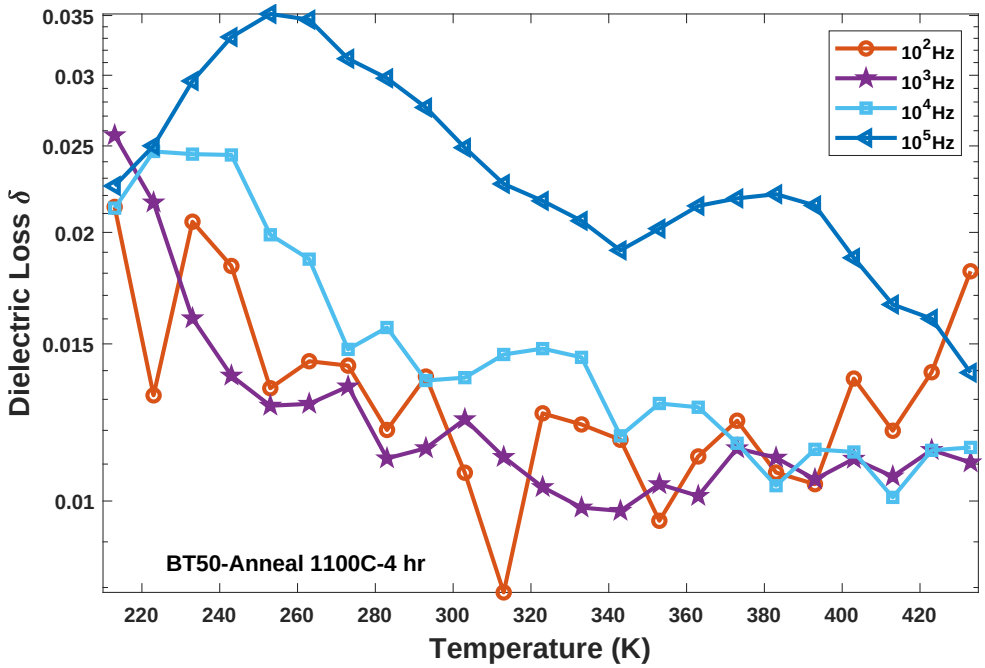

Figure 5.26: Effect of temperature on dielectric loss of BT50 SPS sample annealed at 1100 ^0C for four hours.

11-4) shows different behavior than BT50-11-4. The sample indicates hardly phase transformation at 120 ^0C, and there is no sign of it in other temperature. It is fascinating because the results confirm what we got on DSC results. On DSC just very small peak can be found around this temperature.

The dielectric loss of BT14-SG-11-4 is very noisy at low frequency and hardly can show any trends. At higher frequency, the dielectric loss shows a downward trend by increasing the temperature.

In the case of BT14 SPS not coated sample, the permittivity behave entirely different when they're annealed. The results present that even in low temperature or time annealing process the sample transforms completely to white-yellowish color which is the original color of BTO. All annealed sample doesn't show any sign of SPS sample behavior. The following picture (Fig. 5.29) shows the BT14 SPS Not coated sample annealed at 1100 ^0C for four hours (BT14-NC-11-4) which is similar to other annealed sample. It can clearly be seen two peaks related to phase transformation at 0 ^0C and 120 ^0C.

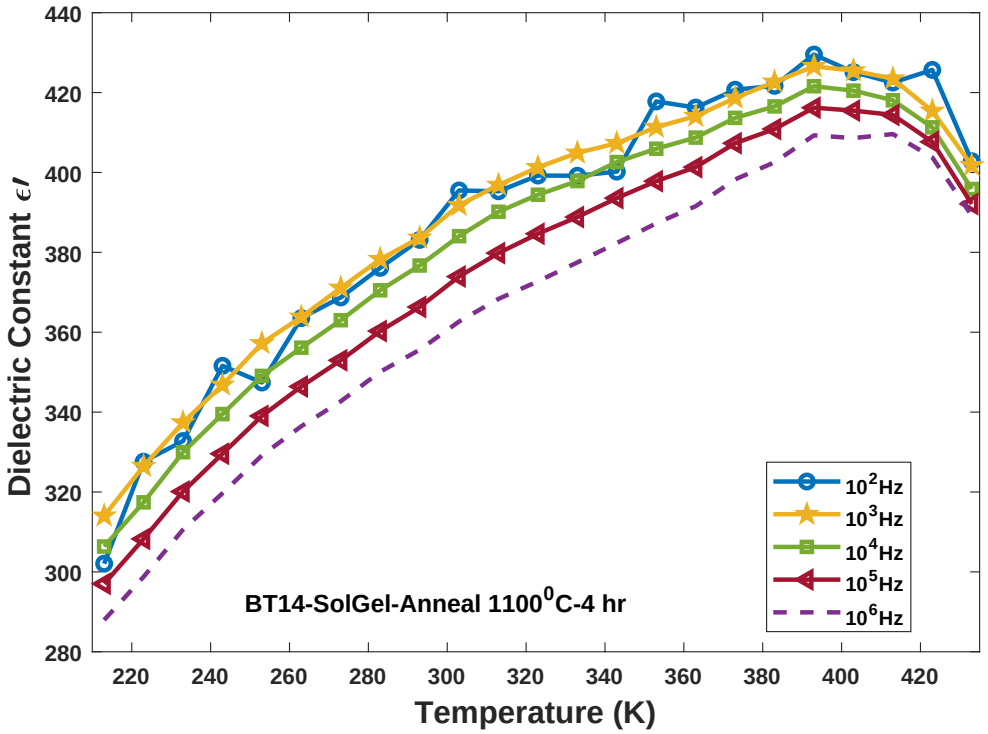

Figure 5.27: Effect of temperature on permittivity of BT14 SPS-SG sample annealed at 1100 ^0C for four hours.

The dielectric loss of BT14-NC-11-4 has temperature dependency similar to the permittivity of the sample. The only difference is that the dependency change by frequency. At low-frequency around 10^2Hz, the process is stronger around 0 ^0C which is shifted to 120 ^0C when the frequency increases to 10^5Hz.

5.3.5 P-E loop

The following figure shows the polarization of sample in the different electrical field (Fig. 5.31). The sample tested for PE loop was Annealed sample which annealed at 1100^0C for four hours. The results show ferroelectric behavior of sample originated form BTO properties with narrow loops. The good breakdown field of 190 kV/cm with a polarization of 32 $\mu C/cm^2$ can be a good candidate for energy storage. The calculated energy stored by the value of 3.3 J/cm^3 is promising material among ceramic composites.

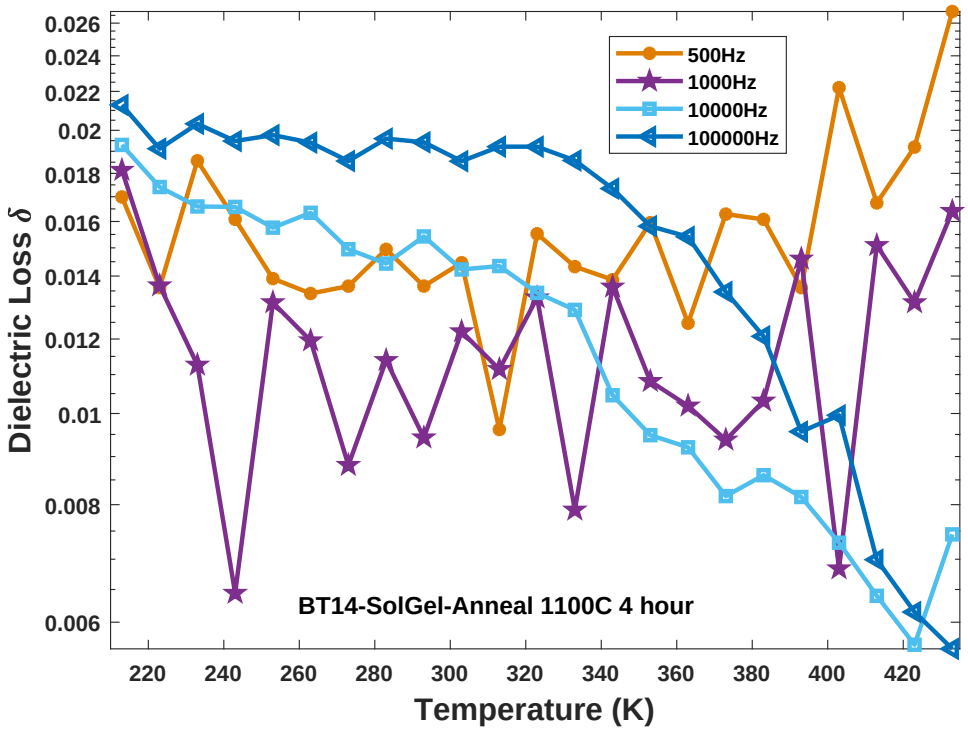

Figure 5.28: Effect of temperature on dielectric loss of BT14 SPS-SG sample annealed at 1100 ^0C for four hours.

The following figure (Fig. 5.32) present the PE loop of BT14 annealed sample at 1100 ^0C for four hours. The loop is as slim as the BT50 sample, and it has a higher breakdown field. However, the loop presented a much smaller polarization than BT50 which is not good for energy storages purpose.

The last two figures (Fig. 5.33, Fig. 5.34) is corresponding to the PE loop of BT14 sample which wasn't coated with SiO_2. The complete ferroelectric behavior can be seen in this figure, and the response is very similar to the Pure BTO. It means that the loop isn't slim and conduction loss is significant in the sample. Compare to BT14 with sol-gel coated SiO_2 it has much smaller breakdown field which is not suitable for energy storage applications.

Unlike the other SPS samples, In uncoated ceramics can be tested by the PE loop even in condition with annealing at low temperature with a short time. The only difference with improving the annealing parameter is on the value of the breakdown field and the polarization. Although, slightly improve in breakdown field can be seen in annealing with a

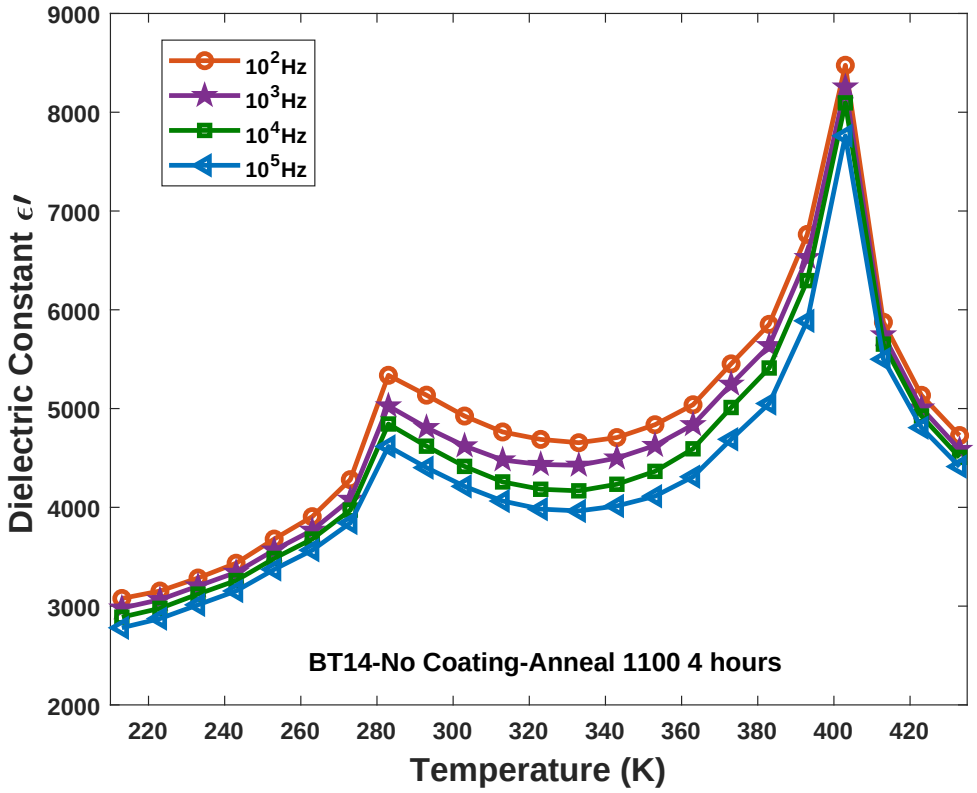

Figure 5.29: Effect of temperature on permittivity of BT14 SPS-NC sample annealed at 1100 ^0C for four hours.

longer time, but the polarization becomes smaller and totally not much change in the width of loop.

The pinch effect in PE loop can be seen in the result of BT14-NC annealed sample. The reason behind it is the defects pinned the motion of domains wall resulted in pinch loop. This effect mostly reported in BTO acceptor doped ceramics due to surface effect which is the gathering of charge defects gathering near the interface like grainboundaries [69], [13], [44]. In this sample, the oxygen vacancies mostly recover by annealing, and the remaining is reform in grainboundaries.

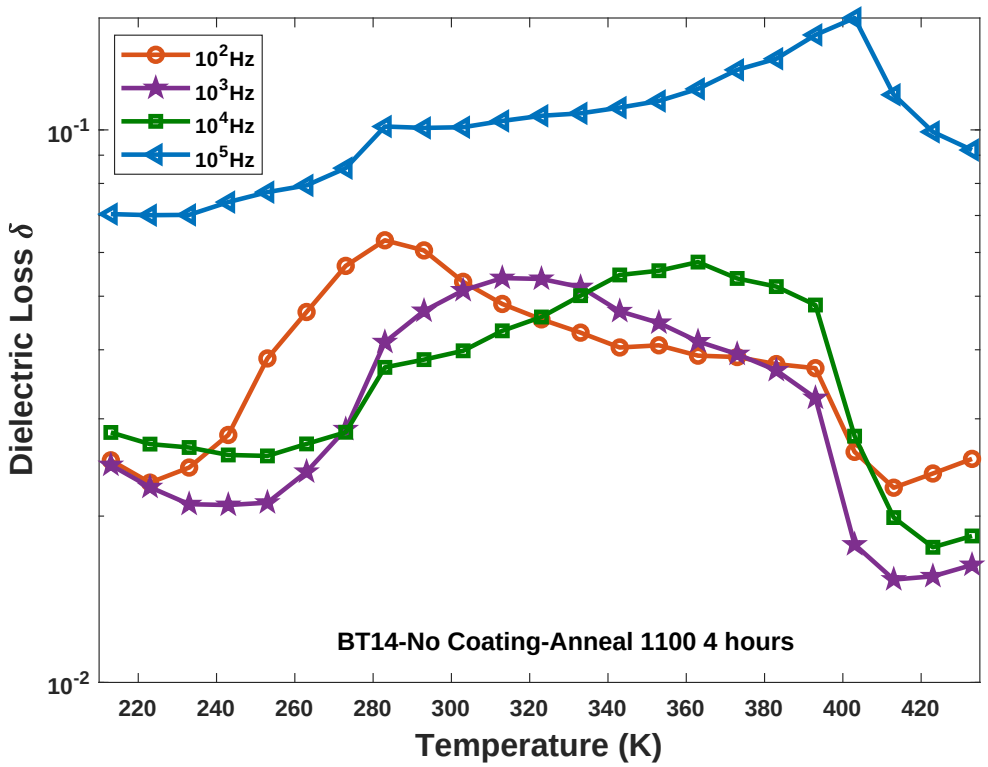

Figure 5.30: Effect of temperature on dielectric loss of BT14 SPS-NC sample annealed at 1100 ^0C for four hours.

5.4 Conclusion

The effect of annealing on dielectric properties of SPS samples was analysis in this chapter. The SPS sample underwent the annealing at 900 ^0C for 4 and 8 hours and 1100 ^0C for 4 hours. The color change can be seen in all samples and extending the annealing process make sample become more like the BTO/SiO_2 ceramic fabricated in the conventional method. The dielectric loss decreases significantly by the process but the permittivity reduced in a small portion. The ceramic behavior suggests that the oxygen vacancies generated by the fabricated process can vanish during the annealing. This cause the sample to undergo significant change by improving the annealing process.

The annealed sample at 900 ^0C for 4 hours shows similar negative permittivity compared to the fresh sample. The DC conductivity plotted against the temperature reveals three

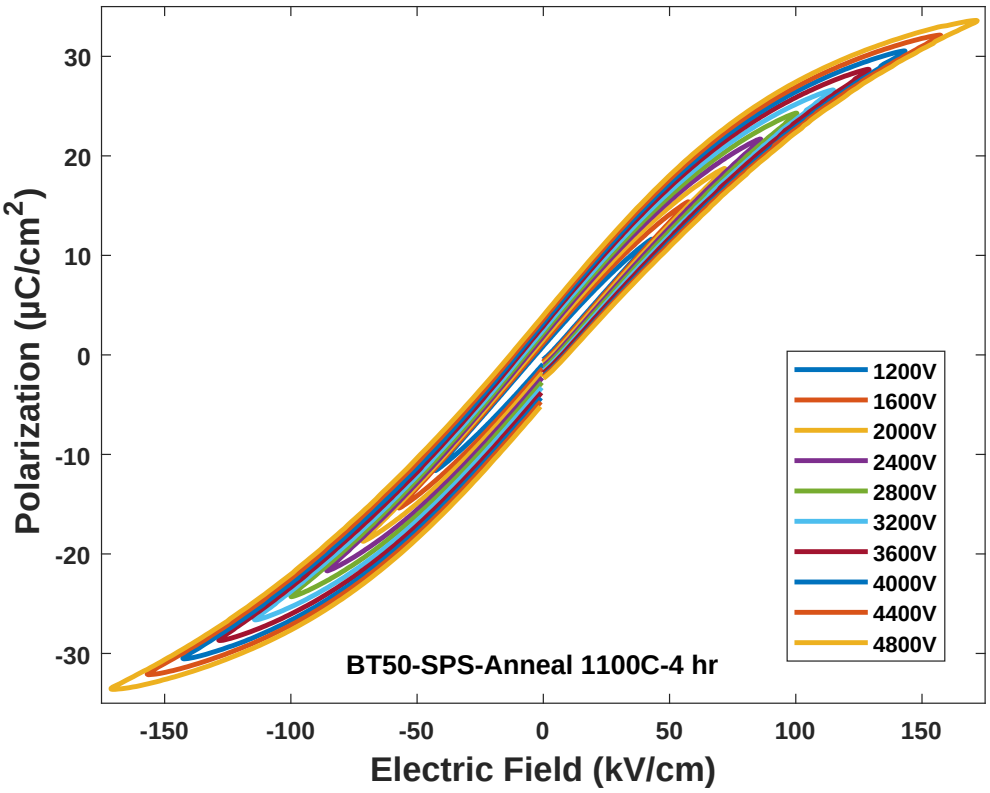

Figure 5.31: PE loop of BT50 SPS sample annealed at 1100 ^0C for 4 hours.

different mechanisms with different activation responsible for dielectric sign change in low-frequency dispersion.

The PE loop test shows proper energy storage for the BT50 sample annealed at 1100 ^0C for four hours. This sample shows a very thin width loop and high polarization with acceptable breakdown field. The PE loop is not much promising for BT14 sample and not coated sample shows a fat loop with low breakdown field.

The DSC result confirms the structure change by phase transformations peaks which responsible for dielectric behavior in different temperature. It is the great interest of the BT14 sample shows no phase transition peaks during DSC, and those behavior match the dielectric behavior with no change in relatively high temperature.

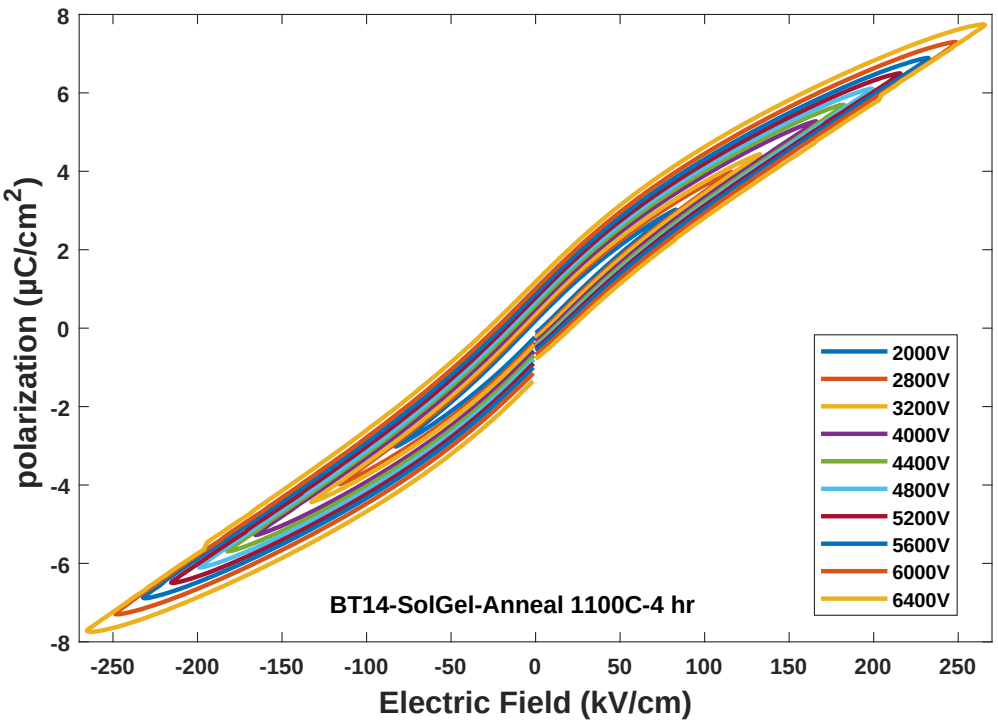

Figure 5.32: PE loop of BT14 SPS sample annealed at 1100 ^0C for 4 hours.

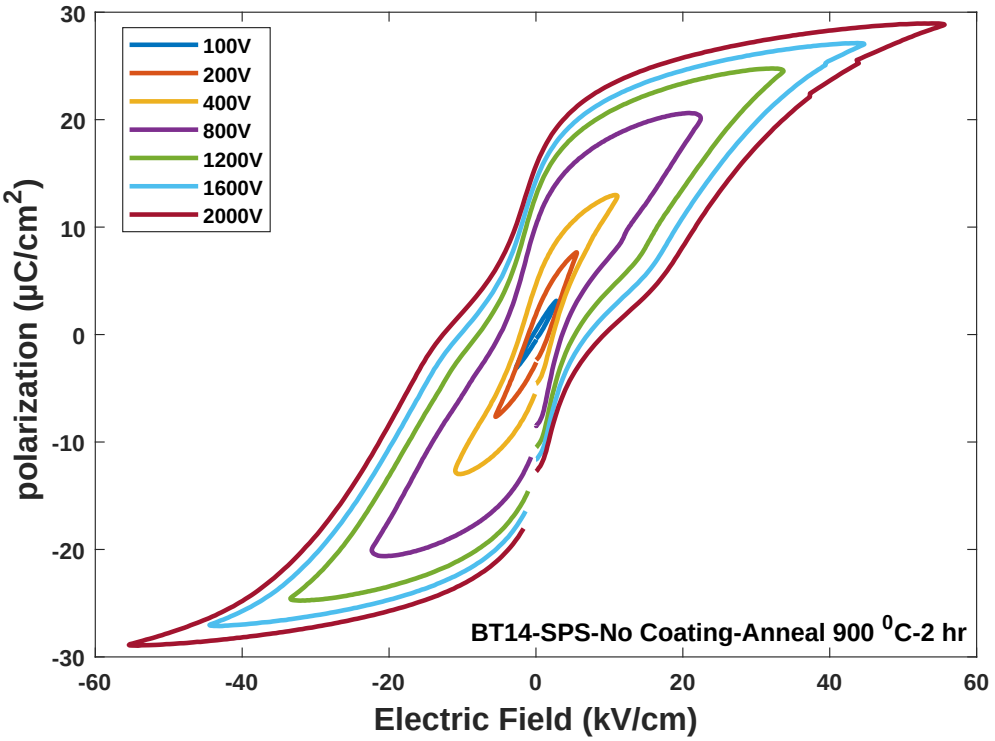

Figure 5.33: PE loop of BT14 SPS sample annealed at 1100 ^0C for 4 hours.

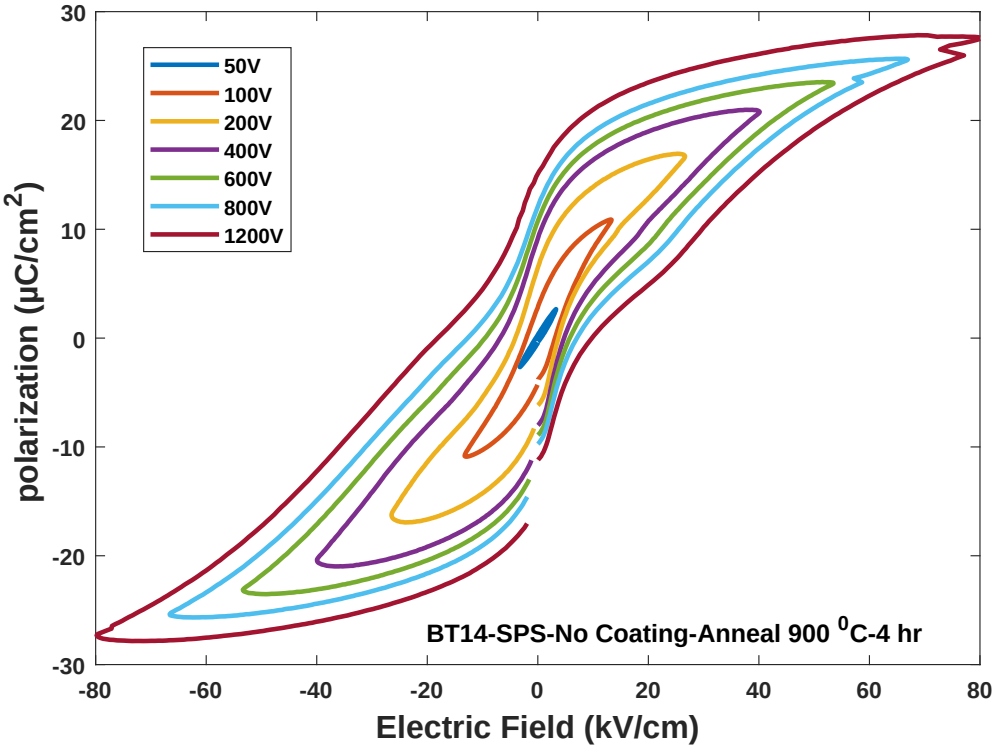

Figure 5.34: PE loop of BT14 SPS sample annealed at 1100 ^0C for 4 hours.

Chapter 6

Final Summary and Future Works

6.1 Summary of created composites

In the first project(third chapter), composites were fabricated by coating various thickness of SiO_2 layer on CCTO particles prepared by the sintering process. The sintering temperatures were chosen based on the eutectic point between SiO_2 and CuO. The following is a summary of the mechanism and properties of ceramics.

1- Sample fabricated at the sintering temperature lower than 1060 ^0C, as expected by increasing the SiO_2 concentration, both permittivity, and the dielectric loss are decreases. Such behavior can simply explain by both mixing laws of composite and IBLC model. Based on IBLC the permittivity of the composite is directly proportional to the grainboundary. These samples show excellent improvement on the nonlinear conductivity and breakdown of composites.

2-In case of samples prepared at a temperature higher than 1060 ^0C we should separate two different situations:

2a- First, composites which filler concentration is not adequate to form eutectic (lower than 25 percent). In this case, the grains become larger by increasing temperature which leads to a slight change in dielectric properties of composites. These composites have acceptable permittivity and dielectric loss.

2b- Second, are the composites with filler concentration more than eutectic. In this composites, the liquid phase can emerge and help to the movement of elements at sintering. Such a process result in the development of a new phase and the formation of defects in the unstable structure of CCTO. Both new phase and defects can make the permittivity increases based on the IBLC and the NBLC model, Respectively. It is fascinating that these composites

show high permittivity up to 10^5 for composites contains more than 30 percent SiO_2 which make such composites much lower loss. These are great candidates for applications like capacitors.

In the second project (Forth chapter), BTO ceramics were sintered by SPS method. The SPS method can form defects inside the ceramics. The main focus of this research is the ceramics with composites of BTO/SiO_2. These defects cause a change in the properties of composite significantly as a follow:

1- The DSC result shows any peaks related to phase transformation for sample composites with SiO_2. The permittivity spectrum also doesn't show any phase transformation peaks for all ceramics. However, there is a small change in activation energy when the sample heated to more than 120 C.

2- The SPS sample posses gigantic permittivity (up to 10^6) compare to composites fabricated in the conventional method. Such behavior is mostly due to charge accumulation of loosely bound electrons in the ceramics.

3- The fabricated ceramics can show negative permittivity in the range of low frequency around 100 Hz by applying DC bias. Such behavior can also be obtained without DC bias at a very low frequency of 0.1 Hz.

4- The fitted result based on the Drude model is prove for the loosely bound electrons, and such composites have lower plasma frequency compare to any other materials as reported till today. Moreover, their both positive and negative permittivity are the largest compared to epsilon negative materials which make these composites Unique materials for dielectric, energy storage and also transistors, electronic cloaking/shielding, metamaterials applications.

In the last chapter(fifth), the effect of annealing on the concentration of oxygen vacancies in BTO SPS composites and its properties was studied. There are the following change and features that annealed ceramics posses:

1- The annealed samples which don't contain SiO_2 can reform back to the original BTO. This sample posses conventional DSC and the permittivity result of BTO ceramics. For the

coated sample, only 120 C peaks are slightly recover..

2- The permittivity and polarization of fully annealed sample show much higher values compared to conventional composites which make these composites great candidate for energy storages.

3- The permittivity of the partially annealed sample still has high values, and dielectric loss decreases significantly in this process which makes them better materials for dielectric purposes.

4- These composites still shows negative permittivity with lower plasma frequency. Such behavior not only proves over the debate of dependant of negative property to the oxygen vacancies but also has a great interest in tunable electronic applications.

6.2 Future work

Based on the results and discussions we have in this dissertation the following are suggestions that can be used in the future works.

1- The CCTO composites also have the potential to shows negative permittivity due to the formation of a new phase and defects in the material.

2- The annealing can generate the gradient in concentration of oxygen vacancies, that make the properties change across the sample thickness. Such a sample can demonstrate abnormal behavior by applying an electrical field.

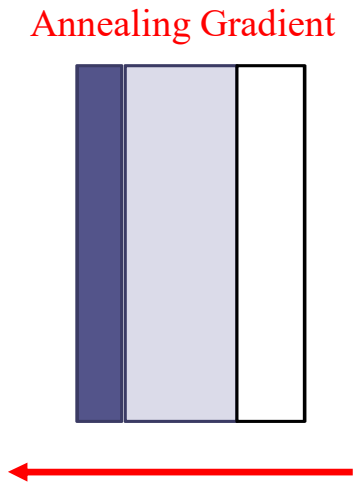

Figure 6.1: Gradient annealing process from specimen surface to the bottom.

3- By producing a partially annealed sample, there is a chance to get materials with high permittivity and high breakdown field which make the energy storage extremely high.

Bibliography

[1] F Amaral, LC Costa, and MA Valente. Decrease in dielectric loss of $cacu_3ti_4o_{12}$ by the addition of teo_2. *Journal of Non-Crystalline Solids*, 357(2):775–781, 2011.

[2] F Amaral, MA Valente, and LC Costa. Dielectric properties of $cacu_3ti_4o_{12}$ ($ccto$) doped with ge_o2. *Journal of Non-Crystalline Solids*, 356(11-17):822–827, 2010.

[3] Mario Aparicio, Andrei Jitianu, and Lisa C Klein. *Sol-gel processing for conventional and alternative energy*. Springer Science & Business Media, 2012.

[4] Aly M Badr, Haroun A Elshaikh, and Ibraheim M Ashraf. Impacts of temperature and frequency on the dielectric properties for insight into the nature of the charge transports in the tl_2s layered single crystals. *Journal of Modern Physics*, 2(01):12, 2011.

[5] Peter Barber, Shiva Balasubramanian, Yogesh Anguchamy, Shushan Gong, Arief Wibowo, Hongsheng Gao, Harry J Ploehn, and Hans-Conrad Zur Loye. Polymer composite and nanocomposite dielectric materials for pulse power energy storage. *Materials*, 2(4):1697–1733, 2009.

[6] Joanna A Bartkowska, Dariusz Bochenek, and Przemysław Niemiec. Multiferroic aurivillius-type bi 6 fe 2- x mn x ti 3 o 18 (0 x 1.5) ceramics with negative dielectric constant. *Applied Physics A*, 124(12):823, 2018.

[7] Aditya Chauhan, Satyanarayan Patel, Rahul Vaish, and Chris R Bowen. Antiferroelectric ceramics for high energy density capacitors. *Materials*, 8(12):8009–8031, 2015.

[8] Min Chen, Zhongyang Wang, Peitao Xie, Zidong Zhang, Laixue Pang, Guohua Fan, Yao Liu, and Runhua Fan. The negative permittivity behavior of carbon nanotubes/yttrium iron garnet composites in the radio frequency. *Materials Letters*, 213:282–285, 2018.

[9] Chuan-bing Cheng, Runhua Fan, Guohua Fan, Hu Liu, Jiao-xia Zhang, Jianxing Shen, Qian Ma, Renbo Wei, and Zhanhu Guo. Tunable negative permittivity and magnetic performance of yttrium iron garnet/polypyrrole metacomposites at the rf frequency. *Journal of Materials Chemistry C*, 2019.

[10] Chuanbing Cheng, Runhua Fan, Zhongyang Wang, Qian Shao, Xingkui Guo, Peitao Xie, Yansheng Yin, Yuliang Zhang, Liqiong An, Yanhua Lei, et al. Tunable and weakly negative permittivity in carbon/silicon nitride composites with different carbonizing temperatures. *Carbon*, 125:103–112, 2017.

[11] Chuanbing Cheng, Kelan Yan, Runhua Fan, Lei Qian, Zidong Zhang, Kai Sun, and Min Chen. Negative permittivity behavior in the carbon/silicon nitride composites prepared by impregnation-carbonization approach. *Carbon*, 96:678–684, 2016.

[12] JH Choi, Y Mao, and JP Chang. Development of hafnium based high-k materialsa review. *Materials Science and Engineering: R: Reports*, 72(6):97–136, 2011.

[13] Jin Hong Choi, Takeshi Yoshimura, Norifumi Fujimura, and Chae Il Cheon. Saturated and pinched ferroelectric hysteresis loops in bifeo 3 ceramics. *Journal of the Korean Physical Society*, 74(3):269–273, 2019.

[14] Biswajit Choudhury, Pawan Chetri, and Amarjyoti Choudhury. Annealing temperature and oxygen-vacancy-dependent variation of lattice strain, band gap and luminescence properties of ceo2 nanoparticles. *Journal of Experimental Nanoscience*, 10(2):103–114, 2015.

[15] CW Chu, F Chen, J Shulman, S Tsui, YY Xue, W Wen, and P Sheng. A negative dielectric constant in nano-particle materials under an electric field at very low frequencies. In *Strongly Correlated Electron Materials: Physics and Nanoengineering*, volume 5932, page 59320X. International Society for Optics and Photonics, 2005.

[16] David R Clarke. Varistor ceramics. *Journal of the American Ceramic Society*, 82(3):485–502, 1999.

[17] S Demirezen, A Kaya, S Altındal Yerişkin, M Balbaşı, and İ Uslu. Frequency and voltage dependent profile of dielectric properties, electric modulus and ac electrical conductivity in the prbacoo nanofiber capacitors. *Results in physics*, 6:180–185, 2016.

[18] OV Dolgov, DA Kirzhnits, and EG Maksimov. On an admissible sign of the static dielectric function of matter. *Reviews of Modern Physics*, 53(1):81, 1981.

[19] Jeppe C Dyre and Thomas B Schrøder. Universality of ac conduction in disordered solids. *Reviews of Modern Physics*, 72(3):873, 2000.

[20] Arthur J Epstein, Fang-Chi Hsu, Nan-Rong Chiou, and Vladimir N Prigodin. Electric-field induced ion-leveraged metal–insulator transition in conducting polymer-based field effect devices. *Current Applied Physics*, 2(4):339–343, 2002.

[21] Diana Estevez, Faxiang Qin, Yang Luo, Le Quan, Yiu-Wing Mai, Larissa Panina, and Hua-Xin Peng. Tunable negative permittivity in nano-carbon coated magnetic microwire polymer metacomposites. *Composites Science and Technology*, 171:206–217, 2019.

[22] AA Felix, Marcelo Ornaghi Orlandi, and José Arana Varela. Schottky-type grain boundaries in *ccto* ceramics. *Solid State Communications*, 151(19):1377–1381, 2011.

[23] ND Gavrilova, VK Novik, AV Vorobyev, and IA Malyshkina. Negative dielectric permittivity of poly (acrylic acid) pressed pellets. *Journal of Non-Crystalline Solids*, 452:1–8, 2016.

[24] Reza Gholipur and Ali Bahari. Effect of electric field on the dielectric and magnetic properties of random nanocomposites. *Materials & Design*, 94:139–147, 2016.

[25] Reza Gholipur and Ali Bahari. Alignment of ag nanoparticles by an external electric field proposed for metamaterial applications. *Current Applied Physics*, 17(7):989–998, 2017.

[26] Keith L Gordon, Jin Ho Kang, Cheol Park, Peter T Lillehei, and Joycelyn S Harrison. A novel negative dielectric constant material based on phosphoric acid doped poly (benzimidazole). *Journal of Applied Polymer Science*, 125(4):2977–2985, 2012.

[27] Keith L Gordon, Jin Ho Kang, Cheol Park, Peter T Lillehei, and Joycelyn S Harrison. Negative dielectric constant material based on ion conducting materials, August 15 2017. US Patent 9,734,932.

[28] Hongbo Gu, Jiang Guo, Suying Wei, and Zhanhu Guo. Polyaniline nanocomposites with negative permittivity. *Journal of Applied Polymer Science*, 130(4):2238–2244, 2013.

[29] Xihong Hao. A review on the dielectric materials for high energy-storage application. *Journal of Advanced Dielectrics*, 3(01):1330001, 2013.

[30] JinLiang He, FengChao Luo, Jun Hu, and YuanHua Lin. *cu* segregation and its effects on the electrical properties of calcium copper titanate. *Science China Technological Sciences*, 54(9):2506–2510, 2011.

[31] Yu-Che Ho, Md Nadim Ferdous Hoque, Elizabeth Stoneham, Juliusz Warzywoda, Tim Dallas, and Zhaoyang Fan. Reduction of oxygen vacancy related traps in tio2 and

the impacts on hybrid perovskite solar cells. *The Journal of Physical Chemistry C*, 121(43):23939–23946, 2017.

[32] Qing Hou, Kelan Yan, Runhua Fan, Kun Zhang, Zidong Zhang, Shibing Pan, and Mingxun Yu. Negative permittivity in fe–si–ni/epoxy magnetic composite materials at high-frequency. *Materials Chemistry and Physics*, 170:113–117, 2016.

[33] Chia-Hung Hsieh, An-Hung Lee, Cheng-Dar Liu, Jin-Lin Han, Kuo-Huang Hsieh, and Sung-Nung Lee. Polyaniline nano-composites with large negative dielectric permittivity. *AIP Advances*, 2(1):012127, 2012.

[34] Rolf E Hummel. *Electronic properties of materials*. Springer Science & Business Media, 2011.

[35] Andrew K Jonscher. Dielectric relaxation in solids. *Journal of Physics D: Applied Physics*, 32(14):R57, 1999.

[36] J Joo, EJ Oh, G Min, AG MacDiarmid, and Arthur Joseph Epstein. Evolution of the conducting state of polyaniline from localized to mesoscopic metallic to intrinsic metallic regimes. *Synthetic metals*, 69(1-3):251–254, 1995.

[37] Kang-Min Kim, Sun-Jung Kim, Jong-Heun Lee, and Doh-Yeon Kim. Microstructural evolution and dielectric properties of sio_2-doped $cacu_3ti_4o_{12}$ ceramics. *Journal of the European Ceramic Society*, 27(13):3991–3995, 2007.

[38] Xuechen Kou, Xiuchao Yao, and Jun Qiu. Negative permittivity and negative permeability of multi-walled carbon nanotubes/polypyrrole nanocomposites. *Organic Electronics*, 38:42–47, 2016.

[39] S Krohns, P Lunkenheimer, SG Ebbinghaus, and A Loidl. Colossal dielectric constants in single-crystalline and ceramic $cacu_3ti_4o_{12}$ investigated by broadband dielectric spectroscopy. *Journal of Applied Physics*, 103(8):084107, 2008.

[40] Seunghwa Kwon, Chien-Chih Huang, MA Subramanian, and David P Cann. Effects of cation stoichiometry on the dielectric properties of $cacu_3ti_4o_{12}$. *Journal of Alloys and Compounds*, 473(1):433–436, 2009.

[41] AN Lagarkov, SM Matytsin, KN Rozanov, and AK Sarychev. Dielectric properties of fiber-filled composites. *Journal of Applied Physics*, 84(7):3806–3814, 1998.

[42] Bin Li, Gang Sui, and Wei-Hong Zhong. Single negative metamaterials in unstructured polymer nanocomposites toward selectable and controllable negative permittivity. *Advanced Materials*, 21(41):4176–4180, 2009.

[43] J Li, AW Sleight, and MA Subramanian. Evidence for internal resistive barriers in a crystal of the giant dielectric constant material: $cacu_3ti_4o_{12}$. *Solid State Communications*, 135(4):260–262, 2005.

[44] Kun Li, Xiao Li Zhu, Xiao Qiang Liu, Xiao Ma, Mao Sen Fu, Jan Kroupa, Stanislav Kamba, and Xiang Ming Chen. Electric-field-induced phase transition and pinched p–e hysteresis loops in pb-free ferroelectrics with a tungsten bronze structure. *NPG Asia Materials*, 10(4):71, 2018.

[45] Laijun Liu, Yanmin Huang, Yunhua Li, Danping Shi, Shaoying Zheng, Shuangshuang Wu, Liang Fang, and Changzheng Hu. Dielectric and non-ohmic properties of $cacu_3ti_4o_{12}$ ceramics modified with nio, sno_2, sio_2, and al_2o_3 additives. *Journal of Materials Science*, 47(5):2294–2299, 2012.

[46] Zhen-Ya Lu, Xiao-Ming Li, and Jian-Qing Wu. Voltage-current nonlinearity of $cacu_3ti_4o_{12}$ ceramics. *Journal of the American Ceramic Society*, 95(2):476–479, 2012.

[47] VV Makarov and AB Sherman. Low-frequency dispersion of the negative dielectric permittivity in c 70 films. *Physics of the Solid State*, 44(11):2200–2203, 2002.

[48] Michio Matsuoka. Nonohmic properties of zinc oxide ceramics. *Japanese Journal of Applied Physics*, 10(6):736, 1971.

[49] Li Min, Chaoming Luo, Lirong Huang, Wengjin Wang, and Qingdong Zeng. Tunable semiconductor metamaterials. In *2018 Asia Communications and Photonics Conference (ACP)*, pages 1–2. IEEE, 2018.

[50] Julie J Mohamed, Sabar D Hutagalung, M Fadzil Ain, Karim Deraman, and Zainal A Ahmad. Microstructure and dielectric properties of $cacu_3ti_4o_{12}$ ceramic. *Materials Letters*, 61(8):1835–1838, 2007.

[51] M Mohammadi, P Alizadeh, and FJ Clemens. Effect of sio_2 on sintering and dielectric properties of $cacu_3ti_4o_{12}$ nanofibers. *Journal of Alloys and Compounds*, 688:270–279, 2016.

[52] Chun-Hong Mu, Peng Liu, Ying He, Jian-Ping Zhou, and Huai-Wu Zhang. An effective method to decrease dielectric loss of $cacu_3ti_4o_{12}$ ceramics. *Journal of Alloys and Compounds*, 471(1):137–141, 2009.

[53] Kazuo Mukae, Kouichi Tsuda, and Ikuo Nagasawa. Non-ohmic properties of *zno*-rare earth metal oxide-co_3o_4 ceramics. *Japanese Journal of Applied Physics*, 16(8):1361, 1977.

[54] Xin Ouyang, Mustafa Habib, Peng Cao, Shanghai Wei, Zhaohui Huang, Weijun Zhang, and Wei Gao. Enhanced extrinsic dielectric response of tio_2 modified $cacu_3ti_4o_{12}$ ceramics. *Ceramics International*, 41(10):13447–13454, 2015.

[55] John B Pendry, AJ Holden, WJ Stewart, and I Youngs. Extremely low frequency plasmons in metallic mesostructures. *Physical review letters*, 76(25):4773, 1996.

[56] Liang Peng, Lixin Ran, Hongsheng Chen, Haifei Zhang, Jin Au Kong, and Tomasz M Grzegorczyk. Experimental observation of left-handed behavior in an array of standard dielectric resonators. *Physical review letters*, 98(15):157403, 2007.

[57] Sidnei Antonio Pianaro, Paulo Roberto Bueno, Paulo Olivi, Elson Longo, and José Arana Varela. Effect of bi_2o_3 addition on the microstructure and electrical properties of the $sno_2.coo.nb_2o_5$ varistor system. *Journal of Materials Science Letters*, 16(8):634–638, 1997.

[58] Lei Qian, Lu Lu, and Runhua Fan. Tunable negative permittivity based on phenolic resin and multi-walled carbon nanotubes. *Rsc Advances*, 5(22):16618–16621, 2015.

[59] Yunpeng Qu, Guohua Fan, Deliang Liu, Yushan Gao, Ciqun Xu, Jun Zhong, Peitao Xie, Yao Liu, Yulin Wu, and Runhua Fan. Functional nano-units prepared by electrostatic self-assembly for three-dimension carbon networks hosted in cacu3ti4o12 ceramics towards radio-frequency negative permittivity. *Journal of Alloys and Compounds*, 743:618–625, 2018.

[60] Michal Rajnak, Zdenko Spitalsky, Bystrik Dolnik, Juraj Kurimsky, Ladislav Tomco, Roman Cimbala, Peter Kopcansky, and Milan Timko. Toward apparent negative permittivity measurement in a magnetic nanofluid with electrically induced clusters. *Physical Review Applied*, 11(2):024032, 2019.

[61] S Anantha Ramakrishna. Physics of negative refractive index materials. *Reports on progress in physics*, 68(2):449, 2005.

[62] M Rapos and JH Calderwood. Dielectric properties of moo3 under the simultaneous action of ac and dc voltages. *Journal of Physics D: Applied Physics*, 7(13):1838, 1974.

[63] Hummel Rolf. Electronic properties of materials, 2000.

[64] Suresh Sagadevan and A Shanmuga Sundaram. A brief review of the relevant dielectric theories of solids. *Latin-American Journal of Physics Education*, 8(3), 2014.

[65] Rainer Schmidt and Derek C Sinclair. $cacu_3ti_4o_{12}$ (*ccto*) ceramics for capacitor applications. *arXiv preprint arXiv:1402.1621*, 2014.

[66] Francesco Scotognella, Giuseppe Della Valle, Ajay Ram Srimath Kandada, Margherita Zavelani-Rossi, Stefano Longhi, Guglielmo Lanzani, and Francesco Tassone. Plasmonics in heavily-doped semiconductor nanocrystals. *The European Physical Journal B*, 86(4):154, 2013.

[67] SF Shao, JL Zhang, P Zheng, and CL Wang. Effect of *cu*-stoichiometry on the dielectric and electric properties in $cacu_3ti_4o_{12}$ ceramics. *Solid state communications*, 142(5):281–286, 2007.

[68] Richard A Shelby, David R Smith, and Seldon Schultz. Experimental verification of a negative index of refraction. *science*, 292(5514):77–79, 2001.

[69] Wei Shi, Qiang Chen, Xi Yue, Lihua Li, Dingquan Xiao, and Jianguo Zhu. Effect of impurity pinning on the hysteresis loop of pstzt ceramics. *Ferroelectrics*, 385(1):6162–168, 2009.

[70] Zhi-cheng Shi, Run-hua Fan, Ke-lan Yan, Kai Sun, Meng Zhang, Cheng-guo Wang, Xiang-fa Liu, and Xi-hua Zhang. Preparation of iron networks hosted in porous alumina with tunable negative permittivity and permeability. *Advanced Functional Materials*, 23(33):4123–4132, 2013.

[71] Zhi-cheng Shi, Run-hua Fan, Zi-dong Zhang, Lei Qian, Meng Gao, Mo Zhang, Li-tuo Zheng, Xi-hua Zhang, and Long-wei Yin. Random composites of nickel networks supported by porous alumina toward double negative materials. *Advanced Materials*, 24(17):2349–2352, 2012.

[72] Zhi-cheng Shi, Fan Mao, Jing Wang, Run-hua Fan, and Xin Wang. Percolative silver/alumina composites with radio frequency dielectric resonance-induced negative permittivity. *RSC Advances*, 5(130):107307–107312, 2015.

[73] Derek C Sinclair, Timothy B Adams, Finlay D Morrison, and Anthony R West. $cacu_3ti_4o_{12}$: one-step internal barrier layer capacitor. *Applied Physics Letters*, 80(12):2153–2155, 2002.

[74] Devendra P Singh, YN Mohapatra, and DC Agrawal. Dielectric and leakage current properties of sol-gel derived calcium copper titanate ($ccto$) thin films and $ccto/zro_2$ multilayers. *Materials Science and Engineering: B*, 157(1):58–65, 2009.

[75] MA Subramanian and AW Sleight. $acu_3ti_4o_{12}$ and $acu_3ru_4o_{12}$ perovskites: high dielectric constants and valence degeneracy. *Solid State Sciences*, 4(3):347–351, 2002.

[76] S Summerfield and PN Butcher. Analysis of ac and dc hopping conductivity in impurity bands and amorphous semiconductors. *Journal of Physics C: Solid State Physics*, 16(2):295, 1983.

[77] Kai Sun, Peitao Xie, Zhongyang Wang, Tongming Su, Qian Shao, JongEun Ryu, Xihua Zhang, Jiang Guo, Akash Shankar, Jianfeng Li, et al. Flexible polydimethylsiloxane/multi-walled carbon nanotubes membranous metacomposites with negative permittivity. *Polymer*, 125:50–57, 2017.

[78] Jing Wang, Zhicheng Shi, Fan Mao, Shougang Chen, and Xin Wang. Bilayer polymer metacomposites containing negative permittivity layer for new high-k materials. *ACS applied materials & interfaces*, 9(2):1793–1800, 2017.

[79] Mao-Hua Wang, Bo Zhang, and Fu Zhou. Preparation and characterization of silica-coated $cacu_3ti_4o_{12}$. *Journal of Electronic Materials*, 43(7):2607–2613, 2014.

[80] Xu-ai Wang, Zhi-cheng Shi, Min Chen, Run-hua Fan, Ke-lan Yan, Kai Sun, Shi-bing Pan, and Ming-xun Yu. Tunable electromagnetic properties in co/al 2 o 3 cermets prepared by wet chemical method. *Journal of the American Ceramic Society*, 97(10):3223–3229, 2014.

[81] YZ Wang, Jinsoo Joo, C-H Hsu, and AJ Epstein. Conductivity and microwave dielectric response of polyaniline and poly (o-toluidine) fibers. *Synthetic Metals*, 69(1-3):267–268, 1995.

[82] Zhongyang Wang, Kai Sun, Peitao Xie, Yao Liu, and Runhua Fan. Generation mechanism of negative permittivity and kramers–kronig relations in batio3/y3fe5o12 multiferroic composites. *Journal of Physics: Condensed Matter*, 29(36):365703, 2017.

[83] Robyn Wangberg, Justin Elser, Evgenii E Narimanov, and Viktor A Podolskiy. Nonmagnetic nanocomposites for optical and infrared negative-refractive-index media. *JOSA B*, 23(3):498–505, 2006.

[84] Haikun Wu, Yuanyuan Qi, Zhongyang Wang, Wen Zhao, Xiaomin Li, and Lei Qian. Low percolation threshold in flexible graphene/acrylic polyurethane composites with tunable negative permittivity. *Composites Science and Technology*, 151:79–84, 2017.

[85] Haikun Wu, Rui Yin, Lei Qian, and Zidong Zhang. Three-dimensional graphene network/phenolic resin composites towards tunable and weakly negative permittivity. *Materials & Design*, 117:18–23, 2017.

[86] Xiaodong Xia, Zheng Zhong, and George J Weng. Maxwell–wagner–sillars mechanism in the frequency dependence of electrical conductivity and dielectric permittivity of graphene-polymer nanocomposites. *Mechanics of Materials*, 109:42–50, 2017.

[87] Peitao Xie, Kai Sun, Zhongyang Wang, Yao Liu, Runhua Fan, Zidong Zhang, and Gerhard Schumacher. Negative permittivity adjusted by sio2-coated metallic particles in percolative composites. *Journal of Alloys and Compounds*, 725:1259–1263, 2017.

[88] LF Xu, PB Qi, XP Song, XJ Luo, and CP Yang. Dielectric relaxation behaviors of pure and pr_6o_{11}-doped $cacu_3ti_4o_{12}$ ceramics in high temperature range. *Journal of Alloys and Compounds*, 509(29):7697–7701, 2011.

[89] Hao Xue, Xiangfeng Guan, Rong Yu, and Zhaoxian Xiong. Dielectric properties and current-voltage nonlinear behavior of $ca_{1-x}sr_xcu_3ti_4o_{12}$ ceramics. *Journal of Alloys and Compounds*, 482(1):L14–L17, 2009.

[90] F Yakuphanoglu, Y Aydogdu, U Schatzschneider, and E Rentschler. Dc and ac conductivity and dielectric properties of the metal-radical compound: Aqua [bis (2-dimethylaminomethyl-4-nit-phenolato)] copper (ii). *Solid state communications*, 128(2-3):63–67, 2003.

[91] Han Yan, Cindy Zhao, Kevin Wang, Lucy Deng, Matthew Ma, and Gu Xu. Negative dielectric constant manifested by static electricity. *Applied Physics Letters*, 102(6):062904, 2013.

[92] Xiuchao Yao, Xuechen Kou, and Jun Qiu. Acidified multi-wall carbon nanotubes/polyaniline composites with high negative permittivity. *Organic Electronics*, 38:55–60, 2016.

[93] Xiuchao Yao, Xuechen Kou, and Jun Qiu. Multi-walled carbon nanotubes/polyaniline composites with negative permittivity and negative permeability. *Carbon*, 107:261–267, 2016.

[94] Xiuchao Yao, Xuechen Kou, and Jun Qiu. Nano-al2o3/pani composites with high negative permittivity. *Organic Electronics*, 39:133–137, 2016.

[95] Xiuchao Yao, Xuechen Kou, and Jun Qiu. Generation mechanism of negative dielectric properties of nano-fe3o4/pani composites. *Materials Chemistry and Physics*, 208:177–182, 2018.

[96] Xiuchao Yao, Xuechen Kou, Jun Qiu, and Mark Moloney. Generation mechanism of negative dielectric properties of metallic oxide crystals/polyaniline composites. *The Journal of Physical Chemistry C*, 120(9):4937–4944, 2016.

[97] DE Yıldız and İ Dökme. Frequency and gate voltage effects on the dielectric properties and electrical conductivity of al/sio2/p-si metal-insulator-semiconductor schottky diodes. *Journal of applied physics*, 110(1):014507, 2011.

[98] SH Zaidi and AK Jonscher. Spectroscopy of delayed electronic transitions in gaas schottky diodes. *Semiconductor science and technology*, 2(9):587, 1987.

[99] Guozhong Zang, Jialiang Zhang, Peng Zheng, Jinfeng Wang, and Chunlei Wang. Grain boundary effect on the dielectric properties of $cacu_3ti_4o_{12}$ ceramics. *Journal of Physics D: Applied Physics*, 38(11):1824, 2005.

[100] Chao Zhang, Zhicheng Shi, Fan Mao, Chaoqiang Yang, Xiaotong Zhu, Jie Yang, Heng Zuo, and Runhua Fan. Flexible polyimide nanocomposites with dc bias induced excellent dielectric tunability and unique nonpercolative negative-k toward intrinsic metamaterials. *ACS applied materials & interfaces*, 10(31):26713–26722, 2018.

[101] Lin Zhang, Patrick Bass, and Z-Y Cheng. Physical aspects of 0-3 dielectric composites. *Journal of Advanced Dielectrics*, 5(02):1550012, 2015.

[102] Lin Zhang, Patrick Bass, Zhi-Min Dang, and Z-Y Cheng. Characterization of percolation behavior in conductor-dielectric 0-3 composites. *Journal of Advanced Dielectrics*, 4(04):1450035, 2014.

[103] LIN Zhang and Z-Y Cheng. Development of polymer-based 0-3 composites with high dielectric constant. *Journal of Advanced Dielectrics*, 1(04):389–406, 2011.

[104] Lin Zhang, Wei Wang, Xiaogang Wang, Patrick Bass, and Z-Y Cheng. Metal-polymer nanocomposites with high percolation threshold and high dielectric constant. *Applied Physics Letters*, 103(23):232903, 2013.

[105] Qiaoli Zhang, Tao Li, Zhenping Chen, Renzhong Xue, and Yongqiang Wang. The non-ohmic and dielectric behavior evolution of $cacu_3ti_4o_{12}$ after heat treatments in oxygen-rich atmosphere. *Materials Science and Engineering: B*, 177(2):168–172, 2012.

[106] Shihai Zhang, Baojin Chu, Xin Xhou, Bret Neese, and Qiming Zhang. High energy density polymer dielectrics for capacitor applications. In *CARTS-CONFERENCE-*, volume 27, page 141. Components Technology Institute Inc., 2007.

[107] Xi Zhang, Suying Wei, Neel Haldolaarachchige, Henry A Colorado, Zhiping Luo, David P Young, and Zhanhu Guo. Magnetoresistive conductive polyaniline–barium titanate nanocomposites with negative permittivity. *The Journal of Physical Chemistry C*, 116(29):15731–15740, 2012.

[108] Xi Zhang, Xingru Yan, Qingliang He, Huige Wei, Jun Long, Jiang Guo, Hongbo Gu, Jingfang Yu, Jingjing Liu, Daowei Ding, et al. Electrically conductive polypropylene nanocomposites with negative permittivity at low carbon nanotube loading levels. *ACS applied materials & interfaces*, 7(11):6125–6138, 2015.

[109] Zi-Dong Zhang, Run-Hua Fan, Zhi-cheng Shi, Shi-Bing Pan, Ke-lan Yan, Kang-ning Sun, Xiang-fa Liu, Xiao Lin Wang, Shi Xue Dou, et al. Tunable negative permittivity behavior and conductor–insulator transition in dual composites prepared by selective reduction reaction. *Journal of Materials Chemistry C*, 1(1):79–85, 2013.

[110] Jiahua Zhu, Suying Wei, Lei Zhang, Yuanbing Mao, Jongeun Ryu, Pallavi Mavinakuli, Amar B Karki, David P Young, and Zhanhu Guo. Conductive polypyrrole/tungsten oxide metacomposites with negative permittivity. *The Journal of Physical Chemistry C*, 114(39):16335–16342, 2010.

[111] ME Zvanut, S Jeddy, E Towett, GM Janowski, C Brooks, and D Schlom. An annealing study of an oxygen vacancy related defect in srtio 3 substrates. *Journal of Applied Physics*, 104(6):064122, 2008.